

A Lattice Investigation of
Heavy Quark Symmetry
in Semi-Leptonic Decays of B Mesons.

Henning Hoerber



Doctor of Philosophy
The University of Edinburgh

1994



To my parents.

Für Oma.

Abstract

In this thesis I study semi-leptonic decays of mesons containing one heavy and one light quark. I describe the necessary theoretical tools of Lattice Gauge Theory and of Heavy Quark Effective Theory.

The six form factors describing the semi-leptonic decays are extracted from a lattice gauge theory calculation. The dependence of the form factors on the masses of the heavy and light quarks is studied.

The results are compared to the predictions of Heavy Quark Symmetry and corrections to the exact symmetry limit of infinitely heavy quarks are analysed.

The slope of the Isgur-Wise function is extracted from the lattice simulation and it is used to extract the Cabbibo-Kobayashi-Maskawa matrix element V_{cb} . The results are compared to those of other authors where possible.

Acknowledgements

This thesis is dedicated to my parents and to my grandmother. Their personal and financial commitment has made it possible for me to spend three wonderful years in Edinburgh. I cannot thank them enough.

Prof. Stuart Pawley stands at the very beginning of this project. His continued support throughout the first year was simply wonderful. I am very grateful.

The quest for mammon finally ended when the Dewar and Ritchie fund granted me support for the last two years of this work. It is gratefully acknowledged.

Working in the Edinburgh QCD group has been most enjoyable. I wish to thank the supervisor trio Brian Pendleton, Ken Bowler and Richard Kenway for tuition, advice and support throughout the three years. Thanks also for making it possible to go to Lat93 and to Seattle !

I am indebted to David Henty and David Richards for continued support, help and interest in the work presented in this thesis. Thanks for answering all the questions !

Throughout this project collaborating with Jim Simone and Laurent Lellouch has been very enjoyable. I have profited enormously from their knowledge and support. I would also like to thank my fellow postgrads Nick Hazel and Hugh Shanahan with whom I have enjoyed working in the early stages of the project and Nick Stanford and John Mehegan for useful discussions.

Thanks go to “the guys”, all the people with whom I have shared an office, lots of coffee breaks and some very nice holidays in the Highlands and in Ireland. To those of you staying on in Edinburgh : good luck with the theses ! See you all soon in “quite boring”.

Very personal thanks go to Aiden, for a wonderful time in Polwarth and a memorable weekend in North Yorkshire, and to Volker not least for all the coffee making and the lifts in the mornings.

Contents

Abstract	iii
Declaration	iv
Acknowledgements	v
Contents	vi
Introduction	1
1 Heavy Quark Symmetries and Meson Decay Form Factors	6
1.1 Heavy Quark Symmetry	7
1.2 Heavy Quark Effective Theory	8
1.3 Weak Meson Decay Form Factors	14
1.4 Phenomenological Applications	25
1.5 Overview	33
2 Lattice Gauge Theory	34
2.1 From Continuum QCD to Lattice QCD	34
2.2 From Lattice QCD to Continuum QCD	42
2.3 Systematic and Statistical Errors	44
3 Lattice Correlation Functions	49
3.1 Interpolating Fields, Two-point Functions and Smearing	49
3.2 Two-Point and Three-Point Functions	51
3.3 Discrete symmetries	56
Overview of Calculation	60
4 Results : Pseudoscalar \rightarrow Pseudoscalar	63
4.1 Introduction	63
4.2 Lattice Parameters	64
4.3 Determination of Z_V	66
4.4 Fitting Procedure and Normalisation	71
4.5 Results for $\beta = 6.2$	84

4.6	Heavy Quark Mass Dependence of $h_+(\omega)$	88
4.7	Light Quark Mass Dependence of $h_+(\omega)$	92
5	Results : Pseudoscalar \rightarrow Vector	101
5.1	Introduction	101
5.2	Axial Current	101
5.3	Axial Current Normalisation Z_A	102
5.4	The Form Factor $h_{A_1}(\omega)$	104
5.5	Heavy Quark Dependence of $h_{A_1}(\omega)$	105
5.6	Light Quark Dependence of $h_{A_1}(\omega)$	111
5.7	The Form Factors $h_{A_2}(\omega)$ and $h_{A_3}(\omega)$	117
5.8	Vector Current	124
6	Discussion and Phenomenological Applications	129
6.1	Slope of the Isgur-Wise Function	129
6.2	Extraction of V_{cb}	133
6.3	Summary	137
6.4	Conclusion	138
	References	140
	Appendix A Two point Functions	149
	Appendix B Radiative Corrections	152
	Appendix C Pseudoscalar \rightarrow Pseudoscalar	154
C.1	$h_+(\omega)$ and $h_-(\omega)$ at fixed light quark mass.	154
C.2	Interpolation of $h_+(\omega)$ to the mass of the strange quark.	162
C.3	Extrapolation of $h_+(\omega)$ to the chiral limit.	165
	Appendix D Pseudoscalar \rightarrow Vector	168
D.1	The form factor $h_{A_1}(\omega)$ at fixed light quark mass	168
D.2	Interpolation of $h_{A_1}(\omega)$ to the mass of the strange quark.	176
D.3	Extrapolation of $h_{A_1}(\omega)$ to the chiral limit.	179

Introduction

This work describes calculations of physical quantities of the Standard Model (SM). The SM successfully describes the strong and electro-weak interactions of the fundamental particles, quarks and leptons, over a wide range of energies. Arguably the two main problems the theory is faced with are the large (> 20) number of free parameters required as input and the lack of theoretical understanding of processes at very low energies (\sim few GeV). In this regime the non-perturbative long-distance forces of the strong interaction, Quantum Chromodynamics (QCD), lead to the confinement of quarks and gluons into hadrons.

Many of the unknown parameters arise in the weak sector of the SM. Most importantly, the quark and lepton masses and the Cabibbo-Kobayashi-Maskawa (CKM) matrix elements, which describe the mixing of mass eigenstates under weak interactions, are all part of the flavour sector. Weak decays of B mesons can help determine many of these quantities. However, the confinement of quarks in hadrons due to the strong interactions plays a crucial role in these processes, one that is a priori impossible to disentangle from the weak interactions. Without an understanding of the non-perturbative part of the interaction it is not possible to extract information on the fundamental parameters of the weak sector.

To reduce the theoretical uncertainties in the calculation of hadronic matrix elements it is instructive to consider certain symmetry limits. Thus, in the light quark sector, the masses of the u and d quarks can be set to 0 to a good approximation, and even the s quark is sometimes taken to be massless. In these limits, the theory yields new relations between physical quantities. Similarly, in the heavy quark sector, regarding the b and c quarks to be infinitely heavy leads to immense simplifications. To make proper use of these symmetry limits it is necessary to formulate them within field theory in such a way that it is possible to incorporate symmetry breaking effects order by order in the expansion parameter, $\frac{m_{\text{light}}}{\Lambda_{\text{QCD}}}$ for chiral symmetry and $\frac{\Lambda_{\text{QCD}}}{m_{\text{heavy}}}$ for heavy quark symmetry. Whereas Chiral Perturba-

tion Theory has been in use for many years, it has only recently become clear that an equivalent effective theory can be formulated for heavy quarks. But although Heavy Quark Effective Theory (HQET) is still a new theory its development over the past few years has already produced a wealth of knowledge and predictions. It is constructed in such a way as to reproduce the low-energy behaviour of systems containing one heavy quark in QCD.

Semi-leptonic decays of \bar{B} mesons (see figure 0.1) are without doubt one of its show-pieces. The discovery of the Isgur-Wise function, one universal form factor instead of six to describe $\bar{B} \rightarrow D l \bar{\nu}$ and $\bar{B} \rightarrow D^* l \bar{\nu}$, prompted a flood of papers. It opened the way to a quasi model-independent extraction of the CKM element V_{cb} and a deepening of our understanding of QCD.

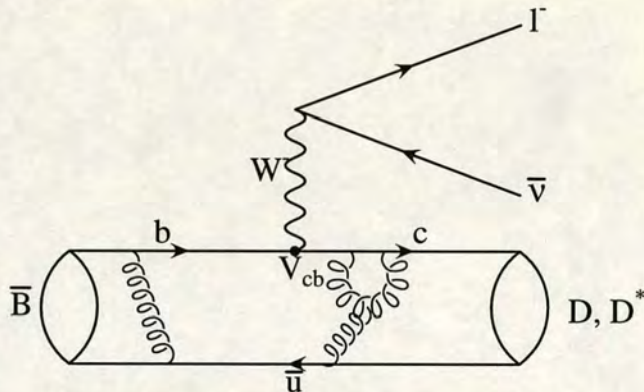


Figure 0.1: Pictorial representation of weak semi-leptonic decays of \bar{B} mesons. Mediated by an electro-weak current the b -quark decays into a c -quark with a light anti-quark as “spectator”. The weak interaction vertex is proportional to the CKM matrix element V_{cb} . For the weak interactions this diagram can be thought of as a Feynman diagram; however, the strong interactions, mediated by the gluons, are non-perturbative.

Nevertheless, tests of the theory are difficult to perform since many of the quantities involve non-perturbative interactions. Although many useful relations between hadronic matrix elements can be derived, it has, so far, not been possible to analytically calculate these quantities without recourse to a model or certain assumptions.

Lattice Gauge Theory (LGT) allows *ab initio* model-independent non-perturbative calculations in QCD. Hadronic weak matrix elements, such as the one of the process in figure 0.1, can be calculated from first principles to an accuracy limited

only by computer resource. LGT is therefore ideally suited to test the predictions of HQET and to analyse symmetry-breaking corrections. The main advantage of Lattice QCD is of course that it is QCD. By this I mean that any Lattice QCD calculation naturally incorporates the effects of long-distance non-perturbative QCD contributions mediated by low energy gluons. This is only slightly marred by the fact that the vast majority of today's lattice calculations are performed in the "quenched approximation", omitting all quark loops. Nevertheless, it is fair to say that Lattice QCD calculations have matured to such an extent that theorists and experimentalists are turning more and more to lattice calculations to help determine the fundamental parameters of the Standard Model.

To evaluate the matrix elements for the semi-leptonic decays $\bar{B} \rightarrow D l \bar{\nu}$ and $\bar{B} \rightarrow D^* l \bar{\nu}$ in a LGT calculation one needs to calculate the hadronic three-point function in which a b quark decays into a c quark, mediated through a vector or axial current $V^\mu = \bar{b}\gamma^\mu c$, $A^\mu = \bar{b}\gamma^\mu\gamma^5 c$, in the presence of a light spectator anti-quark. The three-point function can be represented diagrammatically in analogy to figure 0.1 as shown in figure 0.2.

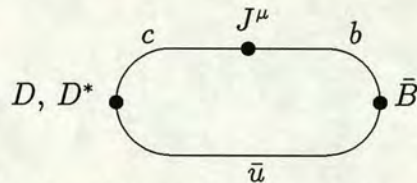


Figure 0.2: The Lattice three-point correlation function needed to extract the hadronic matrix elements of the decays $\bar{B} \rightarrow D l \bar{\nu}$ and $\bar{B} \rightarrow D^* l \bar{\nu}$. The lines represent quark propagators and \bar{B} , D and D^* , and J^μ are lattice operators.

This thesis brings together lattice gauge theory and heavy quark effective theory in an effort to find model-independent predictions for some of the fundamental non-perturbative quantities with which HQET is concerned. The form factors of the decays $\bar{B} \rightarrow D l \bar{\nu}$ and $\bar{B} \rightarrow D^* l \bar{\nu}$ are calculated in a quenched lattice QCD calculation and are presented with a detailed analysis of the statistical and systematical errors. The results are compared to the limit of an exact heavy quark symmetry in which certain form factors vanish and others are identical to a universal form factor, the Isgur-Wise function. Predictions of HQET are limited to the kinematical case where the velocity of the heavy quark inside the hadrons is unchanged; this calculation enables a model-independent determination of the

form factors' dependence on the velocity transfer away from zero recoil. Furthermore I study the symmetry-breaking corrections to the limit of infinitely heavy quarks; at subleading order in the heavy quark expansion several new form factors need to be introduced which are themselves fundamental non-perturbative quantities. Since the masses of the quarks can be varied at will in a LGT simulation, it is possible to study the form factors' dependence on the heavy quark masses in detail.

One of the most important applications of HQET is the extraction of the CKM matrix element V_{cb} . It is possible to determine this quantity by combining experimental data for the decay rates $\bar{B} \rightarrow D^* l \bar{\nu}$ and the value of the Isgur-Wise function at zero recoil predicted by HQET. These determinations of V_{cb} have been termed model-independent in the literature. However, they are faced with two problems. Firstly, it is difficult experimentally to obtain data for the decay rate $\bar{B} \rightarrow D^* l \bar{\nu}$ close to zero recoil and secondly the predictions for the symmetry-breaking corrections, which arise since the b - and c -quarks are not infinitely heavy, are model-dependent predictions. The lattice calculation I present here can help eliminate these uncertainties. Since the form factors have been calculated over a wide range of velocity transfers I will be able to determine their functional form close to zero recoil where experimental data is sparse. This will facilitate the extrapolation to zero recoil since it will allow me to fix the value of the slope of the Isgur-Wise function at zero recoil to its lattice value. Furthermore, the symmetry-breaking corrections to the limit of infinitely heavy quarks can be studied on the lattice in a model-independent way. The size of these corrections at zero recoil has been the focus of much attention recently since it is the main source of theoretical uncertainty in the extraction of V_{cb} .

The plan of this thesis is as follows. In Chapter 1 I give a brief introduction to the HQET focusing on the predictions for semi-leptonic decays. The extraction of V_{cb} , its experimental and theoretical uncertainties, are explained in some detail with the emphasis on a separation of the model-dependent from the model-independent factors. In Chapter 2 I summarise the main aspects of Lattice Gauge Theory and give an overview of the main systematic and statistical uncertainties. Chapter 3 is more technical as I explain the calculation of two- and three-point functions necessary to extract the matrix elements this thesis is concerned with. Chapters

4 and 5 form the core of this work. They contain the analysis of the matrix elements for $\bar{B} \rightarrow D l \bar{\nu}$ and $\bar{B} \rightarrow D^* l \bar{\nu}$ decays. The six form factors parametrising the decays are extracted and their functional form is determined. The functions' dependence on the masses of the heavy and light quarks are analysed and several phenomenologically interesting ratios are calculated. Chapter 6 provides a comparison of the results to those of other authors where possible. The matrix element V_{cb} is extracted combining results of Chapters 4 and 5 with experimental data from the CLEO and ARGUS collaborations. At the end of Chapter 6 I draw my conclusions.

Chapter 1

Heavy Quark Symmetries and Meson Decay Form Factors

In this chapter the ideas of Heavy Quark Symmetry (HQS) are presented. Section 1.2 introduces the Heavy Quark Effective Theory which provides the framework for analysing heavy hadron decays. HQET allows a systematic expansion of hadronic properties in powers of $\frac{1}{m_Q}$, where m_Q denotes the mass of the heavy quark. After a discussion of the infinite mass limit, $m_Q \rightarrow \infty$, in section 1.2.1, the symmetry breaking corrections are analysed in section 1.2.2.

Section 1.3 applies the formalism of HQET to the analysis of semi-leptonic decays of heavy mesons. Again, the discussion is split into an exposé of results at leading order (sections 1.3.1 and 1.3.2) and a subsequent look at symmetry-breaking corrections. Whereas in the limit of infinitely heavy quarks a single function suffices to describe semi-leptonic decays between both heavy pseudoscalar and vector mesons, a larger set of form factors must be introduced at order $\frac{1}{m_Q}$. A second source of symmetry breaking arises from hard gluon exchange. Section 1.3.3 provides a brief description of these corrections which can be calculated perturbatively.

Throughout this chapter an attempt is made to disentangle model-independent predictions from model-dependent ones. This is particularly important for understanding model-independent extractions of the CKM matrix element V_{cb} . In principle, this weak mixing parameter can be obtained in a model-independent way from the measurement of semi-leptonic decays of B mesons. In section 1.4.1 I compare several ways of extracting V_{cb} from different experiments and discuss the relative advantages of these methods and the theoretical uncertainties involved.

Extensive reviews have appeared on this subject recently in which all of the above mentioned topics are treated in detail [1, 2, 3, 4].

1.1 Heavy Quark Symmetry

Analytically, the theory of Quantum Chromodynamics has proved to be intractable at low energies. In this regime the strong coupling, α_s , is of $\mathcal{O}(1)$ so that perturbative methods, using the running coupling as the expansion parameter, fail. Predictions are therefore not based on dynamical (analytical) calculations but rather on symmetries of the theory. This has proven to be very successful for chiral symmetry $SU(3)_L \times SU(3)_R$ which arises in the limit where the masses of the light quarks (up, down and strange) are treated as small compared with the QCD scale. This scale, $\Lambda_{QCD} \sim 0.25 \text{ GeV}$, separates the regions of large and small coupling. It also naturally separates the quarks of the standard model into light quarks and heavy quarks (charm, bottom/beauty and top). For heavy quarks the strong coupling is small at the energy scale of the heavy quarks and QCD interactions on length scales of the order of the heavy quarks' Compton wavelength are perturbative. This is the first reason why strong interactions of systems containing a heavy quark may be simpler than those containing only light quarks [5, 6, 7, 8, 9, 10, 11, 12, 13, 14]. Indeed, if one were to deal with heavy quarks only, heavy meson properties could be calculated from first principles. This idea was used as early as 1975 to predict the properties of charmonium $Q\bar{Q}$ states [15].

But QCD is not that simple for bound states containing a heavy and a light quark in a heavy meson or a heavy quark and two light quarks in a heavy baryon. The size of these states is of order $\frac{1}{\Lambda_{QCD}} \sim 1 \text{ fm}$ and at these distances the coupling α_s becomes large so that the QCD interactions of the light quarks and gluons are confining. This cloud of confined light degrees of freedom in the heavy hadrons has been termed the “brown muck” of hadron physics by Isgur [3]. It is the brown muck which prevents any analytical first-principles calculations in heavy quark physics.

Again, one may use the heaviness of b and c quarks¹ to arrive at a simplification:

¹The top decays too fast to form hadronic bound states; therefore the term “heavy quark” will refer to b and c quarks only.

As the heavy quarks become heavier, their Compton wavelength becomes so small compared to the size of the hadron, $\lambda_Q \ll R_{had}$, that one needs to go to very small distances to see the heavy quarks' structure. But the gluons' coupling to the brown muck is soft, their four-momenta are small compared to the mass of the heavy quark, so they cannot resolve the structure. Consequently the light degrees of freedom are insensitive to the flavour and spin of the heavy quark. Although the colour field of the heavy quark extends out to large distances because of confinement, the chromo-magnetic moment of the heavy quark decouples as $m_Q \rightarrow \infty$. But it is only through such relativistic effects that the spin of the heavy quark couples to the spin of the brown muck. Therefore all heavy quarks look like scalar heavy quarks to the light degrees of freedom. Furthermore, one may consider two hadrons, each containing a single heavy quark, taken to be of different flavour. They are so heavy that they practically define their own center of mass. In the rest frame of the hadron, it is then possible to treat them as static colour charges at the origin. The hadronic systems that can be built around the two different heavy quarks out of the light quarks and gluons will be the same; QCD will distribute the brown muck around the two static colour charges identically and independently of the heavy quark's flavour [16]. It should be clear however, that this observation does not allow one to calculate analytically the configuration of the light degrees of freedom. But the fact that the solution of the QCD field equations are independent of m_Q as $m_Q \rightarrow \infty$ provides model-independent relations between the properties (mass-spectrum [17], decay constants [14, 18, 19], matrix elements [12, 14, 16]) of hadrons containing one heavy quark.

1.2 Heavy Quark Effective Theory

The ideas of HQS can be translated into an effective theory which reproduces the low energy behaviour of QCD. This theory, known as Heavy Quark Effective Theory [20, 21, 22, 23, 24, 25, 26, 27, 28, 29], is best constructed in two steps. First, one considers the limit in which the masses of the heavy quarks are taken to infinity with their four-velocities fixed [26]. The Lagrange density of the effective theory displays a heavy quark spin-flavour symmetry which is not manifest in the full theory of QCD. Its physical content is that the strong interactions of a heavy quark become independent of its mass and spin [16]. As a consequence, the

complexity of hadronic systems results from the strong interactions among the light degrees of freedom only. This leads to relations between hadronic quantities such as decay amplitudes and weak matrix elements. Most importantly for this work, the set of six form factors needed to parametrise the exclusive weak decays $\bar{B} \rightarrow D l \bar{\nu}$ and $\bar{B} \rightarrow D^* l \bar{\nu}$ is replaced by a single universal function, the Isgur-Wise function. The strength of this result lies in the fact that it is a model-independent consequence of QCD in the limit of infinitely heavy quarks [13, 16].

However, heavy quark symmetry is an approximate symmetry since the quark masses are not infinite. In a second step it is therefore necessary to study symmetry breaking-corrections.

1.2.1 Leading Order

The starting point for the construction of HQET is the part of the Lagrange density of full QCD involving the conventional heavy quark field $Q(x)$:

$$\mathcal{L} = \bar{Q}(x)(i\not{D} - m_Q)Q(x) , \quad (1.1)$$

where \not{D} is the covariant derivative

$$D_\mu = \partial_\mu - i\alpha_s A_\mu \quad \not{D} = \gamma^\mu D_\mu . \quad (1.2)$$

The quark momentum P_Q^μ can be split up into a kinetic momentum $m_Q v^\mu$ and a residual momentum k^μ ,

$$P_Q^\mu = m_Q v^\mu + k^\mu , \quad (1.3)$$

where v^μ is the four-velocity of the hadron, satisfying $v \cdot v = 1$. The momenta exchanged between a heavy quark and the light constituents (gluons and light quarks) are much smaller than m_Q . The residual momentum is of order Λ_{QCD} so that, as $m_Q \rightarrow \infty$, the heavy quark is nearly on-shell. The QCD interactions of the heavy quark and the brown muck do not change the heavy quark's velocity or its flavour. Kinks in the heavy quark's trajectory or changes in flavour must be caused by an external non-QCD agency like a weak current.

The global symmetries of HQET in the $m_Q \rightarrow \infty$ limit are strikingly apparent in the Feynman rules of HQET [18, 20, 22, 27]. The heavy quark propagator

becomes

$$\begin{aligned} \frac{i}{\not{P}_Q - m} &\rightarrow \frac{i}{v \cdot k} \frac{1 + \not{v}}{2} + \mathcal{O}\left(\frac{k}{m_Q}\right) \\ &\rightarrow \frac{i}{v \cdot k} P_+, \end{aligned} \quad (1.4)$$

where $P_+(v) = \frac{1}{2}(1 + \not{v})$ is a positive energy projection operator. The property $P_+ \gamma^\mu P_+ = P_+ v^\mu P_+$ means that the vertex between a heavy quark and a gluon can be simplified, too :

$$-ig \gamma^\mu \frac{\lambda^a}{2} \rightarrow -ig v^\mu \frac{\lambda^a}{2}. \quad (1.5)$$

Thus, the propagator of a heavy quark is independent of its mass and since no gamma matrix appears in the HQET coupling of a heavy quark to a gluon, eq. (1.5), the theory exhibits a spin symmetry. The relations eq. (1.4) and eq. (1.5) can be represented graphically as

$$\begin{array}{ccc} \frac{i}{\not{P}_Q - m_Q} & \longrightarrow & \frac{i}{v \cdot k} \\ \text{---} & & \text{---} \\ \text{---} & \longrightarrow & \text{---} \\ -ig \gamma^\mu \frac{\lambda^a}{2} & & -ig v^\mu \frac{\lambda^a}{2} \end{array}$$

These Feynman rules can be derived from the HQET Lagrangian that is obtained from the full QCD Lagrangian by the replacement [26]

$$h_v(x) = e^{im_Q v \cdot x} P_+(v) Q(x). \quad (1.6)$$

The field $h_v(x)$ annihilates a heavy quark with velocity v . The phase factor in eq. (1.6) removes the kinetic momentum so that the effective heavy quark field h_v carries the residual momentum $k \sim \mathcal{O}(\Lambda_{\text{QCD}})$. It is subject to the on-shell

constraint

$$\not{v}h_v = P_+ h_v = h_v, \quad (1.7)$$

which means that the space-time dependence of the heavy quark field is that of a free particle moving with velocity v .

The Lagrangian to lowest order in HQET becomes

$$\begin{aligned} \mathcal{L}_{\text{eff}}^\infty &= \bar{h}_v i v \cdot D h_v \\ &= \bar{h}_v (i v^\mu \partial_\mu + g T_a v^\mu A_\mu^a) h_v. \end{aligned} \quad (1.8)$$

This is not a non-relativistic approximation since the heavy quark's velocity v is completely arbitrary. For each heavy quark in the process under study one has to add a term of the form in eq. (1.8) to the Lagrangian. To describe the decay of a heavy quark $Q(v)$ into another heavy quark of different velocity $Q'(v')$ the Lagrangian would have to be

$$\mathcal{L}_{\text{eff}}^\infty = \bar{h}_v i v \cdot D h_v + \bar{h}_{v'} i v' \cdot D h_{v'}.$$

Heavy quarks with different velocities are not related to each other. This has been termed “velocity superselection rule” by Georgi [26]. Heavy quarks moving at the same velocity are related by a global $SU(2N_h)$ symmetry group, where N_h denotes the number of heavy quarks. Since no masses appear in the Lagrangian, rotations in flavour space leave the Lagrangian of N_h heavy quarks moving at the same velocity unchanged. Since no Dirac matrices appear, $SU(2)$ rotations leave the Lagrangian $\mathcal{L}_{\text{eff}}^\infty$ invariant, too. In the limit of infinitely heavy quarks the QCD interactions are independent of the heavy quark's mass and spin [16, 26].

1.2.2 Order $1/m$

The construction of the effective Lagrangian of HQET in a power series in $\frac{1}{m_Q}$ can be done elegantly in a functional integral approach [30]. Here, I work purely on the classical level.

Since the heavy quark inside the hadron is not exactly on-shell, an additional field is introduced,

$$H_v(x) = e^{im_Q v \cdot x} P_-(v) Q(x), \quad (1.9)$$

with the property

$$\not{v}H_v = -H_v. \quad (1.10)$$

$P_-(v)$ is the projection operator $\frac{1}{2}(1 - \not{v})$. It follows that

$$Q(x) = e^{-im_Q v \cdot x} [h_v(x) + H_v(x)]. \quad (1.11)$$

In the rest frame, h_v corresponds to the upper components of $Q(x)$ and H_v corresponds to the lower components :

$$Q(x)_{\text{rest frame}} = e^{-im_Q t} \begin{pmatrix} h_v(x) \\ H_v(x) \end{pmatrix} \quad (1.12)$$

Inserting the parametrisations eq. (1.9) and eq. (1.6) into the QCD Lagrangian for a single heavy quark and using a decomposition of the covariant derivative into longitudinal and transverse part,

$$\not{D} = \not{v}(v \cdot D) + \not{D}^\perp, \quad v \cdot D^\perp = 0, \quad (1.13)$$

one finds :

$$\mathcal{L}_{\text{eff}} = \bar{h}_v i v \cdot D h_v - \bar{H}_v (i v \cdot D + 2m_Q) H_v + \bar{h}_v i \not{D}_\perp H_v + \bar{H}_v i \not{D}_\perp h_v. \quad (1.14)$$

This equation shows that h_v describes massless degrees of freedom. The fields H_v have twice the mass of the fermions and correspond to the heavy degrees of freedom which will be “integrated out”. This elimination of the heavy degrees of freedom is the first step in the construction of the effective theory. It leads to a nonlocal action functional for the massless fields h_v . In the second step the action is expanded into a series of local operators of increasing dimension by expanding the propagator of H_v in powers of $\frac{1}{m_Q}$ [31, 32, 33, 34, 35]. This gives the operators to arbitrary order in $\frac{1}{m_Q}$; in particular, the action for the HQET including corrections to first order becomes [24, 28]

$$S_v = \int d^4x [\bar{h}_v i v \cdot D h_v + \mathcal{K}_v + \mathcal{M}_v + O(\frac{1}{m_Q^2})], \quad (1.15)$$

with the two operators

$$\mathcal{K}_v = \frac{1}{2m_Q} \bar{h}_v (iD_\perp)^2 h_v \quad (1.16)$$

$$\mathcal{M}_v = \frac{\alpha_s}{4m_Q} \bar{h}_v \sigma_{\mu\nu} F^{\mu\nu} h_v, \quad (1.17)$$

where $F^{\mu\nu}$ is the field strength tensor

$$F^{\mu\nu} = \frac{i}{\alpha_s} [D^\mu, D^\nu]. \quad (1.18)$$

In the rest-frame, $\vec{v} = 0$, one finds

$$\mathcal{K}_v(\vec{v} = 0) = \frac{1}{2m_Q} \bar{h}_v (i\vec{D})^2 h_v \quad (1.19)$$

which is a gauge-covariant form of the kinetic energy due to the off-shell motion of the heavy quark inside the meson. Similarly

$$\mathcal{M}_v(\vec{v} = 0) = \frac{-\alpha_s}{m_Q} \bar{h}_v \vec{S} \cdot \vec{B}_c h_v, \quad (1.20)$$

where S is a spin operator in the rest frame, $S^i = \frac{1}{2} \gamma_5 \gamma^0 \gamma^i$, and $B_c^i = \frac{1}{2} \epsilon^{ijk} F^{jk}$ are the components of the colour-magnetic gluon field. \mathcal{M}_v can therefore be interpreted as a Pauli-like chromo-magnetic hyperfine interaction. Whereas \mathcal{K}_v violates only the heavy quark flavour symmetry, \mathcal{M}_v breaks both flavour and spin symmetry.

The full heavy quark field can be expanded :

$$Q(x) = e^{-im_q v \cdot x} \left[1 + \frac{i \not{D}_\perp}{2m_Q} + \frac{i\alpha_s}{4m_Q^2} \gamma_\mu v_\nu F^{\mu\nu} + \mathcal{O}\left(\frac{1}{m_Q^3}\right) \right] h_v(x), \quad (1.21)$$

which can now be inserted into operators such as a heavy-light current, $V^\mu = \bar{q} \Gamma Q$. However, it is better to rewrite the effective Lagrangian of eq. (1.15) slightly differently, in such a way that the matrix elements of the effective theory become independent of the heavy quark mass [29, 36, 37]. The Lagrangian is rewritten as

$$\mathcal{L}_{\text{eff}} = \bar{h}_v i v \cdot D h_v, \quad (1.22)$$

so that the equation of motion simplifies to

$$iv \cdot D h_v = 0. \quad (1.23)$$

The higher dimension operators are then treated perturbatively as power corrections. The effect of this can be regarded as corrections to the wave function of the heavy meson.

The effective Lagrangian and the effective heavy quark field of eq. (1.21) correctly describe the low-energy long-distance physics of full QCD. Since the heavy quark can also couple to gluons with very high momenta, so-called hard gluons, which can resolve the colour-spin structure, the short-distance physics is not reproduced. However, these effects are of importance in a regime where the coupling constant is small and perturbation theory can be used. In section 1.3.3 I shall briefly sketch the matching of the effective theory onto the full theory at high energies.

1.3 Weak Meson Decay Form Factors

The matrix elements of the semi-leptonic decays of B mesons are parametrised by a set of six form factors :

$$\begin{aligned} \langle D(v') | V^\mu | B(v) \rangle &= h_+(\omega)(v + v')^\mu + h_-(\omega)(v - v')^\mu, \\ \langle D^*(v', \epsilon) | V^\mu | B(v) \rangle &= i h_V(\omega) \epsilon^{\mu\nu\lambda\sigma} \epsilon_\nu^* v'_\lambda v_\sigma, \\ \langle D^*(v', \epsilon) | A^\mu | B(v) \rangle &= h_{A_1}(\omega)(\omega + 1) \epsilon^{*\mu} - [h_{A_2}(\omega) v^\mu + h_{A_3}(\omega) v'^\mu] \epsilon^* \cdot v, \end{aligned} \quad (1.24)$$

where $V^\mu = \bar{c}\gamma^\mu b$, $A^\mu = \bar{c}\gamma^\mu\gamma^5 b$ and \bar{c} and b are the fields of full QCD.

This is the most general decomposition consistent with Lorentz invariance. Using time reversal the form factors can be shown to be real.

The variable $\omega = v \cdot v'$, called velocity-transfer, is related to the momentum transfer $q^2 = (p - p')^2$ by

$$\omega := v \cdot v' = \frac{m_B^2 + m_D^2 - q^2}{2m_B m_D}. \quad (1.25)$$

It is convenient in HQET to work with a mass-independent normalisation of meson

states

$$|M(v)\rangle = m_M^{-\frac{1}{2}} |M(p)\rangle, \quad (1.26)$$

so that the conventional, relativistic normalisation

$$\langle M(p') | M(p) \rangle = 2 E \delta^3(\vec{p} - \vec{p}') \quad (1.27)$$

is replaced by

$$\langle M(v') | M(v) \rangle = 2 \frac{E}{m_M} \delta^3(\vec{p} - \vec{p}'). \quad (1.28)$$

The advantage of this normalisation is that the mass-independent states can be thought of as the eigenstates of the effective Lagrangian \mathcal{L}_{eff} (eq. (1.22)) [29, 36, 37].

1.3.1 Tensor Formalism

To analyse semi-leptonic decays in HQET it is easiest to use the trace formalism [27, 38, 39], where a combined meson spin-wave function is introduced to represent both ground-state pseudoscalar and vector mesons. The wave function

$$\mathcal{M}(v) = \frac{1 + \not{v}}{2} \begin{cases} -\gamma_5; & \text{pseudoscalar meson,} \\ \not{v}; & \text{vector meson,} \end{cases} \quad (1.29)$$

has the correct transformation properties under Lorentz boosts and heavy quark spin rotations. Matrix elements $\langle M'(v') | \mathcal{O} | M(v) \rangle$ in HQET can now be obtained by replacing

$$\begin{aligned} |M(v)\rangle &\rightarrow \mathcal{M}(v) \\ \langle M'(v')| &\rightarrow \overline{\mathcal{M}'}(v') = \gamma_0 \mathcal{M}'(v')^\dagger \gamma_0. \end{aligned} \quad (1.30)$$

The operator \mathcal{O} is replaced by tensors which transform appropriately under the flavour-spin symmetry $SU(4)_v \otimes SU(4)_{v'}$. Finally, the wave functions are put together into invariants of the symmetry where, for each independent invariant, an arbitrary function of the Lorentz invariants is included.

For semi-leptonic weak decays of \bar{B} mesons this implies

$$\langle D(v') | \bar{c}_{v'} \Gamma b_v | \bar{B}(v) \rangle = \text{Tr} \{ (\bar{\mathcal{D}}(v') \Gamma \mathcal{B}(v)) (-\chi_1(\omega) + \chi_2(\omega) \not{v} + \chi_3(\omega) \not{v}' + \chi_4(\omega) \not{v} \not{v}') \}, \quad (1.31)$$

where the functions χ_i also depend on the renormalisation scale, μ , since the current on the left-hand side of eq. (1.31) needs to be renormalised in HQET. Here, $\bar{c}_{v'}$ and b_v are the heavy quark fields of the effective theory, related to the full QCD fields by eq. (1.6). The heavy quark spin indices are contracted for $SU(4)_v \otimes SU(4)_{v'}$ invariance and the trace is formed over the remaining Dirac indices. But using

$$\begin{aligned} \mathcal{M}(v) \not{v} &= -\mathcal{M}(v), \\ \not{v}' \overline{\mathcal{M}}(v') &= -\overline{\mathcal{M}}(v'), \end{aligned} \quad (1.32)$$

one finds that under the trace [27]

$$(\chi_1(\omega) + \chi_2(\omega) \not{v} + \chi_3(\omega) \not{v}' + \chi_4(\omega) \not{v} \not{v}') \equiv -\xi(\omega, \mu), \quad (1.33)$$

and

$$\langle D(v') | \bar{c}_{v'} \Gamma b_v | \bar{B}(v) \rangle = -\xi(\omega, \mu) \text{Tr} \{ \bar{\mathcal{D}}(v') \Gamma \mathcal{B}(v) \}. \quad (1.34)$$

The sign is chosen quite arbitrarily so that the universal function in eq. (1.34) is identical to the Isgur-Wise function first written down by Isgur and Wise in ref. [16]. Performing the traces the following model-independent predictions of HQET for the exclusive weak decays $\bar{B} \rightarrow D l \bar{\nu}$ and $\bar{B} \rightarrow D^* l \bar{\nu}$ in the limit of infinitely heavy quark masses are obtained [16]:

$$\begin{aligned} \langle D(v') | \bar{c}_{v'} \gamma^\mu b_v | B(v) \rangle &= \xi(\omega, \mu) (v + v')^\mu, \\ \langle D^*(v', \epsilon) | \bar{c}_{v'} \gamma^\mu b_v | B(v) \rangle &= i \xi(\omega, \mu) \epsilon^{\mu\nu\alpha\beta} \epsilon_\nu^* v'_\alpha v_\beta, \\ \langle D^*(v', \epsilon) | \bar{c}_{v'} \gamma^\mu \gamma^5 b_v | B(v) \rangle &= \xi(\omega, \mu) [(\omega + 1) \epsilon^{*\mu} - v'^\mu \epsilon^* \cdot v]. \end{aligned} \quad (1.35)$$

Comparing eq. (1.24) with eq. (1.35) one finds that the six form factors conventionally used to describe the weak decays of heavy-light mesons in full QCD are

all related to the universal form factor $\xi(\omega, \mu)$. In the exact symmetry limit :

$$\lim_{m_Q \rightarrow \infty} h_i(\omega) = \alpha_i \xi(\omega, \mu) , \quad (1.36)$$

with coefficients

$$\begin{aligned} \alpha_+ &= \alpha_V = \alpha_{A_1} = \alpha_{A_3} = 1 , \\ \alpha_- &= \alpha_{A_2} = 0 . \end{aligned} \quad (1.37)$$

These relations are, however, spoiled by radiative effects and $\mathcal{O}(\frac{1}{m_Q})$ corrections.

As will be outlined in section 1.3.3 the μ -dependence of the universal form factor cancels that of the Wilson coefficients of the heavy quark currents [41]. One can therefore define a renormalisation-group invariant Isgur-Wise function $\xi(\omega)$ in such a way that the normalisation condition $\xi(\omega, \mu) = 1$ is preserved.

1.3.2 The Isgur-Wise Function

At leading order in the $\frac{1}{m_Q}$ expansion a single universal function describes all weak decays of heavy mesons. It contains all long-distance physics associated with the strong interactions of the light degrees of freedom. This function, the Isgur-Wise function, $\xi(\omega)$, is a fundamental non-perturbative quantity. Heavy Quark Symmetries and Heavy Quark Effective Theory do not predict the dependence of $\xi(\omega)$ on the velocity transfer $\omega = v \cdot v'$.

The following properties of the Isgur-Wise function can be derived. Current conservation yields the normalisation of $\xi(\omega)$ at the zero recoil point, $\omega = 1$, at which the mesons' velocity is unchanged [11]:

$$\xi(1) = 1. \quad (1.38)$$

Furthermore, since $\xi(\omega)$ is the elastic form factor of a ground-state heavy meson, the function must be monotonically decreasing with the velocity transfer, ω .

For small ω one conventionally parametrises $\xi(\omega)$ as

$$\xi(\omega) = 1 - \rho^2(\omega - 1) + \mathcal{O}((\omega - 1)^2) \quad (1.39)$$

$$\xi'(1) = -\rho^2 \quad (1.40)$$

where ρ is called the “slope parameter” or “charge radius”. Since $\xi(\omega)$ is expected to have a positive curvature, this parametrisation will give a lower bound for the slope parameter [42] when fitting experimental data.

Several authors have tried calculating ρ using models and different parametrisations of the Isgur-Wise function, all of which, necessarily, have to incorporate the properties of the universal form factor as described above. Some suggested ansätze are :

$$\begin{aligned} \xi_{\text{BSW}}(\omega) &= \frac{2}{\omega + 1} \exp \left\{ - (2\rho^2 - 1) \frac{\omega - 1}{\omega + 1} \right\}, \\ \xi_{\text{ISGW}}(\omega) &= \exp \left\{ - \rho^2 (\omega - 1) \right\}, \\ \xi_{\text{pole}}(\omega) &= \left(\frac{2}{\omega + 1} \right)^{2\rho^2}. \end{aligned} \quad (1.41)$$

The first function is the form factor derived from an analysis of the Bauer-Stech-Wirbel (BSW) model[40, 44], the second one corresponds to the ISGW model [10] and the third is a pole-type ansatz.

Experimentally, the accessible kinematic region in the semi-leptonic decays $\bar{B} \rightarrow D l \bar{\nu}$ and $\bar{B} \rightarrow D^* l \bar{\nu}$ is in the range $1 < \omega < 1.6$. Knowledge of the Isgur-Wise function close to zero recoil is of particular interest as it enables a determination of V_{cb} . Close to $\omega = 1$ the ansätze of eq. (1.41) give very similar results for $\xi(\omega)$ when inserting the same ρ^2 . A precise value for the parameter ρ^2 is thus equivalent to a determination of the Isgur-Wise function ².

Constraints for ρ^2 have first been determined by Bjorken [38] and Voloshin [45]. Both authors relate ρ^2 to form factors of transitions of a ground-state heavy meson into excited states. Bjorken’s lower and Voloshin’s upper bound give :

$$\frac{1}{4} < \rho^2 < \frac{1}{4} + \frac{m_M - m_Q}{2E_{\min}} \approx \frac{3}{4}, \quad (1.42)$$

²The one-parameter approach has been criticised by Burdman [43]; he suggests a more general parametrisation of $\xi(\omega)$ allowing for an additional term in eq. (1.39), the curvature of the Isgur-Wise function which, with a one-parameter parametrisation, may be fixed to the wrong value. This suggestion will be followed up in the determination of ρ^2 in later chapters.

where $m_M(m_Q)$ denote the masses of the meson(heavy quark) and E_{\min} is the minimum excitation energy relative to the ground-state heavy meson. These bounds are considered to be somewhat uncertain since renormalisation effects have been ignored and it is not clear how to include them (see [1] and references therein); both the slope parameter ρ^2 and the heavy quark mass m_Q are renormalisation-scheme dependent quantities³. Neubert therefore relaxes the upper bound of Voloshin's sum rule to read [1] $0.25 < \rho^2 < 1.0$. The lower bound is not changed because there is evidence, both from experiment [46] and from QCD sum rule results [47], that the contributions of excited states in Bjorken's sum rule are quite sizeable so that the actual value of ρ^2 will be very much larger than 0.25. The QCD sum rule result of ref. [47] which estimates the contributions to the lowest-lying excited states of eq. (1.42) is $0.35 < \rho^2 < 1.15$.

Recently Rafael and Taron [48] have determined a conservative upper bound from analyticity arguments which I combine with Bjorken's lower bound to read :

$$0.25 < \rho^2 < 1.5 \quad (1.43)$$

In section 6.1 the results obtained in this thesis for ρ^2 will be compared with those of other authors.

1.3.3 Renormalisation : Hard gluons

So far, the matrix elements of operators for weak semi-leptonic decays have been obtained in the effective theory. Operators in the full theory can be matched onto a short-distance expansion in terms of operators in the effective theory. Schematically :

$$\bar{Q}'\Gamma Q \rightarrow \sum_i C_i(\mu)J_i + \sum_j \left[\frac{B_j(\mu)}{2m_Q} + \frac{B'_j(\mu)}{2m_{Q'}} \right] \mathcal{O}_j + \mathcal{O}\left(\frac{1}{m_Q^2}\right), \quad (1.44)$$

where the operators $\{J_i\}$ form a complete set of local dimension three current operators,

$$J_i = \bar{h}_{Q'}\Gamma h_Q$$

³Clearly, the slope of a form factor in eq. (1.24) is renormalisation-scheme independent since these are observable quantities. The Isgur-Wise function however is not observable, it is a theoretical tool.

$$\Gamma_i = \begin{cases} \{\gamma^\mu, v^\mu, v'^\mu\}; & \text{vector current,} \\ \{\gamma^\mu \gamma^5, v^\mu \gamma^5, v'^\mu \gamma^5\}; & \text{axial current.} \end{cases} \quad (1.45)$$

The matching was first performed in the leading logarithmic approximation (LLA) [27] where only $\Gamma = \gamma^\mu$ and $\Gamma = \gamma^\mu \gamma^5$ contribute. Then :

$$\bar{c} \gamma_\mu (1 - \gamma_5) b = \left(\frac{\alpha_s(m_b)}{\alpha_s(m_c)} \right)^{\frac{-6}{33-2N_f}} \left(\frac{\alpha_s(m_c)}{\alpha_s(\mu)} \right)^{a_i} \bar{h}_{v'}^c \gamma_\mu (1 - \gamma_5) h_v^b, \quad (1.46)$$

where

$$a_L(\omega) = \frac{8}{33 - 2N_f} (\omega r(\omega) - 1), \quad (1.47)$$

$$r(\omega) = \frac{1}{\sqrt{\omega^2 - 1}} \ln(\omega + \sqrt{\omega^2 - 1}), \quad (1.48)$$

and N_f is the number of quarks in the momentum interval between m_Q and μ .

Since then, the calculation has been carried out to order $\frac{1}{m_Q^2}$ and at next-to-leading-order in perturbation theory. All the elements of the calculation and necessary references can be found in ref. [1]. Here, the result is quoted at leading order :

$$\langle D(v') | \bar{c} \Gamma b | \bar{B}(v) \rangle = -\xi_{\text{ren}}(\omega) \sum_{i=1}^3 \hat{C}_i^{(5)}(m_b, m_c; \omega) \text{Tr} \{ \bar{\mathcal{D}}^*(v') \Gamma_i \mathcal{B}(v) \} + \mathcal{O}\left(\frac{1}{m_Q}\right). \quad (1.49)$$

The μ -dependence of the Wilson coefficients has been factorised into a universal function $K(\omega, \mu)$ which is normalised at zero recoil, $K(1, \mu) = 1$. This is used to define a renormalisation-group invariant Isgur-Wise function

$$\xi_{\text{ren}}(\omega) = \xi(\omega, \mu) K(\omega, \mu), \quad (1.50)$$

with

$$\xi_{\text{ren}}(1) = 1. \quad (1.51)$$

Writing

$$h_i(\omega) = \{\alpha_i + \beta_i(m_b, m_c; \omega) + \mathcal{O}\left(\frac{\Lambda_{QCD}}{m_Q}\right)\} \xi_{\text{ren}}(\omega) \quad (1.52)$$

the matrix elements are obtained by performing the traces in eq. (1.49):

$$\begin{aligned}
h_+(\omega) &= \left[\hat{C}_1(\omega) + \frac{\omega+1}{2} (\hat{C}_2(\omega) + \hat{C}_3(\omega)) \right] \xi_{\text{ren}}(\omega), \\
h_-(\omega) &= \frac{\omega+1}{2} [\hat{C}_2(\omega) - \hat{C}_3(\omega)] \xi_{\text{ren}}(\omega), \\
h_V(\omega) &= \hat{C}_1(\omega) \xi_{\text{ren}}(\omega), \\
h_{A_1}(\omega) &= \hat{C}_1^5(\omega) \xi_{\text{ren}}(\omega), \\
h_{A_2}(\omega) &= \hat{C}_2^5(\omega) \xi_{\text{ren}}(\omega), \\
h_{A_3}(\omega) &= [\hat{C}_1^5(\omega) + \hat{C}_3^5(\omega)] \xi_{\text{ren}}(\omega),
\end{aligned} \tag{1.53}$$

where the dependence of the Wilson coefficients on the masses of the heavy quarks has been suppressed. These functions can be found in ref. [19].

The analysis of ref. [19] shows that the effects of next-to-leading order corrections can be as large as the leading corrections. Numerically, the LLA gives a prediction for the coefficient $\hat{C}_1^5(\omega)$ which is more than 10% too large. Furthermore the form factor $h_+(\omega)$ can be shown to deviate from $h_+(1) = 1$ by terms of order $(m_b - m_c)^2$ only [52]. This constraint is violated by the LLA. In view of a precise determination of the Isgur-Wise function and a determination of V_{cb} it is thus important that Neubert's full next-to-leading order coefficients be used. Corrections to Neubert's computation are of order $\alpha_s^2(z \ln z)^n$ with $n = 0, 1, 2$ and should be smaller than 1%. His results account for the full order α_s dependence of the heavy-quark current on the ratio $z = \frac{m_c}{m_b}$ which, in this lattice calculation, covers the range between 0.6 and 1.

1.3.4 Matrix elements at order $\frac{1}{m_Q}$ and Luke's Theorem

At subleading order in $\frac{1}{m_Q}$ matrix elements receive contributions from higher dimension operators in the effective current and the effective Lagrangian [9, 13, 14]. The basic idea is to leave the heavy quark propagator as its leading order expression and calculate correction terms in the Lagrangian as insertions of operators [29, 36, 37] :

$$\mathcal{L}_{\text{eff}} = \bar{h}_v i v \cdot D h_v + \frac{1}{2m_Q} \mathcal{L}_1 + \mathcal{O}\left(\frac{1}{m_Q^2}\right), \tag{1.54}$$

with

$$\mathcal{L}_1 = \bar{h}_v(iD)^2 h_v + C_{\text{mag}}(\mu) \frac{\alpha_s}{2} \bar{h}_v \sigma_{\mu\nu} F^{\mu\nu} h_v . \quad (1.55)$$

The operator $\bar{h}_v(iD)^2 h_v$ is not renormalised due to the invariance of HQET under reparametrisation of the heavy quark momentum operator [53]. The same symmetry leads to the enormous simplification that all Wilson coefficients appearing at $\mathcal{O}(\frac{1}{m_Q})$ in the weak current can be related to the coefficients appearing at leading order [54].

It was first shown by Luke that at $\mathcal{O}(\frac{1}{m_Q})$ four additional functions and 1 mass parameter $\bar{\Lambda}$ are needed to parametrise the matrix elements of the higher dimension operators [29]. Meanwhile, the perturbative corrections to the subleading form factors have been calculated to next-to-leading order in perturbation theory [54]; the results, written in the form $h_i(\omega) = N_i(\omega; m_b, m_c) \xi_{\text{ren}}(\omega)$, are rather lengthy expressions for $N_i(\omega; m_b, m_c)$. It is more instructive, for understanding the structure of these functions, to work at tree-level.

Consider first the correction to the current due to the insertion of a local dimension four operator. They are of the generic form $\bar{h}_{v'} \Gamma i D_\mu h_v$ with a derivative acting on one of the heavy quark fields. Due to heavy quark symmetry, the structure of Γ is irrelevant. Applying the trace formalism to an operator of this type one finds that the most general form of the matrix element is given by

$$\langle M_2(v') | \bar{h}_{v'} \Gamma i D^\mu h_v | M_1(v) \rangle = -\text{Tr}\{\xi^\mu(v, v', \mu) [\bar{\mathcal{M}}_2(v') \Gamma \mathcal{M}_1(v)]\} , \quad (1.56)$$

where the form factor ξ^μ can be decomposed into three form factors with coefficients v^μ , v'^μ and γ^μ . Conventionally, they are decomposed as

$$\xi^\mu(v, v', \mu) = \xi_+(\omega, \mu)(v^\mu + v'^\mu) + \xi_-(\omega, \mu)(v^\mu - v'^\mu) - \xi_3(\omega, \mu)\gamma^\mu . \quad (1.57)$$

One may now use the equation of motion, $v \cdot D h_v = 0$, to find the constraint

$$0 = \text{Tr}\{\xi_+(\omega, \mu)(1 + \omega) + \xi_-(\omega, \mu)(1 - \omega) - \xi_3(\omega, \mu) \not{v} [\bar{\mathcal{M}}_2(v') \Gamma \mathcal{M}_1(v)]\} , \quad (1.58)$$

which, using eq. (1.32), gives the relation

$$(1 + \omega)\xi_+(\omega, \mu) + (1 - \omega)\xi_-(\omega, \mu) + \xi_3(\omega, \mu) = 0 . \quad (1.59)$$

Another constraint can be derived using the fact that the masses of the heavy quarks have been effectively removed from the wave-functions so that translational invariance applied to a heavy quark current gives

$$\langle M_2(v') | J_{hh}^\mu(x) | M_1(v) \rangle = e^{i\bar{\Lambda}(v'-v) \cdot x} \langle M_2(v') | J_{hh}^\mu(0) | M_1(v) \rangle, \quad (1.60)$$

where

$$\begin{aligned} (m_B v - m_D v') &= (m_b v - m_c v') + \bar{\Lambda}(v - v') \\ \bar{\Lambda} &:= m_B - m_b = m_D - m_c \sim \mathcal{O}(\Lambda_{\text{QCD}}). \end{aligned} \quad (1.61)$$

Next, take the Dirac conjugate of eq. (1.56) with an interchange of variables v and v' :

$$\langle M_2(v') | \bar{h}_v \Gamma(-i \overleftarrow{D}^\mu) h_v | M_1(v) \rangle = -\text{Tr}\{\bar{\xi}^\mu(v', v, \mu) [\overline{\mathcal{M}}_2(v') \Gamma \mathcal{M}_1(v)]\}, \quad (1.62)$$

and use T-invariance to find

$$\bar{\xi}^\mu(v', v, \mu) = \xi_+(\omega, \mu)(v^\mu + v'^\mu) - \xi_-(\omega, \mu)(v^\mu - v'^\mu) - \xi_3(\omega, \mu)\gamma^\mu. \quad (1.63)$$

Thus, one finds the relation

$$\xi^\mu(v, v', \mu) - \bar{\xi}^\mu(v', v, \mu) = \bar{\Lambda}(v - v')^\mu \xi(\omega, \mu). \quad (1.64)$$

These manipulations show that the insertion of the operator $\bar{h}_v \Gamma(-i D^\mu) h_v$ can be described by one new function and the parameter $\bar{\Lambda}$, which is associated with the light degrees of freedom [29, 55]. The scale of deviations from the limit $m_Q \rightarrow \infty$ is set by the dimensionless quantity $\frac{\bar{\Lambda}}{2m_Q}$. One may use the fact that the μ dependence of the functions $\xi_i(\omega, \mu)$ is the same as that of the Isgur-Wise function [1] to introduce a renormalisation-group invariant function $\eta(\omega)$ to parametrise the effect of the local dimension four operator-insertion at the current :

$$\eta(\omega) := \frac{1}{\bar{\Lambda}} \frac{\xi_3(\omega, \mu)}{\xi(\omega, \mu)}. \quad (1.65)$$

Due to the Dirac structure of the operator in eq. (1.56) the function $\eta(\omega)$ breaks both flavour and spin symmetry.

function	normalisation	broken symmetries
$\xi(\omega)$	$\xi(1) = 1$	no
$\eta(\omega)$	no	spin, flavour
$\chi_1(\omega)$	$\chi_1(1) = 0$	flavour
$\chi_2(\omega)$	no	spin, flavour
$\chi_3(\omega)$	$\chi_3(1) = 0$	spin, flavour

Table 1.1: Properties of leading and subleading universal functions in HQET

Next, I turn to symmetry-breaking effects due to insertions of higher-order operators in the effective Lagrangian, see eq. (1.55). Insertions of the operators \mathcal{L}_1 on either of the heavy quark lines can be thought of as corrections to the meson wave functions. These appear since the states of the effective theory are different to those of full QCD.

First look at the kinetic operator in \mathcal{L}_1 , inserted into the heavy b quark line (the matrix element due to an insertion of the operator on the other heavy quark is simply related to the one below by Dirac conjugation and an exchange of the variables v and v'). The kinetic operator has no Dirac structure so that the subleading form-factor will not break the spin symmetry. The matrix element can be parametrised in terms of a single function $\chi_1(\omega, \mu)$:

$$\langle D(v') | i \int d^4x T \{ \bar{h}_v^c \Gamma h_v^b(0), \bar{h}_v^b (iD)^2 h_v^b(x) \} \bar{B}(v) \rangle \sim \chi_1(\omega, \mu) \text{Tr} \{ \bar{D}(v') \Gamma B(v) \}. \quad (1.66)$$

An equivalent investigation of the chromo-magnetic operator, which, through its complicated Dirac structure, will clearly break the spin symmetry, shows that 2 more functions, $\chi_2(\omega, \mu)$ and $\chi_3(\omega, \mu)$, are needed.

The properties of the subleading form factors are collected in table 1.1. Vector current conservation implies that χ_1 and χ_3 vanish at zero recoil. Consequently the two form factors $h_+(\omega)$ and $h_{A_1}(\omega)$ are protected against $\mathcal{O}(\frac{1}{m_Q})$ corrections at zero recoil. This is known as **Luke's Theorem**. In particular this leads to

$$h_{A_1}(1) = \hat{C}_1^5(1; m_b, m_c) + \mathcal{O}(\frac{1}{m_Q^2}), \quad (1.67)$$

$$h_+(1) = \hat{C}_1(1; m_b, m_c) + \hat{C}_2(1; m_b, m_c) + \hat{C}_3(1; m_b, m_c) + \mathcal{O}(\frac{1}{m_Q^2}). \quad (1.68)$$

Since all other form factors of the hadronic matrix elements eq. (1.24) are multiplied by kinematic form factors which disappear at zero recoil Luke's Theorem implies that **there are no terms of $\mathcal{O}(\frac{1}{m_Q})$ in the hadronic matrix elements at $\omega = 1$** . The consequences of Luke's Theorem in the context of a measurement of V_{cb} will be discussed in section 1.4.1.

1.4 Phenomenological Applications

1.4.1 Extraction of V_{cb}

The Cabibbo-Kobayashi-Maskawa (CKM) matrix[56, 57] arises in the Standard Model Lagrangian interaction term which couples the fermion fields and the scalar Higgs doublet. This interaction is written in terms of the weak eigenstates q' of the quark fields :

$$\mathcal{L}_{\text{Yukawa}} = -\frac{g}{\sqrt{2}}(\bar{u}'_L, \bar{c}'_L, \bar{t}'_L)J^\mu \begin{pmatrix} d'_L \\ s'_L \\ b'_L \end{pmatrix} W_\mu^\dagger + \text{h.c.} \quad (1.69)$$

Redefining the quark fields to obtain the observable mass eigenstates has the effect of introducing flavour-changing charged-current interactions via the unitary flavour-mixing CKM matrix :

$$\mathcal{L}_{\text{Yukawa}} = -\frac{g}{\sqrt{2}}(\bar{u}_L, \bar{c}_L, \bar{t}_L)J^\mu V_{\text{CKM}} \begin{pmatrix} d_L \\ s_L \\ b_L \end{pmatrix} W_\mu^\dagger + \text{h.c.}, \quad (1.70)$$

with

$$V_{\text{CKM}} = \begin{pmatrix} V_{ud} & V_{us} & V_{ub} \\ V_{cd} & V_{cs} & V_{cb} \\ V_{td} & V_{ts} & V_{tb} \end{pmatrix}. \quad (1.71)$$

Since the Yukawa-couplings are completely arbitrary complex numbers the elements of the CKM matrix are not predicted by the Standard Model. Through the unitarity constraint - which is the assumption that there are only three quark generations - this means that there are four independent CKM parameters which need to be determined using experimental and theoretical information. For a

detailed discussion of issues surrounding the CKM matrix such as CP-violation and unitarity constraints I refer the reader to the review articles of Buras and Harlander [58] and Nir [59].

The CKM matrix element V_{cb} , which couples a b and a c quark, can be obtained from semi-leptonic decay data in three different ways : the inclusive approach, based on the total semi-leptonic decay width of the B meson and the exclusive determination from the decay amplitudes of either $\bar{B} \rightarrow D l \bar{\nu}$ or $\bar{B} \rightarrow D^* l \bar{\nu}$ extrapolated to the point of zero recoil. All methods have their own experimental and theoretical drawbacks but they rely on the same principal : the decay rates are of the form

$$\text{decay rate} = \left\{ \begin{array}{c} \text{known} \\ \text{factors} \end{array} \right\} \left\{ \begin{array}{c} \text{QCD} \\ \text{factor} \end{array} \right\} |V_{cb}|^2. \quad (1.72)$$

The known factors consist of constants and measurable quantities such as masses and kinematical factors. The QCD factor however is non-perturbative and cannot be obtained from experiment.

In the literature, the focus has been on extracting V_{cb} using the exclusive approach because it has been argued that the uncertainties in the theoretical expression for the total decay rate are too large to allow a precise determination of V_{cb} from the inclusive decay. The parton model formula for the inclusive decay rate has the following form[60]:

$$\Gamma(B \rightarrow X_q l \bar{\nu}) = \frac{G_F^2 m_b^5}{192 \pi^3} \{ \eta_c |V_{cb}|^2 f(\frac{m_c}{m_b}) + \eta_u |V_{ub}|^2 \}, \quad (1.73)$$

where η_c and η_u contain all short-distance QCD corrections and f is a phase-space factor. Since $\frac{|V_{ub}|^2}{|V_{cb}|^2} \leq 1\%$ the contribution from $b \rightarrow u$ can be neglected[61]. Eq. (1.73) is correct at leading order in the heavy quark expansion; non-perturbative corrections have been shown to vanish at $\mathcal{O}(\frac{1}{m_Q})$ [62].

The problem of using eq. (1.73) to determine V_{cb} is rather fundamental. As pointed out in ref. [63, 64, 65], the pole mass is an ill-defined object beyond perturbation theory. It can be shown to exhibit an uncertainty of $\mathcal{O}(\Lambda_{QCD})$ due to renormalon effects. However, for the effective Lagrangian to be invariant under the spin-flavour symmetry group, the heavy quark mass used in the field redefi-

inition eq. (1.6) must be a “physical” mass such as the pole mass or a mass that differs from the pole mass by an amount of order $\mathcal{O}(\Lambda_{QCD})$. The authors of ref. [55] have shown that the introduction of a residual mass term $\delta m = m_Q^{\text{pole}} - m_Q$ leaves physical quantities unaffected : only the combination $(m_Q + \delta m)$ appears in physical matrix elements so that different choices of m_Q are always compensated. Such a residual mass term, which usually in the construction of HQET is set to 0, is necessary in the effective Lagrangian to absorb the ambiguity in the definition of the pole mass. Since δm is independent of m_Q it does not break the flavour symmetry of the effective Lagrangian. Furthermore, in ref. [66], it has recently been shown that the predictions of HQET remain unaffected by the ambiguities introduced through renormalons. All relations between the weak decay form factors and Luke’s Theorem remain valid. However, the parameter $\bar{\Lambda} = m_P - m^{\text{pole}}$, through its dependence on the pole mass, contains a renormalon and thus an ambiguity of $\mathcal{O}(\Lambda_{QCD})$.

In view of these difficulties, and the ongoing debate about the use of perturbation theory in the calculation of the inclusive decay rate [67], I shall only quote the most recent results for $V_{cb}^{\text{inclusive}}$ [68] and subsequently turn to exclusive decays :

$$|V_{cb}| = \begin{cases} 0.039 \pm 0.001(\text{exp.}) \pm 0.005(\text{th.}); & \text{measurement at } \Upsilon(4s) \\ 0.042 \pm 0.002(\text{exp.}) \pm 0.005(\text{th.}); & \text{measurement at } Z^0 \end{cases} \quad (1.74)$$

Exclusive Decays

In the limit of zero lepton mass the differential decay widths for $\bar{B} \rightarrow Dl\bar{\nu}$ and $\bar{B} \rightarrow D^*l\bar{\nu}$ are given by[69]

$$\begin{aligned} \frac{d\Gamma}{d\omega} &= \frac{G_F^2}{48\pi^3} m_B^2 m_{D^{(*)}}^3 \sqrt{(\omega^2 - 1)(\omega + 1)^2} \times |V_{cb}|^2 \times \\ &\begin{cases} (1+r)^2 \frac{\omega-1}{\omega+1} |h_+(\omega) - \frac{m_B - m_{D^{(*)}}}{m_B + m_{D^{(*)}}} h_-(\omega)|^2 & \text{for } \bar{B} \rightarrow Dl\bar{\nu} \\ \left[2(1 - 2\omega r + r^2) [h_{A_1}(\omega)^2 + \frac{\omega-1}{\omega+1} h_V(\omega)^2] \right. \\ \left. + [(\omega - r)h_{A_1}(\omega) - (\omega - 1)(h_{A_3}(\omega) + r h_{A_2}(\omega))]^2 \right] & \text{for } \bar{B} \rightarrow D^*l\bar{\nu} \end{cases} \end{aligned} \quad (1.75)$$

where $r = \frac{m_{D^{(*)}}}{m_B}$.

Eq. (1.75) shows that for both modes the phase space becomes 0 at $\omega = 1$.

$\bar{B} \rightarrow Dl\bar{\nu}$ transitions are suppressed by an additional factor of $(\omega - 1)$ and the decay is experimentally more difficult. On the theoretical side a model-independent extraction of V_{cb} also proves to be more complicated using the mode $\bar{B} \rightarrow Dl\bar{\nu}$. Close to zero recoil the decay rate $\frac{d\Gamma}{d\omega}(\bar{B} \rightarrow Dl\bar{\nu})$ involves both form factors $h_+(\omega)$ and $h_-(\omega)$. Thus, since $h_-(\omega)$ is not protected by Luke's Theorem against $\mathcal{O}(\frac{1}{m_Q})$ corrections at zero recoil, the rate for $\bar{B} \rightarrow Dl\bar{\nu}$ is affected by first-order corrections in the inverse mass of the heavy quarks even at $\omega = 1$. On the other hand, $\bar{B} \rightarrow D^*l\bar{\nu}$ is ideally suited to extract $|V_{cb}|$ since the decay rate is protected by Luke's Theorem against first-order power corrections in $\frac{1}{m_Q}$ at $\omega = 1$ so that:

$$\lim_{\omega \rightarrow 1} \frac{1}{\sqrt{(\omega^2 - 1)}} \frac{d\Gamma(\bar{B} \rightarrow D^*l\bar{\nu})}{d\omega} = \frac{G_F^2 |V_{cb}|^2}{48\pi^3} (m_B - m_{D^*}) m_{D^*}^3 |h_{A_1}(1)|^2 \quad (1.76)$$

where

$$\begin{aligned} h_{A_1}(1) &= 1 + \beta_{A_1}(1) + \mathcal{O}(\frac{1}{m_Q^2}) \\ \text{and} \quad \beta_{A_1}(1) &= -0.01. \end{aligned} \quad (1.77)$$

Therefore, a model-independent determination of V_{cb} is possible via the decay rate of $\bar{B} \rightarrow D^*l\bar{\nu}$ once the non-perturbative $\mathcal{O}(\frac{1}{m_Q^2})$ corrections to $h_{A_1}(1)$ are known whereas for the decay rate $\bar{B} \rightarrow Dl\bar{\nu}$ it is necessary to have an estimate of the $\mathcal{O}(\frac{1}{m_Q})$ corrections to $h_-(1)$. However, this alone does not disqualify the mode $\bar{B} \rightarrow Dl\bar{\nu}$ since further inspection reveals that the $\frac{1}{m_Q}$ corrections to $\bar{B} \rightarrow Dl\bar{\nu}$ are in fact suppressed by a kinematic factor $\frac{m_B - m_D}{m_B + m_D} \approx 0.23$. Similarly to eq. (1.76) one can write

$$\lim_{\omega \rightarrow 1} \frac{1}{(\omega^2 - 1)^{\frac{3}{2}}} \frac{d\Gamma(\bar{B} \rightarrow Dl\bar{\nu})}{d\omega} = \frac{G_F^2 |V_{cb}|^2}{48\pi^3} (m_B + m_D)^2 m_D^3 \times \{1 + \delta_{\text{pert}} + \mathcal{O}(\frac{1}{m_Q})\} \quad (1.78)$$

where the perturbative corrections are known. The non-perturbative corrections are given by [1]⁴

$$\mathcal{O}(\frac{1}{m_Q})_{\bar{B} \rightarrow Dl\bar{\nu}} = 2 \left[\frac{\bar{\Lambda}}{2m_b} + \frac{\bar{\Lambda}}{2m_c} \right] \left[\frac{m_B - m_D}{m_B + m_D} \right] [1 - 2\eta(1)] \quad (1.79)$$

⁴Renormalisation effects have been ignored at $\mathcal{O}(\frac{1}{m_Q})$.

where $\eta(\omega)$ is the subleading Isgur-Wise function arising due to insertions of higher dimension operators in the current. Knowledge of this function is crucial to a determination of V_{cb} from the $\bar{B} \rightarrow Dl\bar{\nu}$ decay rate. Neubert [1] has calculated this function using the QCD sum-rule approach and finds it to be virtually independent of ω : $\eta(\omega) = 0.62 \pm 0.05$. Allowing for a generous error⁵ $\eta(1) = 0.6 \pm 0.3$ gives a very small correction to the decay rate $\bar{B} \rightarrow Dl\bar{\nu}$ at subleading order of 2-3 %. Hence the uncertainty in the normalisation of the decay rate $\bar{B} \rightarrow Dl\bar{\nu}$ at zero recoil could well turn out to be just as small as that of eq. (1.76). Clearly, it would be necessary to verify the sum-rule result for $\eta(\omega)$ and I shall try to do so in chapters 4 and 5. However, since this mode is also experimentally more difficult to measure, I shall now focus on the decay rate for $\bar{B} \rightarrow D^*l\bar{\nu}$.

To disentangle the model-dependent and model-independent parts in the decay rate of $\bar{B} \rightarrow D^*l\bar{\nu}$ it is useful to introduce the ratios of form factors[19]

$$R_1(\omega) = \frac{h_V(\omega)}{h_{A_1}(\omega)}, \quad (1.80)$$

$$R_2(\omega) = \frac{h_{A_3}(\omega) + r h_{A_2}(\omega)}{h_{A_1}(\omega)}, \quad (1.81)$$

in terms of which the decay rate can be written as :

$$\frac{d\Gamma}{d\omega} = \frac{G_F^2}{48\pi^3} (m_B - m_{D^*})^2 m_{D^*}^3 \sqrt{(\omega^2 - 1)(\omega + 1)^2} \times |V_{cb}|^2 \times |h_{A_1}(\omega)|^2 \times \left[2 \frac{(1-2\omega r + r^2)}{(1-r)^2} \left[1 + \frac{(\omega-1)}{(\omega+1)} R_1^2(\omega) \right] + \left[1 - \frac{(\omega-1)}{(1-r)} (1 - R_2(\omega)) \right]^2 \right] \quad (1.82)$$

Taking the ratios of form factors is advantageous as certain subleading form-factors cancel :

$$R_1(\omega) = F_1(\omega) \left(1 + \frac{2\epsilon_c}{\omega + 1} + \frac{2\epsilon_b}{\omega + 1} [1 - 2F_2(\omega)\eta(\omega)] \right), \quad (1.83)$$

where the functions $F_1(\omega)$ and $F_2(\omega)$ are perturbative corrections [1, 19],

$$F_1(\omega) = 1 + \frac{4\alpha_s(m_c)}{3\pi} r(\omega), \quad (1.84)$$

$$F_2(\omega) = 1 + \frac{2\alpha_s(\bar{m})}{3\pi} \frac{(\omega^2 - 1)r(\omega) + (\omega - \frac{m_c}{m_b}) \log z}{1 - 2\omega \frac{m_c}{m_b} + z^2}. \quad (1.85)$$

⁵The error encompasses the model-independent value $\eta(\omega) = \frac{1}{3}$ independent of all sum-rule parameters but excluding radiative corrections.

The expression for the ratio $R_2(\omega)$ is more complicated, however, it is completely insensitive to radiative corrections.

$R_1(\omega)$ is sensitive only to the subleading form factor $\eta(\omega)$ at order $\frac{1}{m_b}$ and thereby a measure of flavour-symmetry breaking, whereas $R_2(\omega)$ is sensitive to $\eta(\omega)$ and the subleading Isgur-Wise function $\chi_3(\omega)$, which arises due to insertions of higher order operators in the effective Lagrangian. It is therefore sensitive to spin- and flavour-symmetry breaking effects (see table 1.1). I shall perform a lattice analysis of these ratios in chapter 5.

In the heavy quark limit both ratios tend to 1 :

$$R_{1,2}(\omega) \rightarrow 1. \quad (1.86)$$

In this case the decay rate simplifies to

$$\begin{aligned} \frac{d\Gamma}{d\omega} = \frac{G_F^2}{48\pi^3} (m_B - m_{D^{(*)}})^2 m_{D^{(*)}}^3 \sqrt{(\omega^2 - 1)(\omega + 1)^2} \times |V_{cb}|^2 \times |h_{A_1}(\omega)|^2 \times \\ \left[1 + \frac{4\omega}{(\omega + 1)} \frac{(1 - 2\omega r + r^2)}{(1 - r)^2} \right]. \end{aligned} \quad (1.87)$$

It is now useful to introduce a new function, which is better suited than the form factor $h_{A_1}(\omega)$ to extract V_{cb} . One defines

$$\hat{\xi}^2(\omega) = \frac{\left[2 \frac{(1-2\omega r+r^2)}{(1-r)^2} \left[1 + \frac{(\omega-1)}{(\omega+1)} R_1^2(\omega) \right] + \left[1 - \frac{(\omega-1)}{(1-r)} (1 - R_2(\omega)) \right]^2 \right] |h_{A_1}(\omega)|^2}{\left[1 + \frac{4\omega}{(\omega + 1)} \frac{(1 - 2\omega r + r^2)}{(1 - r)^2} \right] \eta_A^2} \quad (1.88)$$

where η_A is the short-distance correction factor to $h_{A_1}(\omega)$ at zero recoil, see eq. (1.67). This new function, $\hat{\xi}(\omega)$, is identical to the Isgur-Wise function in the heavy quark limit. Since radiative corrections have been factored out, Luke's Theorem reads :

$$\hat{\xi}(1) = 1 + \mathcal{O}\left(\frac{1}{m_Q^2}\right). \quad (1.89)$$

To extract V_{cb} it now suffices to extrapolate the experimental data for the decay rate in $|V_{cb}| \times \eta_A \hat{\xi}(\omega)$ to $\omega = 1$ to obtain $|V_{cb}| \times [1 + \mathcal{O}(\alpha_s(m_Q), \frac{1}{m_Q^2})]$. Since the short-distance coefficient η_A is known to very high accuracy the only uncertainties in the determination of V_{cb} are

- The size of the $\mathcal{O}(\frac{1}{m_Q^2})$ corrections at zero recoil.
- The value of the slope parameter $\hat{\rho}$ used in the extrapolation to $\omega = 1$; in other words the functional form of $\hat{\xi}(\omega)$. In principle, once sufficient data has become available close to $\omega = 1$, the normalisation condition eq. (1.89) allows for an extraction of V_{cb} without knowledge of the exact functional dependence of the form factor $\hat{\xi}(\omega)$.

Several collaborations have recently presented high-precision data for the decay rate of $\bar{B} \rightarrow D^* l \bar{\nu}$ and they have obtained results for the combination $|V_{cb}| \hat{\xi}(1)$ [46, 71, 72, 73]. Combining these results with predictions for the $\mathcal{O}(\frac{1}{m_Q^2})$ term at $\omega = 1$ gives a quasi model-independent value of $|V_{cb}|$. The magnitude of the $\mathcal{O}(\frac{1}{m_Q^2})$ term has been the focus of some discussion recently. Estimates for this quantity range between 0... – 9%. Combining two different approaches to calculate this quantity [75, 37], Neubert finds a value of [76]

$$|V_{cb}| \hat{\xi}(1) = |V_{cb}| [1 - (5.5 \pm 2.5)\%]. \quad (1.90)$$

To extract $|V_{cb}|$ Neubert[76] then proceeds as follows : take the values of $|V_{cb}| \eta_A \hat{\xi}(1)$ obtained from a linear fit to the experimentally measured decay rates :

$$|V_{cb}| \eta_A \hat{\xi}(1) = 0.0347 \pm 0.0019 \pm 0.0020 \quad \text{CLEO}[71], \quad (1.91)$$

$$|V_{cb}| \eta_A \hat{\xi}(1) = 0.0382 \pm 0.0044 \pm 0.0035 \quad \text{ARGUS}[46], \quad (1.92)$$

$$|V_{cb}| \eta_A \hat{\xi}(1) = 0.0388 \pm 0.0043 \pm 0.0025 \quad \text{ALEPH}[73], \quad (1.93)$$

where the first error is statistical and the second systematic⁶. Following a suggestion by ref. [68] he adds 0.001 ± 0.001 to these values to account for the curvature of the function $\hat{\xi}(\omega)$. Using the prediction of eq. (1.90) the world average of $|V_{cb}|$ is :

$$|V_{cb}| = 0.0399 \pm 0.00269(\text{exp}) \pm 0.0013(\text{th}) = 0.0399 \pm 0.0029. \quad (1.94)$$

Measurements of the differential decay rate also determine the shape of the func-

⁶to obtain these values Neubert uses lifetimes of $\tau_{B^0} = (1.61 \pm 0.08)\text{ps}$ and $\tau_{B^+} = (1.65 \pm 0.07)\text{ps}$ [74] which are different to those of the original papers.

tion $\hat{\xi}(\omega)$. However, since the symmetry-breaking effects away from $\omega = 1$ are unknown, it is difficult to determine the slope of the Isgur-Wise function. Furthermore, the ratios $R_{1,2}(\omega)$ are difficult to obtain experimentally since they involve all four form factors of the decays $\bar{B} \rightarrow D^* l \bar{\nu}$; recently the CLEO collaboration has presented the first experimental measurement of these functions. Performing a three-parameter fit with the two ratios and the slope of the function $\hat{\xi}(\omega)$ as free parameters they determine

$$\begin{aligned} R_1 &= 1.30 \pm 0.36 \pm 0.16, \\ R_2 &= 0.64 \pm 0.26 \pm 0.12, \quad \text{CLEO Collaboration [70, 71]} \\ \hat{\rho}_{\text{linear}} &= 0.84 \pm 0.13 \pm 0.08, \\ \hat{\rho}_{\text{quad}} &= 0.92 \pm 0.64 \pm 0.40. \end{aligned} \quad (1.95)$$

One may use these values to relate the slope factor $\hat{\rho}^2$ to the slope of the Isgur-Wise function ρ^2 . However, due to the symmetry-violations away from $\omega = 1$, which are not predicted by the theory, this relation contains an uncertainty of $\mathcal{O}(\frac{1}{m_Q})$. Using eq. (1.52) and the explicit values of the Wilson coefficient one finds

$$\hat{\rho}^2 = \rho^2 - \frac{1}{6}[R_1^2(1) - 1] - \frac{1}{3} \frac{m_B}{m_B - m_{D^*}}[1 - R_2(1)] + (0.21 \pm 0.02) + \mathcal{O}(\frac{1}{m_Q}) \quad (1.96)$$

Inserting the experimental values obtained by CLEO this means :

$$\hat{\rho}^2 = \rho^2 - 0.1 \pm 0.2 + \mathcal{O}(\frac{1}{m_Q}) \quad \text{CLEO [71, 72]}. \quad (1.97)$$

The ratios $R_{1,2}(1)$ and the slope of the Isgur-Wise function have also been obtained in QCD sum-rule calculations. Using $R_1(1) = 1.3 \pm 0.1$ and $R_2(1) = 0.8 \pm 0.1$ ref. [1] determines

$$-\frac{1}{6}[R_1^2(1) - 1] - \frac{1}{3} \frac{m_B}{m_B - m_{D^*}}[1 - R_2(1)] = -(0.22 \pm 0.06), \quad (1.98)$$

so that

$$\hat{\rho}^2 = \rho^2 \pm 0.06 + \mathcal{O}(\frac{1}{m_Q}) \quad \text{Sum Rules [1]}. \quad (1.99)$$

Whilst many predictions (QCD sum rules, quark models) for the value of ρ^2 exist,

it is clear from eq. (1.96) that a determination of V_{cb} requires a precise model-independent calculation of both ρ^2 and the size of the $\mathcal{O}(\frac{1}{m_Q})$ corrections.

1.5 Overview

In the limit of an exact heavy quark symmetry, $m_{b,c} \rightarrow \infty$, one universal function, the Isgur-Wise function, suffices to describe the semi-leptonic decays of B-mesons, $\bar{B} \rightarrow D l \bar{\nu}$ and $\bar{B} \rightarrow D^* l \bar{\nu}$. Corrections to this picture arise due to hard gluon exchange and the finiteness of the heavy quark masses. The short-distance corrections have been calculated at next-to-leading order in perturbation theory; however, the power corrections in $\frac{1}{m_{b,c}}$ are unknown.

Predictions of heavy quark symmetry are limited to the point where the velocity of the mesons is unchanged due to the weak current, $\omega = 1$. At this point the Isgur-Wise function is normalised to $\xi(1) = 1$ and this can be used to extract the CKM matrix element V_{cb} . The remaining uncertainties arise due to non-perturbative effects which cannot be calculated analytically in a model-independent way. In particular, the slope of the Isgur-Wise function at $\omega = 1$ and the size of the power corrections away from $\omega = 1$ need to be determined.

Chapter 2

Lattice Gauge Theory

Lattice QCD is a regularisation of the theory of strong interactions enabling non-perturbative calculations [77]. These are necessary in extracting the properties of the hadrons which are formed from the fundamental fields of QCD, quarks and gluons. Examples are the calculation of the mass spectrum, matrix elements of operators involving the K , D and B mesons, and the determination of the strong coupling constant ¹.

To date, no other quantitative first-principles approach to non-perturbative QCD is known.

This chapter gives a very brief introduction to Lattice QCD. After providing the necessary definitions I will discuss the sources of errors for the lattice simulation presented in this thesis.

2.1 From Continuum QCD to Lattice QCD

The strong interaction of quarks and gluons is described by the QCD Lagrangian

$$\mathcal{L} = \sum_{q=u,d,s,c,b,\dots} \bar{q}_j (i \not{D}_{jk} - m_q \delta_{jk}) q_k - \frac{1}{4} F_{\mu\nu}^a F^{\mu\nu a}, \quad (2.1)$$

where $j, k = 1, 2, 3$, is the quark-colour index (the Dirac index is dropped for clarity), and $a = 1, \dots, 8$ is the gluon-colour index. Repeated colour indices are summed over.

¹For a more complete overview of the scope of Lattice Calculations see ref. [78].

The covariant derivative is given by

$$D_\mu = \partial_\mu - igA_\mu \quad \not{D} = \gamma^\mu D_\mu . \quad (2.2)$$

The gauge fields A_μ are collected in a matrix $A_\mu = A_\mu^a T^a$ where T^a are the eight generators of the $SU(3)$ symmetry which satisfy the following Lie-Algebra :

$$[T^a, T^b] = if^{abc}T^c \quad \text{tr}(T^a T^b) = \frac{\delta_{ab}}{2} . \quad (2.3)$$

The gauge part of the action is described by the field strength tensor

$$F_{\mu\nu} = F_{\mu\nu}^a T^a = \frac{i}{g}[D_\mu, D_\nu] = \partial_\mu A_\nu - \partial_\nu A_\mu - ig[A_\mu, A_\nu] . \quad (2.4)$$

Euclidean Space

Lattice calculations are performed in Euclidean space which is related to Minkowski space through the rotation

$$t = -i\tau \quad x_E = (\tau, \vec{x}) . \quad (2.5)$$

The Euclidean action is

$$S_E = \int d^4x_E \bar{q}(\gamma_\mu^E \partial_\mu + m)q \quad (2.6)$$

with Euclidean gamma matrices,

$$\gamma_0 = \gamma_4 \quad -i\gamma_i = \gamma_i^E , \quad (2.7)$$

satisfying

$$\{\gamma_\mu^E, \gamma_\nu^E\} = 2\delta_{\mu\nu} \quad \gamma_\mu^{E\dagger} = \gamma_\mu^E . \quad (2.8)$$

Functional Integral

The generating functional in Euclidean space

$$Z_E = \int_{\text{field configurations}} e^{-S_E} , \quad (2.9)$$

where sources are suppressed, looks like the partition function of statistical me-

chanics. This analogy between Euclidean QFT and classical statistical mechanics is exploited to use Monte Carlo methods to calculate expectation values of operators in terms of classical fields:

$$\langle \mathcal{O}(q, \bar{q}, U) \rangle = \frac{1}{Z_E} \int \mathcal{D}q \mathcal{D}\bar{q} \int \mathcal{D}U \mathcal{O}(q, \bar{q}, U) \exp[-S_E(q, \bar{q}, U)] . \quad (2.10)$$

The Feynman path integral is written in terms of the variables of lattice QCD, the quark fields q and \bar{q} , and the gluon field variables U_μ , which are SU(3) matrices replacing the continuum fields A_μ . $S_E(q, \bar{q}, U)$ is the Euclidean continuum action which will now be discretised.

Discretisation

To perform numerical simulations a discrete four-dimensional hypercubic lattice of space-time points separated by the lattice spacing a is introduced. The elements of this lattice are the sites and connections between the sites called links. Defining the variables of Lattice Field Theory only on the elements of the lattice, quark fields on the sites and gauge fields on the links, ensures that eq. (2.9) becomes an integral over a finite number of degrees of freedom when working in a finite volume.

The lattice provides a natural ultraviolet cutoff in momentum space. On a lattice of spatial volume aN_s , with periodic boundary conditions, three-momenta can only take on discrete values

$$\vec{p} = \frac{2\pi}{a}(n_1, n_2, n_3) \frac{1}{N_s} , \quad (2.11)$$

with $-\frac{N_s}{2} < n_i < \frac{N_s}{2}$ and each component is bounded by $\frac{\pi}{a}$.

Lattice QCD is defined as a theory which has as its limit the continuum theory of QCD, (eq. (2.1)), when the lattice spacing a is taken to 0 and the volume of the lattice is taken to infinity in a prescribed way. This will be discussed further below.

Pure Gauge Action

The action S_E is invariant under local SU(3) gauge transformations. A discretisation of the gluonic part of the action which preserves local gauge invariance is

given by the Wilson Gauge Action[77]

$$\int d^4x \sum_{\mu\nu} \frac{1}{2} \text{Tr} F_{\mu\nu} F_{\mu\nu} \longleftrightarrow a^4 \sum_x \sum_{\square} \frac{2}{g^2} (N_c - \text{ReTr} P_{\mu\nu}) , \quad (2.12)$$

where the sum is over all plaquettes $P_{\mu\nu}$ and \square stands for $1 \leq \mu \leq 4$ and $1 \leq \nu \leq \mu$. It is standard to label $\frac{2N_c}{g^2} = \beta$, where N_c denotes the number of colours, so that

$$S_{\text{gauge}} = -\beta \sum_{x, \square} \frac{\text{ReTr} P_{\mu\nu}}{N_c} , \quad (2.13)$$

and the constant terms are ignored. The plaquette is the product of gauge links forming a closed path :

$$P_{\mu\nu} = U_\mu(x) U_\nu(x + a\hat{\mu}) U_\mu^\dagger(x + a\hat{\nu}) U_\nu^\dagger(x) . \quad (2.14)$$

Wilson Fermion Action

The lattice fermion action used in this thesis is constructed as follows. The replacement

$$\begin{cases} \delta_\mu^+ q(x) = q(x + a\hat{\mu}) \\ \delta_\mu^- q(x) = q(x - a\hat{\mu}) \\ \partial_\mu q(x) \rightarrow \frac{1}{2a} [\delta_\mu^+ - \delta_\mu^-] q(x) \end{cases} \quad (2.15)$$

gives an anti-hermitean difference operator and results in what has been termed the “naive” fermion action. It exhibits the well-known fermion doubling problem: one fermi field produces 2^d fermions in d dimensions. The Nielsen-Ninomiya[79] theorem states that there is no local fermion action which has chiral symmetry, no additional states and a real positive transfer matrix. The two most popular approaches in circumventing the doubling problem are the use of “staggered fermions” [80] and “Wilson fermions” [81]. The latter approach follows the suggestion by Wilson in adding a so-called irrelevant operator, an operator that vanishes in the continuum limit, to the naive fermion action.

Following Wilson the derivative operator is taken to be

$$\frac{1}{2a} (1 + \gamma_\mu)(1 - \delta^-) - \frac{1}{2a} (1 - \gamma_\mu)(\delta^+ - 1) = \gamma_\mu \partial_\mu - \frac{a}{2} \delta_\mu , \quad (2.16)$$

where

$$\delta_\mu = \frac{1}{a^2} [\delta^+ + \delta^- - 2] \quad (2.17)$$

and ∂_μ is defined in eq. (2.15).

Minimal coupling of the gauge fields U_μ to the matter fields is achieved through the replacement

$$\begin{cases} \delta_\mu^+ \rightarrow \Delta_\mu^+ = U_\mu \delta_\mu^+ \\ \delta_\mu^- \rightarrow \Delta_\mu^- = U_{-\mu} \delta_\mu^- \\ \delta_\mu \rightarrow \Delta_\mu \end{cases} , \quad (2.18)$$

where $U_{-\mu} = U_\mu^\dagger(x - a\hat{\mu})$. The Wilson fermion action can now be written as the sum of the naïve fermion action,

$$S_{\text{naive}} = a^4 \sum_x \left[m \bar{q}(x) q(x) + \frac{1}{2a} \sum_{\mu=1}^4 \bar{q}(x) \gamma_\mu (\Delta_\mu^+ - \Delta_\mu^-) q(x) \right] \quad (2.19)$$

and the Wilson term

$$S_{\text{Wilson}} = -\frac{a}{2} a^4 \sum_x \sum_{\mu=1}^4 \bar{q}(x) \Delta_\mu q(x) . \quad (2.20)$$

More compactly :

$$S_{\text{Fermion}} = \sum_{x,y} \bar{q}(x) H^{-1}(x, y; U) q(y) , \quad (2.21)$$

where $H^{-1}(x, y; U)$ is the inverse quark propagator and the sum is over the coordinates and spin and colour degrees of freedom. Thus, setting $a = 1$,

$$H^{-1}(x, y; U) = \delta_{x,y} - \kappa \sum_{\mu} \left[(1 - \gamma_\mu) U_\mu \delta_{x+\hat{\mu},y} + (1 + \gamma_\mu) U_\mu^\dagger(y) \delta_{x-\hat{\mu},y} \right] , \quad (2.22)$$

The hopping parameter κ is

$$\kappa = \frac{1}{8 + 2ma} , \quad (2.23)$$

and the bare quark mass is defined as

$$am = \frac{1}{2} \left(\frac{1}{\kappa} - \frac{1}{\kappa_{\text{crit}}} \right) \quad (2.24)$$

where κ_{crit} is the value of the hopping parameter corresponding to zero quark mass which needs to be determined non-perturbatively. The fields have been rescaled

by

$$q(x) \rightarrow \frac{q(x)}{\sqrt{2\kappa}}. \quad (2.25)$$

The additional term in the fermion action removes all unwanted states at the price of explicitly breaking chiral symmetry even when $m = 0$. Chiral symmetry is only regained in the continuum limit with the value of κ tuned to κ_{crit} .

Improvement

Since this is a study of decays of quarks whose masses are large in lattice units, one must worry about controlling discretisation errors. The Wilson fermion action differs from the fermionic term in the continuum action by a discretisation error of $\mathcal{O}(a)$ whereas the gluonic term differs from its continuum counterpart by terms of $\mathcal{O}(a^2)$. The effort to reduce lattice-spacing dependent errors has therefore focused on the fermionic part of the action.

Naively, at quark masses around that of the charm quark, and for lattice spacings $a^{-1} \sim 3\text{GeV}$, one can expect the lattice discretisations errors of $\mathcal{O}(ma)$ to be on the order of $am \sim 40\%$. In order to reduce the discretisation errors, the action eq. (2.21) is modified to an $\mathcal{O}(a)$ -improved action originally proposed by Sheikholeslami and Wohlert[82],

$$S_{\text{Fermion}}^{SW} = S_{\text{Fermion}} - i\frac{\kappa}{2} \sum_{x,\mu,\nu} \bar{q}(x) F_{\mu\nu}(x) \sigma_{\mu\nu} q(x). \quad (2.26)$$

where

$$F_{\mu\nu} = \frac{1}{4} \sum_{\square=1}^4 \left[\frac{P_{\mu\nu}^{\square} - P_{\mu\nu}^{\square\dagger}}{2i} \right]. \quad (2.27)$$

Since this term involves no further derivatives the resulting action, termed the Sheikholeslami-Wohlert or “Clover” Action, couples fields only locally; clearly this is important for the numerical implementation.

Together with a “rotation” of the quark fields, [83],

$$\begin{aligned} q(x) &\longrightarrow \left(1 - \frac{1}{2}\gamma \cdot \vec{D}\right) q(x) \\ \bar{q}(x) &\longrightarrow \bar{q}(x) \left(1 + \frac{1}{2}\gamma \cdot \vec{D}\right), \end{aligned} \quad (2.28)$$

this is equivalent to adding a term

$$\Delta S = a^4 \sum_{x,\mu} \left(\frac{\kappa}{8a} [\bar{q}(x) U_\mu(x) U_\mu(x + \hat{\mu}) q(x + 2\hat{\mu}) + \bar{q}(x + 2\hat{\mu}) U_\mu^\dagger(x + \hat{\mu}) U_\mu^\dagger(x) - 2\bar{q}(x) q(x)] \right) \quad (2.29)$$

to the Wilson action. The action thus obtained guarantees that the leading discretisation errors in matrix element calculations of heavy-quark decays are reduced from $\mathcal{O}(am_Q)$ to $\mathcal{O}(a\alpha_s m_Q)$ and $\mathcal{O}((am_Q)^2)$ [83]. In order to obtain this improvement for matrix elements of semi-leptonic B decays, a “rotated” vector current is used [83] :

$$V_I^\mu \equiv \bar{q}'(x) \tilde{\Gamma}^\mu q(x), \quad (2.30)$$

where

$$\tilde{\Gamma}^\mu = (1 + \frac{1}{2} \gamma \cdot \vec{D}) \gamma^\mu (1 - \frac{1}{2} \gamma \cdot \vec{D}) \quad (2.31)$$

and where the subscript I indicates that V_I^μ is an improved lattice current.

Non-perturbative calculations indicate that this improvement scheme does in fact reduce the systematic error due to the finiteness of the lattice spacing in the calculation of hadronic matrix elements [84]. Recently, the improved action was used to study the heavy quark scaling behaviour of the vector and pseudoscalar decay constants f_P and f_V [85] using both the Wilson and the $\mathcal{O}(a)$ -improved actions. This study is also of interest here, since it allows for the following test of heavy quark symmetry : HQET predicts the simple scaling behaviour

$$\frac{f_P f_V}{M} = (1 + \frac{2}{3\pi} \alpha_s(M) + \dots) [1 + \mathcal{O}(\frac{1}{m_Q})] \quad (2.32)$$

where $M = \frac{m_P + 3m_V}{4}$. This scaling behaviour is found to be very well satisfied with $\mathcal{O}(\frac{1}{m_Q}) \sim 10\%$ working at heavy quark masses corresponding to that of the charm and using an $\mathcal{O}(a)$ -improved action. The result shows that the heavy quark scaling regime is reached fairly early on, at masses around that of the charm. In figure 2.1 the quantity

$$\tilde{U}(M) \equiv U(M) / \left\{ 1 + \frac{8}{3} \frac{\alpha_s(M)}{4\pi} \right\} \quad (2.33)$$

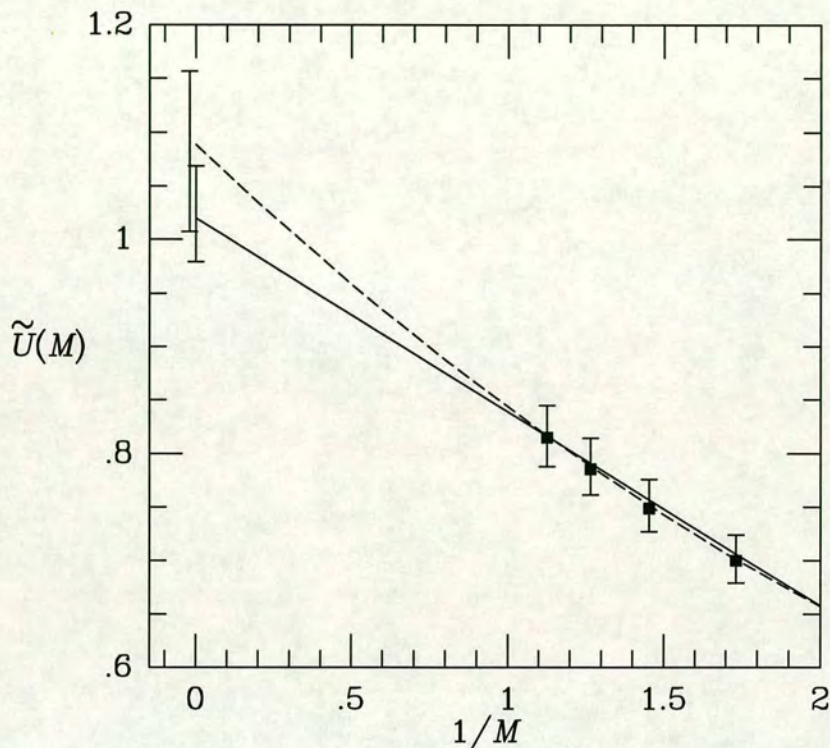


Figure 2.1: The quantity $\tilde{U}(M)$ plotted against the inverse spin-averaged mass. Linear and quadratic fits are represented by the solid and dashed curves, respectively. Also shown are the statistical errors of the extrapolation to the infinite mass limit.

fitted to either a quadratic or a linear function of $1/M$ is shown, where

$$U(M) \equiv \frac{f_V f_P}{M} = \left(1 + \frac{8}{3} \frac{\alpha_s(M)}{4\pi} + \mathcal{O}(1/M) \right), \quad (2.34)$$

and

$$\tilde{U}(M) \equiv U(M) / \left\{ 1 + \frac{8}{3} \frac{\alpha_s(M)}{4\pi} \right\} \quad (2.35)$$

(taken from ref. [85]). Deviations from 1 are seen to be small. However, it should be noted that deviations from the scaling limit for the decay constants f_D and f_B are much larger; non-scaling corrections are of $O(30\%)$ for f_D and $O(10\%)$ for f_B . This is in agreement with results found using the Wilson action if the quark

fields are normalised according to a proposal by Lepage, Kronfeld and Mackenzie [86, 87]. Using their improved quark-field normalisation scheme the authors of ref. [88] and ref. [89] find equally good agreement for eq. (2.32) for data obtained with the Wilson fermion action².

In the calculation presented here, the improved action obtained through the term eq. (2.29) and the rotation eq. (2.28) is used. I shall call this action the Sheikholeslami-Wohlert action. In chapters 4 and 5 lattice-discretisation errors will be discussed in the context of vector- and axial-current normalisation in some detail.

I would like to briefly mention some other possible approaches to the calculation of quantities involving heavy quarks. The formalism described above requires, for the correct propagation of heavy quarks, that the lattice spacing satisfy the condition

$$m_Q a \ll 1. \quad (2.36)$$

However, in order to control finite-size effects, ie in order to fit hadrons on the lattice, one has to work with lattice volumes which are bigger than 1-1.5 fermi. Thus, it is not possible to simulate QCD at the physical mass of the b -quark and one has to work at masses around that of the charm. Scaling laws, such as the one in eq. (2.32) may then be used to extrapolate to higher quark masses. An alternative approach which is the subject of much analysis to date, is the use of a non-relativistic QCD action [91, 92, 93] in which the heavy quark field is a 2-component spinor. Even more drastic is the use of the static approximation[94] in which only the first term of the NRQCD action is kept. This action is widely used to interpolate between the static value of quantities in the limit $m_Q \rightarrow \infty$ and between the values one finds using the full (Wilson or improved) action at the heaviest possible quark masses. No calculations of matrix elements for semi-leptonic decays of B-mesons have been performed using these approaches so far. However, two different calculations to extract the slope of the Isgur-Wise function are being performed which implement directly the HQET on the lattice [95, 96, 97].

²For a review of heavy-light decay constants using both actions see ref. [90].

2.2 From Lattice QCD to Continuum QCD

Lattice QCD is a theory with the following free parameters :

- The bare lattice coupling g .
- The hopping parameters κ_f , where $f = 1, \dots, N_f$, where N_f is the number of flavours.

As in any regularisation scheme, the bare coupling is related to the ultra-violet regulator via a dimensionful cutoff-independent mass parameter Λ_{latt} . The renormalisation group equation gives the following dependency :

$$a = \frac{1}{\Lambda_{\text{latt}}} (\beta_0 g^2)^{-\frac{\beta_1}{2\beta_0^2}} e^{-\frac{1}{2\beta_0 g^2}} [1 + \mathcal{O}(g^2)], \quad (2.37)$$

so that as the coupling goes to 0 the lattice spacing tends to 0. The “scaling regime” is the region in which ratios of physical quantities are independent of the (unphysical) lattice spacing a . Eq. (2.37) defines the “asymptotic scaling regime” in which all physical quantities are independent of a .

In practice, one proceeds as follows :

- the value of κ_{crit} is determined non-perturbatively. To first approximation the square mass of the pion is proportional to the mass of the light quark, $m_\pi^2 \propto m_q$, so that a linear extrapolation of the lattice pion mass in the light kappa values determines κ_{crit} .
- The lattice value of the mass of the ρ particle is used to set the scale a by chirally extrapolating the lattice value m_ρ^{latt} and comparing with the physical value of the ρ particle. In principle any quantity can be used to set the scale and clearly it is best to find a choice which is most insensitive to the lattice mass.
- Scaling has to be verified by calculating the same physical quantity at different values of the lattice spacing $a(g)$. If scaling violations are seen, an extrapolation to $a \rightarrow 0$ has to be performed.

A look at the literature shows that many lattice calculations have been performed to date without the last step. This is also true of the calculation presented here, which works at a single value of the strong coupling. Scaling is assumed but needs to be verified by performing the same calculation at several other values of the lattice spacing.

2.2.1 Renormalisation

Operator matrix elements calculated in a numerical simulation are obtained in a lattice regularisation scheme at a scale $\frac{1}{a}$. However, it is standard to quote results in the continuum \overline{MS} scheme so that a perturbative calculation needs to be performed matching up the two schemes. For the case of the Sheikholeslami-Wohlert action these coefficients have been calculated to one-loop [130]. Denoting the renormalisation coefficients by Z and the quark fields by q ,

$$(\bar{q}\Gamma q)_{\overline{MS}(\mu=\frac{1}{a})} = Z(\bar{q}\Gamma q)_{\text{LAT}}, \quad (2.38)$$

for the vector and the axial current the result is :

$$\begin{aligned} Z_V &= 1 - 0.10 g^2 + \mathcal{O}(g^4), \\ Z_A &= 1 - 0.02 g^2 + \mathcal{O}(g^4). \end{aligned} \quad (2.39)$$

Following a proposal by the authors of ref. [131], the matching coefficients can be improved by using the “boosted coupling”,

$$g^2 = \frac{6}{\beta u_0^4}, \quad u_0 = \left(\frac{1}{8\kappa_{\text{crit}}} \right). \quad (2.40)$$

In chapters 4 and 5 these renormalisation constants will be determined non-perturbatively, thus enabling a comparison with the improved values of eq. (2.39).

2.3 Systematic and Statistical Errors

2.3.1 Systematic Errors

Clearly, the most important source of systematic errors in the simulation presented here is the finite lattice spacing a . To reduce these errors one can either perform

the same calculation at many different and successively smaller lattice spacings to take the continuum limit or, as outlined above, one can try and reduce these errors from the very beginning by choosing a lattice action which is insensitive to a . I will return to this issue in chapters 4 and 5.

Quenching

To calculate expectation values of operators in full QCD one needs to calculate the Feynman path integral given in eq. (2.10). Since this equation looks identical to a statistical mechanics average the whole machinery of Monte Carlo importance sampling becomes available once the theory is discretised as outlined above. The main difference to statistical mechanics is the involvement of anti-commuting Grassmann variables. However, the fermionic action is a quadratic form so that the integration over the fermion fields can be performed analytically. Consider for example a quark propagator : $\mathcal{O} = \langle q(x)\bar{q}(y) \rangle$ and

$$G(x, y) = \frac{1}{Z} \int \mathcal{D}U \det[\mathcal{D} + m] [\mathcal{D} + m]^{-1} e^{-S_{\text{Gauge}}} . \quad (2.41)$$

In general one obtains

$$\langle \mathcal{O}(q, \bar{q}, U) \rangle = \frac{1}{Z} \int \mathcal{D}U \mathcal{T}_O(U) \det[\mathcal{D} + m] e^{-S_{\text{Gauge}}} , \quad (2.42)$$

where $\mathcal{T}_O(U)$ is a functional depending only on the fields U . The direct approach of lattice QCD is to generate configurations of $SU(3)$ matrices U with a probability $P(U) \propto e^{-S_{\text{Gauge}}} \det[\mathcal{D} + m]$ and to calculate the average of $\mathcal{T}_O(U)$ on a finite sample of configurations. This can indeed be done using a Hybrid Monte Carlo algorithm [98] but, since the determinant is a highly non-local object, it is numerically very slow. The vast majority of simulations therefore set the determinant to a constant value : $\det[\mathcal{D} + m] = 1$. The result is the “quenched” or “valence” approximation. It is *a priori* not possible to determine the effect of quenching on the theory since it does not constitute a systematic approach : different quantities will be affected differently. Most importantly one hopes that the main features of full QCD, confinement and asymptotic freedom, remain intact in the quenched theory.

The effect of the determinant in the Feynman path integral is to generate quark loops. In the quenched approximation the gauge coupling therefore runs differently

to that of the full theory. Lattice calculations adjust the quenched gauge coupling at the scale of the cutoff $\frac{1}{a}$ to agree with a coupling at the scale of physics, say for example at the mass of the ρ particle. One of the drawbacks of this procedure, called “setting the scale”, is that different quantities used in this procedure lead to different lattice spacings. In the best case however, one hopes to determine all physics at the chosen scale correctly.

Quenched QCD calculations have proven to be rather successful over the last few years. The light quark spectrum, with quark masses below and at the mass of the strange quark, is in excellent agreement with experiment (see e.g. ref. [99]). Light hadron decay constants and semi-leptonic decays of light mesons have been determined to high accuracy in the quenched theory (see e.g. ref. [100, 101, 102]). In the heavy quark sector the picture is not so clear since it is difficult to disentangle lattice discretisation errors from errors due to quenching.

Finite Volume Effects and Chiral Extrapolation

It is not possible to calculate the quark propagators at the physical values of the masses of the u - and d -quarks. In this limit the system of linear equations for the quark propagators becomes more and more singular. The physical reason for this effect can be seen as follows : the size of the light particles is given approximately by $\frac{1}{\Lambda_{\text{QCD}}} \approx 0.8 fm$ whereas the volume of conventional lattices is around $(1.8 fm)^3$. However, due to the periodic boundary conditions there will be many copies of the hadron and the volume would have to be very large for them not to interact with each other. Since the range of such interactions is of order $\mathcal{O}(\frac{1}{m_\pi})$ one works with unphysically high masses of the light quarks to avoid these interactions. Correlators are therefore calculated at several values of the hopping parameter κ_{light} and extrapolated in κ_{light} according to chiral symmetry to the physical quark masses. It is standard to use only the lowest order chiral perturbation theory result in this procedure and therefore a systematic error is introduced which is however expected to be small.

2.3.2 Statistical Errors

With the chosen discretised action it is possible to evaluate the functional integral using Monte Carlo techniques. Expectation values are calculated on a finite sample

N of gauge configurations :

$$\int \mathcal{D}U f(U) \exp[-S(U)] \approx \frac{1}{N} \sum_{j=1}^N f(U_j). \quad (2.43)$$

The generation of gauge configurations with weight, or probability, $p(U)$, such that

$$p(U) = \exp[-S(U)], \quad (2.44)$$

is described in ref. [103]. Just as in experiments, one has to deal with a statistical error which falls off only as $\frac{1}{\sqrt{N}}$. A large set of gauge configurations however is computationally very expensive. To save computer time, propagators at different values of the hopping parameter κ are calculated on the same set of gauge configurations. Clearly then, different physical quantities will be highly correlated. This is also true of data for the same quantity but on different timeslices. I shall therefore briefly describe how the correlation of the data is taken into account in the fitting of data.

Fitting Correlated Data

The covariance matrix is estimated from the data by

$$\sigma(t_i, t_j) = \frac{1}{N(N-1)} \sum_{k=1}^N (x_k(t_i) - \bar{x}(t_i))(x_k(t_j) - \bar{x}(t_j)), \quad (2.45)$$

where $x_k(t)$ are values of some lattice quantity calculated on a sample of $k = 1 \dots N$ configurations and on timeslice $t_i, i = 1 \dots N_t$. The quantity $\bar{x}(t_i)$ is the configuration average of $x_k(t_i)$. It is often more convenient to work with the correlation matrix,

$$\rho(t_i, t_j) = \frac{\sigma(t_i, t_j)}{\sqrt{\sigma(t_i, t_i)}\sqrt{\sigma(t_j, t_j)}}, \quad (2.46)$$

because the elements of this matrix are normalised in such a way that $\rho(t_i, t_i) = 1$ and $\rho(t_i, t_j) \in [-1, 1]$ so that it is easy to read off how strongly correlated the data on different timeslices is.

In this discussion I am ignoring correlations of the data at different values of the hopping parameter κ . Including these, would make the dimension of the covariance matrix bigger than the number of data values so that the covariance

matrix becomes singular. These correlations can therefore only be included when more configurations become available³. The covariance matrix may also become singular when the fitted data is very highly correlated even if enough data is available [123]. In these cases it is necessary to reduce the covariance matrix or to perform uncorrelated fits.

To fit a model function $f(t; \alpha_r)$ with r parameters to the data, the parameters are varied in order to minimise the χ^2 -function

$$\chi^2(\alpha_r) = \sum_{t_i, t_j} [f(t_i; \alpha_r) - \bar{x}(t_i)] \sigma^{-1}(t_i, t_j) [f(t_j; \alpha_r) - \bar{x}(t_j)], \quad (2.47)$$

where the sum is over all timeslices q the fit is performed on. The goodness of fit is estimated by the ratio $\frac{\chi^2_{\min}}{\text{dof}}$ where dof denotes the number of degrees of freedom, $\text{dof} = q - r$. As a rule of thumb, $\frac{\chi^2_{\min}}{\text{dof}} \sim 1$ indicates a good fit [124].

Bootstrap Resampling

The error of the parameters α_r are estimated according to a bootstrap resampling method [125]. Assume the complete simulation had been performed many times over with different sets of N configurations. Performing a χ^2 -minimisation procedure on each of these hypothetical simulations would yield a distribution for each parameter α_r which could be used to estimate the error in selecting the one particular configuration.

Obviously, it is not possible to generate these additional configurations. However, to mimic this setup one can proceed as follows. The N configurations are resampled randomly, allowing for repetitions, to generate a large number, typically 250, of new simulated ensembles. These ensembles are now used to calculate the distribution of parameters α_r . The quoted error corresponds to the 68% confidence limit of the bootstrap distribution.

³This simulation is performed with $N = 60$.

Chapter 3

Lattice Correlation Functions

In this chapter the lattice techniques for extracting operator matrix elements from numerical simulations are presented.

3.1 Interpolating Fields, Two-point Functions and Smearing

Given a particle, correlation functions are constructed from time-ordered products of field operators χ_h which represent the particle. Thus, to calculate a two-point function defined as

$$c(\vec{x}, t) = \langle 0 | T[\chi_h(x) \chi_h^\dagger(0)] | 0 \rangle, \quad (3.1)$$

it is necessary to find an interpolating field χ_h which maximises the overlap with the physical particle of interest. In principle, any operator such that

$$\langle 0 | \chi_h(0) | h \rangle \neq 0, \quad (3.2)$$

may be used but it is clear that one wishes to construct the interpolating field in such a way that the coupling to radial excitations is small. Here $|h\rangle$ denotes a single particle state for the hadron h .

The simplest choice of interpolating field for pseudoscalar and vector particles is

$$\chi_h = \bar{Q}_b(x) \Gamma Q_a(x), \quad (3.3)$$

where $\Gamma = \gamma_5$ for the pseudoscalar and $\Gamma = \gamma_i$ for the vector particle. These Γ reproduce the quantum numbers $J^{\text{PC}} = 0^{-+}$ and 1^{--} for the pseudoscalar and vector particle respectively. The fields $Q_a(x)$ and $\bar{Q}_b(x)$ are quark field operators of flavour a and b . They are chosen to be at the same space-time point so that no gauge fields need be inserted in order to maintain gauge invariance. Since for

pseudoscalar particles like the B and D mesons, and for vector particles like the D^* , the quark and anti-quark have relative orbital momentum 0, this choice seems reasonable.

However, to enhance the overlap with the ground-state wave-function it is better to use spatially-extended interpolating fields. This is the technique known as *Smearing*. The original proposals [104, 105] for “smeared” interpolating fields were for non-gauge-covariant smearing functions which had to be calculated in a fixed gauge. This problem can be avoided by the use of gauge-covariant sources as suggested in ref. [106, 107]. In this study gauge-invariant Jacobi smearing on the heavy-quark field is used (described in detail in ref. [108]), in which the smeared field, $Q^S(\mathbf{x}, t)$, is defined by

$$Q^S(\mathbf{x}, t) \equiv \sum_{\mathbf{x}'} K(\mathbf{x}, \mathbf{x}') Q(\mathbf{x}', t), \quad (3.4)$$

where the kernel is a scalar function

$$K(\mathbf{x}, \mathbf{x}') = \sum_{n=0}^N \kappa_S^n \Delta^n(\mathbf{x}, \mathbf{x}') \quad (3.5)$$

and

$$\Delta(\mathbf{x}, \mathbf{x}') = \sum_{\mu=1}^3 \{ \delta_{\mathbf{x}', \mathbf{x} - \hat{\mu}} U_{\mu}^{\dagger}(\mathbf{x} - \hat{\mu}, t) + \delta_{\mathbf{x}', \mathbf{x} + \hat{\mu}} U_{\mu}(\mathbf{x}, t) \}. \quad (3.6)$$

Wuppertal smearing [106], which uses the operator $(1 - \kappa_S \Delta)^{-1}$ as the kernel of the smearing, corresponds to $N = \infty$, provided that κ_S is sufficiently small to guarantee convergence. Following the discussion in ref. [108], κ_S is set to 0.25, and the parameter N is used to control the smearing radius, defined by

$$r^2 \equiv \frac{\sum_{\mathbf{x}} |\mathbf{x}|^2 |K(\mathbf{x}, 0)|^2}{\sum_{\mathbf{x}} |K(\mathbf{x}, 0)|^2}. \quad (3.7)$$

The value of N is taken to be $N = 75$ yielding a radius $r = 5.2$.

In terms of the operator Q^S of eq. (3.4), the spatially-extended sources χ used in the calculation of two- and three-point functions are given by

$$\chi(x) = \bar{q}(x) \left(1 + \frac{1}{2} \gamma \cdot \overleftarrow{D} \right) \Gamma \left(1 - \frac{1}{2} \gamma \cdot \overrightarrow{D} \right) Q^S(x), \quad (3.8)$$

where Γ is the appropriate matrix to create a pseudoscalar, vector or axial current and $\bar{q}(x)$ denotes a light anti-quark field.

The use of smearing functions does not significantly complicate the computation of propagators. The quark propagator $H(x, y; U)$ is the basic quantity from which all correlators can be built. It is defined as the Greens' function satisfying the lattice Dirac equation

$$\sum_x (\not{D} + m)(z, x) H(x, y; U) = \delta_{zy}. \quad (3.9)$$

The calculation of n -point functions is described in the next section.

With the fermionic action defined in eq. (2.26), $S_{\text{Fermion}}^{\text{SW}} = \sum \bar{q}(x) H^{-1}(x, y) q(y)$, where the sum is over spin, colour and spatial components, the quark-antiquark correlator in the quenched approximation is

$$\langle \bar{q}(x) q(0) \rangle = \int \mathcal{D}U H(x, 0) e^{-S_{\text{Gauge}}}. \quad (3.10)$$

The inversion of the fermion matrix $H^{-1}(0, x)$ is the numerically most intensive part in calculating Greens Functions. $H^{-1}(0, x)$ is a sparse site \times spin \times colour matrix which needs to be inverted to obtain the quark propagator from the origin to every other point. A study of algorithms to solve the equation

$$H^{-1}(x, y) \phi(y) = J(x), \quad (3.11)$$

for a vector $\phi(y)$, given the source $J(x)$, can be found in ref. [109].

3.2 Two-Point and Three-Point Functions

The correlators are calculated from the functional integral by differentiating the generating functional and performing the Wick contractions of the quark fields to obtain the contributing diagrams. The n -point function is then related formally to the matrix element of physical interest which I shall do explicitly below for the three-point function.



3.2.1 Two-Point Functions

Wick contracting the two-point function defined in eq. (3.1) and “time-slicing” the correlator to project out momenta, one obtains :

$$\begin{aligned} C_{2pt}(\vec{p}, t; U) &= \left\langle \sum_{\vec{x}} e^{i\vec{p}\cdot\vec{x}} c(\vec{x}, t) \right\rangle \\ &= \left\langle \sum_{\vec{x}} e^{i\vec{p}\cdot\vec{x}} \text{Tr} \left[(\Gamma_x)_{\alpha\beta} (\Gamma_0)_{\gamma\delta} H_{\beta\gamma}^{a\ ij}(0, x) H_{\alpha\delta}^{b\ ji}(x, 0) \right] \right\rangle, \end{aligned} \quad (3.12)$$

where i and j are colour; β, γ and δ are spin indices and a and b denote the quark-propagators for quarks of flavour a and b . The brackets $\langle \rangle$ indicate the average over gauge configurations.

The hermiticity relation

$$\gamma_5 H(0, x)^\dagger \gamma_5 = H(x, 0) \quad (3.13)$$

can be used to show that it is only necessary to compute the propagators from the origin to all points in space.

3.2.2 Three-Point Functions

To compute the matrix elements of semi-leptonic decays, the three-point function

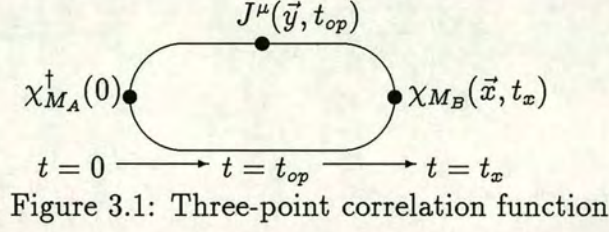
$$C_{PS \rightarrow PS, V}^{3pt\ \mu}(t_x, t_{op}; \vec{p}_B, \vec{q}; U) = \left\langle \sum_{\vec{x}, \vec{y}} e^{i(\vec{p}_B \cdot \vec{x} + \vec{q} \cdot \vec{y})} \langle 0 | \chi_{M_B}(\vec{x}, t_x) J^\mu(\vec{y}, t_{op}) \chi_{M_A}^\dagger(0) | 0 \rangle \right\rangle, \quad (3.14)$$

where $t_x > t_{op} > 0$, is calculated in Euclidean space. The interpolating fields $\chi_{M_A}^\dagger$ and χ_{M_B} create and annihilate hadrons at times 0 and t_x . To project out momenta the operators are weighted with phase factors and summed over the spatial lattice. The particles’ energies are given by :

$$E_B = \sqrt{m_B^2 + |\vec{p}_B|^2}, \quad (3.15)$$

$$E_A = \sqrt{m_A^2 + |\vec{p}_B + \vec{q}|^2}. \quad (3.16)$$

To extract the matrix elements for the semi-leptonic decays $\bar{B} \rightarrow D l \bar{\nu}$ and $\bar{B} \rightarrow D^* l \bar{\nu}$ it is sufficient to consider the case where the particle at the sink, (\vec{x}, t_x) , M_B , is a pseudoscalar. The particle at the source, $t = 0$, M_A , can either be a



pseudoscalar or a vector particle. The current is either vector or axial :

$$J^\mu = \bar{c} \Gamma_J b = \begin{cases} \bar{c} \gamma_\mu b \\ \bar{c} \gamma_\mu \gamma_5 b \end{cases}, \quad (3.17)$$

where I have denoted the quark fields of the b and c quarks in an obvious way.

Performing the Wick contractions one finds

$$C_{PS \rightarrow PS,V}^{3pt\mu}(t_x, t_{op}; \vec{p}_B, \vec{q}; U) = - \sum_{\vec{x}, \vec{y}} e^{i\vec{p}_B \cdot \vec{x}} e^{i\vec{q} \cdot \vec{y}} \text{Tr} \{ H'(y, x) \gamma_5 L(x, 0) \Gamma_{M_A} H(0, y) \Gamma_J \}. \quad (3.18)$$

The propagators of the heavy quarks are given by $H(0, y)$ and $H'(y, x)$ whereas the light quark's propagator is denoted by $L(x, 0)$. I shall drop the explicit average over gauge configurations in the following.

The calculation of the three-point function does not, as it would first seem, require knowledge of the propagator $L(x, 0)$ from the origin to every point x of the lattice. Rather, it is sufficient to calculate the “extended” propagator from 0 to y passing through the timeslice t_x . The extended propagator is defined as [110]:

$$S(0, y; t_x, \vec{p}) = \sum_{\vec{x}} H'(y, x) \gamma_5 L(x, 0) e^{i\vec{p}_B \cdot \vec{x}}. \quad (3.19)$$

Acting on this object with the lattice Dirac operator one finds :

$$\begin{aligned} (\not{D}_y + m) S(0, y; t_x, \vec{p}_B) &= \sum_{\vec{x}} \delta^3(\vec{x} - \vec{y}) \delta(t_x - t_{op}) \gamma_5 L(x, 0) e^{i\vec{p}_B \cdot \vec{x}} \\ &= \gamma_5 L(y, 0) \delta(t_x - t_{op}) e^{i\vec{p}_B \cdot \vec{y}}. \end{aligned} \quad (3.20)$$

One finds that the inversion for the extended propagator requires the light propagator only on a single timeslice. Note also that by solving eq. (3.20) with a pseudoscalar particle at the extension point (\vec{x}, t_x) one can calculate both matrix

elements $\bar{B} \rightarrow D l \bar{\nu}$ and $\bar{B} \rightarrow D^* l \bar{\nu}$ with the same extended propagator. The momentum of the initial particle M_B needs to be fixed for the calculation of $S(0, y; t_x, \vec{p}_B)$ whereas the momentum inserted at the current can be varied when the traces are performed. Thus, in the simulation presented below, the form factors are calculated for a large set of momenta of the final particle but only for two momenta of the initial particle, the \bar{B} -meson, $\vec{p}_B = ((0, 0, 0), (\frac{2\pi}{L}, 0, 0))$.

To examine the behaviour of the three-point function at large times t_{op} and $(t_x - t_{op})$, the lattice completeness relation

$$1 = \frac{1}{L^3} \sum_{\vec{k}} \sum_A \sum_r \frac{1}{2E_A(\vec{k})} |A_r(\vec{k})\rangle \langle A_r(\vec{k})| \quad (3.21)$$

is used to insert two complete sets of states in eq. (3.14). Here r denotes the polarization of the particle A .

Using translational invariance in Euclidean space,

$$O(\vec{x}, t) = e^{\hat{H}t + i\vec{p}\cdot\vec{x}} O(0) e^{-\hat{H}t - i\vec{p}\cdot\vec{x}}, \quad (3.22)$$

and the lattice relation

$$\sum_{\vec{x}} e^{\frac{2\pi i}{L} \vec{x}(\vec{k} - \vec{k}')} = L^3 \delta_{\vec{k}, \vec{k}'}, \quad (3.23)$$

this yields :

$$\begin{aligned} C_{PS \rightarrow PS, V}^{3pt \mu}(t_x, t_{op}; \vec{p}_B, \vec{q}) &= \sum_{A, B} \sum_r \frac{\langle A_r(\vec{p}_A) | \chi_{M_A}^\dagger(0) | 0 \rangle \langle 0 | \chi_{M_B}(0) | B(\vec{p}_B) \rangle}{2E_A(\vec{p}_A) 2E_B(\vec{p}_B)} \times \\ &\times e^{-E_A(\vec{p}_A)t_{op}} e^{-E_B(\vec{p}_B)(t_x - t_{op})} \langle B(\vec{p}_B) | J^\mu(0) | A(\vec{p}_A) \rangle \end{aligned} \quad (3.24)$$

Similar manipulations for the two-point functions of the vector and pseudoscalar particles give the following results :

$$C_V^{2pt \rho} = \sum_r \frac{e^{-E_V t}}{2E_V} Z_V^2(|\vec{p}_V|^2) |\epsilon_\rho^\tau|^2, \quad (3.25)$$

$$C_{PS}^{2pt} = \frac{e^{-E_{PS} t}}{2E_{PS}} Z_{PS}^2(|\vec{p}_{PS}|^2). \quad (3.26)$$

The matrix element of a pseudoscalar is denoted by:

$$Z_{PS}(|\vec{p}|^2) = \langle 0 | \chi_{PS}(0) | P(\vec{p}) \rangle , \quad (3.27)$$

and that of a vector particle by

$$Z_V(|\vec{p}|^2) \epsilon_r^\rho = \langle V_r(\vec{p}) | \chi_V^{\rho\dagger}(0) | 0 \rangle , \quad (3.28)$$

where r is the polarisation index of the vector particle and $|P(\vec{p})\rangle$ and $|V_r(\vec{p})\rangle$ are the single particle states normalized to $\langle P(\vec{p}) | P(\vec{p}) \rangle = L^3 2E_P(\vec{p}) \delta_{\vec{p}\vec{p}'}$. The wave-function factors $Z_{PS}(|\vec{p}|^2)$ and $Z_V(|\vec{p}|^2)$ depend on the meson's momenta since spatially-extended interpolating operators are used.

Taking t_{op} and $(t_x - t_{op})$ to be sufficiently large, only the contribution from the ground state survives :

$$\begin{aligned} C_{PS \rightarrow PS, V}^{\mu\nu}(t_x, t_{op}; \vec{p}_B, \vec{q}) &= \frac{Z_A Z_B}{4E_A(\vec{p}_A)E_B(\vec{p}_B)} e^{-E_A(\vec{p}_A)t_{op}} e^{-E_B(\vec{p}_B)(t_x - t_{op})} \\ &\times \sum_r \epsilon_r^\nu \langle B(\vec{p}_B) | J^\mu(0) | A(\vec{p}_A) \rangle . \end{aligned} \quad (3.29)$$

For pseudoscalar \rightarrow pseudoscalar transitions this simplifies to

$$C_{PS \rightarrow PS}^\mu(t_x, t_{op}; \vec{p}_B, \vec{q}) = \frac{Z_A Z_B}{4E_A E_B} e^{-E_A t_{op}} e^{-E_B(t_x - t_{op})} \langle B(\vec{p}_B) | J^\mu(0) | A(\vec{p}_A) \rangle . \quad (3.30)$$

Thus, once the wave-function factors $Z_A(|\vec{p}_A|)$ and $Z_B(|\vec{p}_B|)$ as well as the energies $E_A(|\vec{p}_A|)$ and $E_B(|\vec{p}_B|)$ have been determined from computations of the two-point correlation functions of the pseudoscalar and vector particles, the matrix element $\langle B(\vec{p}_B) | J^\mu(0) | A(\vec{p}_A) \rangle$ can be computed. This technique can be applied to calculations of the electro-magnetic pion form-factor[111], semi-leptonic decays of light[112, 113, 114, 115, 116, 117] and heavy[120, 121] mesons and rare decays such as $B \rightarrow K^* \gamma$ [118, 119]. Reviews of these calculations can be found in ref. [122].

In this thesis the first results are presented for the calculations of matrix elements of semi-leptonic decays of mesons containing one heavy and one light quark¹. In this case the operator $J^\mu(0)$ is either the vector current $V^\mu(0)$ or the axial current

¹The results of ref. [120, 121] have all been obtained for the case of elastic scattering only.

$A^\mu(0)$.

3.3 Discrete symmetries

The quark propagators are calculated on a finite sample of gauge configurations U . Since the gauge action is invariant under the transformations of parity P , charge conjugation C and time reversal T and the combination CP , the set of all possible configurations contains the symmetry-transformed gauge configurations, too. Rather than computing the observables in the symmetry-transformed gauge configurations, clearly a costly operation, one can make use of the symmetries of the quark propagator to find the value of the observable under consideration in the symmetry-transformed configuration at no additional cost.

3.3.1 Discrete symmetries of the quark propagator

The quark propagators for the Clover action can be shown to satisfy the following relations :

- Hermiticity

$$H(x, y; U) = \gamma_5 H^\dagger(y, x; U) \gamma_5 \quad (3.31)$$

- Parity

$$H(x, y; U) = \gamma_4 H(x^P, y^P; U^P) \gamma_4 \quad (3.32)$$

- Charge Conjugation

$$H(x, y; U) = C H^T(y, x; U^C) C^{-1} \quad (3.33)$$

where $C = \gamma_4 \gamma_2$.

- Time reversal

$$H(x, y; U) = T H(x^T, y^T; U^T) T^{-1} \quad (3.34)$$

where $T = \gamma_4 \gamma_5$.

These symmetries can be used to calculate the three-point function in the set of gauge configurations U, U^P, U^C and U^{CP} and to perform the configuration average over the additional configurations. Applying these symmetries to the two- and

three-point functions can also be used to determine whether the correlators are purely real or imaginary.

3.3.2 Symmetries of the three-point correlator

Parity

Calculating the correlator in the parity-reversed gauge configuration

$$C^{3pt}(t_x, t_y; \vec{p}, \vec{q}; U^P) = - \sum_{\vec{x}, \vec{y}} e^{i\vec{p} \cdot \vec{x}} e^{i\vec{q} \cdot \vec{y}} \text{Tr} \{ \gamma_4 H'(y, x) \gamma_4 \gamma_5 \gamma_4 L(x, 0) \gamma_4 \Gamma_{M_A} \gamma_4 H(0, y) \gamma_4 \Gamma_J \} \quad (3.35)$$

yields the following phases η :

M_A	$J = \gamma_4$	$J = \gamma_j$	Current
γ_5	$\eta = +1$	$\eta = -1$	vector
γ_4	$\eta = -1$	$\eta = +1$	vector
γ_j	$\eta = +1$	$\eta = -1$	vector
γ_4	$\eta = +1$	$\eta = -1$	axial
γ_j	$\eta = -1$	$\eta = +1$	axial

and

$$C^{3pt}(t_x, t_y; \vec{p}, \vec{q}; U^P) = \eta \ C^{3pt}(t_x, t_y; -\vec{p}, -\vec{q}; U) \quad (3.36)$$

Charge Conjugation

A similar analysis for the correlator in the charge-conjugated configuration yields:

$$C^{3pt}(t_x, t_y; \vec{p}, \vec{q}; U^C) = - \sum_{\vec{x}, \vec{y}} e^{i\vec{p} \cdot \vec{x}} e^{i\vec{q} \cdot \vec{y}} \text{Tr} \{ C H'^T(x, y) C^{-1} \gamma_5 C L^T(0, x) C^{-1} \Gamma_M C H^T(y, 0) C^{-1} \Gamma_J \} \quad (3.37)$$

Hermiticity of the quark propagator can be applied to show that

$$C^{3pt}(t_x, t_y; \vec{p}, \vec{q}; U^C) = C^{3pt}(t_x, t_y; -\vec{p}, -\vec{q}; U)^* \quad (3.38)$$

where $*$ denotes the complex conjugate. This identity holds for any combination of indices at the operator and at the source.

CP invariance

Combining C and P invariance allows one to determine whether the three-point-functions are real or imaginary. I denote a pseudoscalar by P , a vector particle by V_4 or V_j depending on what component is used and similarly for the current operator which is either the vector current V or the axial current A . The analysis yields :

- For (particle M_A , operator J) = $(P, V_4), (V_4, V_j), (V_j, V_4), (V_4, A_4), (V_j, A_j)$

$$C^{3pt}(\vec{p}, \vec{q}; U^{CP}) = C^{3pt}(\vec{p}, \vec{q}; U)^* \quad (3.39)$$

and the three-point function is purely real.

- For (particle M_A , operator J) = $(P, V_4), (V_4, V_j), (V_j, V_4), (V_4, A_4), (V_j, A_j)$

$$C^{3pt}(\vec{p}, \vec{q}; U^{CP}) = -C^{3pt}(\vec{p}, \vec{q}; U)^* \quad (3.40)$$

and the three-point function is purely imaginary.

 U, U^P, U^C, U^{CP}

Averaging over this set of configurations is therefore equivalent to making the following replacements :

- For (particle M_A , operator J) = $(P, V_4), (V_4, V_j), (V_j, V_4), (V_4, A_4), (V_j, A_j)$

$$\begin{aligned} & C^{3pt}(\vec{p}, \vec{q}; U) \\ & \rightarrow \frac{1}{4} \{ C^{3pt}(\vec{p}, \vec{q}; U) - C^{3pt}(-\vec{p}, -\vec{q}; U) \\ & \quad + C^{3pt}(-\vec{p}, -\vec{q}; U)^* - C^{3pt}(\vec{p}, \vec{q}; U)^* \} \\ & = \frac{1}{2} i \text{Im} \{ C^{3pt}(\vec{p}, \vec{q}; U) - C^{3pt}(-\vec{p}, -\vec{q}; U) \} \end{aligned} \quad (3.41)$$

- For (particle M_A , operator J) = $(P, V_4), (V_4, V_j), (V_j, V_4), (V_4, A_4), (V_j, A_j)$

$$\begin{aligned} & C^{3pt}(\vec{p}, \vec{q}; U) \\ & \rightarrow \frac{1}{4} \{ C^{3pt}(\vec{p}, \vec{q}; U) + C^{3pt}(-\vec{p}, -\vec{q}; U) \\ & \quad + C^{3pt}(-\vec{p}, -\vec{q}; U)^* + C^{3pt}(\vec{p}, \vec{q}; U)^* \} \end{aligned}$$

$$= \frac{1}{2} \text{Re}\{C^{3pt}(\vec{p}, \vec{q}; U) + C^{3pt}(-\vec{p}, -\vec{q}; U)\} \quad (3.42)$$

Time Reversal

Time reversal can be used very effectively by choosing the extension point $t_x = 24$ since the correlators can then be averaged over the values for t and $48 - t$. This procedure is sometimes referred to as “folding”.

A similar analysis can be carried out for the two-point correlators and the averaging procedure was also implemented in the calculation presented here.

Overview of Calculation

The calculation of three point functions is computationally very expensive. To save computer time, the same set of heavy and light propagators is used to calculate as many different correlators as possible. Thus, the UKQCD collaboration has calculated the hadronic matrix elements for the decays $\bar{B} \rightarrow D l \bar{\nu}$, $\bar{B} \rightarrow D^* l \bar{\nu}$ and $B \rightarrow K^* \gamma$ in one numerical simulation. This amounts to a total number of 60 operators : the first 36 are for heavy to heavy pseudoscalar Isgur-Wise data, and the remaining 24 for the $B \rightarrow K^* \gamma$ decay. This set of operators is shown in table 3.1, using the notation (Γ_1, Γ_2) to represent a decay from a pseudoscalar particle to a particle with an interpolating operator Γ_1 , via a current Γ_2 . Note that these are Euclidean matrices, so that 4 corresponds to the temporal index.

The momentum injected in the pseudoscalar was fixed to two values, $\vec{p}_B = (0, 0, 0)$ and $\vec{p}_B = (1, 0, 0)$, when generating the extended propagators. A larger number of incoming momenta needed to be injected at the operator in order to cover a large range of velocity or momentum transfer, q^2 , and all values of $|\vec{q}| < 2$ were used. Denoting the incoming vector momentum by \vec{p}_{D,D^*} the outgoing pseudoscalar momentum by \vec{p}_B (see figure 3.2), the momentum transfer is given by

$$\vec{q} = \vec{p}_{D,D^*} - \vec{p}_B, \quad (3.43)$$

The complete sets of momenta are shown in tables 3.2 and 3.3. For $\vec{p}_B = 0$, $\vec{q} = \vec{p}_{D,D^*}$ and all possible momenta combinations of $|\vec{p}_{D,D^*}| < 2$ were used. For $\vec{p}_B = (1, 0, 0)$, the situation is more complicated. As the data was calculated in

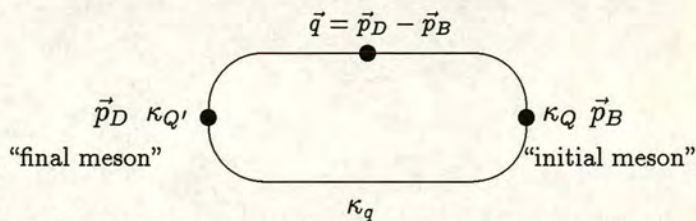


Figure 3.2: Lattice momenta – notational conventions.

#	(Γ_1, Γ_2)	#	(Γ_1, Γ_2)
1	γ_5, γ_1	31	$\gamma_3, \gamma_3\gamma_5$
2	γ_5, γ_2	32	$\gamma_3, \gamma_4\gamma_5$
3	γ_5, γ_3	33	$\gamma_4, \gamma_1\gamma_5$
4	γ_5, γ_4	34	$\gamma_4, \gamma_2\gamma_5$
5	γ_1, γ_1	35	$\gamma_4, \gamma_3\gamma_5$
6	γ_1, γ_2	36	$\gamma_4, \gamma_4\gamma_5$
7	γ_1, γ_3	37	γ_1, σ_{34}
8	γ_1, γ_4	38	γ_1, σ_{24}
9	γ_2, γ_1	39	γ_1, σ_{23}
10	γ_2, γ_2	40	γ_1, σ_{14}
11	γ_2, γ_3	41	γ_1, σ_{13}
12	γ_2, γ_4	42	γ_1, σ_{12}
13	γ_3, γ_1	43	γ_2, σ_{34}
14	γ_3, γ_2	44	γ_2, σ_{24}
15	γ_3, γ_3	45	γ_2, σ_{23}
16	γ_3, γ_4	46	γ_2, σ_{14}
17	γ_4, γ_1	47	γ_2, σ_{13}
18	γ_4, γ_2	48	γ_2, σ_{12}
19	γ_4, γ_3	49	γ_3, σ_{34}
20	γ_4, γ_4	50	γ_3, σ_{24}
21	$\gamma_1, \gamma_1\gamma_5$	51	γ_3, σ_{23}
22	$\gamma_1, \gamma_2\gamma_5$	52	γ_3, σ_{14}
23	$\gamma_1, \gamma_3\gamma_5$	53	γ_3, σ_{13}
24	$\gamma_1, \gamma_4\gamma_5$	54	γ_3, σ_{12}
25	$\gamma_2, \gamma_1\gamma_5$	55	γ_4, σ_{34}
26	$\gamma_2, \gamma_2\gamma_5$	56	γ_4, σ_{24}
27	$\gamma_2, \gamma_3\gamma_5$	57	γ_4, σ_{23}
28	$\gamma_2, \gamma_4\gamma_5$	58	γ_4, σ_{14}
29	$\gamma_4, \gamma_1\gamma_5$	59	γ_4, σ_{13}
30	$\gamma_4, \gamma_2\gamma_5$	60	γ_4, σ_{12}

Table 3.1: The set of 60 operators for which the hadronic matrix elements of pseudoscalar to pseudoscalar and pseudoscalar to vector decays were simulated.

	\vec{p}_{D,D^*}	\vec{q}		\vec{p}_{D,D^*}	\vec{q}
1	(0,0,0)	(0,0,0)	10	(0,1,-1)	(0,1,-1)
2	(1,0,0)	(1,0,0)	11	(1,1,1)	(1,1,1)
3	(0,1,0)	(0,1,0)	12	(-1,1,1)	(-1,1,1)
4	(0,0,1)	(0,0,1)	13	(1,-1,1)	(1,-1,1)
5	(1,1,0)	(1,1,0)	14	(1,1,-1)	(1,1,-1)
6	(1,0,1)	(1,0,1)	15	(2,0,0)	(2,0,0)
7	(0,1,1)	(0,1,1)	16	(0,2,0)	(0,2,0)
8	(1,-1,0)	(1,-1,0)	17	(0,0,2)	(0,0,2)
9	(1,0,-1)	(1,0,-1)			

Table 3.2: Momenta \vec{p}_{D,D^*} for $\vec{p}_B = (0, 0, 0)$.

	\vec{p}_{D,D^*}	\vec{q}		\vec{p}_{D,D^*}	\vec{q}
1	(0,0,0)	(-1,0,0)	11	(1,0,-1)	(0,0,-1)
2	(1,0,0)	(0,0,0)	12	(0,1,1)	(-1,1,1)
3	(-1,0,0)	(-2,0,0)	13	(0,1,-1)	(-1,1,-1)
4	(0,1,0)	(-1,1,0)	14	(0,-1,1)	(-1,-1,1)
5	(0,-1,0)	(-1,-1,0)	15	(0,-1,-1)	(-1,-1,-1)
6	(0,0,1)	(-1,0,1)	16	(1,1,1)	(0,1,1)
7	(0,0,-1)	(-1,0,-1)	17	(1,-1,1)	(0,-1,1)
8	(1,1,0)	(0,1,0)	18	(1,1,-1)	(0,1,-1)
9	(1,0,1)	(0,0,1)	19	(1,-1,-1)	(0,-1,-1)
10	(1,-1,0)	(0,-1,0)	20	(2,0,0)	(1,0,0)

Table 3.3: Momenta \vec{p}_{D,D^*} for $\vec{p}_B = (1, 0, 0)$.

terms of \vec{q} up to 2, there is a less complete set of \vec{p}_{D,D^*} .

Chapter 4

Results : Pseudoscalar \rightarrow Pseudoscalar

In this chapter I present numerical results of the lattice data for the form factors of the decay $\bar{B} \rightarrow Dl\bar{\nu}$.

To start, a precise determination of the vector current renormalisation constant Z_V is performed allowing for an estimate of $\mathcal{O}(am_Q)$ effects in heavy quark currents on the lattice. In section 4.4 fitting procedures are explored to establish how best to determine the form factors; this is closely related to the discussion of how to normalise the data properly to obtain continuum matrix elements. Section 4.5 contains the results for the form factors $h_+(\omega)$ and $h_-(\omega)$ obtained from the simulation at $\beta = 6.2$. Fits to obtain ρ^2 , the slope of the Isgur-Wise function at $\omega = 1$ are performed using some of the ansätze introduced in section 1.3.2. An attempt is made in section 4.6 to quantify $\frac{1}{m_Q}$ corrections. Section 4.7 analyses the form factors' dependence on the mass of the light spectator quark.

4.1 Introduction

The hadronic matrix element $\langle V|J^\mu|P\rangle$ for the decay $\bar{B} \rightarrow Dl\bar{\nu}$ can be obtained from the lattice correlator $\langle 0|\chi_D(x)V_I^\mu(\vec{y}, t_{\text{op}})\chi_B^\dagger(0)|0\rangle$, where χ_D and χ_B^\dagger are interpolating fields for the P mesons consisting of a light anti-quark and a heavy quark. The improved current V_I has been defined in eq. (2.30). This correlator is calculated numerically in Euclidean space using the functional integral

$$\langle 0|\chi_D(x)V_I^\mu(\vec{y}, t_{\text{op}})\chi_B^\dagger(0)|0\rangle = \frac{1}{Z} \int \mathcal{D}U \text{Tr}[H'(y, x)\gamma_5 L(x, 0)\Gamma_D H(0, y)\Gamma^\mu] e^{-S[U]}, \quad (4.1)$$

where $H'(y, x)$, $L(x, 0)$ and $H(0, y)$ are the propagators of the light and heavy quarks. Working in momentum space, the asymptotic form of the three-point

function in Euclidean space is given by

$$\begin{aligned}
 C_{3pt}^\mu(t_x, t_{op}; \vec{p}_B; U) &= \sum_{\vec{x}\vec{y}} e^{i\vec{p}_B\vec{x}} e^{i\vec{q}\vec{y}} \langle 0 | \chi_B(\vec{x}, t_x) V_I^\mu(\vec{y}, t_{op}) \chi_D^\dagger(0) | 0 \rangle \\
 &\longrightarrow \\
 \frac{Z_D(|\vec{p}_D|)}{2E_D(\vec{p}_D)} \frac{Z_B(|\vec{p}_B|)}{2E_B(\vec{p}_B)} e^{-E_D(\vec{p}_D)t_{op}} e^{-E_B(\vec{p}_B)(t_x - t_{op})} &\times \langle D, \vec{p}_D | V_I^\mu | B, \vec{p}_B \rangle,
 \end{aligned} \tag{4.2}$$

where time reversal invariance has been used. Equation 4.2 is correct, provided the three points in the correlator are sufficiently separated in time, $t_{op}, (t_x - t_{op}) \gg 1$ so that the ground-state contribution dominates. $E_D(\vec{p}_D)$ and $E_B(\vec{p}_B)$ are the energies of the D- and B-meson and their wave-function factors have been denoted by $Z_D(|\vec{p}_D|)$ and $Z_B(|\vec{p}_B|)$. They are determined from a fit to the asymptotic form of the two-point functions for large Euclidean times

$$\begin{aligned}
 C_{2pt}(t, \vec{p}) &= \sum_{\vec{x}} e^{i\vec{p}\vec{x}} \langle \chi_P(\vec{x}, t) \chi_P^\dagger(\vec{0}, 0) \rangle \\
 &\rightarrow Z_P^2(|\vec{p}|) \frac{e^{-E_P(\vec{p})\frac{T}{2}}}{E_P(\vec{p})} \cosh\left(E_P(\vec{p})\left[t - \frac{T}{2}\right]\right),
 \end{aligned} \tag{4.3}$$

where T is the time-extent of the lattice and P stands for either the B or the D meson. These meson two-point functions have been calculated for all combinations of heavy-light kappa values tabulated in 4.1 for momenta up to $\frac{\pi}{12}$. The asymptotic form of the correlator is fitted to eq. (4.3) on time-slices $t = 11$ to $t = 22$. Results of these fits are tabulated in Appendix A.

Once the factors associated with the two-point functions are known, the matrix element in eq. (4.2) contains the two unknown form factors $h_+^L(\omega)$ and $h_-^L(\omega)$:

$$\langle D, \vec{p}_D | V_I^\mu | B, \vec{p}_B \rangle = \sqrt{m_B m_D} \left[(v_B + v_D)^\mu h_+^L(\omega) + (v_B - v_D)^\mu h_-^L(\omega) \right] \tag{4.4}$$

They are related to the physical form factors by the multiplicative renormalisation constant Z_V : $h_L^\pm = \frac{h_L^\pm}{Z_V}$; its determination is the subject of section 4.3.

4.2 Lattice Parameters

This simulation was performed using a set of 60 quenched gauge configurations on a $24^3 \times 48$ lattice at a coupling corresponding to $\beta = 6.2$. The configurations were generated as part of the UKQCD project with periodic boundary conditions

60 gauge configurations		
$\kappa_{Q'}$	κ_q	κ_Q
0.133	0.14144	0.129
0.129		
0.125		
0.121		
0.133	0.14144	0.133
0.125		0.125

Table 4.1: Data set at $\beta = 6.2$.

using the Hybrid Over-Relaxed algorithm [126] with the Wilson gauge action introduced in eq. (2.12). The lattice spacing, determined from the string tension, is $a^{-1} = 2.73(5)$ GeV [127]. In physical units this corresponds to a lattice spacing of approximately 0.07 fm and a spacial extent of 1.68 fm. The Over-Relaxed Minimal Residual algorithm with red-black preconditioning was used to calculate the propagators [109] with the $\mathcal{O}(a)$ -improved Sheikholeslami-Wohlert action, introduced in eq. (2.26). This is done with periodic boundary conditions in the spatial and anti-periodic boundary conditions in the temporal direction. Smearing, as outlined in section 3.1, was implemented for the operators creating a meson at the origin. The hopping parameters for the calculation are shown in table 4.1. Each of the final heavy quark hopping-parameters $\kappa_{Q'}$ has been combined with any of the light spectator anti-quarks κ_q ¹ and initial heavy hopping-parameters κ_Q . Since, both for the case of pseudoscalar \rightarrow pseudoscalar and pseudoscalar \rightarrow vector, the lattice particle with hopping parameter κ_Q is always a pseudoscalar, this particle will be called the “initial meson”².

Frequently, the data-set will be split into the “degenerate” and the “non-degenerate” case; the first refers to the set of hopping-parameters for which initial and final meson masses are identical, the elastic scattering; the latter comprises all other hopping-parameter combinations. Note that for the two degenerate decays with hopping parameters 0.125 and 0.133, the form factors have only been calculated at one value of the light quark mass, 0.14144.

¹The light anti-quark will frequently be called “light quark” for simplicity.

²The three-point function is calculated in its time-reversed form to allow for the use of previously calculated light propagators.

\vec{p}_B	(0, 0, 0)		(1, 0, 0)			
\vec{q}	(0,0,0)	(1,0,0)	(-1,0,0)	(0,0,0)	(-2,0,0)	(-1,1,0)
\vec{p}_D	(0,0,0)	(1,0,0)	(0,0,0)	(1,0,0)	(-1,0,0)	(0,1,0)
# mom	1	6	1	1	1	4

Table 4.2: Momenta at $\beta = 6.2$ in lattice units.

Momenta

The complete set of momentum combinations for which the matrix elements have been calculated are shown in tables 3.2 and 3.3. To minimise statistical and systematic errors, correlators with initial or final momenta equal or greater than $|\vec{p}| = \sqrt{2}(\pi/12)$ are not used. Momenta resulting in the same q^2 - and therefore the same velocity transfer ω - are averaged. Table 4.2 shows the momenta used in the analysis of this and the following chapter. All momenta are in lattice units so that $\frac{2\pi}{L} = 1$. The lower row in table 4.2 indicates how many equivalent momenta are averaged over for the temporal components of the lattice current, $\mu = 4$. As can be seen from table 4.2 there are two channels for which the velocity of the meson is unchanged by the electro-weak current. Whereas the combination $(0, 0, 0) \rightarrow (0, 0, 0)$ fulfills the zero-recoil condition, $\omega = v \cdot v' = 1$, regardless of the masses, the channel $(1, 0, 0) \rightarrow (1, 0, 0)$ gives zero recoil only for the degenerate case.

Statistics are enhanced by choosing the time t_x at which the initial meson is destroyed to be half-way across the time-extent of the lattice, $t_x = 24$. The three-point function is symmetrised about this point using Euclidean time reversal. The time position of the current is varied in the interval $t_{op} = 7 - 16$.

4.3 Determination of Z_V

In the continuum the lattice vector current is related to the physical current $V^\mu = \bar{Q}_1 \gamma^\mu Q_2$ by a renormalisation constant Z_V :

$$V^\mu = Z_V V_I^\mu + \mathcal{O}(a\alpha_s) + \mathcal{O}(a^2) , \quad (4.5)$$

where the lattice vector current is the “improved” operator defined in eq. (2.30), $V_I^\mu = \bar{Q}_1 \tilde{\Gamma}^\mu Q_2$, and $\tilde{\Gamma}$ is defined in eq. (2.31) (see section 2.1), with two heavy quarks Q_1 and Q_2 .

$\beta = 6.2$			$\beta = 6.0$		
κ_Q	$m_Q^0 a$	Z_V^{HL}	κ_Q	$m_Q^0 a$	Z_V^{HL}
0.133	0.236	0.8913^{+2}_{-1}	0.129	0.365	0.920^{+1}_{-1}
0.129	0.324	0.9177^{+3}_{-2}	0.125	0.448	0.945^{+1}_{-1}
0.125	0.410	0.9428^{+4}_{-2}	0.120	0.549	0.973^{+2}_{-2}
0.121	0.494	0.9659^{+5}_{-3}			

Table 4.3: The normalisation constant Z_V^{HL} as a function of the mass of the heavy quark. The value of κ_q is 0.14144 at $\beta = 6.2$ and 0.144 at $\beta = 6.0$.

The renormalisation constant Z_V can be determined very precisely by evaluating the ratio

$$Z_V^{HL} = \frac{C_{2pt}(t_x, \vec{p})}{C_{3pt}^{\mu=4}(t_{op}, t_x, \vec{p}, \vec{q} = \mathbf{0})} , \quad (4.6)$$

where $C_{3pt}^{\mu=4}(t_{op}, t_x, \vec{p}, \vec{q} = \mathbf{0})$ is the three-point function of the forward matrix element $\langle P, \vec{p} | V_I^\mu | P, \vec{p} \rangle$. The renormalisation constant for a particular heavy quark current obtained in this way is denoted by Z_V^{HL} . Unless explicitly stated the momentum is taken to be $\vec{p} = \mathbf{0}$.

Formally, discretisation errors for V_I^μ are of $\mathcal{O}(\alpha_s m_Q a)$ and $\mathcal{O}(m_Q^2 a^2)$ (see section 2.1). For light quark currents, where the operators χ and χ^\dagger in eq. (4.2) annihilate and create mesons with two light quarks, the renormalisation constant determined using eq. (4.6) at $\beta = 6.2$ and for a hopping parameter $\kappa_q = 0.14144$ is found to be $Z_V^{\text{light}} = 0.831(1)$ [128]. Using the chiral Ward identities the authors of ref. [129] find $Z_V = 0.815(6)$. These results are in excellent agreement with the value from one-loop perturbation theory [130]

$$Z_V = 1 - 0.10g^2 + \mathcal{O}(g^4) = 0.834 + \mathcal{O}(g^4) , \quad (4.7)$$

evaluated using the coupling constant obtained from the mean field resummation of tadpole diagrams [131] :

$$g^2 = \frac{6}{\beta u_0^4} , u_0 = \left(\frac{1}{8\kappa_{crit}} \right) . \quad (4.8)$$

These results show that for light quarks the discretisation errors are small. The difference between Z_V and Z_V^{HL} will give a measure of the size of discretisation errors for heavy quark currents.

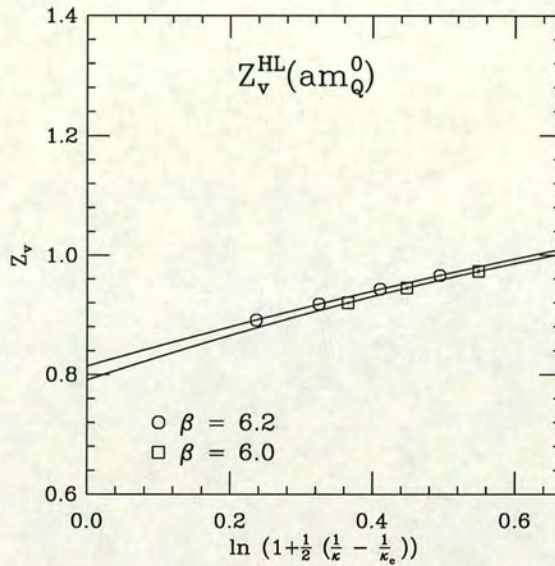


Figure 4.1: The renormalisation constant Z_V^{HL} as a function of $m_Q^0 a$. The solid lines represent fits to quadratic functions of $m_Q^0 a$ for the data at the two different values of β . The errors on the points are smaller than the size of the symbols.

In table (4.3) Z_V^{HL} obtained with $\vec{p} = \mathbf{0}$ is shown as a function of the bare heavy quark mass,

$$m_Q^0 a = \ln\left\{1 + \frac{1}{2}\left(\frac{1}{\kappa} - \frac{1}{\kappa_{\text{crit}}}\right)\right\}. \quad (4.9)$$

The light quark masses correspond to $\kappa = 0.14144$ at $\beta = 6.2$ and $\kappa = 0.144$ at $\beta = 6.0$. The second data set is obtained using the same gluonic and fermionic action but with a bigger lattice spacing of $a^{-1} = 2.0$ GeV. The lattice size is $16^3 \times 48$ so that the volumes of the two lattices at $\beta = 6.2$ and $\beta = 6.0$ are practically identical. The physical light quark masses are both slightly larger than the strange quark.

Fig. 4.1 shows the results of a fit of the two data sets to a quadratic function in $m_Q^0 a$. Since the results at the two values of β are consistent it is reasonable to conclude that the discretisation errors are indeed functions of $m_Q^0 a$ only. Results of the fits to

$$Z_V^{HL} = A + Bm_Q^0 a + C(m_Q^0 a)^2 \quad (4.10)$$

are shown in table 4.4. For two of the heavy masses at $\beta = 6.2$, corresponding

β	A	B	C
6.2	0.814^{+2}_{-2}	0.342^{+12}_{-12}	-0.072^{+18}_{-18}
6.0	0.791^{+4}_{-4}	0.397^{+18}_{-18}	-0.120^{+20}_{-20}

Table 4.4: Results of fits to $Z_V^{HL} = A + Bm_Q^0 a + C(m_Q^0 a)^2$ at the two values of β and a light quark mass of $\kappa_q = 0.14144$.

to $\kappa_Q = 0.129$ and $\kappa_Q = 0.121$, values of Z_V^{HL} were calculated for three values of the light-quark mass. Table 4.5 shows that Z_V^{HL} is practically independent of the mass of the light quark.

Furthermore, table 4.5 contains results for Z_V^{HL} evaluated using the forward matrix element with $\vec{p} = (1, 0, 0)$. In this case it is possible to obtain Z_V^{HL} from the ratio eq. (4.6) for Lorentz index $\mu = 4$ and $\mu = 1$ separately. In the latter case one has

$$Z_V^{HL}(\mu = 1) = \frac{p^1}{E} \frac{C_2(t_x, \vec{p})}{C_3^{\mu=1}(t, t_x, \vec{p})}, \quad (4.11)$$

where E is the energy of the meson with momentum $\vec{p} = (1, 0, 0)$. Table 4.5 shows that the difference in results for Z_V^{HL} obtained with $\vec{p} = (1, 0, 0)$ and $\vec{p} = \vec{0}$ is less than 1% for the temporal component. On the other hand, the difference between $Z_V^{HL}(\mu = 4)$ and $Z_V^{HL}(\mu = 1)$ for the case $\vec{p} = (1, 0, 0)$ is slightly bigger. For Lorentz index $\mu = 1$ it is no longer the charge operator appearing in C_3 and the statistical error is much larger. The discrepancy between the two values of Z_V^{HL} for $\vec{p} = (1, 0, 0)$ and $\vec{p} = (0, 0, 0)$ is not bigger than 1.5σ and this could be a purely statistical effect. Figure 4.2 shows fits of the three different Z_V^{HL} to a quadratic in $m_Q^0 a$. Taking the values $Z_V^{HL}(\mu = 4)$ as the best value for $Z_V^{HL}(m_Q^0 a)$ table 4.5 shows that the values differ from the value for light quarks by about 10-20 % for the range of quark masses used in the calculation of three-point functions; for $\kappa_Q = 0.129$, which corresponds approximately to the mass of the charm, the discretisation error is approximately 12 %. This is consistent with the expectation that the errors are of $\mathcal{O}(\alpha_s m_Q a)$ and $\mathcal{O}(m_Q^2 a^2)$. For $Z_V^{HL}(\mu = 1)$ the discretisation error is found to be as large as 40 %.

Since $\mathcal{O}(m_Q a)$ effects can become quite large for heavy quarks it would be unreasonable to use the perturbative value of Z_V to normalise the data. The issue of normalisation will be addressed further in section 4.4.

μ and \vec{p}	κ_Q	Z_V^{HL}		
		$\kappa_q = 0.14144$	$\kappa_q = 0.14226$	$\kappa_q = 0.14262$
$\mu = 4, \vec{p} = \vec{0}$	0.133	0.8913^{+1}_{-1}		
$\mu = 4, \vec{p} = \vec{0}$	0.129	0.9177^{+3}_{-2}	0.9168^{+4}_{-4}	0.9165^{+5}_{-6}
$\mu = 4, \vec{p} = \vec{0}$	0.125	0.9428^{+4}_{-2}		
$\mu = 4, \vec{p} = \vec{0}$	0.121	0.9659^{+5}_{-4}	0.9656^{+6}_{-6}	0.9658^{+8}_{-11}
$\mu = 4, \vec{p} = (\pi/12, 0, 0)$	0.133	0.8976^{+10}_{-6}		
$\mu = 4, \vec{p} = (\pi/12, 0, 0)$	0.129	0.9248^{+9}_{-7}	0.9242^{+14}_{-12}	0.9240^{+24}_{-24}
$\mu = 4, \vec{p} = (\pi/12, 0, 0)$	0.125	0.9498^{+7}_{-8}		
$\mu = 4, \vec{p} = (\pi/12, 0, 0)$	0.121	0.9729^{+7}_{-9}	0.9734^{+12}_{-16}	0.9746^{+27}_{-25}
$\mu = 1, \vec{p} = (\pi/12, 0, 0)$	0.133	0.949^{+57}_{-56}		
$\mu = 1, \vec{p} = (\pi/12, 0, 0)$	0.129	0.994^{+57}_{-63}	0.982^{+83}_{-86}	0.924^{+134}_{-118}
$\mu = 1, \vec{p} = (\pi/12, 0, 0)$	0.125	1.042^{+53}_{-67}		
$\mu = 1, \vec{p} = (\pi/12, 0, 0)$	0.121	1.084^{+60}_{-75}	1.089^{+94}_{-116}	1.059^{+165}_{-160}

Table 4.5: Values of Z_V^{HL} for different choices of the Lorentz index μ , momenta \vec{p} , and light quark masses (given by κ_q).

It is worthwhile taking another look at the statistical error for $Z_V^{HL}(\mu = 4)$ obtained from the ratio eq. (4.6). These errors are tiny, due to a nearly complete cancellation of the fluctuations in the numerator and denominator. To achieve this cancellation it is necessary to have precisely the same momenta for two- and three-point function. In particular for the three-point function calculated with one lattice unit of momentum in the x -direction, $\vec{p} = (1, 0, 0)$, the two-point function must not be averaged over the equivalent momenta $((\pm 1, 0, 0), (0, \pm 1, 0), (0, 0, \pm 1))$, as is standard procedure to determine the energies and wave-function factors of the mesons. Table 4.6 shows how choosing the correct two-point function leads to better cancellation in the ratio eq. (4.6). The first column is the usual Z_V^{HL} obtained from the three-point function with momenta $(0, 0, 0) \rightarrow (0, 0, 0)$. Columns 2, 3 and 4 all use the three-point function with $\vec{p}_i = (1, 0, 0) \rightarrow \vec{p}_f = (1, 0, 0)$, but differ in the choice of two-point function. Method 2, ($|\vec{p}| = 1$), averages over all six possible orientations of the spatial momentum. Method 3, ($|p_x| = 1$), regains some of the correlations between numerator and denominator by only averaging over $\vec{p} = \pm(1, 0, 0)$. Method 4 uses the two-point function at the same value of momentum as the three-point function, $\vec{p} = (1, 0, 0)$ only.

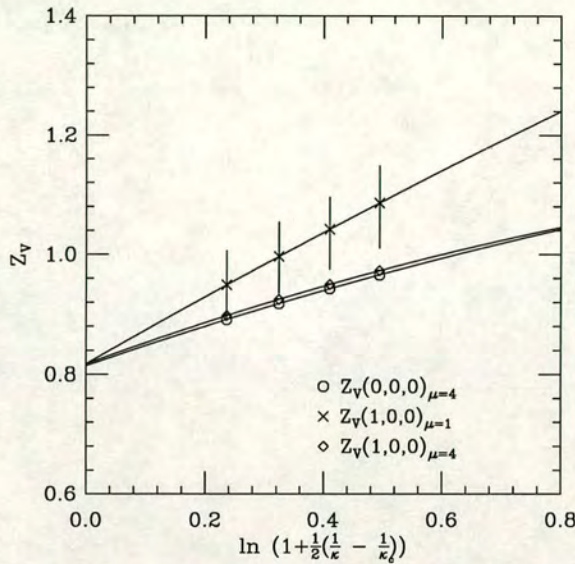


Figure 4.2: The renormalisation constant Z_V^{HL} as a function of $m_Q^0 a$ at two different momenta and Lorent indices.

κ_h	κ_l	$\mathbf{p} = 0$	$ \mathbf{p} = 1$	$ p_x = 1$	$p_x = 1$
0.129	0.14144	0.9176^{+3}_{-3}	0.96^{+3}_{-4}	0.93^{+2}_{-3}	0.925^{+1}_{-1}
0.121	0.14144	0.9659^{+4}_{-4}	1.00^{+3}_{-4}	0.97^{+2}_{-3}	0.973^{+1}_{-1}

Table 4.6: Comparison of Z_V^{HL} obtained from eq. (4.6) using the same three-point function but differently averaged two-point functions. Column 1 is Z_V^{HL} for $\vec{p} = (0,0,0)$. This is to be compared with column 4 which contains the Z_V^{HL} for $\vec{p} = (1,0,0)$ obtained with the two-point function which has momentum only in the x -direction.

Table 4.6 shows that the errors decrease as more mutual correlations between the three-point and two-point functions are regained. The values obtained by method 4 are remarkably accurate, and only differ from the zero momentum numbers by 1%. The values obtained with two-point functions averaged over two or six momenta are relatively high although consistent with column four within errors.

4.4 Fitting Procedure and Normalisation

It is possible to cancel the time dependence of the three-point function by dividing out the appropriate two-point correlators :

$$R^\mu(\vec{p}_B, \vec{q}, t_x, t_{op}) := \frac{C^{3\mu}(\vec{p}_B, \vec{q}, t_x, t_{op})}{C_D^2(\vec{p}_D, t_{op}) C_B^2(\vec{p}_B, (t_x - t_{op}))} \longrightarrow \frac{1}{Z_D(|\vec{p}_D|) Z_B(|\vec{p}_D|)} \sqrt{m_B m_D} \left[(v_B + v_D)^\mu h_+^L(\omega) + (v_B - v_D)^\mu h_-^L(\omega) \right] \quad (4.12)$$

In so doing, one has to be sure that the two-point functions are asymptotic in the region of time-slices where the ratio eq. (4.12) is fitted. This may not be the case for momenta of magnitude $\sqrt{2}$ and higher. For smaller momenta, fitting the ratio R^μ must yield values of $h_+^L(\omega)$ and $h_-^L(\omega)$ consistent with those obtained from a fit to eq. (4.2) with the energies and masses of the mesons frozen to their fitted values. I shall perform a comparison of these two fitting methods in section 4.4.2.

Extracting $h_+(\omega)$

Depending on what momentum combination is considered, eq. (4.12) yields between one and three equations to determine $h_+^L(\omega)$ and $h_-^L(\omega)$. Numerically, the time component, $\mu = 4$, is the cleanest channel. This component is used to extract $h_+(\omega)$ under the assumption that the contribution of $h_-(\omega)$ is negligible, $h_-(\omega) = 0$. Indeed, this is exact for the degenerate transitions as a consequence of current conservation. For non-degenerate transitions the error introduced by this approximation is of $\mathcal{O}(\alpha_s(m_Q), \alpha_s(m'_Q), \frac{1}{m_Q})$ since, to leading order in the $\frac{1}{m_Q}$ expansion one has

$$h_-(\omega) = \left[0 + \beta_-(\omega) + \mathcal{O}\left(\frac{1}{m_Q}\right) \right] \xi(\omega) , \quad (4.13)$$

where $\beta_-(\omega)$ are the radiative corrections known to $\mathcal{O}(\alpha_s)$. The leading power corrections are proportional to ϵ_Q and $\epsilon_{Q'}$ with a proportionality factor independent of the heavy quark masses. Furthermore, since $h_-(\omega)$ must vanish for $\epsilon_Q = \epsilon_{Q'}$, the leading power corrections must be proportional to $\epsilon_Q - \epsilon_{Q'}^3$. Thus, the error made on $h_+(\omega)$ in setting $h_-(\omega) = 0$ in the time component of eq. (4.2) to lowest

³I am ignoring radiative corrections at $\mathcal{O}(\frac{1}{m_Q})$.

order in $\frac{1}{m_Q}$ is

$$\frac{\delta h_+(\omega)}{h_+(\omega)} = \left| \frac{(v-v')^0}{(v+v')^0} \frac{[\beta^-(\omega) + (\epsilon_Q - \epsilon_{Q'})\delta_{1/m_Q}(\omega)]}{(\beta^+(\omega) + 1)} \right|, \quad (4.14)$$

with a function $\delta_{\frac{1}{m_Q}}(\omega)$ which is estimated to be of order 1. For the transitions considered $|\frac{(v-v')^0}{(v+v')^0}| < 0.02$. Using Neubert's short-distance corrections one finds $\beta^+(\omega)$ values as small as -0.07 and $|\beta^-(\omega)|$ as large as $+0.02$ for the transitions of the heaviest to the lightest quark. For this case the power corrections are largest: $|\epsilon_Q - \epsilon_{Q'}| = 0.1$ where the parameter $\bar{\Lambda}$ has been set to 0.5GeV [1]. Thus for the worst case $\frac{\delta h_+(\omega)}{h_+(\omega)} < 0.25\%$. This error can be increased if $\delta_{\frac{1}{m_Q}}(\omega)$ is much larger than 1; but even assuming this function were around 4, $\frac{\delta h_+(\omega)}{h_+(\omega)}$ remains below 1% because the ratio $\frac{(v-v')^0}{(v+v')^0}$ is so small. Therefore one may safely estimate

$$\frac{\delta h_+(\omega)}{h_+(\omega)} < 1\%, \quad (4.15)$$

and the time component of eq. (4.12) with $h_-(\omega) \equiv 0$ will give a precise determination of $h_+(\omega)$. Clearly, eq. (4.15) needs to be verified once $h_-(\omega)$ has been extracted; to do so I proceed as follows.

Extracting $h_-(\omega)$

Having calculated $h_+^L(\omega)$ in the above way, $h_-^L(\omega)$ is found by fitting to all available components of eq. (4.12) whilst holding $h_+^L(\omega)$ fixed to its time-component value. The fit is determined by minimizing a χ^2 function which takes into account correlations between different times for each component μ and cross correlations between different equations labelled by μ . The χ^2/dof therefore expresses how good the data fits the form of eq. (4.12) and how compatible the decomposition in terms of $h_+^L(\omega)$ and $h_-^L(\omega)$ is. If unreasonably high χ^2/dof were to be found this would indicate that the value to which $h_+^L(\omega)$ is frozen does not agree with the decomposition of the spatial equations. Equally, reasonable χ^2/dof - and, of course, small $h_-^L(\omega)$ - validate this method.

The reason $h_+^L(\omega)$ is fixed to obtain $h_-^L(\omega)$ is motivated by the fact that the temporal and spatial components of eq. (4.12) are not quite compatible : recall that the determination of Z_V^{HL} showed that the discretisation errors on the three-

point functions differed by up to 10% between temporal and spatial channels. This issue is closely related to the one of normalisation of the form factors h_{\pm}^L and will be further discussed below. A consistency check can be performed by fitting to all components of eq. (4.12) with both form factors as free parameters. The $h_+(\omega)$ obtained in this way should agree with the $h_+(\omega)$ obtained from the temporal component only. Equally, one may choose to perform fits without correlations between equations taken into account and this will also be tested.

Normalisation

The lattice vector current is related to the physical current by eq. (4.5) so that the physical h_{\pm} are obtained by the same prescription :

$$h_{\pm}(\omega) = Z_V h_{\pm}^L(\omega) . \quad (4.16)$$

Since discretisation errors of the three-point functions proportional to $\mathcal{O}(am_Q)$ are fairly large, see section 4.3, it is unreasonable to use the perturbatively determined Z_V . A more suitable choice of normalisation will lead to better control of discretisation errors and hence to more meaningful results for $h_{\pm}(\omega)$.

Table (4.3) shows that the normalisation depends mildly on the mass of the heavy quark. The three-point correlators are therefore normalised depending on their heavy quark content. For the degenerate data set this is straightforward : current conservation implies

$$Z_V^{\text{HL}} h_+^L(1) = h_+(1) = 1 . \quad (4.17)$$

The $(0,0,0) \rightarrow (0,0,0)$ recoil channel can therefore be used to calculate a Z_V^{HL} which incorporates all zero-recoil discretisation errors. Assuming that the momentum dependence of $\mathcal{O}(a)$ effects is small, using eq. (4.17) cancels discretisation errors when used to normalise the temporal equation of eq. (4.12).

For the non-degenerate data-set it is a priori not clear how to proceed since the heavy quark current is no longer conserved. Nevertheless, as discussed in section 4.6, the form factor $h_+(\omega)$ is unaffected by $\frac{1}{m_Q}$ effects at zero recoil. Eq. (4.17) is modified to

$$Z_V^{\text{HL}} h_+^L(1) = h_+(1) = \left[1 + \beta^+(1) + \mathcal{O}\left(\frac{1}{m_Q^2}\right)\right] \xi(1) . \quad (4.18)$$

Assuming that $\mathcal{O}(\frac{1}{m_Q^2})$ corrections are negligible at $\omega = 1$ one can therefore normalise the data for both the degenerate and non-degenerate case by :

$$\begin{aligned} h_+(w) &= \frac{h_+^L(w)}{h_+^L(1)}(1 + \beta_+(1)) \\ h_-(w) &= \frac{h_-^L(w)}{h_+^L(1)}(1 + \beta_+(1)) \end{aligned} \quad (4.19)$$

The error introduced for the non-degenerate data-set can be estimated as follows: calling h_+^{correct} the correctly normalised physical form factor which incorporates $\frac{1}{m_Q^2}$ corrections at zero recoil, denoted by δ_{1/m^2} , one finds :

$$h_+^{\text{correct}} = h_+(w) \times \frac{1 + \beta_+(1) + \delta_{1/m^2}}{1 + \beta_+(1)} \quad (4.20)$$

$$\simeq [1 + \delta_{1/m^2}] h_+(w) . \quad (4.21)$$

Thus, supposing that the size of the second-order power corrections are of the order -5%, as predicted by ref. [76], the correct physical form factor would be 5% smaller than the one extracted here. However, ratios of form factors will be free of this uncertainty. In section 4.6 power corrections at order $\frac{1}{m_Q}$ will be analysed and this will give an indication to what extent $\frac{1}{m_Q^2}$ corrections in eq. (4.18) can be neglected. I note also, that the degenerate data-set will be free of this theoretical uncertainty.

In principle, the forward matrix element for the mesons with one unit of momentum in the x direction may also be used to normalise the data. For degenerate transitions the forward matrix element for momenta $(1, 0, 0) \rightarrow (1, 0, 0)$ gives a non-zero temporal and spatial component which can be used to normalise the respective channels. This is particularly important since section 4.3 has shown that discretisation errors are much larger for the spatial channels. However, for the non-degenerate data set the channel $(1, 0, 0) \rightarrow (1, 0, 0)$ does not correspond to zero recoil. Therefore, in order to treat the complete data set in a consistent way, the form factors will always be normalised by the temporal recoil, $Z_V^{\text{HL}}((0, 0, 0) \rightarrow (0, 0, 0), \mu = 4)$.

It is important to note that because $h_+(\omega)$ is obtained from the correctly normalised temporal component of eq. (4.12) it does not suffer from the discrepancy

in normalisation between temporal and spatial equations. This discrepancy is absorbed completely by the form factor $h_-(\omega)$ which is obtained from both temporal and spatial equations. For the degenerate data set, where $h_-(\omega) = 0$ by current conservation, the value of $h_-(\omega)$ obtained on the lattice is a measure of the size of the discrepancy. For non-degenerate transitions the values of $h_-(\omega)$ can be used to put bounds on the physical $h_-(\omega)$.

There are two ways of enforcing the normalisation eq. (4.19) on the lattice. One can normalise the three-point functions by the fitted value of $Z_V^{\text{HL}} = \frac{1+\beta^+(1)}{h_+^L(1)}$. Equivalently, all form factors can be normalised by fitting directly to the ratio of the three-point function and its corresponding zero-recoil channel. Both methods have been tried and do not differ significantly. In the following all normalisation will be done using the fitted values of $\frac{1+\beta^+(1)}{h_+^L(1)}$.

4.4.1 Radiative Corrections

The radiative corrections are calculated according to Neubert's short distance expansion [19]. For this purpose the heavy quark mass is defined as

$$m_Q = \frac{a^{-1}}{4}(3m_V^\chi + m_{\text{PS}}^\chi) - \bar{\Lambda} , \quad (4.22)$$

where m_{PS}^χ and m_V^χ are the chirally extrapolated masses of the vector and pseudoscalar particles in lattice units (see Appendix A). These masses correspond to heavy-light mesons with a massless anti-quark; in this case the parameter $\bar{\Lambda}$ is taken to be 500 MeV[1].

Since the calculation is performed in quenched lattice QCD the number of quark flavours is set to 0 and no particle thresholds are assumed in Neubert's expressions⁴. In Appendix B values of $\beta^+(\omega)$ are tabulated for various combinations of heavy-quark masses and over the range of ω for which $h_+(\omega)$ has been calculated.

The equivalent radiative correction factors to $h_-(\omega)$ have also been calculated : they are completely negligible.

⁴See however the discussion of quenching in section 2.3.1 : the lattice cutoff is adjusted to incorporate the effects of quenching. It is therefore not clear how to run quenched lattice QCD results.

4.4.2 Choosing a fitting method

The kinematics of this simulation are such that $h_{\pm}^L(\omega)$ have been calculated for a range of ω very close to zero recoil, $\omega = 1$. The set of points in this region with the smallest errors will dominate the determination of the form-factors' ω -dependence and, subsequently, that of the Isgur-Wise function. Ideally, choosing a particular fitting method should not affect the determination of a fit-parameter as for example ρ^2 . In this section I make an attempt expose to what extent different procedures of fitting affect the form factors. For clarity this study will be made on a subset of the degenerate data only; recall that for this data set $h_-(\omega) \equiv 0$ is a consequence of current conservation.

In the previous section the following possible fitting methods have emerged which differ in the way the exponential decay of the three-point function is determined :

- Method \mathcal{A} :
$$\frac{1}{h_+^L(1)} C_{3pt}^\mu(\vec{p}_B, \vec{q}, t_x, t_{op}).$$

The form factors are normalised by the fitted value of $h_+^L(1)$. Energies and wavefunction factors are frozen to their fitted values from the two-point function fits.

- Method \mathcal{B} :
$$\frac{1}{h_+^L(1)} R^\mu(\vec{p}_B, \vec{q}, t_x, t_{op}).$$

The data is normalised as in \mathcal{A} . The exponential decay of the three-point function is cancelled by the appropriate two-point functions.

$h_+(\omega)$

It is natural to expect the three-point functions to reach their asymptotic form half way between the point where the initial meson is created ($t_x = 24$) and where the final meson is destroyed ($t = 0$). Unless otherwise stated, the three-point functions are therefore fitted on time-slices 11, 12 and 13.

Table 4.7 contains results for $h_+(\omega)$ at the heaviest quark masses obtained with both methods. I include some of the higher momenta, which are dropped in the analysis of subsequent chapters, for comparison. The data is plotted in figure 4.3. Errors on ω are not shown and the points are shifted with respect to each other

$\kappa_Q = 2100 \longrightarrow \kappa_{Q'} = 2100, \quad \kappa_q = 4144$						
			Method \mathcal{A}		Method \mathcal{B}	
\mathbf{p}_B	\mathbf{p}'_D	ω	$\frac{h_+(\omega)}{1+\beta_+(\omega)}$	χ^2/dof	$\frac{h_+(\omega)}{1+\beta_+(\omega)}$	χ^2/dof
(0,0,0)	(0,0,0)	1.000^{+0}_-0	1.000^{+0}_-0	3.2/2	1.000^{+0}_-0	1.1/2
(0,0,0)	(1,0,0)	1.037^{+1}_-1	0.91^{+2}_-3	13/2	0.96^{+1}_-1	3.3/2
(0,0,0)	(1,1,0)	1.067^{+3}_-3	0.87^{+2}_-2	0.43/2	0.89^{+2}_-2	2.5/2
(1,0,0)	(0,0,0)	1.037^{+1}_-1	0.89^{+2}_-2	6.4/2	0.91^{+2}_-1	1.1/2
(1,0,0)	(1,0,0)	0.996^{+5}_-5	0.96^{+4}_-4	0.99/2	0.97^{+5}_-5	0.5/2
(1,0,0)	(-1,0,0)	1.157^{+2}_-2	0.78^{+4}_-3	2/2	0.81^{+4}_-3	2.1/2
(1,0,0)	(0,1,0)	1.076^{+2}_-2	0.86^{+3}_-3	3.2/2	0.88^{+3}_-2	0.41/2
(1,0,0)	(1,1,0)	1.021^{+5}_-5	0.90^{+3}_-6	1.1/2	0.89^{+6}_-7	0.91/2
(1,0,0)	(0,1,1)	1.102^{+6}_-6	0.79^{+4}_-3	0.25/2	0.81^{+4}_-3	1.4/2

Table 4.7: Values of the physical $\frac{h_+(\omega)}{(1+\beta_+(\omega))}$ obtained with the two fitting methods \mathcal{A} and \mathcal{B} ; see text for details.

to enable a comparison of the errors; the correct ω is that of the points on the left, method \mathcal{B} , depicted by the crosses \times .

The first observation is that fitting to the ratio R^μ , method \mathcal{B} , results in very low χ^2/dof , indicating that there is a very good cancellation of the exponential. Good plateaus are found around $t_{op} = 12$, as expected, for all momenta and all heavy-quark mass combinations. Examples of such plateaus are shown in figure 4.4. The data exhibit plateaus between $t_{op} = 11$ and $t_{op} = 13$ for all momenta; however, the data is not asymptotic on more than the three time-slices. Recall that the extension point $t_x = 24$ was chosen to enable the use of Euclidean time-reversal. A simulation with the initial and final meson further apart would possibly allow for greater scope in the variation of t_{op} albeit at the cost of not being able to average the correlator with its time-symmetric counterpart.

In comparison, using method \mathcal{A} results in larger χ^2/dof . Using this method the data favours fits on time-slices 12-14 when the B-meson has zero momentum, and time-slices 11-13 when $\vec{p}_B = (1, 0, 0)$.

To extract values of the energies and wave function factors the two-point functions are fitted on time slices 11-22. It is possible that the two-point functions for higher momenta are not yet fully asymptotic on the time slices for which the

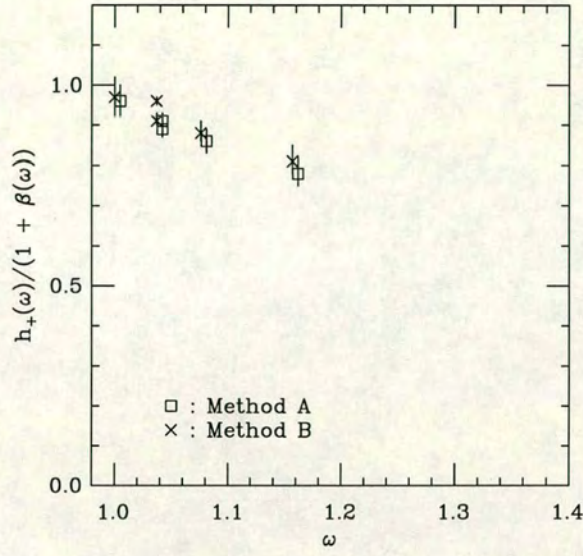


Figure 4.3: Comparison of fitting methods : $\mathcal{A} = \square$, $\mathcal{B} = \times$.

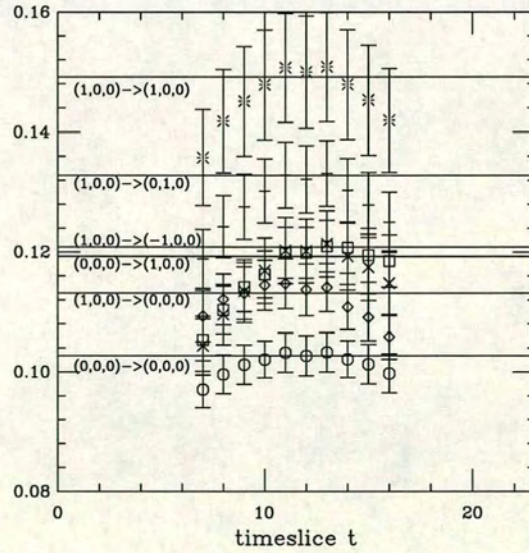


Figure 4.4: A set of plateaus for $\kappa_Q = \kappa_{Q'} = 0.121$ and $\kappa_q = 0.14144$. The data-points correspond to the ratio eq. (4.12). The plateaus are obtained from a correlated fit on $t = 11, 12, 13$.

three-point functions are fitted. This would mean that the ground state energies and wave-function factors are not properly isolated, leading to an overestimation of the two-point functions. In table 4.7 no such effect is seen, indicating that maybe too much caution has been applied. However, the situation deteriorates somewhat when going to lighter anti-quark masses; thus, when determining the ω dependence of the form factors, momenta equal or bigger than $\sqrt{2}$ will be excluded.

Overall, the two methods are remarkably consistent. However, for both methods, figure (4.3) shows a slightly larger discrepancy between the momentum combinations $(0,0,0) \rightarrow (1,0,0)$ and $(1,0,0) \rightarrow (0,0,0)$. This occurs over the whole range of hopping parameters : the values of $h_+((0,0,0) \rightarrow (1,0,0))$ and $h_+((1,0,0) \rightarrow (0,0,0))$ correspond to the same velocity transfer ω since the masses of the initial and final particle are identical. The reason for this discrepancy can be found in the way the two form factors are extracted : the three-point function from which $h_+((0,0,0) \rightarrow (1,0,0))$ is obtained is found by averaging the set of six momenta $(\pm 1, 0, 0)$, $(0, \pm 1, 0)$ and $(0, 0, \pm 1)$ whereas $h_+((1,0,0) \rightarrow (0,0,0))$ is determined from a three-point function which explores only the x -direction. In both cases the wave-function factors and energies of the two-point functions have been averaged over all six momenta. Thus, the inconsistency of the two values is interpreted as a statistical fluctuation. This is the same effect encountered in section 4.3 where the value of Z_V^{HL} obtained from the ratio eq. (4.6) when evaluated with a three-point function in the x -direction and a two-point function averaged over all directions comes out too high.

As pointed out above, method \mathcal{B} yields smaller χ^2/dof in comparison to method \mathcal{A} . The only momentum combination for which any significant change, compared to the error bars, between the two methods is observed is $h_+((0,0,0) \rightarrow (1,0,0))$. Using method \mathcal{A} these values are lower thus making them more compatible with the equivalent momentum $h_+((1,0,0) \rightarrow (0,0,0))$. The large values of χ^2 for this method are due to the fact that the exponential falloff of the three-point correlators is slightly different to the one with the energies fixed to their fitted values from the two-point functions.

To allow for a better fit to the exponential decay of the three-point functions for method \mathcal{A} , two approaches have been tried. Firstly, a simultaneous fit to the two- and three-point functions was performed. On the limited number of

configurations available this clearly reduces the number of time-slices the fit to the two-point functions can be performed on. The errors are thus so drastically increased that consistency is achieved through loss of accuracy.

A better approach is to allow one additional parameter in eq. (4.2) and fit to

$$C^{3\mu}(\vec{p}_B, \vec{q}, t_x, t_{op}) \times e^{-\delta E t_{op}}, \quad (4.23)$$

which is tantamount to letting the fit determine the energy of the final particle, the D-meson. Understandably, this method leads to an increase in the errors for $h_+(\omega)$ and to low χ^2/dof . The surprising result is that the values of $\delta E/E$ are found to be less than 0.1% for any combination of heavy and light quark hopping-parameters and for all of the momentum combinations. Using this method, the values of $h_+((1,0,0) \rightarrow (0,0,0))$ and $h_+((0,0,0) \rightarrow (1,0,0))$ are in excellent agreement. All other momenta are consistent with those of figure 4.3. However, this approach poses certain problems. Firstly, it is in principle inconsistent to allow for changes in the energies while holding the wave-function factors fixed. This is somewhat defused by the fact that the values of δE are all consistent with 0. Secondly, there is no clear way of generalising this method to the case where fits are performed simultaneously to more than one four-vector-component of the three-point function. For this reason this method will not be pursued further. It has however given further evidence that the inconsistency between the values of $h_+((1,0,0) \rightarrow (0,0,0))$ and $h_+((0,0,0) \rightarrow (1,0,0))$ is of a statistical nature only.

Another momentum combination which warrants some attention is $h_+((1,0,0) \rightarrow (1,0,0))$. For degenerate transitions this point corresponds to zero recoil and therefore, due to current conservation, $h_+(\omega)$ must be equal to one. As can be seen from figure 4.3 the values of $h_+((1,0,0) \rightarrow (1,0,0))$ are slightly lower than 1. At a light anti-quark mass corresponding to $\kappa_q = 0.14144$, $h_+(\omega)$ is consistent with 1 within 1σ ; for lighter anti-quark masses the situation becomes worse. As for the case discussed previously, this inconsistency arises because the three-point function explores only the x -direction. For this particular momentum one can calculate $h_+((1,0,0) \rightarrow (1,0,0))$ in an alternative way which uses the same three-point function and the same method of normalisation but the wave-function factors and energies are cancelled by the unaveraged two-point function pointing

in the x -direction only. Using the values of Z_V^{HL} from table 4.5 in section 4.3 one finds values of $h_+(\omega)$,

$$h_+((1, 0, 0) \rightarrow (1, 0, 0)) = \frac{Z_V^{\text{HL}}(\mu = 4, (0, 0, 0) \rightarrow (0, 0, 0))}{Z_V^{\text{HL}}(\mu = 4, (1, 0, 0) \rightarrow (1, 0, 0))}, \quad (4.24)$$

equal to one to within 1% independent of the light spectator quark mass.

To summarize the findings so far : the two fitting methods are found to give consistent results within errors. Momentum combinations which seem to yield slightly inconsistent results were investigated and the inconsistencies were shown to arise due to the same statistical fluctuation which was encountered at the end of section 4.3 in the determination of Z_V^{HL} .

$h_-(\omega)$

Finally, $h_-(\omega)$ is extracted using all available components of eq. (4.12) with $h_+(\omega)$ frozen to its temporal value. Method \mathcal{B} is chosen since it leads to significantly better χ^2 in the extraction of $h_+(\omega)$.

$\kappa_Q = 2100 \rightarrow \kappa_{Q'} = 2100, \quad \kappa_q = 4144$				
			Method \mathcal{B}	
\mathbf{p}_B	\mathbf{p}'_D	ω	$h_-(\omega)$	χ^2/dof
(0,0,0)	(1,0,0)	1.037^{+1}_{-1}	-0.09^{+3}_{-3}	21/5
(1,0,0)	(0,0,0)	1.036^{+2}_{-2}	0.04^{+3}_{-3}	2/5
(1,0,0)	(-1,0,0)	1.153^{+4}_{-4}	-0.00^{+1}_{-1}	3.7/5
(1,0,0)	(0,1,0)	1.072^{+5}_{-5}	0.00^{+1}_{-1}	16/8

Table 4.8: Values of $h_-(\omega)$ obtained with the fitting method \mathcal{B} , described in the text.

Table 4.8 shows the resulting values of $h_-(\omega)$. Radiative corrections are not applied to $h_-(\omega)$ since they are very small and because $h_-(\omega)$ suffers from potentially large discretisation errors so that its physical interpretation is not entirely clear. The number of degrees of freedom (dof) varies from momentum combination to momentum combination because the number of non-vanishing equations used to determine both form factors varies between one and three; since all equations are fitted on three time slices $dof = 7$ corresponds to three, $dof = 4$ to two and $dof = 1$ to one equation.

The χ^2 for these fits can be quite large. This is due to the fact that all errors due to the discrepancy in the normalisation are soaked up by $h_-(\omega)$. The analysis of section 4.3 has shown that the discretisation errors are different for temporal and spatial equations and the fitting method here ignores this fact by freezing $h_+(\omega)$ to its temporal value. Thus, the three-point functions are not being fitted to a form which allows for these discrepancies and this forcibly creates high χ^2/dof . Nevertheless, this is the only way to keep $h_+(\omega)$ free from large discretisation errors. Slightly improved χ^2/dof are obtained by not taking into account correlations between equations but no significant change in $h_-(\omega)$ is observed. Finally, the data was also fitted allowing both $h_+(\omega)$ and $h_-(\omega)$ to vary; this results in compatible values for both form factors, too.

Table 4.8 shows that $h_-(\omega)$ takes on values greater than 0 whereas current conservation requires $h_-(\omega) \equiv 0$. However, in section 4.3 it was shown that the spatial components of the three-point functions are low by up to 15% compared to the temporal components (resulting in larger Z_V^{HL} for $\mu = 1$). This is compatible with $|h_-(\omega)|$ taking on values as large as 0.15 as found in table 4.8. To the level of accuracy with which $h_-(\omega)$ can be determined it is therefore concluded that for the degenerate dataset $h_-(\omega)$ is consistent with 0.

Using this bound on $h_-(\omega)$ it is now possible to quantify the error made on $h_+(\omega)$ from fits to the temporal equation of eq. (4.12) only. Using eq. (4.14) one finds

$$\delta h_+(\omega)_{\max} = \left| \frac{(v - v')^0}{(v + v')^0} \right|_{\max} \frac{h_-(\omega)_{\max}}{h_+(\omega)_{\min}} \sim 0.07 \times \frac{0.1}{0.6} \sim 1\% . \quad (4.25)$$

The systematic error due to this approximation is thus very small.

Recap and summary

An extensive study was carried out to understand the systematics of several fitting methods and different normalisations of the data. Having found consistency, the following fitting method will be used. The form factor $h_+^L(\omega)$ is determined from a fit to the temporal equation of eq. (4.12) alone. The form factor $h_-^L(\omega)$ is found by a fit to all available components of eq. (4.12) with $h_+^L(\omega)$ frozen to its temporal value. The data will be normalised subsequently by taking the ratios $\frac{h_+^L(\omega)}{h_+^L(1)}(1 + \beta_+(1))$ and $\frac{h_-^L(\omega)}{h_-^L(1)}(1 + \beta_+(1))$. Only momenta smaller than $\sqrt{2}$ will be

included in fits since higher momenta possibly have large systematic errors.

4.5 Results for $\beta = 6.2$

The results for $h_+(\omega)$ and $h_-(\omega)$ for all heavy and light quark mass combinations are tabled in Appendix C.

In figure 4.5 the form factors $\frac{h_+(\omega)}{1+\beta^+(\omega)}$ and $h_-(\omega)$ are plotted for all different mass and momentum combinations at the heaviest of the light hopping parameters, $\kappa_q = 0.14144$. It is a surprising result that the data for $\frac{h_+(\omega)}{1+\beta^+(\omega)}$ falls on such a smooth curve. From this plot it is clear that it is a non-trivial task to find the heavy-quark mass dependence; points with very close values of ω are equal within errors independent of what mass or momentum is used. This is a first indication that corrections proportional to the inverse power of the heavy quark masses are not very large; this will be investigated further in section 4.6.

The smoothness of the data is also an indication that $\mathcal{O}(am_Q)$ errors are fairly well under control and that the approximation of setting $h_-(\omega) \equiv 0$ for all mass combinations is fairly reasonable. This is underlined by the fact that the values found for $h_-(\omega)$ are such that $|h_-(\omega)| < 0.2$. This is in fact a conservative estimate since the points in figure 4.5 which yield the largest $h_-(\omega)$ result from the momentum combination $(1, 0, 0) \rightarrow (1, 0, 0)$ for which the coefficient in the equation which determines $h_-(\omega)$, eq. (4.12), is a small number when the masses of the initial and final heavy quarks become identical. To the accuracy with which $h_-(\omega)$ can be determined with the chosen fitting method (see the discussion in section 4.4.2), it is therefore concluded that the form factor $h_-(\omega)$ is small for all ω :

$$|h_-(\omega)| < 0.1 . \quad (4.26)$$

4.5.1 Extracting ρ^2

The form factor $h_+(\omega)$ is related to the Isgur-Wise function $\xi(\omega)$ by

$$h_+(\omega) = [1 + \beta^+(\omega) + \gamma^+(\omega, m_Q)] \xi(\omega) , \quad (4.27)$$

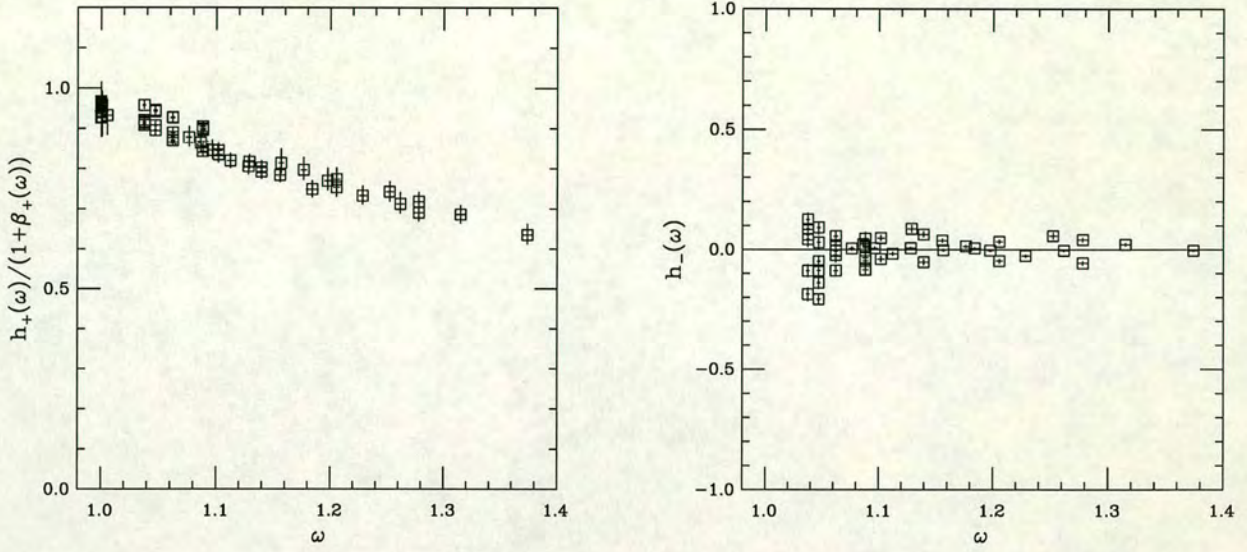


Figure 4.5: All data points over the whole range of masses and momenta for the form factors $\frac{h_+(\omega)}{1+\beta_+(\omega)}$ and $h_-(\omega)$ at $\kappa_q = 0.14144$.

where $\gamma^+(\omega, m_Q)$ incorporates all $\mathcal{O}(\frac{1}{m_Q})$ effects and m_Q stands for either of the heavy quarks. Thus one may write

$$\frac{h_+(\omega)}{1+\beta_+(\omega)} \simeq [1 + \gamma^+(\omega, m_Q)] \xi(\omega) . \quad (4.28)$$

To determine $\rho^2 = -\xi'(1)$ it is necessary to know the size of all corrections to the limit of infinitely heavy quark masses. Heavy Quark Symmetries do not predict the size of these corrections; the only model-independent information available is at the zero-recoil point. Here, the form factor $h_+(\omega)$ is protected against $\mathcal{O}(\frac{1}{m_Q})$ corrections by Luke's Theorem (see section 1.3.4). This has been used to normalise the data according to

$$h_+(\omega) = \frac{h_+^L(\omega)}{h_+^L(1)} [1 + \beta_+(1)] , \quad (4.29)$$

with

$$h_+^L(1) = \frac{1}{Z_{\text{HL}}^V} [1 + \beta_+(1) + \mathcal{O}(\frac{1}{m_Q^2})] . \quad (4.30)$$

For the degenerate case $\mathcal{O}(\frac{1}{m_Q^2}) \equiv 0$ due to current conservation. For the non-

		$N\xi_{\text{BSW}}(\omega)$			$\xi_{\text{BSW}}(\omega)$	
κ_Q	$\kappa_{Q'}$	$\tilde{\rho}^2$	N	χ^2/dof	$\tilde{\rho}^2$	χ^2/dof
2100	2100	1.4^{+3}_{-3}	0.99^{+1}_{-1}	9.4/3	1.5^{+3}_{-3}	9.7/4
2500	2500	1.4^{+2}_{-2}	0.99^{+1}_{-1}	12/3	1.5^{+2}_{-2}	12/4
2900	2900	1.5^{+2}_{-2}	0.99^{+1}_{-1}	13/3	1.5^{+2}_{-2}	13/4
3300	3300	1.4^{+1}_{-1}	0.99^{+1}_{-1}	12/3	1.5^{+1}_{-1}	12/4

Table 4.9: Values of $\tilde{\rho}^2$ and N for the elastic scattering at $\kappa_q = 0.14144$ from fits to $N\xi_{\text{BSW}}(\omega)$ and $\xi_{\text{BSW}}(\omega)$.

degenerate data set a systematic error has a priori been introduced through the normalisation procedure by setting $\mathcal{O}(\frac{1}{m_Q^2}) = 0$ at $\omega = 1$. Away from zero recoil both the degenerate and non-degenerate data-sets will be affected by power corrections so that the functional forms of $\xi(\omega)$ and $h_+(\omega)$ may differ. For the degenerate data set these corrections can be expected to be rather small close to $\omega = 1$. To test this assumption I shall focus first on the degenerate data-set at the heaviest anti-quark mass; this will provide a rough estimate of the size of power corrections. In section 4.6 this analysis is extended to include all masses of the initial and final heavy quarks.

$\kappa_q = 0.14144$ - elastic scattering

Figures 4.6 show fits of the four degenerate data sets to one of the proposed functions for $\xi(\omega)$:

$$\xi_{\text{BSW}}(\omega) = \frac{2}{\omega + 1} \exp \left\{ - (2\tilde{\rho}^2 - 1) \frac{\omega - 1}{\omega + 1} \right\}. \quad (4.31)$$

The slope is denoted by $\tilde{\rho}$ to emphasize that it may be different from the slope of the Isgur-Wise function. To start, a normalisation factor N is allowed to incorporate for the overall uncertainty in the normalisation of the data on the lattice so that a two-parameter fit is performed to $N\xi_{\text{BSW}}(\omega)$. The fits are then repeated setting $N=1$.

The resulting slopes are shown in table 4.9. The fits result in relatively large χ^2/dof . This is due to the discrepancy of the measurements of the momenta $(1, 0, 0) \rightarrow (0, 0, 0)$ and $(0, 0, 0) \rightarrow (1, 0, 0)$ as discussed in section 4.4.2. Remark-

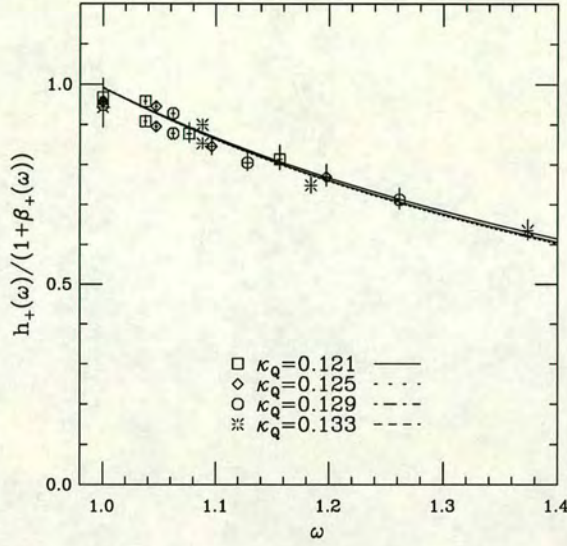


Figure 4.6: Fits to BSW-function for the four cases of elastic scattering at $\kappa_q = 0.14144$. An overall normalisation factor is allowed.

ably, one finds no variation in $\tilde{\rho}^2$ suggesting that $\mathcal{O}(\frac{1}{m_Q})$ effects are small in the range of ω explored.

To establish that this is not due to the particular choice of parametrisation the data is also fitted to a quadratic function

$$\xi_{\text{quad}}(\omega) = 1 - \tilde{\rho}^2(\omega - 1) + \frac{c}{2}(\omega - 1)^2. \quad (4.32)$$

This parametrisation is valid close to $\omega = 1$ and is more general than the specific parametrisation of BSW. The results of the quadratic fits are shown in table (4.10).

The fits confirm that the four data sets yield the same slope parameter. This would mean that at the heavy quark masses used in this simulation the scaling regime is reached and $\frac{h_+(\omega)}{1+\beta_+(\omega)}$ is an Isgur-Wise function. An extrapolation to the chiral limit would then yield the Isgur-Wise function relevant to $\bar{B} \rightarrow D l \bar{\nu}$ and $\bar{B} \rightarrow D^* l \bar{\nu}$ decays. Furthermore, the normalisation factor N is found to be 1 in the two-parameter fits; this validates the normalisation procedure.

		$N\xi_{\text{quad}}(\omega)$				$\xi_{\text{quad}}(\omega)$		
κ_Q	$\kappa_{Q'}$	$\tilde{\rho}^2$	c	N	χ^2/dof	$\tilde{\rho}^2$	c	χ^2/dof
2100	2100	1.5^{+7}_{-9}	$4.2^{+7.1}_{-9.2}$	1.00^{+2}_{-3}	9.4/3	1.6^{+3}_{-4}	$5.6^{+4.1}_{-4.1}$	9.4/4
2500	2500	1.5^{+6}_{-6}	$3.6^{+4.7}_{-5.6}$	1.00^{+2}_{-3}	12/3	1.6^{+3}_{-3}	$4.2^{+2.2}_{-2.1}$	12/4
2900	2900	1.6^{+5}_{-5}	$3.4^{+2.8}_{-3.1}$	1.00^{+2}_{-3}	13/3	1.6^{+2}_{-2}	$3.5^{+1.1}_{-1.2}$	13/4
3300	3300	1.6^{+3}_{-3}	$3.1^{+1.2}_{-1.5}$	1.00^{+2}_{-3}	11/3	1.5^{+2}_{-2}	2.7^{+6}_{-7}	11/4

Table 4.10: Values of $\tilde{\rho}^2$ and N for the elastic scattering at $\kappa_q = 0.14144$ from fits to $N\xi_{\text{quad}}(\omega)$ and $\xi_{\text{quad}}(\omega)$.

To further substantiate the claim that power corrections are small, the data at all heavy quark masses will be used in the following section to quantify $\mathcal{O}(\frac{1}{m_Q})$ corrections more precisely. This will be done at the heaviest light-quark mass, $\kappa_q = 0.14144$, as this is the data with the smallest statistical errors and, at this light quark value, the simulation was performed over a slightly larger range of heavy quark masses. It will be assumed, in what follows, that the findings at this light quark mass give a valid description of the heavy quark mass dependence at lighter masses of the spectator quark.

4.6 Heavy Quark Mass Dependence of $h_+(\omega)$

Recall from section 1.3.4 that the scale of $\frac{1}{m_Q}$ corrections is set by the parameter $\bar{\Lambda}$, eq. (1.61). Putting $\epsilon_{Q^{(\prime)}} = \frac{\bar{\Lambda}}{2m_{Q^{(\prime)}}}$, the corrections at higher order in $\frac{1}{m_Q}$ can be written in terms of two functions :

$$\frac{h_+(\omega)}{1 + \beta_+(\omega)} \simeq [1 + \gamma^+(\omega)] \xi(\omega) , \quad (4.33)$$

with

$$\gamma_{Q \rightarrow Q'}^+(\omega) = g_Q(\omega, \alpha_s(m_Q), z) \epsilon_Q + g_{Q'}(\omega, \alpha_s(m_{Q'}), z) \epsilon_{Q'} + \mathcal{O}(\epsilon_Q^2, \epsilon_{Q'}^2, \epsilon_Q \epsilon_{Q'}) . \quad (4.34)$$

Since the mass of the light spectator quark is nonzero the energy carried by the light degrees of freedom will differ to its value in the chiral limit by an amount equal to the mass difference of the heavy quarks. Using eq. (4.22), which defines

the spin-averaged heavy quark masses, one finds

$$\bar{\Lambda}_{4144} - \bar{\Lambda}^\chi = m_{Q\,4144} - m_Q = \frac{a^{-1}}{4} [3(m_V^{4144} - m_V^\chi) + (m_P^{4144} - m_P^\chi)], \quad (4.35)$$

which gives

$$\bar{\Lambda}_{4144} = 0.63 \text{ GeV} . \quad (4.36)$$

Furthermore,

$$\epsilon_{Q^{(')}} = \frac{\bar{\Lambda}_{4144}}{2m_{Q^{(')}}} , \quad (4.37)$$

$$z = \frac{m_Q}{m_{Q'}} . \quad (4.38)$$

The functions g_Q and $g_{Q'}$ are matrix elements of dimension five operators evaluated at order $\mathcal{O}(\epsilon_{Q^{(')}}^0)$. These two functions must be equal when $Q = Q'$. The amount by which they differ will partly be governed by logarithms of the heavy quark masses, as indicated by the presence of the running coupling in the functions' arguments. The functions will also depend differently on the variable z . However, since the difference between g_Q and $g_{Q'}$ is one of radiative corrections it is very small. In what follows this difference will be neglected so that eq. (4.34) simplifies to

$$\gamma_{Q \rightarrow Q'}^+(\omega) = g(\omega)(\epsilon_Q + \epsilon_{Q'}) + \mathcal{O}(\epsilon_Q^2, \epsilon_{Q'}^2, \epsilon_Q \epsilon_{Q'}) . \quad (4.39)$$

To evaluate the function $g(\omega)$ it is necessary to have a set of $h_+(\omega)$ at a fixed ω for different masses of initial or final mesons. This is achieved when the momentum of one of the mesons vanishes since ω then becomes independent of that meson's mass. There are four such values of ω for which this is the case. For each of these four points there are four measurements of $h_+(\omega)$. One of these is used to normalise the remaining three. Thus, for example for vanishing initial meson momentum, the following ratio is constructed :

$$\begin{aligned} R^+(\omega, x) &= \frac{1}{\epsilon_{Q_1}} \left[1 - \frac{h_+^{Q \rightarrow Q'}(\omega)/(1 + \beta_+^{Q \rightarrow Q'}(\omega))}{h_+^{Q_1 \rightarrow Q'}(\omega)/(1 + \beta_+^{Q_1 \rightarrow Q'}(\omega))} \right] \\ &= g(\omega) \left(1 - \frac{m_{Q_1}}{m_Q} \right) + \mathcal{O}(\epsilon_Q^2, \epsilon_{Q'}^2, \epsilon_Q \epsilon_{Q'}) . \end{aligned} \quad (4.40)$$

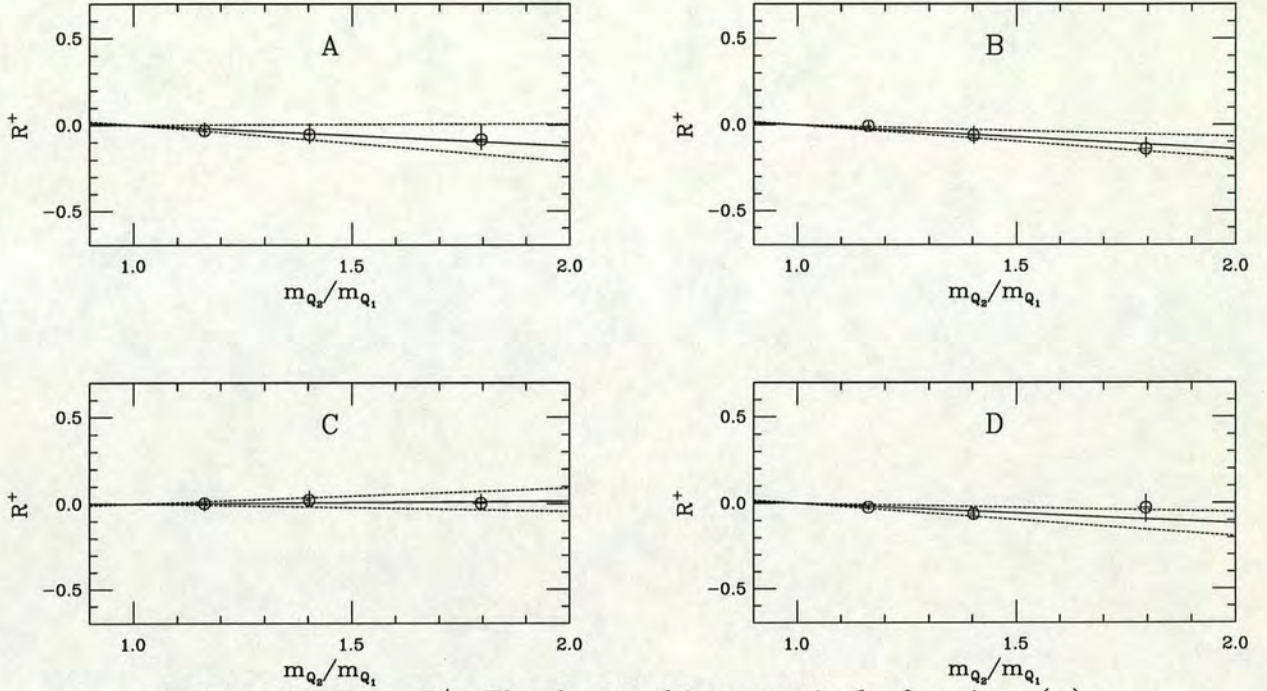


Figure 4.7: Fits to R^+ . The slope and intercept is the function $g(\omega)$.

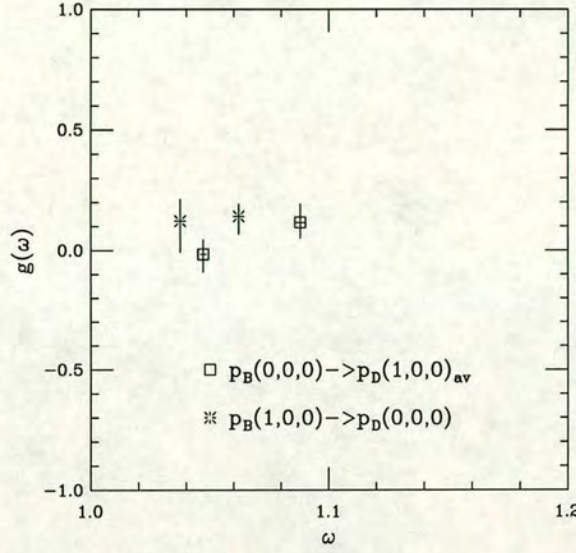
The resulting three data points for each ω are fitted to a straight line the slope and intercept of which is $g(\omega)$. The details of the fits are summarized in table 4.11. In figure 4.7 the data is plotted with the fits for each of the four ω . The data for R^+ satisfies the parametrisation of eq. (4.40) surprisingly well.

The resulting $g(\omega)$ is shown in figure 4.8. The function is consistent with zero over the range of recoils ω that have been studied : $1 < \omega < 1.1$. Although this is a very small range of velocity transfers there is no apparent trend in $g(\omega)$ and this could indicate that $g(\omega)$ remains small over the experimentally interesting range, $1 < \omega < 1.5$. Unless the $\mathcal{O}(\epsilon_{Q^{(i)}})$ corrections are cancelled by higher order $\epsilon_{Q^{(i)}}^n$ corrections in the ω -interval that has been studied, this means that $\mathcal{O}(\epsilon_{Q^{(i)}})$ corrections are genuinely small, as are all higher-order corrections. Thus, for $h_+(\omega)$ the flavour component of the heavy-quark symmetry is well satisfied in the charmed sector. This is somewhat surprising since for the decay constant f_D of the pseudoscalar D meson the authors of ref. [85], in a very similar study, find the $\mathcal{O}(\epsilon_c)$ corrections to the heavy-quark limit to be in the order of 30%.

Since $g(\omega)$ is found to be consistent with zero, the neglect of power corrections

pt	κ_{D^*}	κ_B	\mathbf{p}_{D^*}	\mathbf{p}_B	ω	x	R^+
A	0.121	0.121	(0,0,0)	(1,0,0)	1.037^{+1}_{-1}	1.00	0
	0.125					1.16	-0.032^{+46}_{-34}
	0.129					1.40	-0.056^{+63}_{-49}
	0.133					1.80	-0.084^{+86}_{-56}
	$g(\omega) = 0.122^{+90}_{-130}$ with $\chi^2/\text{dof}=0.1/2$						
B	0.121	0.129	(0,0,0)	(1,0,0)	1.062^{+2}_{-2}	1.00	0
	0.125					1.16	-0.007^{+22}_{-15}
	0.129					1.40	-0.062^{+50}_{-47}
	0.133					1.80	-0.139^{+64}_{-49}
	$g(\omega) = 0.141^{+51}_{-73}$ with $\chi^2/\text{dof}=0.9/2$						
C	0.125	0.121	(1,0,0)	(0,0,0)	1.047^{+1}_{-1}	1.00	0
	0.125					1.16	0.003^{+33}_{-38}
	0.129					1.40	0.023^{+51}_{-36}
	0.133					1.80	0.003^{+51}_{-39}
	$g(\omega) = -0.162^{+78}_{-101}$ with $\chi^2/\text{dof}=0.3/2$						
D	0.133	0.121	(1,0,0)	(0,0,0)	1.088^{+2}_{-2}	1.00	0
	0.125					1.16	-0.024^{+17}_{-16}
	0.129					1.40	-0.062^{+33}_{-35}
	0.133					1.80	-0.027^{+75}_{-81}
	$g(\omega) = 0.117^{+76}_{-66}$ with $\chi^2/\text{dof}=1/2$						

Table 4.11: Power corrections to $h_{A_1}(\omega)$ for four values of ω when $\kappa_q = 0.14144$. See text for definition of R^+ and $g(w)$.

Figure 4.8: The subleading form factor $g(\omega)$.

in determining the value of $h_+^L(1)$ used to normalise both $h_+^L(\omega)$ and $h_-^L(\omega)$ is justified. Since no mass dependence of $\frac{h_+(\omega)}{1+\beta_+(\omega)}$ is found one can combine data at fixed light quark mass of different initial and final heavy quark masses. This will be done in the following section to determine the light quark behaviour of $h_+(\omega)$. The fact that $\mathcal{O}(\epsilon_{Q^{(\prime\prime)}})$ corrections are negligible also means that the functions $\frac{h_+(\omega)}{1+\beta_+(\omega)}$ are effectively Isgur-Wise functions. Thus, when $\kappa_q = \kappa_{crit}$, the Isgur-Wise function obtained is the one relevant to $\bar{B} \rightarrow D l \bar{\nu}$ decays and to elastic \bar{B} and D scattering. Furthermore, an interpolation to the mass of the strange quark, $\kappa_q = \kappa_s$ will yield $\xi_s(\omega)$, the Isgur-Wise function relevant to $\bar{B}_s \rightarrow D_s l \bar{\nu}$ decays and to elastic \bar{B}_s and D_s scattering. However, since the range over which $g(\omega)$ has been calculated is very small, care needs to be applied in the determination of the slope ρ^2 . In principle, only values of $h_+(\omega)$ determined in the regime $1 \leq \omega \leq 1.1$ should be used to determine ρ^2 as the $\mathcal{O}(\frac{1}{m_Q})$ corrections further out have not been tested.

4.7 Light Quark Mass Dependence of $h_+(\omega)$

Chiral Extrapolation

To determine the Isgur-Wise function relevant to semi-leptonic decays with a light anti-quark \bar{u} or \bar{d} the results for $h_+(\omega)$ are extrapolated to vanishing light anti-quark mass $\kappa_{\text{crit}} = 0.14315$ [132].

The extrapolations are linear in the bare quark masses

$$am_q = \frac{1}{2} \left(\frac{1}{\kappa_q} - \frac{1}{\kappa_{\text{crit}}} \right). \quad (4.41)$$

Both $h_+(\omega)$ and ω are fitted to functions of the form $c_1(am_q) + c_2$ independently. The values of c_2 are the chirally extrapolated $h_+(\omega)_{\text{crit}}$ and ω_{crit} .

The results of the chiral extrapolations are tabled in Appendix C.2. All fits result in small χ^2/dof with the possible exception of the momentum combination $(1,0,0) \rightarrow (1,0,0)$. This channel corresponds to zero recoil when the masses of the initial and final heavy quarks are identical. As was discussed in section 4.4.2 the constraint $h_+((1,0,0) \rightarrow (1,0,0)) = 1$ is not very well satisfied. This was seen to arise due to a statistical fluctuation in the way the three-point function for this particular channel had been calculated. The constraint is less and less well satisfied for lighter anti-quarks. The correlated extrapolation tries to fix the downward trend in the data and does so at the expense of a large χ^2/dof .

The form factor $h_-(\omega)$ is not extrapolated since it suffers from large discretisation errors and is therefore not entirely physical.

Interpolation to the Strange Quark

The same linear fits as for the chiral extrapolation are used to interpolate to the mass of the strange quark, $\kappa_s = 0.1419$ [132]. The interpolated results for $h_+(\omega)_s$ and ω_s are given by $c_1(am_s) + c_2$ where m_s is the improved bare mass of the strange quark. These values can also be found in Appendix C.2.

Since it has been established in the previous section that $\frac{h_+(\omega)}{1+\beta_+(\omega)}$ is an Isgur-Wise function, the form factors with different initial and final heavy quark masses at fixed light-quark mass are combined in this section to determine the light quark

behaviour and the slope of the Isgur-Wise functions at the light-quark masses of a \bar{u} or \bar{d} and \bar{s} . However, in view of the fact that $\mathcal{O}(\frac{1}{m_Q})$ corrections have only been tested in the range $1 \leq \omega \leq 1.1$, these slope values may be contaminated by symmetry-breaking effects at larger ω . Furthermore, momentum-dependent lattice artefacts will be studied below to determine the size of the systematic error. The slope parameters obtained in this section are therefore not the absolute best values of ρ^2 : however, fitting all data points at fixed light quark mass allows for a determination of the form factors' dependence on the light quark masses.

Results of fits to the function suggested by BSW are shown in figure 4.9 for both $\kappa_q = \kappa_{\text{crit}}$ and $\kappa_q = \kappa_{\text{strange}}$. The full line is for the fit to $N \xi_{\text{BSW}}(\omega)_q$, the dashed lines represent fits to the same function with $N = 1$.

Since the dependence of the Isgur-Wise function on the velocity transfer ω is a priori unknown $\xi(\omega)_q$ is also fitted to a quadratic parametrisation

$$\xi_{\text{quad}}(\omega)_q = 1 - \rho^2(\omega - 1) + \frac{c}{2}(\omega - 1)^2, \quad (4.42)$$

where c is the curvature of the Isgur-Wise function at zero recoil. Setting $c = 0$ yields a lower bound on the slope parameter.

The fit results for the different parametrisations at the three light-quark values, $\kappa_q = 0.14144, 0.14226, 0.14262$ and for $\kappa_q = \kappa_s$ and $\kappa_q = \kappa_{\text{crit}}$ are presented in table 4.12 ⁵.

The fact that the values of χ^2/dof are relatively high should not be taken as an indication that the parametrisations described above are poor representations of the data. The large χ^2 are mainly due to the discrepancy between the measurements of $h_+((1,0,0) \rightarrow (0,0,0))$ and $h_+((0,0,0) \rightarrow (1,0,0))$ which has been discussed in detail in section 4.4.2. Furthermore, it was shown that $h_+((1,0,0) \rightarrow (1,0,0))$ is a poor representation of the form factor due to a statistical fluctuation. One should therefore not look at the absolute magnitude of χ^2/dof to determine the goodness of fit but rather at the relative performance of different parametrisations. One then finds that better fits are achieved with all functions when the

⁵Other parametrisations of the Isgur-Wise function give virtually the same parameters as ξ_{BSW} and are therefore not tabled.

$N \xi_{\text{BSW}}(\omega)$				$\xi_{\text{BSW}}(\omega)$			
κ_q	ρ^2	N	$\chi^2/d.o.f.$	ρ^2	$\chi^2/d.o.f.$		
0.14144	1.4^{+1}_{-1}	0.99^{+1}_{-1}	150/58	1.5^{+1}_{-1}	160/59		
κ_s	1.3^{+2}_{-2}	0.98^{+1}_{-1}	80/38	1.5^{+2}_{-2}	89/39		
0.14226	0.9^{+2}_{-2}	0.95^{+2}_{-2}	94/38	1.5^{+2}_{-2}	130/39		
0.14262	0.6^{+3}_{-3}	0.92^{+2}_{-3}	87/38	1.5^{+3}_{-3}	140/39		
κ_{crit}	0.9^{+2}_{-3}	0.95^{+3}_{-2}	47/38	1.4^{+2}_{-2}	74/39		
$N \xi_{\text{lin}}(\omega)$				$\xi_{\text{lin}}(\omega)$			
κ_q	ρ^2	N	$\chi^2/d.o.f.$	ρ^2	$\chi^2/d.o.f.$		
0.14144	1.0^{+1}_{-1}	0.97^{+1}_{-1}	160/58	1.3^{+1}_{-1}	240/59		
κ_s	1.0^{+1}_{-1}	0.97^{+1}_{-1}	86/38	1.2^{+1}_{-1}	130/39		
0.14226	0.8^{+2}_{-2}	0.95^{+2}_{-1}	95/38	1.2^{+1}_{-1}	170/39		
0.14262	0.5^{+3}_{-3}	0.92^{+2}_{-2}	87/38	1.2^{+2}_{-2}	160/39		
κ_{crit}	0.7^{+2}_{-2}	0.94^{+2}_{-2}	49/38	1.1^{+1}_{-2}	110/39		
$N \xi_{\text{quad}}(\omega)$				$\xi_{\text{quad}}(\omega)$			
κ_q	ρ^2	c	N	$\chi^2/d.o.f.$	ρ^2	c	$\chi^2/d.o.f.$
0.14144	1.4^{+2}_{-2}	$2.8^{+9}_{-1.1}$	0.99^{+1}_{-1}	140/57	1.6^{+2}_{-2}	3.7^{+9}_{-9}	150/58
κ_s	1.4^{+2}_{-3}	$3.2^{+1.2}_{-1.5}$	0.99^{+2}_{-2}	78/37	1.6^{+2}_{-2}	$4.3^{+1.2}_{-1.4}$	80/38
0.14226	1.0^{+3}_{-3}	$1.7^{+1.7}_{-1.9}$	0.96^{+2}_{-1}	93/37	1.7^{+2}_{-2}	$6.1^{+1.6}_{-1.8}$	110/38
0.14262	0.6^{+5}_{-5}	$0.6^{+2.5}_{-2.9}$	0.92^{+3}_{-3}	87/37	1.9^{+3}_{-3}	$7.9^{+2.3}_{-2.4}$	110/38
κ_{crit}	1.2^{+3}_{-4}	$3.1^{+1.6}_{-2.0}$	0.97^{+3}_{-3}	45/37	1.7^{+3}_{-3}	$5.9^{+1.7}_{-1.9}$	51/38

Table 4.12: Results of fits of the data for $h_+(\omega)/(1 + \beta^+(\omega))$ to the parametrisations $\xi_{\text{BSW}}(\omega)$, $\xi_{\text{lin}}(\omega)$ and $\xi_{\text{quad}}(\omega)$ with and without the additional parameter N , as described in the text. For fixed κ_q , all heavy-quark mass combinations were used. Only transitions with initial and final meson momenta less or equal to $\pi/(12a)$ were included. Here $\kappa_{\text{crit}} = 0.14315(2)$ and $\kappa_s = 0.1419(1)$.

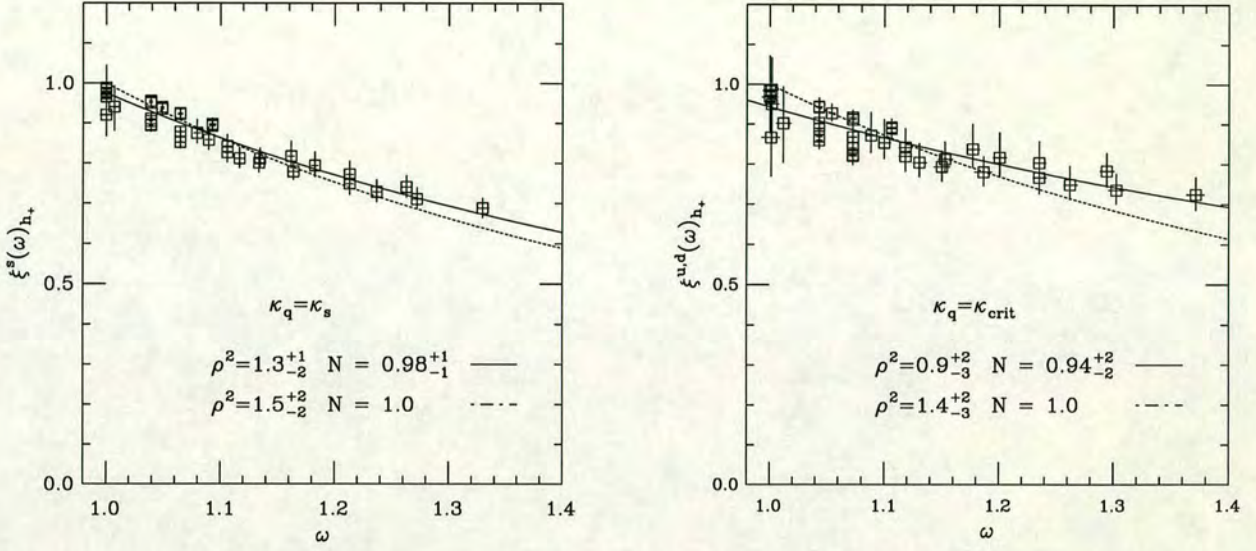


Figure 4.9: Fits to $\xi_{\text{BSW}}(\omega)_q$ and $N \xi_{\text{BSW}}(\omega)_q$ to all data points (using all mass combinations and momenta) in the chiral limit (right plot) and at the strange light-quark mass (left plot).

additional parameter N is allowed. The χ^2/dof does not particularly favour any of the parametrisations when the normalisation is not fixed to 1. As expected, a linear fit yields the lowest value of ρ^2 since it is the only parametrisation which does not allow a positive curvature. Since fits to $N\xi(\omega)_{\text{BSW}}$ and $N\xi(\omega)_{\text{quad}}$ result in virtually identical values of ρ^2 the BSW parametrisation will be taken as the standard form since it has one less parameter and yields slightly lower χ^2/dof .

4.7.1 Systematic error

To judge how good the values of ρ^2 that have been obtained in the previous section are, one needs a quantification of the systematic errors.

It is not possible to estimate the size of the $\mathcal{O}(am_Q)$ effects proportional to the momentum transfer; these effects cannot be disentangled from the form factors' own functional dependence on q^2 ; this can only be done by comparing the results presented here with data on lattices of different lattice spacings.

The size of discretisation errors proportional to $\mathcal{O}(a|\vec{p}|)$ at zero recoil can be

estimated by comparing the renormalisation constants Z_V^{HL} obtained from the forward matrix elements $(0,0,0) \rightarrow (0,0,0)$ and $(1,0,0) \rightarrow (1,0,0)$. One finds

$$\left| \frac{Z_V^{\text{HL}}((1,0,0) \rightarrow (1,0,0), \mu=4)}{Z_V^{\text{HL}}((0,0,0) \rightarrow (0,0,0), \mu=4)} - 1 \right| < 1\% , \quad (4.43)$$

for the degenerate data set. These errors can therefore be safely neglected.

In the previous section it was shown that power corrections to $\frac{h_+(\omega)}{1+\beta_+(\omega)}$ are small. In fact, this is also an indication that remaining mass-dependent discretisation errors in $\xi(\omega)_s$ and $\xi(\omega)_{u,d}$ are small. However, discretisation errors proportional to $\alpha_s a p$, where p is the magnitude of the incoming or outgoing meson can be analysed as follows.

For fixed initial and final meson momenta the data for all heavy quark mass combinations for $\xi(\omega)_s$ and $\xi(\omega)_{u,d}$ are fitted to $N\xi(\omega)_{\text{BSW}}$. The coefficients of the artefact terms are the same within each such momentum set and different from set to set. The variation in the results of the fits will give an indication of how large these artefacts are, although this issue cannot be disentangled from the statistical variations that were found in section 4.4.2. In particular, when the initial and final momentum magnitudes in two different sets are the same, the variation must be attributed to these statistical fluctuations and not to the difference in $\alpha_s a p_i$ and $\alpha_s a p_f$.

The results of these fits to the different momentum sets are shown in table 4.13 and in figure 4.10. The values of ρ^2 for the different momentum sets are quite

		$N\xi_{\text{BSW}}(\omega)_{u,d}$			$N\xi_{\text{BSW}}(\omega)_s$		
\vec{p}_B	\vec{p}_{D^*}	ρ^2	N	χ^2/dof	ρ^2	N	χ^2/dof
(0,0,0)	(1,0,0)	0.9^{+4}_{-3}	0.98^{+3}_{-3}	0.1/10	1.2^{+2}_{-2}	1.00^{+2}_{-1}	0.1/10
(1,0,0)	(0,0,0)	1.7^{+6}_{-6}	0.95^{+5}_{-4}	0.2/10	1.8^{+4}_{-3}	0.96^{+2}_{-2}	0.1/10
(1,0,0)	(0,1,0)	0.9^{+5}_{-4}	0.95^{+1}_{-1}	0.2/10	1.5^{+3}_{-2}	0.97^{+5}_{-4}	0.1/10
(1,0,0)	(-1,0,0)	0.9^{+3}_{-3}	0.95^{+1}_{-1}	0.7/10	1.2^{+2}_{-2}	0.97^{+7}_{-5}	0.1/10

Table 4.13: Values of ρ^2 and N from different momentum sets and all heavy quark mass combinations at $\kappa_q = \kappa_{\text{crit}}$.

compatible within each other and with the values obtained from fits to all data

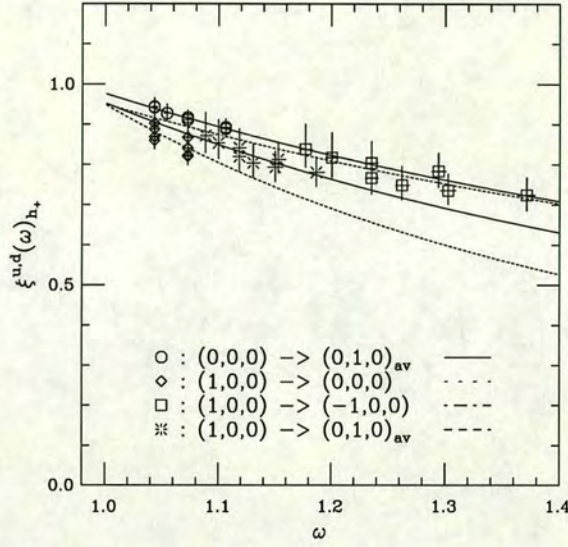


Figure 4.10: Fits to all masses for different momentum combinations. Consistent slope parameters are found for all momenta with the exception of the combination $h_+((1,0,0) \rightarrow (0,0,0))$.

and momenta (see table 4.12). The exception is the combination $h_+((1,0,0) \rightarrow (0,0,0))$. This discrepancy has been encountered before : it has been interpreted as a statistical fluctuation, due to the fact that the correlator for this momentum explores only the x -direction, rather than a systematic error proportional to $\alpha_s ap$. In fact, the same problem arises for the momentum $h_+((1,0,0) \rightarrow (1,0,0))$, which, for degenerate heavy quarks, should give $\xi(1) = 1$. Using the chosen fitting method, this condition is clearly violated; however, for this data-set, it is possible to use a different method to extract the form factor by calculating

$$h_+((1,0,0) \rightarrow (1,0,0)) = \frac{Z_V^{\text{HL}}(\mu = 4, (0,0,0) \rightarrow (0,0,0))}{Z_V^{\text{HL}}(\mu = 4, (1,0,0) \rightarrow (1,0,0))}. \quad (4.44)$$

Here, the Z_V^{HL} are obtained with two- and three-point functions which both explore only the x -direction (see section 4.3) and therefore retain far more correlations. Using this method one obtains values of $h_+((1,0,0) \rightarrow (1,0,0)) = 1$ to within 1% even when going to lighter anti-quark masses.

It is reassuring that the value of N is very close to 1 for the case $h_+((0,0,0) \rightarrow$

$(1, 0, 0)$) because the corresponding data are clearly the best points : these data-points should have the smallest discretisation errors because the momenta of the incoming and outgoing mesons are less than or equal to the initial and final momenta of the other momentum sets. They are also the points for which the normalisation procedure is optimal because they are obtained from three-point functions which are much more correlated with the three-point functions which are used to calculate the normalisation factor $h_+^L(1)$ than any of the other data points. This is due to the fact that for this one particular momentum, the three-point function is built using the same exponentiated propagator as for $h_+^L(1)$. These data points also have the smallest statistical errors since they have been obtained from an average of six different momenta. Finally, the ω for these points are all in the range $1 \leq 1.1$: thus, they will be free of $\mathcal{O}(\frac{1}{m_Q})$ effects as found in section 4.6, and can be safely used to extract a slope parameter free of any power corrections in $\frac{1}{m_Q}$. Clearly then, this momentum combination is best suited to determine the slope of the Isgur-Wise function without introducing the statistical and systematic errors which are inherent to the other momentum combinations.

4.7.2 The Isgur-Wise Function

Following the comments of the previous section, the procedure to determine ρ^2 will be as follows : all heavy-quark mass combinations for $h_+((0, 0, 0) \rightarrow (1, 0, 0))$ are fitted to ξ_{BSW} with the normalisation fixed to $N = 1$. This gives the central value and the statistical error for ρ^2 . The systematic error is obtained by allowing a spread in the values of ρ^2 which encompasses the two central values obtained from a fit to all data points to ξ_{BSW} and to $N\xi_{\text{BSW}}$, as shown in figure 4.9. Thus, the results for the slope of the Isgur-Wise function at $\omega = 1$ are

$$\rho_{u,d}^2 = 1.2_{-3}^{+3}(\text{stat.})_{-3}^{+2}(\text{syst.}) \quad (4.45)$$

for $\xi_{u,d}(\omega)$ and

$$\rho_s^2 = 1.2_{-2}^{+2}(\text{stat.})_{-0}^{+3}(\text{syst.}) \quad (4.46)$$

for $\xi_s(\omega)$.

The values found using this method, chosen to minimise the systematic errors and the $\mathcal{O}(\frac{1}{m_Q})$ contaminations, are in excellent agreement with the fits to all

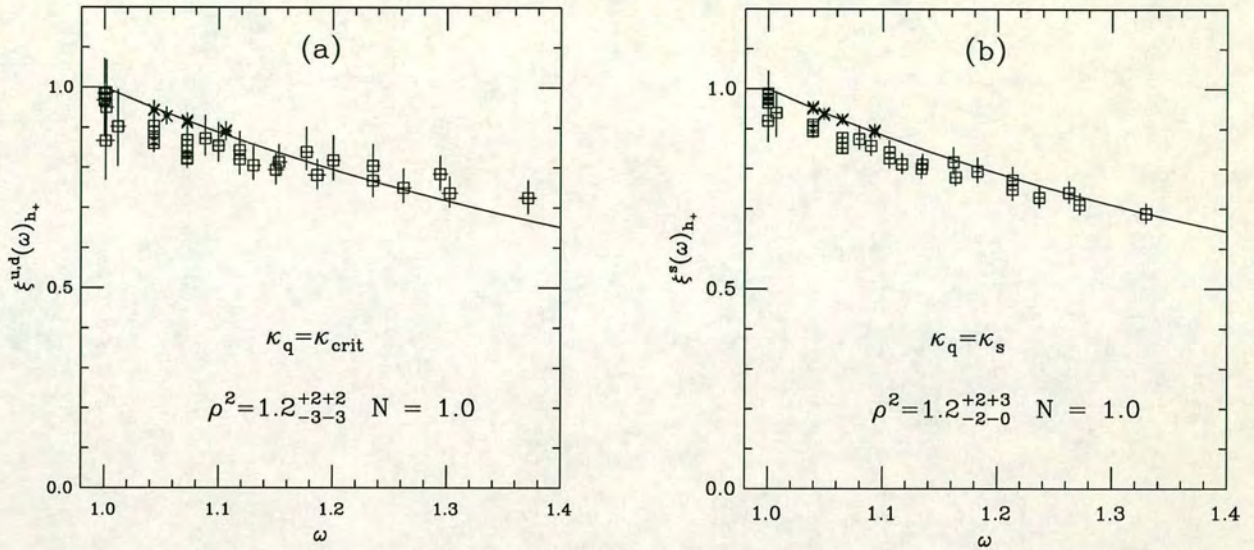


Figure 4.11: The Isgur-Wise function for a spectator quark whose mass is (a) zero and (b) the strange quark mass. The points denoted by * have been used to obtain the fits which give the best values of ρ^2 and the statistical errors quoted in eq. (4.45). The normalisation is fixed to 1. See text before eq. (4.45) for details.

data points (see table 4.12 and figures 4.9). The errors are by far large enough to encompass the small fluctuations in the central values of ρ^2 found when fitting the data to other possible parametrisations.

The discussion of these results and a comparison to predictions by other authors is postponed till the end of next chapter in which an attempt will be made to extract ρ^2 from the form factor $h_{A_1}(\omega)$ of the decay $\bar{B} \rightarrow D^* l \bar{\nu}$.

Chapter 5

Results : Pseudoscalar \rightarrow Vector

In this chapter results are presented for the form factors of the decay $\bar{B} \rightarrow D^* l \bar{\nu}$. Starting in section 5.2 the form factors contributing to the axial current are analysed and section 5.8 contains results for the vector current form factor.

5.1 Introduction

The lattice parameters of this simulation are identical to those of the decay $\bar{B} \rightarrow D l \bar{\nu}$ and can be found in section 4.2.

Recall from section 1.3 that four form factors are needed to describe the matrix elements of $\bar{B} \rightarrow D^* l \bar{\nu}$:

$$\begin{aligned} \langle D^*(v', \epsilon) | V^\mu | B(v) \rangle &= i h_V(\omega) \epsilon^{\mu\nu\lambda\sigma} \epsilon_\nu^* v'_\lambda v_\sigma, \\ \langle D^*(v', \epsilon) | A^\mu | B(v) \rangle &= h_{A_1}(\omega)(\omega + 1) \epsilon^{*\mu} - [h_{A_2}(\omega) v^\mu + h_{A_3}(\omega) v'^\mu] \epsilon^* \cdot v. \end{aligned} \quad (5.1)$$

The calculation proceeds much the same way as the calculation of the matrix elements of the $\bar{B} \rightarrow D l \bar{\nu}$ decay. The lattice correlator $\langle 0 | \chi_D^*(x) J_I^\mu(\vec{y}, t_{\text{op}}) \chi_B^\dagger(0) | 0 \rangle$ is calculated, where χ_D^* is the appropriate interpolating field for a vector meson and J_I^μ is the lattice axial or vector current.

5.2 Axial Current

The asymptotic form of the three-point function in Euclidean space is given by

$$\begin{aligned} C_{3pt}^{\mu\nu}(t_x, t_{op}; \vec{p}_B; U) \sum_{\vec{x}\vec{y}} e^{i\vec{p}_B \vec{x}} e^{i\vec{q}\vec{y}} \langle 0 | \chi_B(\vec{x}, t_x) A_I^\mu(\vec{y}, t_{op}) \chi_{D^*}^{\nu\dagger}(0) | 0 \rangle &\longrightarrow \\ \frac{Z_{D^*}(|\vec{p}_{D^*}|)}{2E_{D^*}(\vec{p}_{D^*})} \frac{Z_B(|\vec{p}_B|)}{2E_B(\vec{p}_B)} e^{-E_{D^*}(\vec{p}_{D^*})t_{op}} e^{-E_B(\vec{p}_B)(t_x - t_{op})} \times \sum_{\tau} \epsilon_\tau^{\nu*} \langle D^*, \vec{p}_{D^*} | A_I^\mu | B, \vec{p}_B \rangle, & (5.2) \end{aligned}$$

where $q^\mu = (p_{D^*} - p_B)^\mu$. Defining

$$A^{\mu\nu} = \sum_r \epsilon_r^{\nu*} \langle D^*, \vec{p}_{D^*} | V_I^\mu | B, \vec{p}_B \rangle \quad (5.3)$$

and performing the sum over polarisations one finds the Minkowski space relation:

$$\begin{aligned} A^{\mu\nu} = & \sqrt{m_B m_{D^*}} \left[(-g^{\mu\nu} + \frac{p_{D^*}^\mu \cdot p_{D^*}^\nu}{m_{D^*}^2}) (\omega + 1) h_{A_1}(\omega) \right] \\ & - \frac{1}{\sqrt{m_B m_{D^*}}} \left[\frac{p_B \cdot p_{D^*}}{m_{D^*}^2} p_{D^*}^\nu - p_B^\nu \right] [h_{A_2}(\omega) p_B^\mu + h_{A_3}(\omega) p_{D^*}^\mu] \end{aligned} \quad (5.4)$$

where I have converted back to a mass-dependent normalisation. For any momentum combination of the final and initial mesons this yields sufficient equations to determine the three form factors. The energies and wave function factors are determined from eq. (4.3) and the equivalent correlator for the vector meson :

$$\begin{aligned} C_{2pt,P}(t, \vec{p}) &= \sum_{\vec{x}} e^{i\vec{p}\vec{x}} \langle \chi_P(\vec{x}, t) \chi_P^\dagger(\vec{0}, 0) \rangle \\ &\rightarrow Z_P^2(|\vec{p}|) \frac{e^{-E_P(\vec{p})\frac{T}{2}}}{E_P(\vec{p})} \cosh \left(E_P(\vec{p}) \left[t - \frac{T}{2} \right] \right), \end{aligned} \quad (5.5)$$

$$\begin{aligned} C_{2pt,V}^{\mu\nu}(t, \vec{p}) &= \sum_{\vec{x}} e^{i\vec{p}\vec{x}} \langle \chi_V^\mu(\vec{x}, t) \chi_V^{\nu\dagger}(\vec{0}, 0) \rangle \\ &\rightarrow \left(-g_{\mu\nu} + \frac{p_\mu p_\nu}{m_V^2} \right) Z_V^2(|\vec{p}|) \frac{e^{-E_V(\vec{p})\frac{T}{2}}}{E_V(\vec{p})} \cosh \left(E_V(\vec{p}) \left[t - \frac{T}{2} \right] \right) \end{aligned} \quad (5.7)$$

Before proceeding to present results for the form factors it is necessary to relate the lattice axial current to the continuum axial current. This is the subject of the following section.

5.3 Axial Current Normalisation Z_A

The lattice form factors $h^L(\omega)$ contributing to the axial lattice current A_I^μ are related to form factors in the continuum by a multiplicative renormalisation constant Z_A

$$h_*(\omega) = Z_A h_*^L(\omega), \quad (5.8)$$

where

$$A_{\text{cont}}^\mu = Z_A A_I^\mu + \mathcal{O}(a\alpha_s) + \mathcal{O}(a^2) , \quad (5.9)$$

and h_* stands for $h_{A_1}(\omega)$, $h_{A_2}(\omega)$ and $h_{A_3}(\omega)$. Since the axial current is not conserved, Z_A cannot be determined as precisely as the renormalisation constant of the lattice vector current Z_V (see section 4.3). The procedure followed to determine Z_A is therefore the same as the one used to determine Z_V for the non-degenerate data-set of the pseudoscalar matrix elements. It is motivated by Luke's Theorem which states that $h_{A_1}(\omega)$ is unaffected by $\frac{1}{m_Q}$ corrections at the zero recoil point, $\omega = 1$. One can therefore write

$$Z_A^{\text{HL}} h_{A_1}^L(1) = \left[1 + \beta_{A_1}(1) + \mathcal{O}\left(\frac{1}{m_Q^2}\right) \right] \xi(1) . \quad (5.10)$$

Values of the perturbatively calculable radiative corrections, given by $\beta_{A_1}(\omega)$ and calculated using Neubert's short-distance expansion are tabulated in Appendix B. Once again, the superscript HL indicates that a different normalisation constant will be used which depends on the quark content of the mesons involved in the process. This procedure should help eliminate some of the remaining lattice artefacts of $\mathcal{O}(am_Q)$.

Using the fact that for $\vec{p}_B = \vec{p}_{D^*} = (0, 0, 0)$ eq. (5.4) simplifies to

$$A^{\mu\nu} = \sqrt{m_B m_{D^*}} (\omega + 1) (-g^{\mu\nu} + \delta_{\mu\nu} \delta_{\mu 0}) h_{A_1}(\omega) , \quad (5.11)$$

Z_A^{HL} can be determined by fitting $[A^{11}(0, 0, 0) + A^{22}(0, 0, 0) + A^{33}(0, 0, 0)]$ to a constant function. All axial form factors are then normalised by

$$h_*(\omega) = \frac{h_*^L(\omega)}{h_{A_1}^L(1)} [1 + \beta_{A_1}(1)] . \quad (5.12)$$

As for the case of $h_+(\omega)$ this normalisation procedure introduces an error of the size of the $\frac{1}{m_Q^2}$ corrections to $h_{A_1}(\omega)$ at $\omega = 1$. This error cannot be avoided.

Figure 5.1 shows Z_A^{HL} as a function of the bare heavy quark mass $m_Q^0 a$,

$$Z_A^{\text{HL}} = A + B m_Q^0 a + C (m_Q^0 a)^2 , \quad (5.13)$$

with the fit parameters shown in table 5.1. Table 5.2 contains results for Z_A^{HL}

β	A	B	C
6.2	1.03^{+3}_{-3}	0.1^{+1}_{-1}	0.1^{+1}_{-1}

Table 5.1: Results of fits to $Z_A^{HL} = A + Bm_Q^0 a + C(m_Q^0 a)^2$ at a light quark mass of $\kappa_q = 0.14144$.

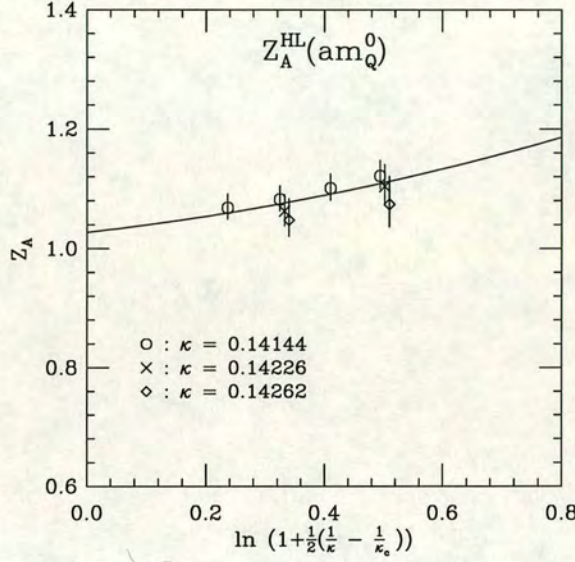


Figure 5.1: The renormalisation constant Z_A^{HL} as functions of $m_Q^0 a$. The solid lines represents a fit to a quadratic functions of $m_Q^0 a$ for the data at $\kappa_q = 0.14144$.

for the heavy kappa values and at three masses of the light quark. The results indicate that Z_A^{HL} depends only mildly on the heavy and light quark masses.

The values calculated here can be compared to the value of Z_A found in one-loop perturbation theory for the $\mathcal{O}(a)$ -improved action [130]

$$Z_A = 1 - 0.02g^2 + \mathcal{O}(g^4) = 0.97, \quad (5.14)$$

using the boosted coupling g as defined in section 2.2.1. A recent non-perturbative calculation however found a much larger value, $Z_A = 1.09$, at $\beta = 6.0$. This was obtained by requiring that the correctly normalised currents obey the continuum Ward identities [128]. Possibly, the inclusion of the $\mathcal{O}(g^4)$ will close the gap between the perturbative and non-perturbative values.

κ_Q	$m_Q^0 a$	Z_A^{HL}		
		$\kappa_q = 0.14144$	$\kappa_q = 0.14226$	$\kappa_q = 0.14262$
0.121	0.4943	$1.12 \pm \frac{3}{2}$	$1.10 \pm \frac{3}{3}$	$1.07 \pm \frac{5}{4}$
0.125	0.4102	$1.10 \pm \frac{2}{2}$		
0.129	0.3243	$1.08 \pm \frac{2}{2}$	$1.06 \pm \frac{3}{2}$	$1.05 \pm \frac{4}{3}$
0.133	0.2363	$1.07 \pm \frac{2}{2}$		

Table 5.2: Values of Z_A^{HL} for the degenerate data set.

5.4 The Form Factor $h_{A_1}(\omega)$

Eq. (5.4) shows that $h_{A_1}(\omega)$ can be determined for any momentum using the spatial-spatial component

$$A^{ii}(p_B^i = 0, p_{D^*}^i = 0) = \sqrt{m_B m_{D^*}}(\omega + 1)h_{A_1}(\omega) . \quad (5.15)$$

Neither $h_{A_2}(\omega)$ nor $h_{A_3}(\omega)$ contribute to these particular channels regardless of the initial and final meson masses. Together with the fact that $\mathcal{O}(\frac{1}{m_Q})$ corrections are expected to be small over the range of ω explored here, due to Luke's Theorem, this offers the possibility of extracting a precise value of the slope of the Isgur-Wise function.

To determine $h_{A_1}(\omega)$ the ratio

$$R^{\mu\nu}(\vec{p}_B, \vec{q}, t_x, t_{\text{op}}) := \frac{C_{3pt}^{\mu\nu}(\vec{p}_B, \vec{q}, t_B, t_{\text{op}})}{C_{2pt,D^*}(\vec{p}_{D^*}, t_{\text{op}})C_{2pt,B}(\vec{p}_B, (t_B - t_{\text{op}}))} \quad (5.16)$$

is fitted to a constant, where the three-point function at large Euclidean times is given by eq. (5.2) and the two-point correlators at large Euclidean times are given by eq. (5.5) and eq. (5.7).

The procedure followed here is similar to the one for the determination of $h_+(\omega)$. To start, all heavy quark mass combinations at the largest spectator quark mass are studied in an attempt to quantify $\mathcal{O}(\frac{1}{m_Q})$ corrections to the infinite quark mass limit. In section 5.6 the light-quark dependence of $h_{A_1}(\omega)$ is investigated.

The momenta used for fits to determine the functional form of $\frac{h_{A_1}(\omega)}{1+\beta_{A_1}}$ are shown in table 5.3. For all momenta good plateaus are found on timeslices $t_{\text{op}} = 11, 12, 13$.

\vec{p}_B	(0, 0, 0)		(1, 0, 0)			
\vec{p}_{D^*}	(0,0,0)	(1,0,0)	(0,0,0)	(1,0,0)	(-1,0,0)	(0,1,0)

Table 5.3: Momenta in lattice units used to determine ρ^2 . The momentum combination $(0, 0, 0) \rightarrow (0, 0, 0)$ is used to normalise the data after the fit.

5.5 Heavy Quark Dependence of $h_{A_1}(\omega)$

In the study of the heavy quark dependence of the form factor $h_+(\omega)$, section 4.6, $\mathcal{O}(\frac{1}{m_Q})$ were found to be negligible close to $\omega = 1$ so that $\frac{h_+(\omega)}{1+\beta_+(\omega)}$ is effectively an Isgur-Wise function. This analysis tested the flavour component of heavy quark symmetry. In this section a similar analysis will be performed for the form factor $h_{A_1}(\omega)$ thus probing both the spin and flavour components of the symmetry. As in section 4.6, this study will be performed at the heaviest mass of the spectator quark, $\kappa_q = 0.14144$; in the sequel it will be presumed that the heavy quark mass dependence at this light quark mass is a valid representation of the dependence at lighter spectator quark masses.

To get an indication of the size of symmetry-breaking effects figure 5.2 shows the data at $\kappa_q = 0.14144$ for the two form factors $h_{A_1}(\omega)$ and $h_+(\omega)$ for the complete degenerate data set. The plot shows no significant difference between the form factors close to $\omega = 1$. This is not unexpected since, of the six form factors needed to describe the semi-leptonic decays $\bar{B} \rightarrow D l \bar{\nu}$ and $\bar{B} \rightarrow D^* l \bar{\nu}$, only $h_+(\omega)$ and $h_{A_1}(\omega)$ are protected against $\mathcal{O}(\frac{1}{m_Q})$ at zero recoil.

A simple probe of the size of these corrections can be obtained by performing fits to the BSW parametrisation for a fixed mass of the b -quark and different masses of the c -quark. Figure 5.3 shows these fits for the heaviest of the b -quarks, corresponding to $\kappa_Q = 0.121$ and all four c -quark values. There is no trend in ρ^2 at all, all fits give a value of $\rho^2 = 1.0$ with a normalisation just below 1.

To substantiate this point further the ratio

$$\frac{h_{A_1}(\omega)[1 + \beta_{A_1}(\omega)]^{-1}}{h_+(\omega)[1 + \beta_+(\omega)]^{-1}}(\omega) = 1 + \gamma_{A_1}(\omega) \quad (5.17)$$

is calculated. In eq. (5.17) the fact that $\mathcal{O}(\frac{1}{m_Q})$ corrections to $h_+(\omega)$ are small has been used to set $\gamma_{h_+}(\omega) \equiv 0$, so that $h_+(\omega)[1 + \beta_+(\omega)]^{-1} = \xi(\omega)$. In principle,

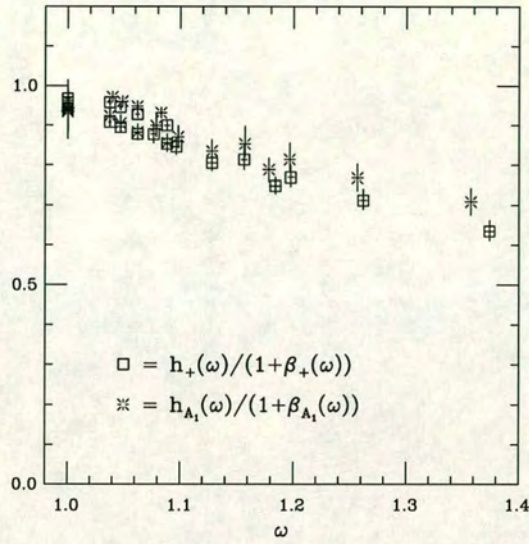


Figure 5.2: The degenerate dataset for the two form factors protected by Luke's Theorem, $h_{A_1}(\omega)$ and $h_+(\omega)$. Close to $\omega = 1$ the data lies exactly on top of each other; for larger ω there is a small trend towards $h_{A_1}(\omega) > h_+(\omega)$.

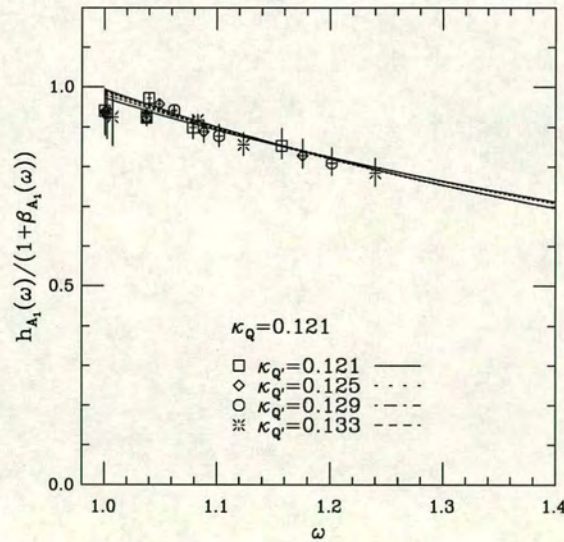


Figure 5.3: BSW fits for the fixed b -quark mass, $\kappa_Q = 0.121$ and varying masses of the c -quark. All fits result in the same slope parameter indicating that $\mathcal{O}(\frac{1}{m_Q})$ effects are small for $h_{A_1}(\omega)$.

there is only one kinematical case for which the form factors $h_+(\omega)$ and $h_{A_1}(\omega)$ have been calculated at the same velocity transfer. This is achieved, when the momentum of the D and the D^* is $\mathbf{0}$ and $\vec{p}_B = (1, 0, 0)$. In this case

$$\omega_{B \rightarrow D l \bar{\nu}} = \omega_{B \rightarrow D^* l \bar{\nu}} = \frac{E_B}{m_B} \quad (5.18)$$

so that the ratio can be calculated at four values of ω , corresponding to the four heavy quark masses of the b -quark. However, the mass difference between the D and the D^* is an $\mathcal{O}(\frac{1}{m_Q})$ effect in HQET. Therefore the velocity transfers ω are essentially degenerate to very high accuracy and one can use all momenta to calculate the ratio eq. (5.17).

Figure 5.4 shows that no significant deviation from 1 is found for the ratio close to $\omega = 1$ as expected from figure 5.2. Further out, however, one finds values for $\gamma_{A_1}(\omega)$ around 3 to 5%, albeit consistent with 0 at the 1σ level. In figure 5.4 different mass combinations have not been distinguished; to show that this is possible it is necessary to study the heavy-quark mass dependence of the function $\gamma_{A_1}(\omega)$.

One may decompose the function $\gamma_{A_1}^{Q \rightarrow Q'}(\omega)$ describing the $\mathcal{O}(\frac{1}{m_Q})$ corrections into two functions g_Q and $g_{Q'}$ just as in the case of $h_+(\omega)$, see section 4.6 :

$$\gamma_{A_1}^{Q \rightarrow Q'}(\omega) = g_Q^{A_1}(\omega, \alpha_s(m_Q), z) \epsilon_Q + g_{Q'}^{A_1}(\omega, \alpha_s(m_{Q'}), z) \epsilon_{Q'} + \mathcal{O}(\epsilon_Q^2, \epsilon_{Q'}^2, \epsilon_Q \epsilon_{Q'}) . \quad (5.19)$$

However, it is no longer the case that $g_Q^{A_1} = g_{Q'}^{A_1}$ when $Q = Q'$ - as I assumed in section 4.6 for the case of γ_{h_+} , since the structure of the higher dimension operators that the functions describe are different. In what follows the analysis above together with the results of section 4.6 will be taken as justification to set the $\mathcal{O}(\frac{1}{m_Q})$ corrections proportional to $\frac{1}{m_b}$ to 0, $g_Q^{A_1}(\omega, \alpha_s(m_Q), z) = 0$. This approximation is nearly exact at tree level. It introduces an error which can be estimated using Neubert's expressions for the functions $N_i(\omega)$, $h_i(\omega) = N_i(\omega)\xi(\omega)$ [1]. One finds that the difference is suppressed by a kinematical factor $\frac{(\omega-1)}{(\omega+1)}$ which multiplies the ϵ_b term. The error is therefore negligible in the region close to $\omega = 1$.

One may then perform an analysis similar to that of section 4.6 to extract the

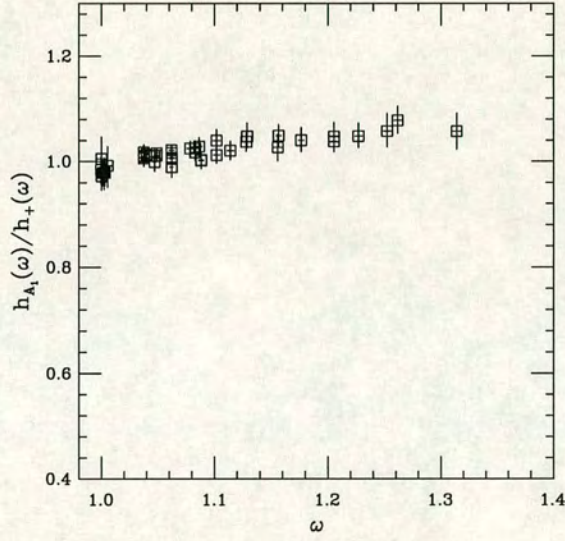


Figure 5.4: The ratio $\frac{h_{A_1}(\omega)[1+\beta_{A_1}(\omega)]^{-1}}{h_+(\omega)[1+\beta_+(\omega)]^{-1}}$. Since $\mathcal{O}(\frac{1}{m_Q})$ corrections to $h_+(\omega)$ are negligible, $h_+(\omega)[1+\beta_+(\omega)]^{-1} = \xi(\omega)$ and the deviation from one of the plotted ratio gives the size of $\mathcal{O}(\frac{1}{m_Q})$ corrections to $h_{A_1}(\omega)[1+\beta_{A_1}(\omega)]^{-1}$.

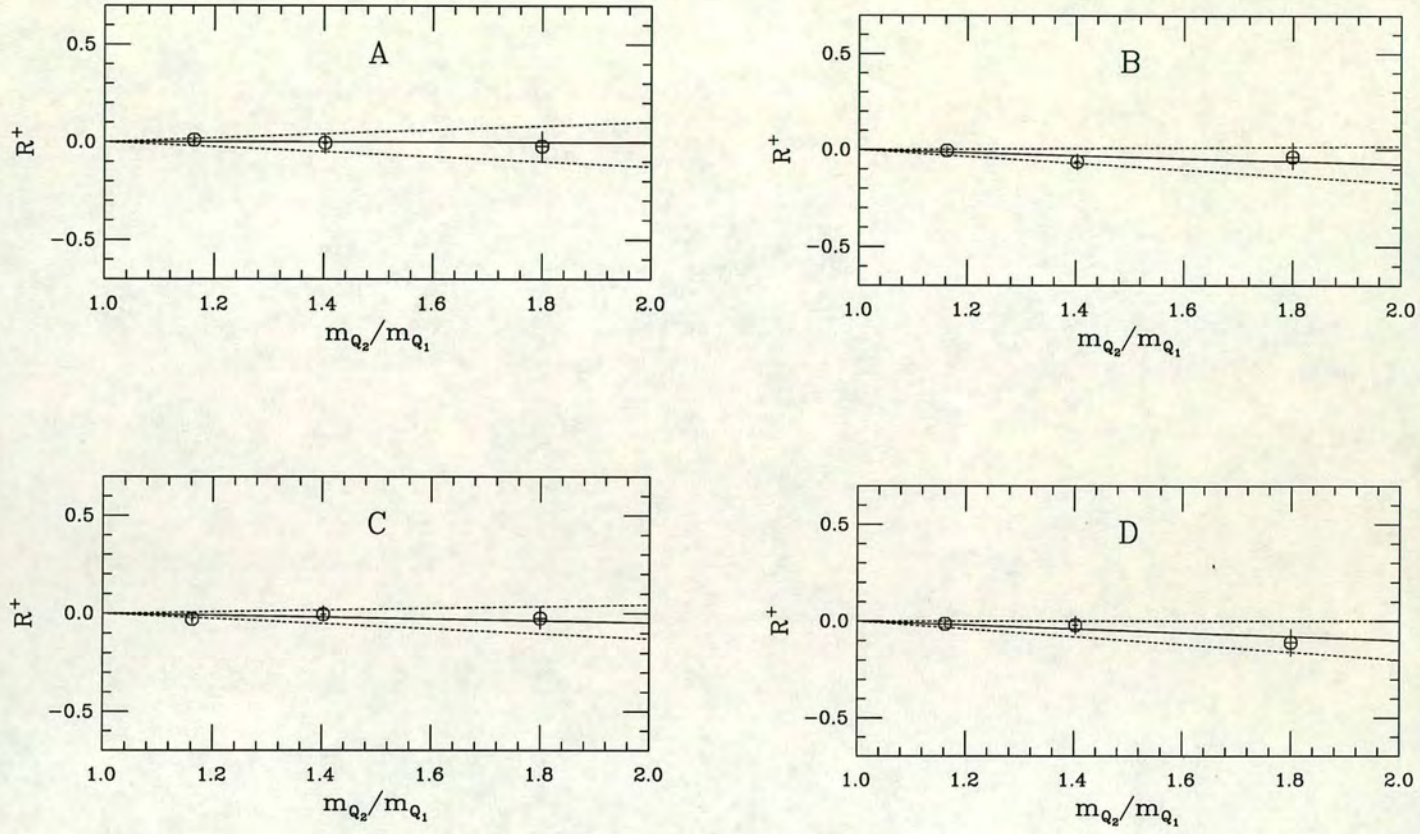


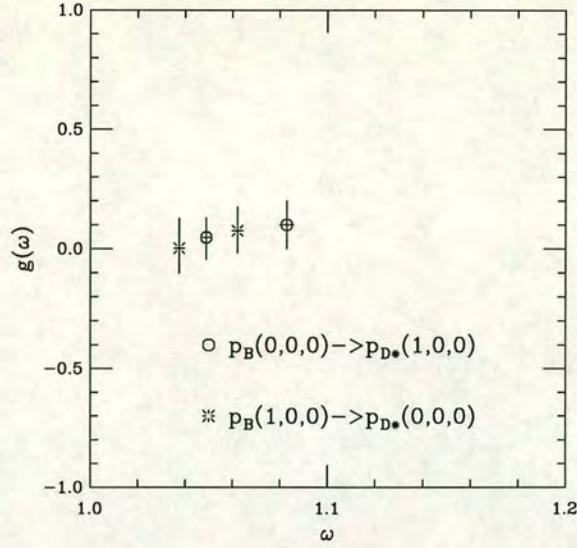
Figure 5.5: The ratios R^+ which are fitted to $R^+ = g^{A_1}(\omega)(1 - \frac{m_{Q_2}}{m_{Q_1}})$ as a function of $\frac{m_{Q_2}}{m_{Q_1}}$.

ratio

$$R^{A_1}(\omega, x) = \frac{1}{\epsilon_{Q_2}} \left[1 - \frac{h_{A_1}^{Q \rightarrow Q_1}(\omega)/(1 + \beta_{A_1}^{Q \rightarrow Q_1}(\omega))}{h_{A_1}^{Q \rightarrow Q_2}(\omega)/(1 + \beta_{A_1}^{Q \rightarrow Q_2}(\omega))} \right] \quad (5.20)$$

$$= g^{A_1}(\omega) \left(1 - \frac{m_{Q_2}}{m_{Q_1}} \right). \quad (5.21)$$

The details of these fits are shown in table 5.4. The function $g^{A_1}(\omega)$ is shown in figure 5.6. There is no significant deviation from $g^{A_1}(\omega) = 0$. This is astounding in view of the fact that the heavy quark masses in the B- and D^* -meson have been varied such that the expansion parameter $\epsilon_{Q^{(\prime)}}$ lies between 1/4 and 1/8. Thus both the flavour- and spin-symmetry sector of heavy-quark symmetry are being tested. Assuming that higher order corrections in $\epsilon_{Q^{(\prime)}}$ do not cancel the $\mathcal{O}(\epsilon_{Q^{(\prime)}})$

Figure 5.6: The function $g^{A_1}(\omega)$.

corrections it is therefore concluded that $h_{A_1}(\omega)$ is unaffected by $\mathcal{O}(\frac{1}{m_Q})$ corrections in the range $1 < \omega < 1.1$. For higher values of ω there are, unfortunately, no kinematical situations allowing for a similar type of analysis. Figure 5.4 shows that the $\mathcal{O}(\frac{1}{m_Q})$ effects are smaller than 5% in the range $1 < \omega < 1.4$. It is also possible to detect this trend in figure 5.6 as there is a small rise in the central value of $g^{A_1}(\omega)$ with growing ω .

It is clear that the slope parameter ρ^2 is determined mainly by the points close to zero recoil. Since, in this regime, $g^{A_1}(\omega) \simeq 0$, the functions $h_{A_1}(\omega)$ are effectively Isgur-Wise functions. In particular, if only points with $\omega < 1.1$ are used to find the value of ρ^2 , this slope should be free of $\mathcal{O}(\frac{1}{m_Q})$ corrections. This is what will be done below.

5.6 Light Quark Dependence of $h_{A_1}(\omega)$

Appendix D contains the result of the interpolations of the form factor $h_{A_1}(\omega)$ to the chiral limit and of the interpolations to the mass of the strange quark. Assuming that $\mathcal{O}(\frac{1}{m_Q})$ corrections are indeed small, these form factors are the Isgur-Wise functions relevant to $B \rightarrow D^*$ decay and $B_s \rightarrow D_s^*$ decays. The chiral limit is taken in the same way as for $h_+(\omega)$, see section 4.7. Both ω and $h_{A_1}(\omega)$ are extrapolated independently and linearly in the bare quark masses to $\kappa_q = \kappa_{\text{crit}} = 0.14315$. The same linear fit is used to interpolate to $\kappa_q = \kappa_s = 0.1419$.

pt	κ_{D^*}	κ_B	\mathbf{p}_{D^*}	\mathbf{p}_B	ω	x	R^+
A	0.121	0.121	(0,0,0)	(1,0,0)	1.037^{+1}_{-1}	1.00	0
	0.125					1.16	0.010^{+21}_{-23}
	0.129					1.40	-0.006^{+45}_{-52}
	0.133					1.80	-0.022^{+74}_{-81}
	$g^{A_1}(\omega) = 0.002^{+24}_{-104}$ with $\chi^2/\text{dof}=0/2$						
B	0.121	0.129	(0,0,0)	(1,0,0)	1.062^{+2}_{-2}	1.00	0
	0.125					1.16	-0.004^{+18}_{-19}
	0.129					1.40	-0.062^{+39}_{-41}
	0.133					1.80	-0.037^{+74}_{-62}
	$g^{A_1}(\omega) = 0.075^{+51}_{-73}$ with $\chi^2/\text{dof}=0.9/2$						
C	0.125	0.121	(1,0,0)	(0,0,0)	1.049^{+2}_{-2}	1.00	0
	0.125					1.16	-0.028^{+22}_{-20}
	0.129					1.40	-0.005^{+41}_{-34}
	0.133					1.80	-0.025^{+59}_{-53}
	$g^{A_1}(\omega) = 0.047^{+82}_{-91}$ with $\chi^2/\text{dof}=1.1/2$						
D	0.133	0.121	(1,0,0)	(0,0,0)	1.083^{+3}_{-3}	1.00	0
	0.125					1.16	-0.013^{+22}_{-19}
	0.129					1.40	-0.020^{+45}_{-45}
	0.133					1.80	-0.109^{+67}_{-68}
	$g^{A_1}(\omega) = 0.099^{+00}_{-99}$ with $\chi^2/\text{dof}=0.4/2$						

Table 5.4: Power corrections to $h_{A_1}(\omega)$ for two values of ω when $\kappa_q = 0.14144$. See text for definition of R^+ and $g^{A_1}(\omega)$

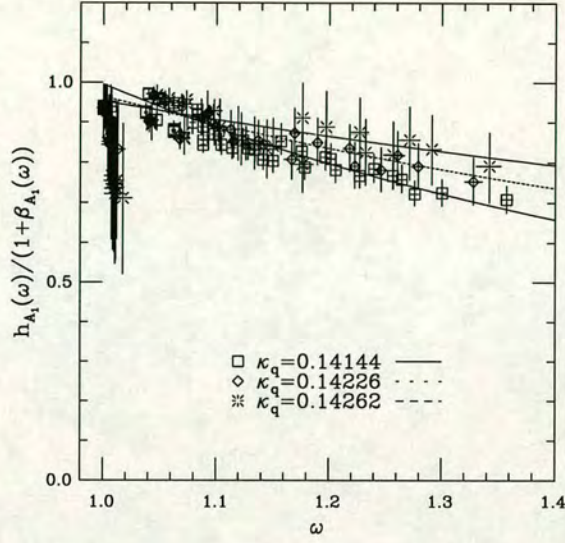


Figure 5.7: BSW fits using all heavy quark combinations at the three light quark masses. The fitted function is $N \xi_{\text{BSW}}(\omega)$.

Figure 5.7 shows the data for all mass and momentum combinations at the three masses of the light quark. The situation is very similar to what was found for the form factor $h_+(\omega)$. In particular the channel $h_{A_1}((1,0,0) \rightarrow (1,0,0))$, which is very close to zero recoil deteriorates towards smaller masses of the spectator quark so that it is more and more difficult to satisfy the condition $\xi(1) = 1$.

Fits have been performed to the BSW parametrisation to all data points at κ_{crit} and κ_s , see figure 5.8. These fits incorporate all systematic errors. They are therefore not the best possible determination of ρ^2 but they can be used to study the light quark dependence of $h_{A_1}(\omega)$. Comparing the values of table 5.5, one finds a small downward trend in ρ^2 with decreasing light quark mass; this trend is slightly smaller when the normalisation factor N is set to 1. These results are in excellent agreement with the findings for the form factor $h_+(\omega)$, see table 4.12.

To find the best values of ρ^2 the same procedure as for $h_+(\omega)$ is adopted : only the momentum combination $(0,0,0) \rightarrow (0,1,0)_{\text{av}}$ is fitted to the BSW parametrisation since this represents the best data with the smallest statistical and systematic

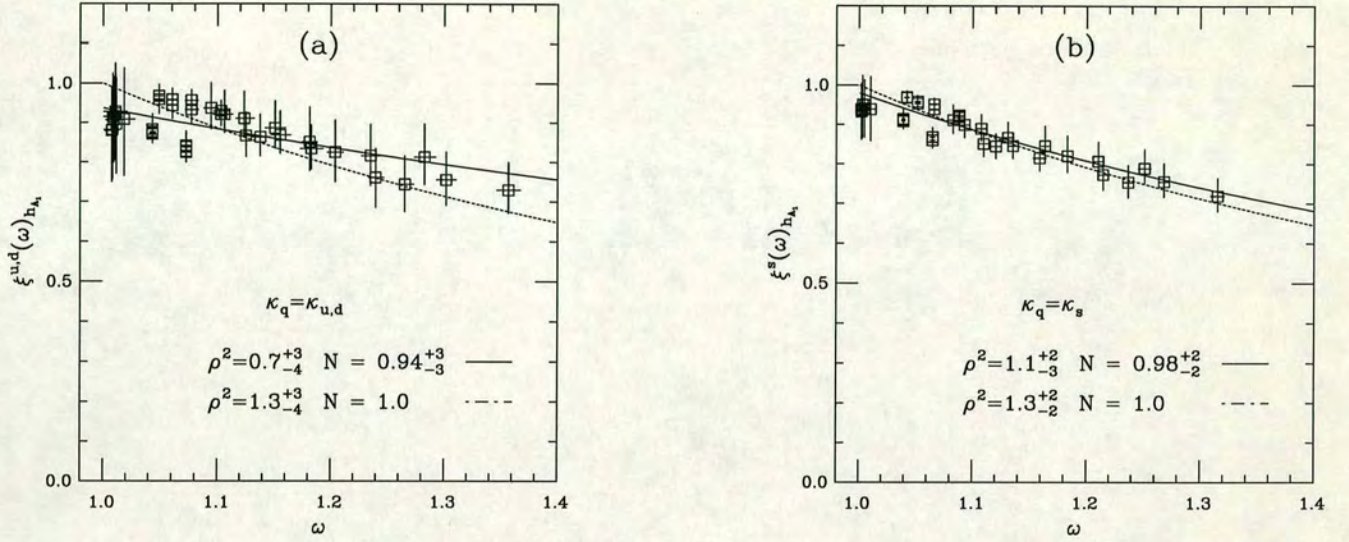


Figure 5.8: BSW fits using all heavy quark combinations for a spectator quark whose mass is (a) zero and (b) the mass of a strange quark. The fit-functions are $N \xi_{\text{BSW}}(\omega)$ and $\xi_{\text{BSW}}(\omega)$.

κ_q	$N \xi_{\text{BSW}}(\omega)$			$\xi_{\text{BSW}}(\omega)$	
	ρ^2	N	χ^2/dof	ρ^2	χ^2/dof
0.14144	1.2^{+2}_{-2}	1.00^{+1}_{-1}	110/58	1.2^{+2}_{-2}	110/58
κ_s	1.1^{+2}_{-3}	0.98^{+2}_{-2}	57/38	1.3^{+2}_{-2}	61/39
0.14226	0.8^{+3}_{-3}	0.96^{+2}_{-2}	58/38	1.1^{+3}_{-3}	60/39
0.14262	0.5^{+4}_{-4}	0.95^{+4}_{-3}	35/38	1.0^{+3}_{-3}	44/39
κ_{crit}	0.7^{+3}_{-4}	0.94^{+3}_{-3}	46/38	1.3^{+3}_{-4}	65/39

Table 5.5: Values of ρ^2 and N from fits to all heavy quark mass combinations at the three light quark masses, at the mass of the strange quark and in the chiral limit.

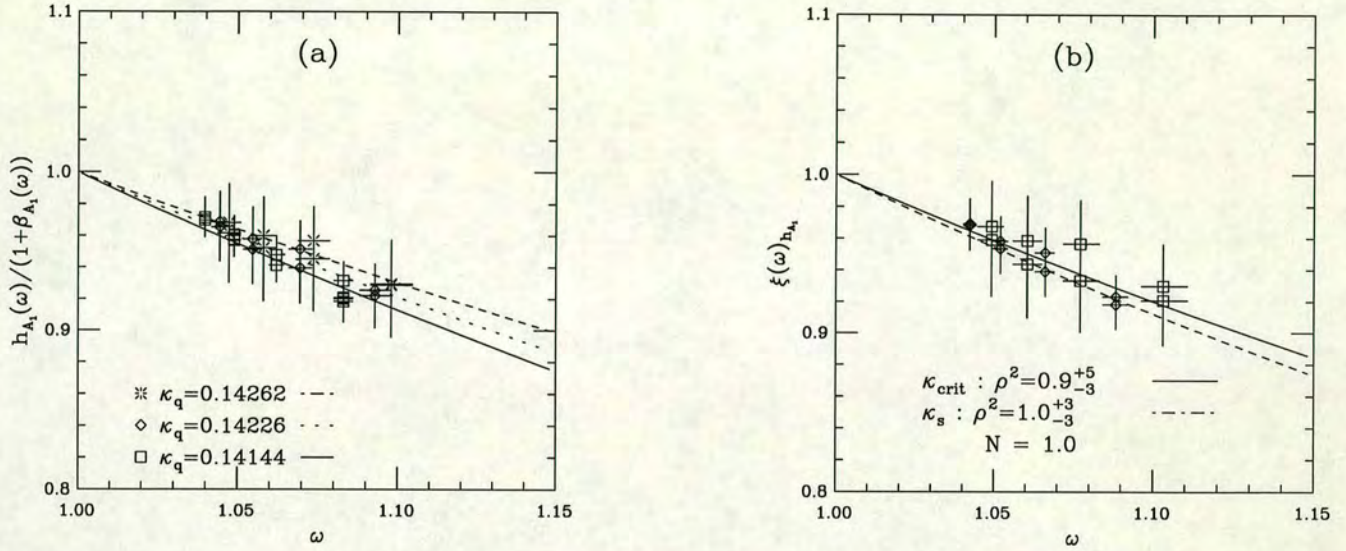


Figure 5.9: BSW fits using all heavy quark combinations for the momentum $h_{A_1}((0,0,0) \rightarrow (1,0,0))$ for a spectator quark with (a) varying mass (b) the mass zero and the mass of the strange quark. The fit-function is $\xi_{\text{BSW}}(\omega)$.

error. These data points will also be free of $\mathcal{O}(\frac{1}{m_Q})$ contaminations since they lie in the interval close to $\omega = 1$, where the function $g^{A_1}(\omega)$ is zero. Doing this one finds a rather more smooth behaviour of ρ^2 with the light quark mass; these values are shown in table 5.6. Figure 5.9 shows how subtle this effect is (note the scale !). These values are in good agreement with those found when fitting all momenta.

The spread in the central values of fits to all momentum and mass combinations with N both free and fixed to 1 is taken into account by the systematic error. The central value for ρ^2 is taken from table 5.6 with $N = 1$. Thus :

$$\rho_{u,d}^2 = 0.9_{-3}^{+5}(\text{stat.})_{-2}^{+4}(\text{syst.}) \quad (5.22)$$

and

$$\rho_s^2 = 1.0_{-3}^{+3}(\text{stat.})_{-0}^{+3}(\text{syst.}) . \quad (5.23)$$

For a discussion of these results I refer the reader to chapter 6.

κ_q	$N\xi_{\text{BSW}}(\omega)$			$\xi_{\text{BSW}}(\omega)$	
	ρ^2	N	χ^2/dof	ρ^2	χ^2/dof
0.14144	1.2^{+2}_{-2}	1.01^{+2}_{-2}	1/10	0.9^{+2}_{-2}	0.2/11
κ_s	1.1^{+2}_{-3}	0.98^{+2}_{-2}	0.4/6	1.0^{+3}_{-3}	0.3/7
0.14226	1.0^{+4}_{-3}	1.01^{+2}_{-2}	0.3/6	0.8^{+3}_{-3}	0.4/7
0.14262	0.8^{+5}_{-4}	1.00^{+4}_{-3}	0.2/6	0.7^{+4}_{-3}	0.2/7
κ_{crit}	0.7^{+3}_{-4}	0.94^{+3}_{-3}	0.2/6	0.9^{+5}_{-3}	0.2/7

Table 5.6: Values of ρ^2 and N from fits to all heavy quark mass combinations using the momentum combination $(0,0,0) \rightarrow (0,1,0)_{\text{av}}$ at the three light quark masses, at the mass of the strange quark and in the chiral limit.

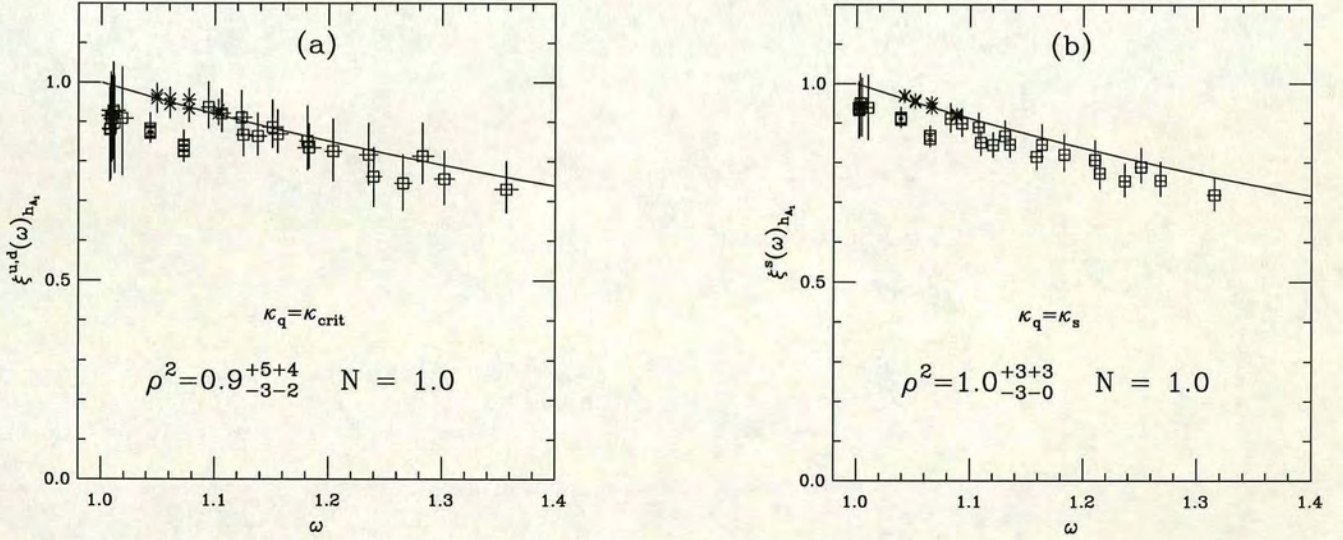


Figure 5.10: The Isgur-Wise function obtained from $h_{A_1}(\omega)$ for a spectator quark whose mass is (a) zero and (b) the mass of the strange quark. The points denoted by * are the best data which have been used to determine the slopes from a fit to $\xi_{\text{BSW}}(\omega)$.

5.7 The Form Factors $h_{A_2}(\omega)$ and $h_{A_3}(\omega)$

In this section the determination of the form factors $h_{A_2}(\omega)$ and $h_{A_3}(\omega)$ is described.

To extract the axial current form factors $h_{A_2}(\omega)$ and $h_{A_3}(\omega)$ the following approach is adopted :

- The form factor $h_{A_1}(\omega)$ is fixed to its value obtained from the spatial-spatial component $A^{ii}(p_B^i = 0, p_{D^*}^i = 0)$.
- A maximum of the available equations $A^{\mu\nu}$ is used. Only components which are numerically very noisy are discarded. In practice this means that for $\vec{p}_B = (0, 0, 0)$ the three components $A^{ii}(p_B^i \neq 0, p_{D^*}^i \neq 0)$, A^{0i} and A^{i0} are fitted, with correlations between timeslices and across components taken into account.
- For $\vec{p}_B = (1, 0, 0)$ the cases $i = 1$ and $i = 2, 3$ need to be treated differently. For $\vec{p}_{D^*} = (0, 0, 0)$ only the components A^{11} and A^{01} contribute. For $\vec{p}_{D^*} = (1, 0, 0)$ and $\vec{p}_{D^*} = (-1, 0, 0)$ there are four additional components of which three are used : A^{11} , A^{01} and A^{10} . The temporal-temporal component A^{00} is very noisy and has next-to vanishing kinematical factors for $h_{A_2}(\omega)$ and $h_{A_3}(\omega)$; it is therefore not used. Indeed, for $\vec{p}_{D^*} = (1, 0, 0)$ all kinematical factors for $h_{A_2}(\omega)$ and $h_{A_3}(\omega)$ are small so that the form factors for this momentum combination cannot be determined.
- For the momentum combination $\vec{p}_{D^*} = (0, 1, 0)$ the situation is more complicated since a total of 7 additional components can be used. It is clear from section 4.3 that temporal and spatial components can have very different discretisation errors : using all available components therefore results in high χ^2/dof . The results of these fits are nevertheless shown (only A^{00} is excluded as it is very noisy) since there is a priori no good argument for eliminating any particular component. The χ^2/dof are slightly better when using a block-diagonal covariance matrix or when performing an uncorrelated fit. However, the values for $h_{A_2}(\omega)$ and $h_{A_3}(\omega)$ remain practically unchanged. Better χ^2/dof of 1-2 are obtained when using only 4 or 5 of the available components. The values for $h_{A_3}(\omega)$ are not very strongly affected

but $h_{A_2}(\omega)$ starts to fluctuate quite strongly. Within 1σ however all values are consistent.

Eq. (5.4) shows that the coefficients of $h_{A_2}(\omega)$ and $h_{A_3}(\omega)$ are proportional to the square of the four-momenta involved. Since $\frac{(am)^2}{(ap_i)^2} \propto \mathcal{O}(10)$ the matrix elements are practically saturated by the contribution of $h_{A_1}(\omega)$ and one cannot expect to determine $h_{A_{2,3}}$ to very high accuracy unless the matrix elements have been obtained with incredibly good statistics.

In figure 5.11 I show an example of a multi-plateau for the matrix element with momenta $\vec{p}_B = (1, 0, 0)$ and $\vec{D}^* = (0, 0, 0)$. The first component, A^{22} is not refitted:

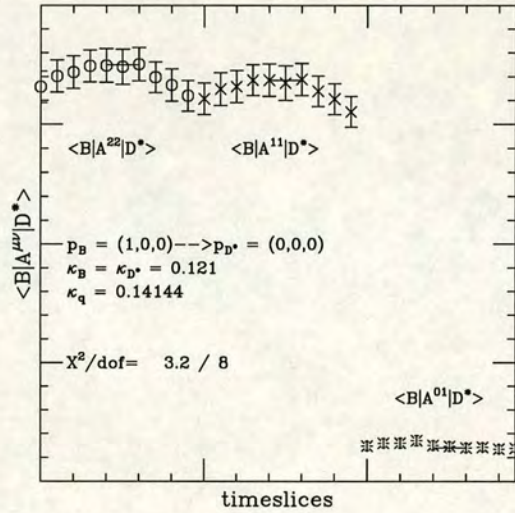


Figure 5.11: Examples of matrix elements with different Lorentz indices used to extract the form factors $h_{A_2}(\omega)$ and $h_{A_3}(\omega)$.

it is the matrix element which was used to determine $h_{A_1}(\omega)$. For this particular momentum only, two additional components are available to determine $h_{A_2}(\omega)$ and $h_{A_3}(\omega)$. These two components can be fitted with very low χ^2/dof , holding $h_{A_1}(\omega)$ fixed to its value from the component A^{22} , with correlations between timeslices and equations taken into account. They exhibit clear plateaus around $t = 11$. This plot shows that the problem in determining $h_{A_2}(\omega)$ and $h_{A_3}(\omega)$ does not result from poor data for their matrix elements but rather it is due to this being

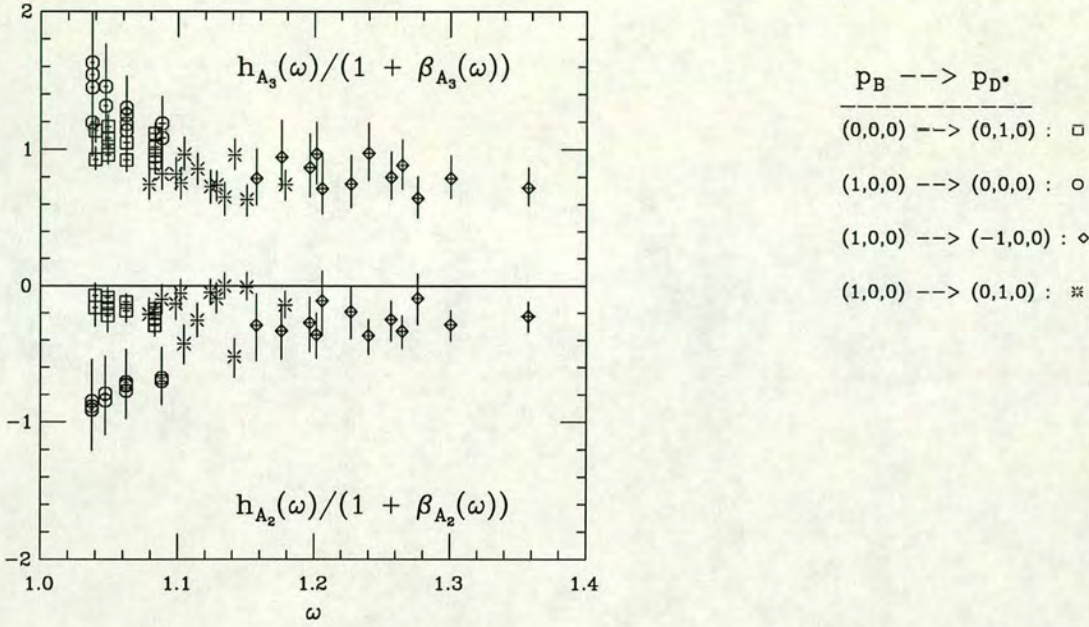


Figure 5.12: The form factors $\frac{h_{A_2}(\omega)}{(1+\beta_{A_2}(\omega))}$ and $\frac{h_{A_3}(\omega)}{(1+\beta_{A_3}(\omega))}$ at $\kappa_q = 0.14144$. Different momenta are distinguished by the symbols shown on the right.

an $\mathcal{O}(p^2)$ effect. Explicitly, the equations for this momentum are :

$$\begin{aligned}
 A^{22} = A^{33} &= \sqrt{(m_B m_{D^*})} (\omega + 1) h_{A_1}(\omega), \\
 A^{11} &= \sqrt{(m_B m_{D^*})} (\omega + 1) h_{A_1}(\omega) + \frac{1}{\sqrt{(m_B m_{D^*})}} (p_B^1)^2 h_{A_2}(\omega), \\
 A^{01} &= \frac{1}{\sqrt{(m_B m_{D^*})}} p_B^1 [h_{A_2}(\omega) E_B + h_{A_3}(\omega) E_D]
 \end{aligned} \tag{5.24}$$

Since the first two matrix elements are very nearly equal these equations are very badly conditioned to determine $h_{A_2}(\omega)$: although the matrix element is no worse than the one used to determine $h_{A_1}(\omega)$ to very high accuracy, it is not good enough to find $h_{A_2}(\omega)$.

In figure 5.12 all heavy-quark mass combinations for both form factors are plotted at $\kappa_q = 0.14144$. Different momenta have been given different symbols. They will be affected not only by the statistical fluctuations that have been observed in the calculation of the other form factors but also by different systematic effects

depending on how many components have been used to extract them.

Since the data is affected by potentially large systematic errors it is difficult to draw decisive conclusions. The form factor $h_{A_2}(\omega)$ is consistent with 0, as predicted by HQS for the scaling regime. There is however a trend to $h_{A_2}(\omega) < 0$. The momentum combination $(1, 0, 0) \rightarrow (0, 0, 0)$ warrants special examination : it seems to indicate larger $\frac{1}{m_Q}$ corrections. This can be due to two problems. Firstly, as I have shown in the above example, the form factors for this momentum are extracted from two equations with a matrix which is very close to being singular. Secondly, this particular momentum channel has been seen before to deviate somewhat from determinations of all form factors at equivalent or close ω using the momentum $(0, 0, 0) \rightarrow (1, 0, 0)$. The form factors using the momentum $(0, 0, 0) \rightarrow (1, 0, 0)$ are obtained from the average of six momenta, $\vec{p}_{D^*} = ((\pm 1, 0, 0), (0, \pm 1, 0), (0, 0, \pm 1))$, whereas the form factor from $\vec{p}_B = (1, 0, 0)$ explores only the x -direction. The $1 - 2\sigma$ discrepancy between the two are therefore interpreted as being due to the different statistical ensembles they have been obtained from. Since the momentum combination $(0, 0, 0) \rightarrow (1, 0, 0)$ is obtained from a larger set of momenta it is likely to yield a better value of $h_{A_2}(\omega)$ and $h_{A_3}(\omega)$. The form factor $h_{A_3}(\omega)$, which in the infinite quark-mass limit is an Isgur-Wise function, shows a small decrease with increasing ω . From figure 5.12 I conclude that it is not possible to extract information from this lattice calculation on the physical form factors $h_{A_2}(\omega)$ and $h_{A_3}(\omega)$. Results presented below on the size of $\mathcal{O}(\frac{1}{m_Q})$ corrections are to be taken as bounds and not as absolute values. Some methods will be presented for extracting subleading form factors. No attempt will be made to study the light-quark dependence; in particular, I will always work at the heaviest mass of the anti-quark, $\kappa_q = 0.14144$, a chiral extrapolation will not be performed.

To evaluate the size of the $\frac{1}{m_Q}$ corrections the radiatively corrected ratios $\frac{h_{A_2}(\omega)}{h_{A_1}(\omega)}$ and $\frac{h_{A_3}(\omega)}{h_{A_1}(\omega)}$ are plotted in figure 5.13. Since $h_{A_1}(\omega)$ has vanishing $\frac{1}{m_Q}$ corrections, one has

$$\frac{h_{A_2}(\omega)}{h_{A_1}(\omega)} \left[\frac{1 + \beta_{A_1}(\omega)}{1 + \beta_{A_2}(\omega)} \right] = \gamma_{A_2}(\omega) \quad (5.25)$$

$$\frac{h_{A_3}(\omega)}{h_{A_1}(\omega)} \left[\frac{1 + \beta_{A_1}(\omega)}{1 + \beta_{A_3}(\omega)} \right] = 1 + \gamma_{A_3}(\omega) . \quad (5.26)$$

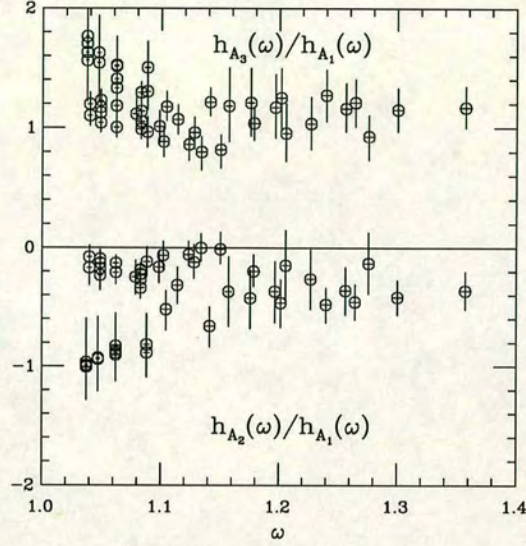


Figure 5.13: The ratios $\frac{h_{A_2}(\omega)}{(1+\beta_{A_2}(\omega))} / \frac{h_{A_1}(\omega)}{(1+\beta_{A_1}(\omega))}$ and $\frac{h_{A_3}(\omega)}{(1+\beta_{A_3}(\omega))} / \frac{h_{A_1}(\omega)}{(1+\beta_{A_1}(\omega))}$ at $\kappa_q = 0.14144$.

The interesting feature is that γ_{A_2} and γ_{A_3} have opposite signs :

$$\gamma_{A_3} > 0, \quad (5.27)$$

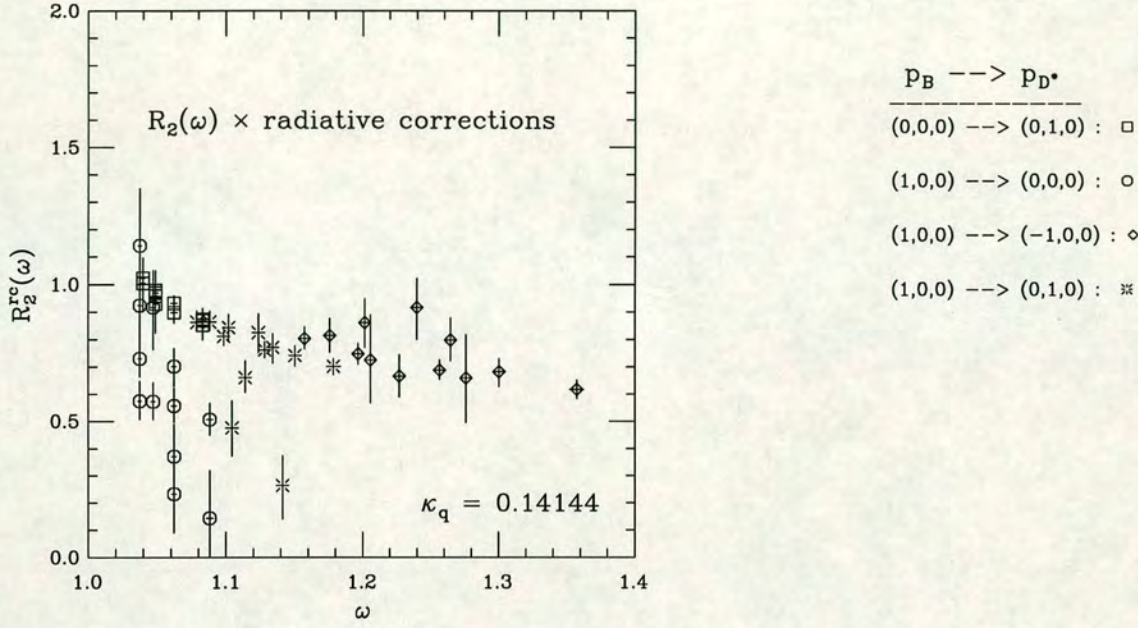
$$\gamma_{A_2} < 0. \quad (5.28)$$

The data is too noisy to detect any significant dependence of the $\frac{1}{m_Q}$ corrections on the velocity transfer.

In figure 5.14 the ratio

$$R_2 = \frac{h_{A_3}(\omega) + \frac{m_{D^*}}{m_B} h_{A_2}(\omega)}{h_{A_1}(\omega)} \quad (5.29)$$

is plotted as a function of ω . Radiative corrections have been applied and are found to be negligible. Recall from chapter 1 that this ratio relates the form factor $\hat{\rho}$ arising in the expression for the decay rate of $\bar{B} \rightarrow D^* l \bar{\nu}$ to the form factor of the Isgur-Wise function ρ . As in figure 5.12 different momenta have been assigned different symbols. Were it not for some wild fluctuations for the values of R_2 obtained from the momentum $(1, 0, 0) \rightarrow (0, 0, 0)$ (given by the octagons) this

Figure 5.14: The ratio $R_2(\omega)$ at $\kappa_q = 0.14144$.

result could be taken as evidence for the relation $R_2(1) = 1$ which corresponds to the exact heavy quark limit.

In figure 5.15 I show a subset of the values of $R_2(\omega)$ for fixed mass of the b quark and four values of the c quark. The errors for R_2 for this data are very small due to the cancellations in the ratio of form factors. The systematic error is therefore even more pronounced in figure 5.15 and the discrepancy of the values of $R_2(\omega)$ close to $\omega = 1$ is not reconcilable. I have presented some possible explanations as to why this momentum combination does not allow for a precise determination of $h_{A_2}(\omega)$ and $h_{A_3}(\omega)$. It is most likely that R_2 is strongly affected by lattice artefacts and the systematic errors due to different $\mathcal{O}(am)$ effects of the components $A^{\mu\nu}$ that are used to extract form factors with different momenta. It is therefore not possible to present any definitive conclusions on this quantity and its dependence on ω . However, it is most likely that

$$R_2(\omega) \leq 1. \quad (5.30)$$

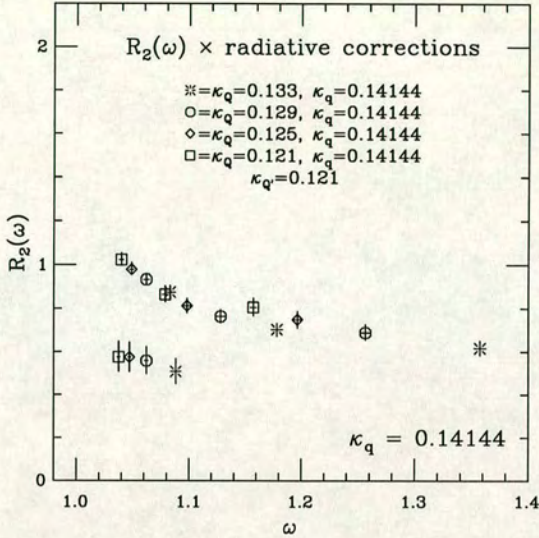


Figure 5.15: The ratio $R_2(\omega)$ for $\kappa_Q = 0.121$ and four values of $\kappa_{Q'}$ at $\kappa_q = 0.14144$.

5.8 Vector Current

In this section the vector form factor relevant to $\bar{B} \rightarrow D^* l \bar{\nu}$ decay is extracted. The Minkowski matrix element is parametrised in terms of the single function $h_V(\omega)$ as follows :

$$\langle D_r^* | V^\mu | \bar{B} \rangle = i h_V(\omega) \epsilon_r^{*\beta} \epsilon^{\mu\beta\lambda\sigma} v'_\lambda v_\sigma . \quad (5.31)$$

Defining

$$V^{\mu\nu} := \sum_r \epsilon_r^{\nu*} \langle D_r^* | V^\mu | \bar{B} \rangle \quad (5.32)$$

and performing the sum over polarisations one finds :

$$\begin{aligned} V^{\mu\nu} &= 2im_B m_{D^*} h_V(\omega) \sum_r \epsilon_r^{\nu*} \epsilon^{\mu\beta\lambda\sigma} \epsilon^{\beta*} v'_\lambda v_\sigma \\ &= \frac{i h_V(\omega)}{\sqrt{m_B m_{D^*}}} g^{\nu\beta} \epsilon^{\mu\beta\lambda\sigma} v'_\lambda v_\sigma \end{aligned} \quad (5.33)$$

where I have converted back to a mass-dependent normalisation. Summing over $\sigma = 0, 1$ - only the correlator for $\vec{p}_B = (0, 0, 0)$ and $(1, 0, 0)$ is calculated - gives a set of relations

$$\begin{aligned} V^{23} &= -V^{32} = \frac{i h_V(\omega)}{\sqrt{m_B m_{D^*}}} \{ p_{D^*}^1 E_B - E_{D^*} p_B^1 \} , \\ V^{12} &= -V^{21} = \frac{i h_V(\omega)}{\sqrt{m_B m_{D^*}}} p_{D^*}^3 E_B , \\ V^{31} &= -V^{13} = \frac{i h_V(\omega)}{\sqrt{m_B m_{D^*}}} p_{D^*}^2 E_B . \end{aligned} \quad (5.34)$$

For $\vec{p}_B = (0, 0, 0)$ all components are averaged whereas for $\vec{p}_B = (1, 0, 0)$ the first equation and the two lower equations are fitted simultaneously with the correlations between equations and time-slices taken into account.

Since the forward matrix element, $v = v' = \mathbf{0}$, vanishes, the lattice form factors $h_V^L(\omega)$ are normalised using the form factor $h_+^L(1)$:

$$h_V(\omega) = \frac{h_V^L(\omega)}{h_+^L(1)} (1 + \beta_+(1)) . \quad (5.35)$$

Figure 5.16 shows the results of these fits at the heaviest mass of the light spectator

quark for all heavy-quark and momentum combinations. The plateaus in these fits are far less pronounced than the ones for $h_+(\omega)$ and $h_{A_1}(\omega)$; different momenta need to be fitted on different plateaus, [(10, 11, 12); (11, 12, 13); (12, 13, 14)]. The statistical errors for the values of $h_V(\omega)$ are fairly large : this can be due partly to the fact that the matrix element is proportional to v^2 and partly to the fact that one cannot achieve too good a cancellation in the errors by normalising with a different form factor.

Clearly, $h_V(\omega)$ is not an Isgur-Wise function : there are large $\frac{1}{m_Q}$ corrections. For comparison, the form-factor $\frac{h_{A_1}(\omega)}{1+\beta_{A_1}(\omega)}$, which was shown to have vanishing corrections proportional to $\frac{1}{m_Q}$, is plotted as is the deviation of the ratio of both form factors from unity :

$$\frac{h_V(\omega)}{h_{A_1}(\omega)} \frac{(1 + \beta_{A_1}(\omega))}{(1 + \beta_V(\omega))} - 1 = R_1(\omega) \frac{(1 + \beta_{A_1}(\omega))}{(1 + \beta_V(\omega))} - 1 \quad (5.36)$$

$$\simeq \gamma_V(\omega). \quad (5.37)$$

where, in the last line, I have assumed that $\gamma_{A_1}(\omega) = 0$ for all ω . The plot shows that the ratio $\frac{h_V(\omega)}{h_{A_1}(\omega)} \frac{1+\beta_{A_1}(\omega)}{1+\beta_V(\omega)}$ is bigger than 1 by 10 to 30 %. Note that figure 5.16 shows all data at $\kappa_q = 0.14144$ regardless of the initial and final heavy quark masses although there may be different $\mathcal{O}(\frac{1}{m_Q})$ corrections within the data-set. However, since the errors are slightly larger compared to those of $h_{A_1}(\omega)$. I shall make no attempt at finding the exact mass dependence of the function $\gamma_V(\omega)$. The deviation of the radiatively corrected $R_1(\omega)$ from 1 exhibits a linear behaviour in ω with a small positive slope. The discontinuity at around $\omega = 1.2$ is interpreted as a statistical fluctuation; indeed, this function is smoothed out for the data at lighter masses of the spectator quark.

In eq. (5.36) the perturbative symmetry-breaking corrections have been explicitly factored out. Equivalently (see chapter 1) one can write :

$$R_1(\omega) = F_1(\omega) \left(1 + \frac{2\epsilon_c}{\omega + 1} + \frac{2\epsilon_b}{\omega + 1} [1 - 2F_2(\omega)\eta(\omega)] \right), \quad (5.38)$$

where the perturbative functions F_1 and F_2 can be found in chapter 1. Both the QCD and the $\frac{1}{m_c}$ corrections are positive, so that the deviations from 1 are expected to be large. To determine a value of R_1 at $\omega = 1$ I perform a fit to all

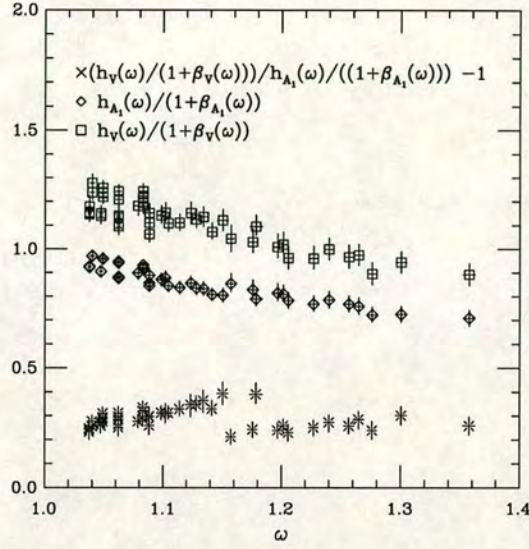


Figure 5.16: The form factors $h_V(\omega)$ and $h_{A_1}(\omega)$ and $R_1(\omega) \frac{(1+\beta_{A_1}(\omega))}{(1+\beta_V(\omega))} - 1$ at $\kappa_q = 0.14144$.

data points $\frac{h_V(\omega)}{(1+\beta_V(\omega))}$ to the function $N\xi_{\text{BSW}}$ where

$$R_1(1) = \frac{h_V(1)}{h_{A_1}(1)} = N \frac{[1 + \beta_V(1)]}{[1 + \beta_{A_1}(1)]} \quad (5.39)$$

This fit, for $\kappa_1 = 0.14144$ is shown in figure 5.17. I find a normalisation of $N = 1.3(3)$; to convert this value to a prediction for $R_1(1)$, N is multiplied by the radiative factors $\frac{[1+\beta_V(1)]}{[1+\beta_{A_1}(1)]}$ which leads to a value of $R_1(1) = 1.4(3)$. This is in good agreement with the experimental determination of the CLEO collaboration, $R_1(1) = 1.3(3)$ and also with QCD sum rule calculations, $R_1(1) = 1.3(1)$.

Studying the light quark dependence of the form factor $h_V(\omega)$ and the ratio $R_1(\omega)$ proves difficult as the data becomes a lot noisier towards lighter spectator quark masses. Performing BSW fits to $\frac{h_V(\omega)}{(1+\beta_V(\omega))}$ one finds a downward trend in the normalisation N . This is also true of $R_1(\omega) \frac{(1+\beta_{A_1}(\omega))}{(1+\beta_V(\omega))} - 1$ whose chirally extrapolated values are shown in figure 5.18. This seems to indicate values of $R_1(1)$ which are rather closer to the heavy quark limit, $R_1(1) = 1$ than the one found above. However the data close to $\omega = 1$ are very unclear as to whether the ratio tends to $R_1(1) = 1$, as in the heavy-quark limit, or to a larger value. I shall therefore

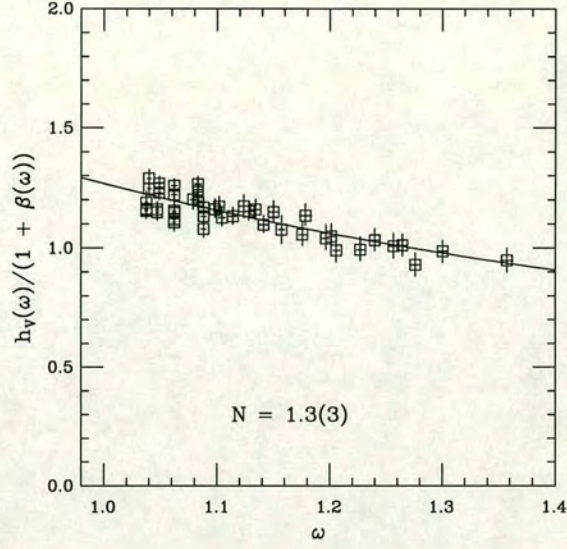


Figure 5.17: A BSW fit to the data $\frac{h_V(\omega)}{(1+\beta_V(\omega))}$ at $\kappa_q = 0.14144$ for all heavy quark masses and momentum combinations.

only use the chirally extrapolated data to correct the value of $R_1(1)$ found at $\kappa_q = 0.14144$ to a marginally lower value :

$$R_1(1) = 1.3 \pm 3 \quad (5.40)$$

The $\frac{1}{m_b}$ corrections to R_1 depend solely on the subleading form factor $\eta(\omega)$, the functions $\chi_i(\omega)$, due to insertions of higher order operators in the heavy quark lines do not appear. This allows one, in principle, to extract $\eta(\omega)$, once the parameter $\bar{\Lambda}$ is fixed. Following the discussion of section 4.6, I set $\bar{\Lambda}_{4144} = 0.63 \text{ GeV}$. The resulting values for $\eta(\omega)$ are shown in figure 5.19. Unfortunately, the result is not very clear as there are large fluctuations in $\eta(\omega)$ for values of ω which are close. One can only put very mild bounds on $\eta(\omega)$:

$$0 < \eta(\omega) < 1. \quad (5.41)$$

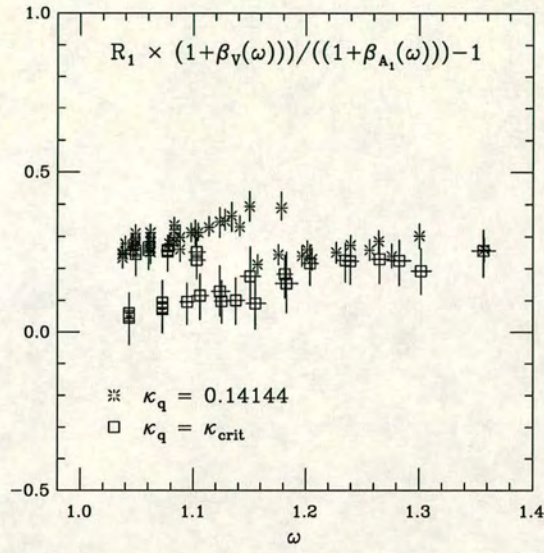


Figure 5.18: The $R_1(\omega) \frac{(1 + \beta_{A_1}(\omega))}{(1 + \beta_V(\omega))} - 1$ at a massless spectator quark and at a spectator quark of $\kappa_q = 0.14144$.

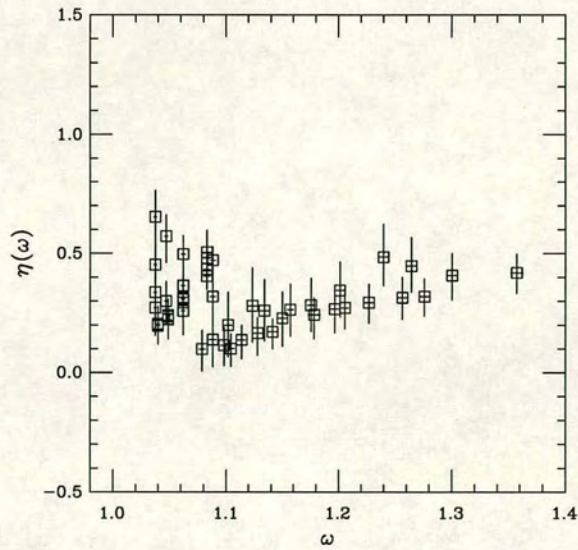


Figure 5.19: The subleading form factor $\eta(\omega)$ at $\kappa_q = 0.14144$.

Chapter 6

Discussion and Phenomenological Applications

In this chapter the results of chapters 4 and 5 are summarised. In section 6.2 the element V_{cb} of the quark-mixing matrix is determined in a model-independent fashion using the lattice value of the slope of the Isgur-Wise function. The results are compared to those of other authors.

6.1 Slope of the Isgur-Wise Function

In chapters 4 and 5 the two form factors $h_+(\omega)$ and $h_{A_1}(\omega)$ were tested for heavy quark symmetry violations. Unfortunately, this was only possible in the velocity interval $1 < \omega < 1.1$ where $\mathcal{O}(\frac{1}{m_Q})$ effects for both form factors are expected to be small due to Luke's Theorem. This theorem states that violations to the heavy quark symmetry limit to the radiatively corrected form factors $h_+(\omega)$ and $h_{A_1}(\omega)$ are of $\mathcal{O}(\frac{1}{m_Q^2})$ only at $\omega = 1$. Neither of the two form factors exhibited any $\mathcal{O}(\frac{1}{m_Q})$ corrections in the regime $\omega < 1.1$. Simple tests indicate that these effects remain small over the whole velocity interval $1 < \omega < 1.4$. Fits to the BSW function showed no variation in the slope factors when fitting data of different initial or final heavy quark masses. However, the ratio $\frac{h_{A_1}(\omega)}{h_+(\omega)}$ shows a small upward trend and is consistent with $\mathcal{O}(\frac{1}{m_Q})$ corrections as large as 4% at $\omega = 1.4$.

Both form factors were used independently to extract the slope of the Isgur-Wise function at zero recoil. Only data with $\omega < 1.1$ was used. To minimise the systematic error the momentum combination $\vec{p}_B = \mathbf{0} \rightarrow \vec{p}_{D^*} = (0, 1, 0)_{av}$ was fitted, where the final momentum is the average of six momenta. In these fits, the values of the form factors at zero recoil was fixed to 1. Correlations between the data was not taken into account. In the chiral limit the two determinations yield

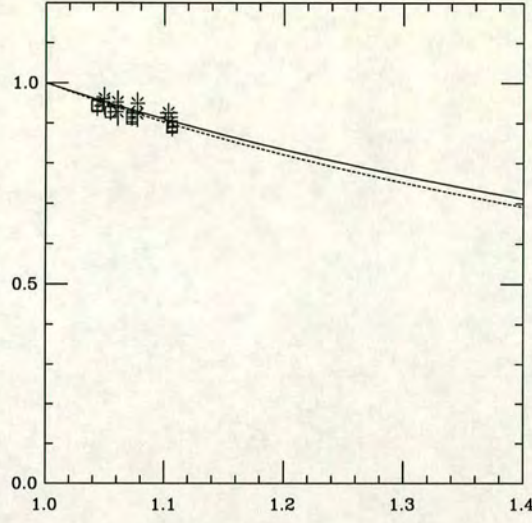


Figure 6.1: Determinations of the slope of the Isgur-Wise function using correlated least- χ^2 -fits from data obtained for the form factors $h_+(\omega)$ and $h_{A_1}(\omega)$.

the slopes

$$\rho_{u,d}^2 = 1.2_{-3}^{+3}(\text{stat.})_{-3}^{+2}(\text{syst.}) \quad \text{for } h_+(\omega), \quad (6.1)$$

$$\rho_{u,d}^2 = 0.9_{-3}^{+5}(\text{stat.})_{-2}^{+4}(\text{syst.}) \quad \text{for } h_{A_1}(\omega). \quad (6.2)$$

The statistical error can be further reduced by performing correlated fits : reassuringly these fits bring the two values of ρ^2 even closer. One finds :

$$\rho_{u,d}^2 = 1.0_{-2}^{+2}(\text{stat.}) \quad \text{for } h_+(\omega), \quad (6.3)$$

$$\rho_{u,d}^2 = 1.1_{-2}^{+2}(\text{stat.}) \quad \text{for } h_{A_1}(\omega), \quad (6.4)$$

and these two fits are shown in figure 6.1. The correlations in the data are high; this can lead to rather peculiar effects [123] which is why I have chosen to exclude correlations when fitting the form factors to different functions of ω in chapters 4 and 5. It is possible that one such effect of high correlations can be seen in figure 6.1 : although none of the data for $h_{A_1}(\omega)$ lies below $h_+(\omega)$ fitting $h_{A_1}(\omega)$ leads to the smaller slope. In this case the effect is fairly small as both values of ρ^2 of

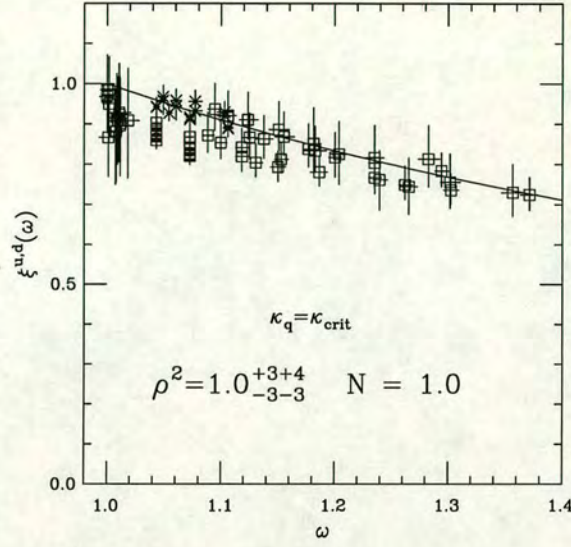


Figure 6.2: The combined data for the form factors $h_{A_1}(\omega)$ and $h_+(\omega)$ and the best fit to the function $\xi_{\text{BSW}}(\omega)$ using the points denoted by *. The systematic error encompasses the slopes obtained from fits to all data points to the two functions $\xi_{\text{BSW}}(\omega)$ and $N\xi_{\text{BSW}}(\omega)$.

the correlated fit are consistent with those of the uncorrelated fit.

Figure 6.2 shows the combined data for $h_{A_1}(\omega)$ and $h_+(\omega)$ for all heavy quark masses in the chiral limit. I have combined the above fit results of eq. (6.3) to find a value

$$\rho_{u,d}^2 = 1.0^{+3}_{-3}(\text{stat.})^{+4}_{-3}(\text{syst.}). \quad (6.5)$$

Other parametrisations yield values which are consistent with eq. (6.5).

In table 6.1 I compare the lattice result of this work with those of other authors. There is only one other lattice value available to date [120] which is obtained working with a mass of the light anti-quark of around the strange mass. This value should therefore be compared to the value of ρ_s^2 which I present below.

The value of ρ^2 of this work is safely above the lower bound of Bjorken [38] and below any of the upper bounds obtained by various authors.

The light quark behaviour of the Isgur-Wise function was also studied. Interpolated

Reference	$-\xi'_{u,d}(1)$
This work (UKQCD)	$1.0^{+3}_{-3}(\text{stat})^{+4}_{-3}(\text{syst})$
Bernard, Shen and Soni[120]	$1.24(26)(\text{stat.})(26)(\text{syst.})$
de Rafael and Taron[48]	$\rho^2 < 1.42$
Close and Wambach[137]	$1.35 + \mathcal{O}((\omega - 1)^2)$
Neubert[1]	$0.66(5)$
Voloshin[45]	$1.4(3)$
Bjorken[38]	$\rho^2 > 0.25$
Blok and Shifman[47]	$0.35 < \rho^2 < 1.15$
Hogaasen and Sadzikowski[133]	0.98
Rosner[136]	$1.59(43)$
Burdman[43]	$1.08(10)$
Dai, Huang and Jin[138]	$1.05(20)$

Table 6.1: Comparison of this lattice result for $-\xi'_{u,d}(1)$ to the theoretical predictions of various authors.

tions in the light quark mass of the data yield the value of the Isgur-Wise function at the mass of the strange quark. The same strategy is adopted to find the central values and errors as in the chiral limit. The two values obtained from independent fits to $h_{A_1}(\omega)$ and $h_+(\omega)$,

$$\rho_s^2 = 1.2^{+2}_{-2}(\text{stat.}) \quad \text{for } h_+(\omega), \quad (6.6)$$

$$\rho_s^2 = 1.0^{+3}_{-3}(\text{stat.}) \quad \text{for } h_{A_1}(\omega), \quad (6.7)$$

are combined to give

$$\rho_s^2 = 1.1^{+3}_{-3}(\text{stat.})^{+3}_{-1}(\text{syst.}). \quad (6.8)$$

The best fits and the complete data set are shown in figure 6.3.

Comparing the values of ρ^2 in the chiral limit and at the strange mass one finds a slight decrease of the slope parameter with decreasing light anti-quark mass. The light quark dependence is however rather weak and consistent with an Isgur-Wise function which is independent of the mass of the light spectator quark. The behaviour found here is in agreement with the calculations of ref. [133] and ref. [137]. The first calculation is based on an improved bag model and is an extension of earlier work by the authors of ref. [134]. The authors of ref. [137] have analysed the form factors in an improved ISGW quark-model and find values which are also close to the QCD sum rule result of ref. [1]. It is noted however

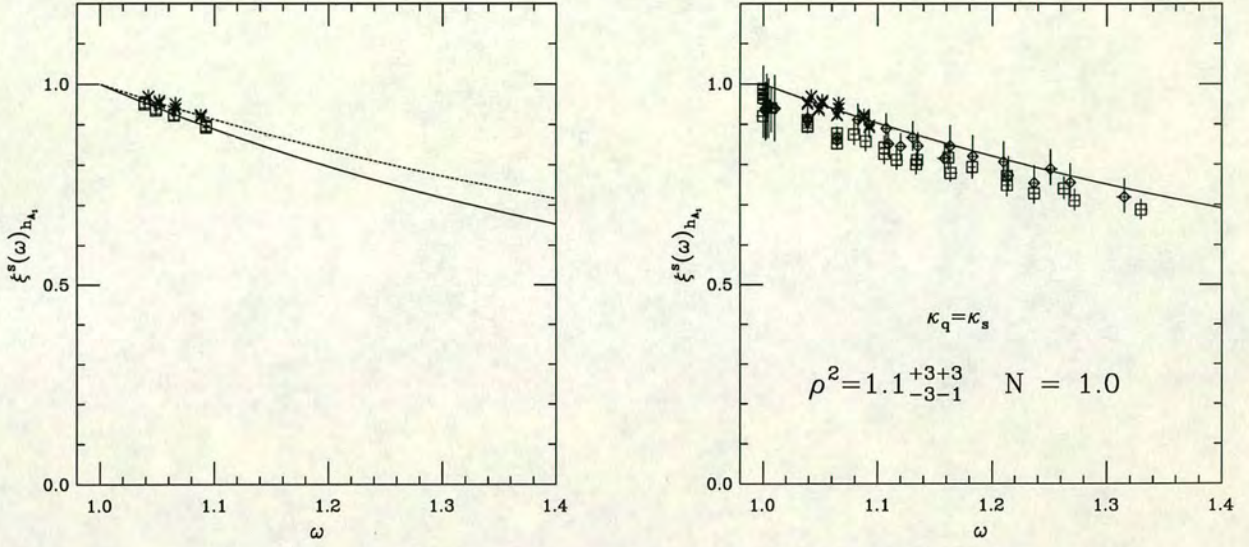


Figure 6.3: The combined data for the form factors $h_{A_1}(\omega)$ and $h_+(\omega)$ and the best fit to the function $\xi_{BSW}(\omega)$ using only the momentum $(1, 0, 0) \rightarrow (0, 0, 0)$ fitted to $\xi_{BSW}(\omega)$ at the mass of the strange spectator quark.

that a contradicting result is obtained in Chiral Perturbation Theory [139].

6.2 Extraction of V_{cb}

In chapter 1 I showed how data of the decay rate $\bar{B} \rightarrow D^* l \bar{\nu}$ can be used to extract the CKM matrix element V_{cb} once the slope of the Isgur-Wise function and the $\frac{1}{m_Q}$ corrections are known. Schematically :

$$\frac{d\Gamma}{d\omega}(\bar{B} \rightarrow D^* l \bar{\nu}) = \mathcal{K} \eta_A^2 \hat{\xi}^2(\omega) \left[1 + \frac{4\omega}{\omega+1} \frac{1-2\omega r + r^2}{(1-r)^2} \right] |V_{cb}|^2, \quad (6.9)$$

where \mathcal{K} are known factors, η_A^2 are the known radiative corrections at $\omega = 1$ and $\hat{\xi}(\omega)$ is related to the form factor $h_{A_1}(\omega)$ through

$$\hat{\xi}^2(\omega) = \frac{\left[2 \frac{(1-2\omega r + r^2)}{(1-r)^2} \left[1 + \frac{(\omega-1)}{(\omega+1)} R_1^2(\omega) \right] + \left[1 - \frac{(\omega-1)}{(1-r)} (1 - R_2(\omega)) \right]^2 \right] |h_{A_1}(\omega)|^2}{\left[1 + \frac{4\omega}{(\omega+1)} \frac{(1-2\omega r + r^2)}{(1-r)^2} \right] \eta_A^2}. \quad (6.10)$$

The slope of $\hat{\xi}$ is related to the slope of the Isgur-Wise function via eq. (1.96)

$$\hat{\rho}^2 = \rho^2 - \frac{1}{6}[R_1^2(1) - 1] - \frac{1}{3} \frac{m_B}{m_B - m_{D^*}}[1 - R_2(1)] + (0.21 \pm 0.02) + \mathcal{O}\left(\frac{1}{m_Q}\right).$$

In the previous section a precise value of the slope of the Isgur-Wise function ρ^2 has been determined and it was also found that the $\mathcal{O}(\frac{1}{m_Q})$ corrections are negligible. In chapter 5 the ratio $R_1(1)$ was determined :

$$R_1(1) = 1.3 \pm 0.3, \quad (6.11)$$

which agrees well with the experimental value from CLEO [70] and predictions from QCD sum rules [1]. However, it was not possible to extract the ratio $R_2(1)$. I shall therefore use the experimental result obtained by the CLEO-collaboration:

$$R_2(1) = 0.6 \pm 0.3 \quad \text{CLEO [70]}, \quad (6.12)$$

to predict :

$$\hat{\rho}^2 = \rho^2 - 0.1 \pm 0.1. \quad (6.13)$$

The uncertainty in this result is due to that of the values of $R_2(1)$ and $R_1(1)$. This result can now be used in conjunction with the lattice value of ρ^2 and the measurements of $\frac{d\Gamma}{d\omega}(\bar{B} \rightarrow D^* l \bar{\nu})$ to calculate the product $|V_{cb}|\hat{\xi}(1) = |V_{cb}|[1 + \mathcal{O}(\frac{1}{m_Q^2})]$. Although one can expect the corrections of order $\frac{1}{m_Q^2}$ to be small since the calculation has shown that corrections at order $\frac{1}{m_Q}$ are negligible, this issue could not be resolved by the lattice simulation. This is partly due to the fact that the lattice currents need to be related to the continuum \overline{MS} currents through renormalisation constants whose calculation introduces an error of $\mathcal{O}(\frac{1}{m_Q^2})$ at $\omega = 1$. However, for the case of elastic scattering, current conservation implies that these corrections vanish to all orders in $\frac{1}{m_Q}$ at zero recoil. Since I have not seen a different behaviour of the elastic and inelastic scattering when extracting values of ρ^2 , the $\mathcal{O}(\frac{1}{m_Q^2})$ are predicted to be negligible. I therefore set

$$|V_{cb}|\hat{\xi}(1) = |V_{cb}|. \quad (6.14)$$

As there is some consensus [76] that the $\mathcal{O}(\frac{1}{m_Q^2})$ corrections are negative, the extracted values of $|V_{cb}|$ can be regarded as lower bounds.

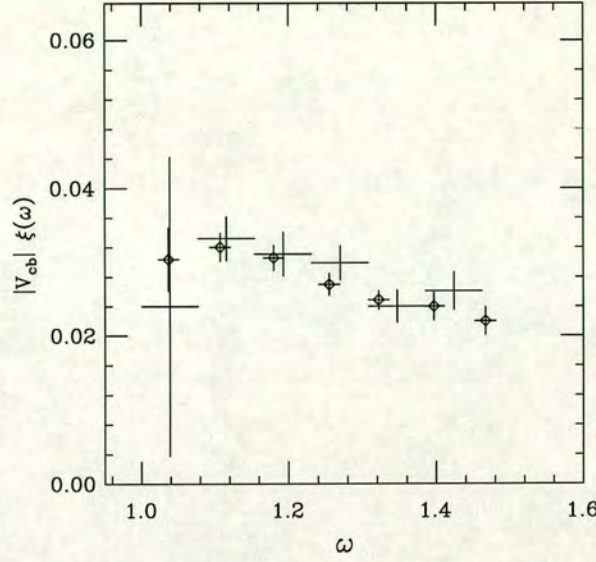


Figure 6.4: Data of the decay rate $\bar{B} \rightarrow D^* l \bar{\nu}$ obtained by the CLEO Collaboration. The diamonds represent the most recent data of ref. [71, 72] and the + are the data previously presented by CLEO (taken from ref. [140]).

In figure 6.4 I show a plot of a very recent measurement [71, 72]¹ of the decay rate $\frac{d\Gamma}{d\omega}(\bar{B} \rightarrow D^* l \bar{\nu})$ with the previous results of the same collaboration [140]. The plot gives an indication of the improvement which has been achieved in the measurement of the decay rate. Unfortunately, the most recent data has not been made available. To determine V_{cb} I shall therefore use data obtained by the CLEO and ARGUS collaborations which was compiled in ref. [140].

To start I perform two-parameter fits of the experimental data to the parametrisations $|V_{cb}|\xi_{BSW}(\omega)$ and $|V_{cb}|\xi_{lin}(\omega)$. The two parameters are $\hat{\rho}^2$ and V_{cb} and the results for these parameters are summarized in table 6.2. Using the BSW parametrisation yields a rather high value of $\hat{\rho}^2$ for the ARGUS data. I note however that much improved data has been presented in ref. [46].

Next I turn to determinations of V_{cb} combining the experimental data with the lattice results of this thesis. In figure 6.5 I show least- χ^2 -fits to the experimental

¹I have taken the liberty of reading off the data from figure 12 in ref. [72]. These new data points are therefore not exact.

Experiment	$\xi_{\text{BSW}}(\omega)$			$\xi_{\text{lin}}(\omega)$		
	$ V_{\text{cb}} $	$\hat{\rho}^2$	$\chi^2/d.o.f.$	$ V_{\text{cb}} $	$\hat{\rho}^2$	$\chi^2/d.o.f.$
ARGUS	0.046(2)	2.4(1)	3.6/6	0.039(2)	1.2(1)	4.4/6
CLEO II	0.037(2)	1.2(1)	2.4/4	0.035(1)	0.8(1)	2.4/4

Table 6.2: Results for $|V_{\text{cb}}|$ and the slope parameter $\hat{\rho}^2$ from a fit of $|V_{\text{cb}}|\xi_{\text{BSW}}(\omega)$ and $|V_{\text{cb}}|\xi_{\text{lin}}(\omega)$ to experimental data. The experimental data are obtained from the differential branching ratio for $\bar{B} \rightarrow D^* l \bar{\nu}$ decays assuming a B meson lifetime of 1.63ps [74]. The quoted errors are simple gaussian χ^2 -errors and do not include systematics. They must therefore not be taken too seriously. The data have been compiled by [140]. These values should be compared with the values obtained recently in references [46, 72, 73] which I have presented on page 31. Out of curiosity I note that performing similar fits to the new CLEO data [72] I find values of $\hat{\rho}_{\text{BSW}}^2 = 1.2(1)$, $|V_{\text{cbBSW}}| = 0.0348(10)$ and $\hat{\rho}_{\text{lin}}^2 = 0.8(1)$ and $|V_{\text{cblin}}| = 0.0334(10)$. These values compare rather well with those obtained with a more sophisticated fitting procedure by the CLEO collaboration.

Experiment	$ V_{\text{cb}} $	$\chi^2/d.o.f.$
ARGUS	$0.033(2)^{+2+}_{-2-}{}^{3+}_{-2-}{}^1_{-1}$	9.6/7
CLEO II	$0.036(1)^{+1+}_{-2-}{}^{4+}_{-2-}{}^1_{-1}$	2.7/5

Table 6.3: Results for $|V_{\text{cb}}|$ from a fit of $|V_{\text{cb}}|\hat{\xi}_{\text{BSW}}(\omega)$ to experimental data with $\hat{\xi}_{\text{BSW}}(\omega)$ fixed by the lattice computation. The experimental data are obtained from the differential branching ratio for $\bar{B} \rightarrow D^* l \bar{\nu}$ decays assuming a B meson lifetime of 1.63ps [74]. In the $|V_{\text{cb}}|$ column, the first set of errors is due to experimental uncertainties, the second set of errors results from the lattice statistical errors on $\hat{\rho}^2$, the third, from the lattice systematic errors on $\hat{\rho}^2$ and the last from the uncertainty in the values of $R_{1,2}(1)$.

data for $|V_{\text{cb}}|\xi_{u,d}(\omega)$ where the only parameter is $|V_{\text{cb}}|$. The slope $\hat{\rho}^2$ is obtained from the lattice value of the slope of the Isgur-Wise function, eq. (6.5), $\rho_{u,d}^2 = 1.0^{+3}_{-3}(\text{stat.})^{+4}_{-3}(\text{syst.})$, and eq. (6.13) to find :

$$\hat{\rho}^2 = 0.9^{+3}_{-3}(\text{stat.})^{+4}_{-3}(\text{syst.})^{+1}_{-1}(R_{1,2}), \quad (6.15)$$

where the last uncertainty is due to the errors of $R_1(1)$ and $R_2(1)$. The B meson lifetime is taken to be 1.63 ps [74]. The results of these fits are summarized in table 6.3.

The values of V_{cb} obtained using the lattice value of $\hat{\rho}^2$ are comparably low to the V_{cb} values obtained from two-parameter fits to the experimental data. Comparing

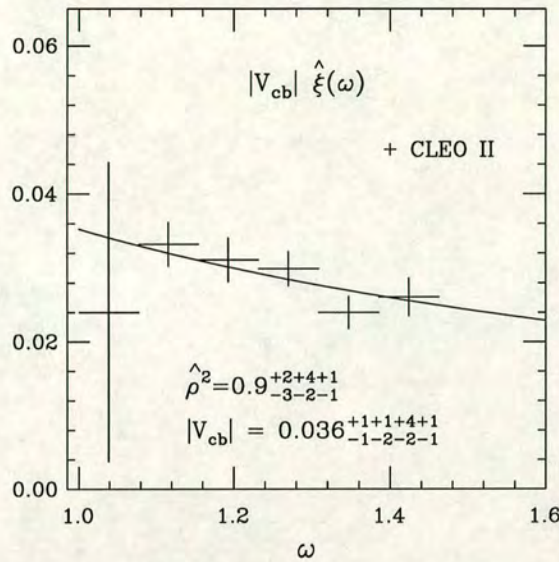


Figure 6.5: Determination of V_{cb} combining CLEO data and the lattice result of $\hat{\rho}^2$.

these results to the most recent world average of $V_{cb} = 0.040 \pm 0.003$ [76] is difficult since the data have improved rather drastically. I will therefore only point out the differences in the procedure I have adopted to extract a value of V_{cb} , to the procedure of ref. [76]. Firstly, I have set the $\mathcal{O}(\frac{1}{m_Q^2})$ corrections to zero at $\omega = 1$ whereas ref. [76] assumes these corrections to be $(-5.5 \pm 2.5)\%$. Including such a correction factor would, for example, increase the CLEO II value to $V_{cb, \text{LAT}} = 0.038(4)$. Another difference may be found in the different choice of function used to extrapolate the decay rate data. The results of table 6.3 have been obtained using the BSW function whereas ref. [76] performs linear fits and adds a value of 0.001 ± 0.001 to the V_{cb} obtained in this way.

6.3 Summary

I have presented a lattice QCD calculation of the matrix elements of the semi-leptonic decays $\bar{B} \rightarrow D l \bar{\nu}$ and $\bar{B} \rightarrow D^* l \bar{\nu}$. The simulation was performed in the quenched approximation on a sample size of 60 gauge configurations at three values of the light quark and four values of the initial and final heavy quark masses. To reduce lattice artefacts proportional to the lattice spacing a an $\mathcal{O}(a)$ improved

action proposed by Sheikholeslami and Wohlert was used.

The six form factors relevant to the decays $\bar{B} \rightarrow D l \bar{\nu}$ and $\bar{B} \rightarrow D^* l \bar{\nu}$ have been extracted. Clean signals enabled a precise determination of the form factors $h_{A_1}(\omega)$ and $h_+(\omega)$. Remaining lattice artefacts were investigated in a calculation of the renormalisation constant Z_V which relates the lattice current to its \overline{MS} equivalent. For the time component of the matrix element these effects are found to be relatively well under control, however, there is a rather large discrepancy, of the order of 15%, between the temporal and spatial components.

The data for $h_+(\omega)$ and $h_{A_1}(\omega)$ were fitted to several functions and it was found that the BSW parametrisation describes the ω -dependence of the data well. The large range of quark masses at which the calculation was performed allowed a detailed study of the heavy-quark dependence of the form factors. It was found that $\mathcal{O}(\frac{1}{m_Q})$ corrections are completely negligible in the range $1 \leq \omega \leq 1.1$. Thus, the form factors are effectively Isgur-Wise functions and they were used to extract the slope parameter ρ^2 .

Extrapolations to the chiral limit, in which the spectator anti-quark is massless, and interpolations to the strange quark mass were performed for $h_+(\omega)$ and $h_{A_1}(\omega)$. The light quark dependence of the Isgur-Wise function was found to be weak with a slight decrease of the slope with decreasing light quark mass.

The calculation of $h_-(\omega)$, $h_{A_2}(\omega)$, $h_{A_3}(\omega)$ and $h_V(\omega)$ proved more difficult. This is due in part to difficulties with the lattice normalisation procedure and errors proportional to the lattice spacing. The functions $h_{A_2}(\omega)$ and $h_{A_3}(\omega)$ are difficult to extract as the terms in the matrix elements proportional to $h_{A_2}(\omega)$ and $h_{A_3}(\omega)$ are very small compared to the $h_{A_1}(\omega)$ term. Ratios of form factors have been analysed in which several sub-leading form factors cancel. Even though these quantities suffer from large statistical and systematic uncertainties, the methods developed should prove useful when better statistics are available.

Finally, the obtained lattice values were used to calculate the slope parameter $\hat{\rho}^2$ relevant for an extraction of the CKM matrix element V_{cb} . Combining experimental data for the decay rate of $\bar{B} \rightarrow D^* l \bar{\nu}$ with this number a value of V_{cb} was obtained.

6.4 Conclusion

The calculation of three-point functions on the lattice in heavy quark physics is a relatively young field. In this thesis, I have demonstrated the feasibility and the usefulness of such calculations. For several quantities with small systematic errors model-independent predictions have been presented, adding useful information to the predictions of HQET which are limited to the kinematical endpoint $\omega = 1$.

Possibly the most surprising result is that the form factors $h_+(\omega)$ and $h_{A_1}(\omega)$ are found to be independent of the heavy and initial quark masses at which the simulation was performed. Thus, the heavy quark limit is reached at quark masses around that of the charm. This allows for an extraction of the slope of the Isgur-Wise function with rather small uncertainties. This slope factor, ρ^2 , is often used to extract the CKM matrix element V_{cb} . There are, however, corrections which need to be taken into account. These corrections are due to contributions of three other form factors, $h_{A_{2,3}}$ and h_V , contributing to the matrix elements $\bar{B} \rightarrow D^* l \bar{\nu}$. The lattice calculation of these form factors has proven to be very difficult as these form factors are kinematically suppressed and susceptible to errors proportional to the lattice spacing. This is also true for the extraction of subleading form factors contributing at $\mathcal{O}(\frac{1}{m_Q})$ to the matrix elements. Although higher statistics will certainly improve on the results presented here it seems questionable whether these quantities can be reliably extracted using the discretised action of Sheikholeslami and Wohlert. It is possible that other actions, such as a discretised version of the NRQCD action, will prove more successful in this mass regime.

References

- [1] M. Neubert, SLAC preprint SLAC-PUB-6263 (1993), to appear in Phys. Rep.
- [2] H. Georgi, in: Perspectives in the Standard Model, Proceedings of the Theoretical Advanced Study Institute in Elementary Particle Physics (TASI-91), Boulder, Colorado, 1991, edited by R.K. Ellis, C.T. Hill, and J.D. Lykken (World Scientific, Singapore, 1992), p. 589.
- [3] N. Isgur and M.B. Wise, in: Heavy Flavours, edited by A.J. Buras and M. Lindner (World Scientific, Singapore, 1992), p. 234.
- [4] T. Mannel, in: QCD-20 Years Later, Proceedings of the Workshop on QCD, Aachen, Germany, 1992, edited by P.M. Zerwas and H.A. Kastrup (World Scientific, Singapore, 1993), p. 634.
- [5] H.D. Politzer, Phys. Rev. Lett. **30**, 1346 (1973).
- [6] M. Suzuki, Nucl. Phys. B **258**, 553 (1985).
- [7] B. Grinstein, M.B. Wise, and N. Isgur, Phys. Rev. Lett. **56**, 298 (1986).
- [8] T. Altomari and L. Wolfenstein, Phys. Rev. Lett. **58**, 1583 (1987).
- [9] E.V. Shuryak, Phys. Lett. B **93**, 134 (1980); Nucl. Phys. B **198**, 83 (1982).
- [10] N. Isgur, D. Scora, B. Grinstein, and M.B. Wise, Phys. Rev. D **39**, 799 (1989).
- [11] J.E. Paschalis and G.J. Gounaris, Nucl. Phys. B **222**, 473 (1983); F.E. Close, G.J. Gounaris, and J.E. Paschalis, Phys. Lett. B **149**, 209 (1984).
- [12] S. Nussinov and W. Wetzel, Phys. Rev. D **36**, 130 (1987).
- [13] M.B. Voloshin and M.A. Shifman, Yad. Fiz. **45**, 463 (1987) [Sov. J. Nucl. Phys. **45**, 292 (1987)].

- [14] M.B. Voloshin and M.A. Shifman, *Yad. Fiz.* **47**, 801 (1988) [*Sov. J. Nucl. Phys.* **47**, 511 (1988)].
- [15] T. Appelquist and H.D. Politzer, *Phys. Rev. Lett.* **34**, 43 (1975).
- [16] N. Isgur and M.B. Wise, *Phys. Lett. B* **232**, 113 (1989); **237**, 527 (1990).
- [17] N. Isgur and M.B. Wise, *Phys. Rev. Lett.* **66**, 1130 (1991).
- [18] H.D. Politzer and M.B. Wise, *Phys. Lett. B* **206**, 681 (1988); **208**, 504 (1988).
- [19] M. Neubert, *Phys. Rev. D* **46**, 3914 (1992).
- [20] E. Eichten and F. Feinberg, *Phys. Rev. D* **23**, 2724 (1981).
- [21] W.E. Caswell and G.P. Lepage, *Phys. Lett. B* **167**, 437 (1986).
- [22] E. Eichten, in: *Field Theory on the Lattice*, edited by A. Billoire et al., *Nucl. Phys. B (Proc. Suppl.)* **4**, 170 (1988).
- [23] G.P. Lepage and B.A. Thacker, in: *Field Theory on the Lattice*, edited by A. Billoire et al., *Nucl. Phys. B (Proc. Suppl.)* **4**, 199 (1988).
- [24] E. Eichten and B. Hill, *Phys. Lett. B* **234**, 511 (1990); **243**, 427 (1990).
- [25] B. Grinstein, *Nucl. Phys. B* **339**, 253 (1990).
- [26] H. Georgi, *Phys. Lett. B* **240**, 447 (1990).
- [27] A.F. Falk, H. Georgi, B. Grinstein, and M.B. Wise, *Nucl. Phys. B* **343**, 1 (1990).
- [28] A.F. Falk, B. Grinstein, and M.E. Luke, *Nucl. Phys. B* **357**, 185 (1991).
- [29] M.E. Luke, *Phys. Lett. B* **252**, 447 (1990).
- [30] T. Mannel, W. Roberts and Z. Ryzak, *Nucl. Phys. B* **368**, 204 (1992).
- [31] M.A. Shifman, A.I. Vainshtein, and V.I. Zakharov, *Nucl. Phys. B* **120**, 316 (1977).
- [32] E. Witten, *Nucl. Phys. B* **122**, 109 (1977).

- [33] J. Polchinski, Nucl. Phys. B **231**, 269 (1984).
- [34] K. Wilson, Phys. Rev. **179**, 1499 (1969); Phys. Rev. D **3**, 1818 (1971).
- [35] W. Zimmermann, Ann. of Phys. **77**, 536 (1973); **77**, 570 (1973).
- [36] H. Georgi, B. Grinstein, and M.B. Wise, Phys. Lett. B **252**, 456 (1990).
- [37] A.F. Falk and M. Neubert, Phys. Rev. D **47**, 2965 (1993); **47**, 2982 (1993).
- [38] J.D. Bjorken, in: Results and Perspectives in Particle Physics, Proceedings of the 4th Rencontres de Physique de la Vallée d'Aoste, La Thuile, Italy, 1990, edited by M. Greco (Editions Frontières, Gif-sur-Yvette, 1990), p. 583; in: Gauge Bosons and Heavy Quarks, Proceedings of the 18th SLAC Summer Institute on Particle Physics, Stanford, California, 1990, edited by J.F. Hawthorne (SLAC Report No. 378, Stanford, 1991), p. 167.
- [39] A.F. Falk, Nucl. Phys. B **378**, 79 (1992).
- [40] M. Wirbel, B. Stech and M. Bauer, Z. Phys. C **29**, 637 (1985); M. Bauer, B. Stech, and M. Wirbel, Z. Phys. C **34**, 103 (1987).
- [41] M. Neubert, Phys. Rev. D **46**, 2212 (1992).
- [42] M. Neubert, Phys. Lett. B **264**, 455 (1991).
- [43] G. Burdman, Phys. Lett. B **284**, 133 (1992).
- [44] M. Neubert and V. Rieckert, Nucl. Phys. B **382**, 97 (1992).
- [45] M.B. Voloshin, Phys. Rev. D **46**, 3062 (1992).
- [46] H. Albrecht et al. (ARGUS collaboration), Z. Phys. C **57**, 533 (1993).
- [47] B. Blok and M. Shifman, Phys. Rev. D **47**, 2949 (1993).
- [48] E. de Rafael and J. Taron, Marseille preprint CPT-93/P.2908, June 1993.
- [49] M. Neubert, Phys. Rev. D **45**, 2451 (1992); **47**, 4063 (1993).
- [50] M. Neubert, V. Rieckert, B. Stech, and Q.P. Xu, in: Heavy Flavours, edited by A.J. Buras and M. Lindner (World Scientific, Singapore, 1992), p. 286.

- [51] A.V. Radyushkin, Phys. Lett. B **271**, 218 (1991).
- [52] M. Ademollo and R. Gatto, Phys. Rev. Lett. **13**, 264 (1964).
- [53] M. Luke and A.V. Manohar, Phys. Lett. B **286**, 348 (1992).
- [54] M. Neubert, Phys. Lett. B **306**, 357 (1993); Phys. Rev. D **49**, 1542 (1994).
- [55] A.F. Falk, M. Neubert, and M.E. Luke, Nucl. Phys. B **388**, 363 (1992).
- [56] N. Cabibbo, Phys. Rev. Lett. **10**, 531 (1963).
- [57] M. Kobayashi and K. Maskawa, Prog. Theor. Phys. **49**, 652 (1973).
- [58] A.J. Buras and M.K. Harlander, in: Heavy Flavours, edited by A.J. Buras and M. Lindner (World Scientific, Singapore, 1992), p. 58.
- [59] Y. Nir, in: The Third Family and the Physics of Flavour, Proceedings of the 20th SLAC Summer Institute on Particle Physics, Stanford, California, 1992, edited by L. Vassilian (SLAC Report No. 412, Stanford, 1993), p. 81; Y. Nir and H.R. Quinn, Annu. Rev. Nucl. Part. Sci. **42**, 221 (1992).
- [60] N. Cabibbo and L. Maiani, Phys. Lett. B **79**, 109 (1978).
- [61] Particle Data Group, K. Hikasa et al., Phys. Rev. D **45**, S1 (1992).
- [62] J. Chay, H. Georgi and B. Grinstein, Phys. Lett. B **247**, 399 (1990).
- [63] B.H. Smith and M.B. Voloshin, Minneapolis Report No. TPI-MINN-94/5-T (1994), hep-ph/9401357.
- [64] I. Bigi et al., CERN Report No. CERN-TH.7171/94 (1994), hep-ph/9402360.
- [65] M. Beneke and V.M. Braun, München Report No. MPI-PhT/94-9 (1994), hep-ph/9402364.
- [66] M. Neubert and C.T. Sachrajda, CERN Report No. CERN-TH.7312/94 (1994), hep-ph/9407394.
- [67] M. Luke, M. Savage and M. Wise, hep-ph 9409287.

- [68] R. Patterson, to appear in: Proceedings of the 27th International Conference on High Energy Physics, Glasgow, Scotland, July 1994.
- [69] F.J. Gilman and R.L. Singleton, Jr., Phys. Rev. D **41**, 142 (1990).
- [70] R. Kutschke (CLEO Collaboration), to appear in: Proceedings of the 27th International Conference on High Energy Physics, Glasgow, Scotland, July 1994.
- [71] T. Browder (CLEO Collaboration), to appear in: Proceedings of the 27th International Conference on High Energy Physics, Glasgow, Scotland, July 1994.
- [72] B. Barish et al. (CLEO Collaboration), Cornell preprint CNS 94/1285 (1994).
- [73] L. Scot (ALEPH Collaboration), to appear in: Proceedings of the 27th International Conference on High Energy Physics, Glasgow, Scotland, July 1994.
- [74] F. deJongh, to appear in: Proceedings of the 27th International Conference on High Energy Physics, Glasgow, Scotland, July 1994.
- [75] M. Shifman, N. G. Uraltsev and A. Vainshtein, Minnesota preprint TPI-MINN-94/13-T (1994).
- [76] M. Neubert, CERN preprint CERN-TH.7935/94 (1994).
- [77] K. G. Wilson, Phys. Rev. D **10**, 2445 (1974).
- [78] Proceedings of the 1992 symposium of Lattice Field Theory, Amsterdam, The Netherlands, Nucl. Phys. (Proc. Suppl.) B **30**; Proceedings of the 1993 symposium of Lattice Field Theory, Dallas, Texas, Nucl. Phys. (Proc. Suppl.) B **34**.
- [79] H. Nielsen and M. Ninomiya, Nucl. Phys. B **185**, 20 (1981).
- [80] T. Banks, J. Kogut and L. Susskind, Phys. Rev. D **13**, 1043 (1976).
- [81] K. G. Wilson, in New Phenomena in Subnuclear Physics, edited by A. Zichichi, Plenum, New York (1977).

- [82] B. Sheikholeslami & R. Wohlert, Nucl. Phys. B **259** (1985) 572.
- [83] G. Heatlie, C.T. Sachrajda, G. Martinelli, C. Pittori & G.C. Rossi, Nucl. Phys. B **352** (1991) 266.
- [84] G. Martinelli, C.T. Sachrajda & A. Vladikas, Nucl. Phys. B **358** (1991) 212.
- [85] UKQCD Collaboration, R. M. Baxter et al., Phys. Rev. D **49**, 1594 (1994).
- [86] G.P. Lepage & P.B. Mackenzie, Nucl. Phys. B (Proc. Suppl.) **20** (1991) 173; Fermilab Preprint FERMILAB-PUB-91-355-T-REV, September 1992.
- [87] A. S. Kronfeld, Nucl. Phys. (Proc. Suppl.) B **30**, 445 (1993).
- [88] UKQCD Collaboration, J. N. Simone et al., Nucl. Phys. (Proc. Suppl.) B **30**, 461 (1993).
- [89] C. W. Bernard, J. N. Labrenz and A. Soni, UW-PT-93-06, WASH-U-HEP-93-30, BNL-49068, hep-lat 9306009 (1993).
- [90] R. Sommer, Desy Preprint DESY 94-011, Wuppertal Preprint WUB 94-04, January 1994.
- [91] G. P. Lepage and B. A. Thacker, in: Field Theory on the Lattice, edited by A. Billoire et al., Nucl. Phys. B (proc. Suppl.) **4**, 199 (1988).
- [92] B. A. Thacker and G. P. Lepage, Phys. Rev. D **43** 196 (1991).
- [93] G. P. Lepage et al., Phys. Rev. D **46** 4052 (1992).
- [94] E. Eichten, in: Field Theory on the Lattice, edited by A. Billoire et al., Nucl. Phys. B (proc. Suppl.) **4**, 170 (1988).
- [95] J. E. Mandula and M. C. Ogilvie, hep-lat/9408006.
- [96] U. Aglietti and S. Capitani, Preprint Roma1 993-94, hep-ph/9401335.
- [97] J. Mehegan, Ph.D. Thesis, Physics Department, University of Edinburgh, unpublished (1994).
- [98] S. Duane et al., Phys. Lett. B **195**, 216 (1987).
- [99] F. Butler et al., Phys. Rev. Lett. **70**, 2849 (1993).

- [100] V. Lubicz et al., Phys. Lett. B **274**, 415 (1992).
- [101] C. Bernard, A. El-Khadra and A. Soni, Phys. Rev. D **45**, 869 (1992).
- [102] UKQCD Collaboration, D. Richards et al., Nucl. Phys. B (Proc. Suppl.) **34**, 411 (1994).
- [103] N. Cabibbo and E. Marinari, Phys. Lett. B **119**, 387 (1982).
- [104] R. D. Kenway, in Proceedings of XII International Conference on HEP, Leipzig (1984) 51, eds. A. Meyer and E. Wieczore.
- [105] A. Billoire, E. Marinari, and G. Parisi, Phys. Lett. B **162** (1985) 160.
- [106] S. Güsken et al., Nucl. Phys. B (Proc. Suppl.) **17** (1990) 361 and Phys. Lett. B **227**, 266 (1989).
- [107] E. Eichten, G. Hockney, and H. B. Thacker, Nucl. Phys. B (Proc. Suppl.) **17**, 529 (1990).
- [108] UKQCD Collaboration, C.R. Allton et al., Phys. Rev. D **47**, 5128 (1993).
- [109] A.D. Simpson, *Algorithms for lattice QCD*, Ph.D. thesis, University of Edinburgh (1991).
- [110] C. Bernard and A. Soni, Nucl. Phys. B (Proc. Suppl.) **9**, 155 (1989).
- [111] G. Martinelli and C.T. Sachrajda, Nucl. Phys. B **306**, 865 (1988).
- [112] M. Crisafulli, G. Martinelli, V.J. Hill, C.T. Sachrajda, Phys. Lett. B **223**, 90 (1989). V. Lubicz, G. Martinelli and C.T. Sachrajda, Nucl. Phys. B **356**, 301 (1991). V. Lubicz, G. Martinelli, M.S. McCarthy and C.T. Sachrajda, Phys. Lett. B **274**, 415 (1992).
- [113] C. Bernard, A. El-Khadra and A. Soni, Phys. Rev. D **43**, 2140 (1991).
C. Bernard, A. El-Khadra and A. Soni, Phys. Rev. D **45**, 869 (1992).
- [114] UKQCD Collaboration, Edinburgh Preprint 94/546, to be published.
- [115] A. Abada, et al., Nucl. Phys. B **416**, 675 (1994).
- [116] R. Gupta, T. Bhattacharya and D. Daniel, preprint LA UR-93-3580.

- [117] A. Abada et al., ELC and APE Collaborations, in Lattice'93, Nucl. Phys. B (Proc. Suppl.) **34**, 477 (1994).
- [118] UKQCD Collaboration, K. C. Bowler *et al.*, Phys. Rev. Lett. **72**, 1398 (1994), hep-lat 9311004.
- [119] C. Bernard, P. Hsieh, and A. Soni, Phys. Rev. Lett. **72**, 1402 (1994), hep-lat 9311011.
- [120] C. Bernard, Y. Shen, and A. Soni, Phys. Lett. B **317**, 164 (1993).
- [121] UKQCD Collaboration, S. P. Booth et al., Phys. Rev. Lett. **72**, 462 (1994).
- [122] C.W. Bernard and A. Soni, "Lattice Approach to Electroweak Matrix Elements", Brookhaven National Laboratory Preprint BNL-47585 (1992), to be published in "Quantum Fields on the Computer", ed.M.Creutz, World Scientific; A.S. Kronfeld and P.B. Mackenzie, "Progress in QCD using Lattice Gauge Theory", Fermilab Preprint PUB-93/058-T (1993), to be published in the Annual Review of Nuclear and Particle Science.
- [123] C. Michael, Phys. Rev. D **49**,2616 (1994).
- [124] W. H. Press et al., Numerical Recipes in C, Cambridge Press (1988).
- [125] B. Efron, SIAM Review **21**, 460 (1979).
- [126] UKQCD Collaboration, C.R. Allton et al. Phys. Lett. B **284**, 377 (1992).
- [127] UKQCD Collaboration, R.M. Baxter et al. Phys. Rev. D **49**, 1594 (1994).
- [128] UKQCD Collaboration, Edinburgh Preprint 94/545, unpublished.
- [129] G. Martinelli, S.Petrarca. C. T. Sachrajda and A. Vladikas, Phys. Lett. B **311**, 241 (1993).
- [130] A. Borelli, R. Frezotti, E. Gabrielli and C. Pittori, Nucl. Phys. B **409**, 382 (1993).
- [131] G. Lepage and P. Mackenzie, Phys. Rev. D **48**, 2250 (1993).
- [132] UKQCD Collaboration, C.R. Allton et al., Phys. Rev. D **49**, 474 (1994).

- [133] H. Hógaasen and M. Sadzikowski, Jagellonian University preprint TPJU-9-94 (February 1994), hep-ph 9402279.
- [134] M. Sadzikowski and K. Zalewski, Z. Phys. C **59**, 677 (1993).
- [135] B. Blok and M. Shifman, Phys. Rev. D **47**, 2949 (1993).
- [136] J. L. Rosner, Phys. Rev. D **42**, 3732 (1990).
- [137] F. E. Close and A. Wambach, Oxford University Theory Preprint OUTP - 94 09P, RAL-94-041 (1994).
- [138] Y. B. Dai, C. S. Huang and H. Y. Jin, Z. Phys. C **56**, 707 (1992).
- [139] E. Jenkins and M. J. Savage, Phys. Lett. B **281**, 331 (1992).
- [140] "Semileptonic B Decays", S. Stone, in "B Decays", ed. S. Stone, 2nd Edition (World Scientific, Singapore, 1994).

Appendix A

Two point Functions

Pseudoscalar Meson

Table A.4: Wavefunction factors, Z^2 , and energies, E_P for the heavy-light, pseudoscalar mesons and for two values of momentum, $|\mathbf{p}|$. The energies are quoted in lattice units ($a^{-1} \simeq 2.7\text{GeV}$ [127]). The $\chi^2/d.o.f.$ for the fits which give these results are all on the order of 1. The fitting range is $11 \leq t < 23$.

$\kappa_q = 0.14144$								
κ_Q	0.121		0.125		0.129		0.133	
$ \mathbf{p} $	Z^2	E_P	Z^2	E_P	Z^2	E_P	Z^2	E_P
0	18.0^{+6}_{-6}	0.924^{+2}_{-2}	16.4^{+5}_{-5}	0.823^{+2}_{-2}	14.5^{+5}_{-5}	0.716^{+2}_{-2}	12.5^{+4}_{-3}	0.600^{+2}_{-2}
$\pi/12a$	12.5^{+6}_{-6}	0.959^{+3}_{-3}	11.5^{+5}_{-5}	0.862^{+3}_{-3}	10.4^{+5}_{-5}	0.760^{+3}_{-3}	9.1^{+4}_{-4}	0.654^{+3}_{-3}
$\kappa_q = 0.14226$								
κ_Q	0.121		0.125		0.129		0.133	
$ \mathbf{p} $	Z^2	E_P	Z^2	E_P	Z^2	E_P	Z^2	E_P
0	15.5^{+6}_{-6}	0.901^{+3}_{-3}	14.2^{+6}_{-6}	0.800^{+3}_{-3}	12.8^{+5}_{-5}	0.693^{+3}_{-3}	11.0^{+4}_{-4}	0.576^{+3}_{-3}
$\pi/12a$	10.6^{+6}_{-6}	0.938^{+4}_{-4}	9.8^{+6}_{-5}	0.841^{+4}_{-4}	8.9^{+5}_{-5}	0.740^{+4}_{-3}	7.8^{+4}_{-4}	0.632^{+3}_{-3}
$\kappa_q = 0.14262$								
κ_Q	0.121		0.125		0.129		0.133	
$ \mathbf{p} $	Z^2	E_P	Z^2	E_P	Z^2	E_P	Z^2	E_P
0	14.7^{+8}_{-8}	0.892^{+4}_{-5}	13.5^{+7}_{-6}	0.791^{+4}_{-4}	12.1^{+6}_{-5}	0.683^{+4}_{-4}	10.4^{+5}_{-5}	0.566^{+3}_{-3}
$\pi/12a$	10.0^{+6}_{-7}	0.930^{+5}_{-5}	9.3^{+6}_{-6}	0.833^{+4}_{-5}	8.4^{+5}_{-5}	0.732^{+4}_{-5}	7.4^{+5}_{-4}	0.624^{+4}_{-4}

Vector Meson

Table A.5: Wavefunction factors, Z^2 , and energies, E_V for the heavy-light, vector mesons and for two values of momentum, $|\mathbf{p}|$. For details see section 5.4. The energies are quoted in lattice units ($a^{-1} \simeq 2.7\text{GeV}$ [127]). The $\chi^2/d.o.f.$ for the fits which give these results are all on the order of 1. The fitting range is $11 \leq t < 23$.

$\kappa_q = 0.14144$								
κ_Q	0.121		0.125		0.129		0.133	
$ \mathbf{p} $	Z^2	E_V	Z^2	E_V	Z^2	E_V	Z^2	E_V
0	25.6^{+8}_{-9}	0.944^{+3}_{-3}	25.5^{+8}_{-8}	0.847^{+2}_{-3}	25.1^{+8}_{-8}	0.745^{+3}_{-3}	24.2^{+7}_{-8}	0.638^{+3}_{-3}
$\pi/12a$	18.2^{+8}_{-9}	0.982^{+3}_{-4}	18.3^{+8}_{-9}	0.888^{+2}_{-3}	18.2^{+8}_{-8}	0.791^{+2}_{-3}	17.9^{+8}_{-8}	0.690^{+3}_{-3}
$\kappa_q = 0.14226$								
κ_Q	0.121		0.125		0.129		0.133	
$ \mathbf{p} $	Z^2	E_P	Z^2	E_P	Z^2	E_P	Z^2	E_P
0	$22.1^{+9}_{-1.0}$	0.921^{+3}_{-4}	22.1^{+9}_{-9}	0.823^{+4}_{-3}	21.8^{+9}_{-9}	0.722^{+4}_{-4}	21.2^{+8}_{-9}	0.614^{+4}_{-4}
$\pi/12a$	15.8^{+9}_{-8}	0.962^{+4}_{-4}	16.0^{+9}_{-8}	0.868^{+4}_{-4}	16.0^{+9}_{-7}	0.772^{+4}_{-4}	15.7^{+8}_{-7}	0.671^{+4}_{-4}
$\kappa_q = 0.14262$								
κ_Q	0.121		0.125		0.129		0.133	
$ \mathbf{p} $	Z^2	E_P	Z^2	E_P	Z^2	E_P	Z^2	E_P
0	$20.9^{+1.3}_{-1.1}$	0.911^{+6}_{-5}	$21.0^{+1.4}_{-1.1}$	0.814^{+6}_{-4}	$20.9^{+1.4}_{-1.2}$	0.712^{+6}_{-4}	$20.3^{+1.3}_{-1.2}$	0.605^{+6}_{-5}
$\pi/12a$	$14.9^{+1.1}_{-9}$	0.954^{+6}_{-6}	$15.1^{+1.1}_{-9}$	0.861^{+5}_{-6}	$15.3^{+1.1}_{-8}$	0.765^{+6}_{-5}	$15.1^{+1.2}_{-8}$	0.664^{+6}_{-6}

Heavy Quark Masses

Table A.6: Physical heavy-quark masses corresponding to different values the heavy-quark hopping parameter κ_Q . They are obtained from the corresponding chirally-extrapolated pseudoscalar and vector meson masses as described in section 4.4.1. For completeness I also tabulate the chirally-extrapolated meson masses in lattice units ($a^{-1} \simeq 2.7$ GeV [127]). These masses were obtained by linear extrapolation of the masses m_P and m_V obtained with the three values of the light antiquark hopping $\kappa_q = 0.14144, 0.14226, 0.14262$. The χ^2/dof for the chiral extrapolations are all on the order of 1. The meson masses were computed as described in section 5.4 and are listed above. All two-point functions are fitted on the range $11 \leq t < 23$.

κ_Q	m_P^x	m_V^x	m_Q [GeV]
0.121	0.875^{+4}_{-4}	0.895^{+5}_{-6}	1.90
0.125	0.774^{+4}_{-4}	0.797^{+5}_{-6}	1.64
0.129	0.666^{+4}_{-4}	0.695^{+5}_{-6}	1.36
0.133	0.548^{+4}_{-3}	0.586^{+5}_{-5}	1.06

Appendix B

Radiative Corrections

Table B.7: The radiative corrections $\beta^+(\omega)$ for the form factor $h_+(\omega)$ calculated according to Neubert's short-distance expansion [19]. For details see section 4.4.1.

	ω				
$\kappa_Q \rightarrow \kappa_{Q'}$	1.0	1.1	1.2	1.3	1.4
$0.121 \rightarrow 0.121$	0	-0.0245	-0.0472	-0.0683	-0.0881
$0.121 \rightarrow 0.125$	0.0166	-0.0075	-0.0301	-0.0511	-0.0709
$0.121 \rightarrow 0.129$	0.0372	0.0129	-0.0092	-0.0302	-0.0499
$0.121 \rightarrow 0.133$	0.0632	0.0401	0.0183	-0.0022	-0.0217
$0.125 \rightarrow 0.125$	0	-0.0234	-0.0452	-0.0654	-0.0845
$0.125 \rightarrow 0.129$	0.0240	0.0010	-0.0205	-0.0407	-0.0597
$0.125 \rightarrow 0.133$	0.0548	0.0325	0.0115	-0.0084	-0.0273
$0.129 \rightarrow 0.129$	0	-0.0219	-0.0423	-0.0614	-0.0793
$0.129 \rightarrow 0.133$	0.0386	0.0174	-0.0026	-0.0215	-0.0394
$0.133 \rightarrow 0.133$	0	-0.0194	-0.0378	-0.0549	-0.0710

Table B.8: The radiative corrections β_{A_1} for the form factor $h_{A_1}(\omega)$ calculated according to Neubert's short-distance expansion [19]. For details see section 4.4.1.

$\kappa_Q \rightarrow \kappa_{Q'}$	ω				
	1.0	1.1	1.2	1.3	1.4
$0.121 \rightarrow 0.121$	-0.0424	-0.0682	-0.0922	-0.1146	-0.1356
$0.121 \rightarrow 0.125$	-0.0305	-0.0484	-0.0651	-0.0808	-0.0956
$0.121 \rightarrow 0.129$	-0.0153	-0.0311	-0.0459	-0.0599	-0.0730
$0.121 \rightarrow 0.133$	0.0022	-0.0108	-0.0231	-0.0347	-0.0456
$0.125 \rightarrow 0.125$	-0.0453	-0.0702	-0.0934	-0.1151	-0.1354
$0.125 \rightarrow 0.129$	-0.0274	-0.0431	-0.0580	-0.0719	-0.0850
$0.125 \rightarrow 0.133$	-0.0059	-0.0185	-0.0305	-0.0417	-0.0524
$0.129 \rightarrow 0.129$	-0.0498	-0.0734	-0.0955	-0.1162	-0.1357
$0.129 \rightarrow 0.133$	-0.0209	-0.0332	-0.0449	-0.0559	-0.0664
$0.133 \rightarrow 0.133$	-0.0579	-0.0796	-0.0999	-0.1191	-0.1371

Appendix C

Pseudoscalar \rightarrow Pseudoscalar

C.1 $h_+(\omega)$ and $h_-(\omega)$ at fixed light quark mass.

This appendix lists all values of the form factors $h_+(\omega)$ and $h_-(\omega)$ of the decay $\bar{B} \rightarrow D l \bar{\nu}$. For details of the fitting method see section 4.

In the following tables I use the notation :

- $h_+^L(\omega)$ = the value of the lattice form factor as defined by eq. (4.12). No radiative corrections have been applied.
- $h_+(\omega)^{\text{rc}} = \frac{h_+^L(\omega)}{1+\beta_+(\omega)} \times \frac{1+\beta_+(1)}{h_+^L(1)}$. This is the radiatively corrected and normalised *physical* form factor.
- $h_-(\omega) = h_-^L(\omega) \times \frac{1+\beta_+(1)}{h_+^L(1)}$. This is the normalised form factor without radiative corrections.

$\kappa_Q = 2100 \longrightarrow \kappa_{Q'} = 2100, \quad \kappa_q = 4144$							
\mathbf{p}	\mathbf{p}'	ω	$h_+^L(\omega)$	$h_+(\omega)^{\text{rc}}$	χ^2/dof	$h_-(\omega)$	χ^2/dof
(0,0,0)	(0,0,0)	1.000_{-0}^{+0}	1.00_{-2}^{+2}	1.00_{-0}^{+0}	1.1/2	0.00_{-0}^{+0}	0/0
(0,0,0)	(1,0,0)	1.037_{-1}^{+1}	0.95_{-2}^{+2}	0.96_{-1}^{+1}	3.3/2	-0.09_{-3}^{+3}	21/5
(1,0,0)	(0,0,0)	1.037_{-1}^{+1}	0.90_{-2}^{+2}	0.91_{-1}^{+2}	0.98/2	0.04_{-3}^{+3}	2/5
(1,0,0)	(1,0,0)	0.996_{-3}^{+2}	0.97_{-5}^{+5}	0.97_{-5}^{+5}	0.52/2	0.00_{-0}^{+0}	0/0
(1,0,0)	(-1,0,0)	1.157_{-2}^{+2}	0.79_{-3}^{+3}	0.82_{-3}^{+4}	2.1/2	-0.00_{-1}^{+1}	3.7/5
(1,0,0)	(0,1,0)	1.076_{-2}^{+2}	0.86_{-2}^{+3}	0.88_{-2}^{+3}	0.41/2	0.00_{-1}^{+1}	16/8
$\kappa_Q = 2100 \longrightarrow \kappa_{Q'} = 2500, \quad \kappa_q = 4144$							
\mathbf{p}	\mathbf{p}'	ω	$h_+^L(\omega)$	$h_+(\omega)^{\text{rc}}$	χ^2/dof	$h_-(\omega)$	χ^2/dof
(0,0,0)	(0,0,0)	1.000_{-0}^{+0}	1.01_{-2}^{+2}	1.00_{-0}^{+0}	0.79/2	0.00_{-0}^{+0}	0/0
(0,0,0)	(1,0,0)	1.047_{-1}^{+1}	0.95_{-3}^{+2}	0.95_{-1}^{+1}	3.5/2	-0.05_{-3}^{+2}	20/5
(1,0,0)	(0,0,0)	1.037_{-1}^{+1}	0.92_{-2}^{+2}	0.92_{-1}^{+1}	0.64/2	0.06_{-3}^{+3}	1.3/5
(1,0,0)	(1,0,0)	0.996_{-3}^{+3}	0.98_{-5}^{+5}	0.97_{-5}^{+5}	0.67/2	$-1.46_{-0.88}^{+1.2}$	2.7/5
(1,0,0)	(-1,0,0)	1.176_{-2}^{+3}	0.77_{-3}^{+3}	0.80_{-2}^{+3}	1.5/2	0.01_{-1}^{+1}	3.4/5
(1,0,0)	(0,1,0)	1.086_{-3}^{+3}	0.86_{-2}^{+3}	0.86_{-2}^{+2}	0.24/2	0.02_{-1}^{+1}	13/8
$\kappa_Q = 2100 \longrightarrow \kappa_{Q'} = 2900, \quad \kappa_q = 4144$							
\mathbf{p}	\mathbf{p}'	ω	$h_+^L(\omega)$	$h_+(\omega)^{\text{rc}}$	χ^2/dof	$h_-(\omega)$	χ^2/dof
(0,0,0)	(0,0,0)	1.000_{-0}^{+0}	1.02_{-2}^{+2}	1.00_{-0}^{+0}	0.65/2	0.00_{-0}^{+0}	0/0
(0,0,0)	(1,0,0)	1.062_{-2}^{+2}	0.94_{-2}^{+2}	0.93_{-1}^{+1}	3.8/2	-0.01_{-3}^{+3}	20/5
(1,0,0)	(0,0,0)	1.037_{-1}^{+1}	0.93_{-2}^{+2}	0.92_{-1}^{+1}	0.34/2	0.09_{-3}^{+3}	0.66/5
(1,0,0)	(1,0,0)	0.998_{-3}^{+3}	0.98_{-6}^{+5}	0.96_{-5}^{+4}	0.9/2	$-0.40_{-0.42}^{+53}$	3.2/5
(1,0,0)	(-1,0,0)	1.205_{-3}^{+3}	0.76_{-3}^{+3}	0.77_{-2}^{+3}	0.89/2	0.03_{-1}^{+1}	3.3/5
(1,0,0)	(0,1,0)	1.102_{-3}^{+3}	0.85_{-2}^{+3}	0.85_{-2}^{+2}	0.19/2	0.05_{-1}^{+1}	9.6/8
$\kappa_Q = 2100 \longrightarrow \kappa_{Q'} = 3300, \quad \kappa_q = 4144$							
\mathbf{p}	\mathbf{p}'	ω	$h_+^L(\omega)$	$h_+(\omega)^{\text{rc}}$	χ^2/dof	$h_-(\omega)$	χ^2/dof
(0,0,0)	(0,0,0)	1.000_{-0}^{+0}	1.04_{-2}^{+2}	1.00_{-0}^{+0}	0.63/2	0.00_{-0}^{+0}	0/0
(0,0,0)	(1,0,0)	1.088_{-2}^{+2}	0.91_{-2}^{+2}	0.90_{-1}^{+1}	4.3/2	0.05_{-3}^{+3}	18/5
(1,0,0)	(0,0,0)	1.037_{-1}^{+1}	0.95_{-2}^{+2}	0.92_{-1}^{+1}	0.15/2	0.13_{-3}^{+3}	0.41/5
(1,0,0)	(1,0,0)	1.005_{-4}^{+4}	0.96_{-6}^{+5}	0.93_{-5}^{+4}	1.4/2	$0.02_{-0.28}^{+0.35}$	3.6/5
(1,0,0)	(-1,0,0)	1.252_{-3}^{+3}	0.73_{-3}^{+3}	0.74_{-2}^{+3}	0.33/2	0.06_{-1}^{+1}	3.4/5
(1,0,0)	(0,1,0)	1.129_{-3}^{+4}	0.82_{-2}^{+3}	0.82_{-2}^{+2}	0.2/2	0.09_{-1}^{+2}	7.3/8

$\kappa_Q = 2900 \longrightarrow \kappa_{Q'} = 2100, \quad \kappa_q = 4144$							
p	p'	ω	$h_+^L(\omega)$	$h_+(\omega)^{rc}$	χ^2/dof	$h_-(\omega)$	χ^2/dof
(0,0,0)	(0,0,0)	1.000_{-0}^{+0}	1.05_{-2}^{+2}	1.00_{-0}^{+0}	0.12/2	0.00_{-0}^{+0}	0/0
(0,0,0)	(1,0,0)	1.037_{-1}^{+1}	1.00_{-2}^{+2}	0.96_{-1}^{+1}	2.5/2	-0.19_{-3}^{+3}	23/5
(1,0,0)	(0,0,0)	1.062_{-2}^{+2}	0.90_{-2}^{+2}	0.87_{-1}^{+1}	0.8/2	-0.02_{-3}^{+3}	1.4/5
(1,0,0)	(1,0,0)	0.998_{-3}^{+3}	1.01_{-5}^{+5}	0.96_{-4}^{+5}	0.11/2	$0.81_{0.53}^{0.37}$	1.7/5
(1,0,0)	(-1,0,0)	1.205_{-3}^{+3}	0.76_{-3}^{+3}	0.75_{-2}^{+3}	6.2/2	-0.05_{-1}^{+1}	8.6/5
(1,0,0)	(0,1,0)	1.102_{-3}^{+3}	0.86_{-2}^{+3}	0.84_{-2}^{+2}	0.85/2	-0.04_{-1}^{+1}	16/8
$\kappa_Q = 2900 \longrightarrow \kappa_{Q'} = 2500, \quad \kappa_q = 4144$							
p	p'	ω	$h_+^L(\omega)$	$h_+(\omega)^{rc}$	χ^2/dof	$h_-(\omega)$	χ^2/dof
(0,0,0)	(0,0,0)	1.000_{-0}^{+0}	1.06_{-2}^{+2}	1.00_{-0}^{+0}	0.2/2	0.00_{-0}^{+0}	0/0
(0,0,0)	(1,0,0)	1.047_{-1}^{+1}	0.99_{-2}^{+2}	0.94_{-1}^{+1}	2.7/2	-0.14_{-3}^{+2}	23/5
(1,0,0)	(0,0,0)	1.062_{-2}^{+2}	0.91_{-2}^{+2}	0.87_{-1}^{+1}	0.64/2	-0.01_{-3}^{+3}	0.97/5
(1,0,0)	(1,0,0)	0.996_{-3}^{+3}	1.02_{-5}^{+5}	0.96_{-4}^{+4}	0.24/2	$1.31_{0.96}^{0.65}$	2.3/5
(1,0,0)	(-1,0,0)	1.228_{-3}^{+3}	0.74_{-3}^{+3}	0.73_{-2}^{+2}	5.2/2	-0.03_{-1}^{+0}	8.2/5
(1,0,0)	(0,1,0)	1.112_{-3}^{+3}	0.85_{-2}^{+3}	0.82_{-2}^{+2}	0.53/2	-0.02_{-1}^{+1}	12/8
$\kappa_Q = 2900 \longrightarrow \kappa_{Q'} = 2900, \quad \kappa_q = 4144$							
p	p'	ω	$h_+^L(\omega)$	$h_+(\omega)^{rc}$	χ^2/dof	$h_-(\omega)$	χ^2/dof
(0,0,0)	(0,0,0)	1.000_{-0}^{+0}	1.07_{-2}^{+2}	1.00_{-0}^{+0}	2.7/2	0.00_{-0}^{+0}	0/0
(0,0,0)	(1,0,0)	1.062_{-2}^{+2}	0.98_{-2}^{+2}	0.93_{-1}^{+1}	3/2	-0.09_{-2}^{+2}	23/5
(1,0,0)	(0,0,0)	1.062_{-2}^{+2}	0.93_{-2}^{+2}	0.88_{-1}^{+1}	0.4/2	0.02_{-3}^{+2}	0.49/5
(1,0,0)	(1,0,0)	0.995_{-4}^{+4}	1.02_{-6}^{+5}	0.95_{-4}^{+4}	1.2/2	0.00_{-0}^{+0}	0/0
(1,0,0)	(-1,0,0)	1.262_{-3}^{+3}	0.72_{-2}^{+3}	0.71_{-2}^{+3}	3.8/2	-0.00_{-1}^{+0}	7.6/5
(1,0,0)	(0,1,0)	1.128_{-4}^{+4}	0.84_{-2}^{+3}	0.81_{-2}^{+2}	0.31/2	0.01_{-4}^{+0}	8.9/8
$\kappa_Q = 2900 \longrightarrow \kappa_{Q'} = 3300, \quad \kappa_q = 4144$							
p	p'	ω	$h_+^L(\omega)$	$h_+(\omega)^{rc}$	χ^2/dof	$h_-(\omega)$	χ^2/dof
(0,0,0)	(0,0,0)	1.000_{-0}^{+0}	1.08_{-2}^{+2}	1.00_{-0}^{+0}	1/2	0.00_{-0}^{+0}	0/0
(0,0,0)	(1,0,0)	1.088_{-2}^{+2}	0.96_{-2}^{+2}	0.91_{-1}^{+1}	3.5/2	-0.03_{-2}^{+2}	22/5
(1,0,0)	(0,0,0)	1.062_{-2}^{+2}	0.95_{-2}^{+2}	0.89_{-1}^{+1}	0.21/2	0.06_{-3}^{+2}	0.32/5
(1,0,0)	(1,0,0)	0.996_{-4}^{+5}	1.00_{-6}^{+6}	0.93_{-5}^{+4}	2.2/2	$-0.19_{0.63}^{0.84}$	4.2/5
(1,0,0)	(-1,0,0)	1.315_{-4}^{+4}	0.70_{-2}^{+3}	0.69_{-2}^{+2}	2/2	0.02_{-0}^{+1}	6.8/5
(1,0,0)	(0,1,0)	1.156_{-4}^{+4}	0.82_{-2}^{+3}	0.78_{-2}^{+2}	0.21/2	0.04_{-1}^{+1}	6.3/8

$\kappa_Q = 2500 \longrightarrow \kappa_{Q'} = 2500, \quad \kappa_q = 4144$							
\mathbf{p}	\mathbf{p}'	ω	$h_+^L(\omega)$	$h_+(\omega)^{\text{rc}}$	χ^2/dof	$h_-(\omega)$	χ^2/dof
(0,0,0)	(0,0,0)	1.000_{-0}^{+0}	1.04_{-2}^{+2}	1.00_{-0}^{+0}	1.8/2	0.00_{-0}^{+0}	0/0
(0,0,0)	(1,0,0)	1.047_{-1}^{+1}	0.97_{-2}^{+2}	0.95_{-1}^{+1}	3.1/2	-0.09_{-3}^{+2}	23/5
(1,0,0)	(0,0,0)	1.047_{-1}^{+1}	0.92_{-2}^{+2}	0.90_{-1}^{+1}	0.63/2	0.03_{-3}^{+3}	1.1/5
(1,0,0)	(1,0,0)	0.995_{-3}^{+3}	0.99_{-5}^{+5}	0.96_{-4}^{+4}	0.83/2	0.00_{-0}^{+0}	0/0
(1,0,0)	(-1,0,0)	1.198_{-3}^{+3}	0.76_{-3}^{+3}	0.77_{-2}^{+3}	3/2	-0.00_{-0}^{+0}	5.6/5
(1,0,0)	(0,1,0)	1.096_{-3}^{+3}	0.86_{-2}^{+3}	0.85_{-2}^{+3}	0.43/2	0.01_{-1}^{+1}	13/8
$\kappa_Q = 2500 \longrightarrow \kappa_{Q'} = 3300, \quad \kappa_q = 4144$							
\mathbf{p}	\mathbf{p}'	ω	$h_+^L(\omega)$	$h_+(\omega)^{\text{rc}}$	χ^2/dof	$h_-(\omega)$	χ^2/dof
(0,0,0)	(0,0,0)	1.000_{-0}^{+0}	1.06_{-2}^{+2}	1.00_{-0}^{+0}	0.74/2	0.00_{-0}^{+0}	0/0
(0,0,0)	(1,0,0)	1.088_{-2}^{+2}	0.93_{-2}^{+2}	0.90_{-1}^{+1}	4/2	0.01_{-2}^{+3}	21/5
(1,0,0)	(0,0,0)	1.047_{-1}^{+1}	0.95_{-2}^{+2}	0.91_{-1}^{+1}	0.17/2	0.09_{-3}^{+2}	0.33/5
(1,0,0)	(1,0,0)	1.001_{-4}^{+4}	0.98_{-6}^{+5}	0.93_{-5}^{+4}	1.8/2	$-0.05_{-0.37}^{+0.5}$	3.9/5
(1,0,0)	(-1,0,0)	1.278_{-3}^{+4}	0.72_{-3}^{+3}	0.72_{-2}^{+2}	0.94/2	0.04_{-1}^{+1}	4.9/5
(1,0,0)	(0,1,0)	1.139_{-4}^{+4}	0.82_{-2}^{+3}	0.80_{-2}^{+2}	0.23/2	0.06_{-1}^{+1}	6.9/8
$\kappa_Q = 3300 \longrightarrow \kappa_{Q'} = 2500, \quad \kappa_q = 4144$							
\mathbf{p}	\mathbf{p}'	ω	$h_+^L(\omega)$	$h_+(\omega)^{\text{rc}}$	χ^2/dof	$h_-(\omega)$	χ^2/dof
(0,0,0)	(0,0,0)	1.000_{-0}^{+0}	1.09_{-2}^{+2}	1.00_{-0}^{+0}	0.083/2	0.00_{-0}^{+0}	0/0
(0,0,0)	(1,0,0)	1.047_{-1}^{+1}	1.02_{-2}^{+2}	0.95_{-1}^{+1}	2.3/2	-0.21_{-2}^{+2}	21/5
(1,0,0)	(0,0,0)	1.088_{-2}^{+2}	0.90_{-2}^{+2}	0.84_{-1}^{+1}	0.68/2	-0.05_{-3}^{+2}	0.84/5
(1,0,0)	(1,0,0)	1.001_{-4}^{+4}	1.04_{-7}^{+5}	0.95_{-4}^{+4}	0.072/2	$0.51_{-0.45}^{+0.34}$	1.8/5
(1,0,0)	(-1,0,0)	1.278_{-3}^{+4}	0.71_{-2}^{+3}	0.69_{-2}^{+2}	7.3/2	-0.06_{-1}^{+1}	9.9/5
(1,0,0)	(0,1,0)	1.139_{-4}^{+4}	0.84_{-2}^{+3}	0.79_{-2}^{+2}	0.38/2	-0.05_{-1}^{+1}	10/8
$\kappa_Q = 3300 \longrightarrow \kappa_{Q'} = 3300, \quad \kappa_q = 4144$							
\mathbf{p}	\mathbf{p}'	ω	$h_+^L(\omega)$	$h_+(\omega)^{\text{rc}}$	χ^2/dof	$h_-(\omega)$	χ^2/dof
(0,0,0)	(0,0,0)	1.000_{-0}^{+0}	1.11_{-2}^{+2}	1.00_{-0}^{+0}	3.1/2	0.00_{-0}^{+0}	0/0
(0,0,0)	(1,0,0)	1.088_{-2}^{+2}	0.98_{-2}^{+2}	0.90_{-1}^{+1}	2.8/2	-0.08_{-2}^{+2}	21/5
(1,0,0)	(0,0,0)	1.088_{-2}^{+2}	0.93_{-2}^{+2}	0.85_{-1}^{+1}	0.32/2	0.01_{-3}^{+2}	0.43/5
(1,0,0)	(1,0,0)	0.994_{-5}^{+6}	1.05_{-6}^{+6}	0.94_{-5}^{+5}	1.5/2	0.00_{-0}^{+0}	0/0
(1,0,0)	(-1,0,0)	1.374_{-5}^{+5}	0.66_{-3}^{+3}	0.64_{-2}^{+3}	3.4/2	-0.00_{-0}^{+0}	8.2/5
(1,0,0)	(0,1,0)	1.184_{-5}^{+5}	0.81_{-2}^{+3}	0.75_{-2}^{+2}	0.16/2	0.01_{-0}^{+0}	5.3/8

$\kappa_Q = 2100 \longrightarrow \kappa_{Q'} = 2100, \quad \kappa_q = 4226$							
p	p'	ω	$h_+^L(\omega)$	$h_+(\omega)^{rc}$	χ^2/dof	$h_-(\omega)$	χ^2/dof
(0,0,0)	(0,0,0)	1.000^{+0}_{-0}	1.01^{+3}_{-2}	1.00^{+0}_{-0}	0.35/2	0.00^{+0}_{-0}	0/0
(0,0,0)	(1,0,0)	1.040^{+2}_{-2}	0.95^{+3}_{-3}	0.95^{+2}_{-1}	3/2	-0.10^{+4}_{-4}	19/5
(1,0,0)	(0,0,0)	1.040^{+2}_{-2}	0.88^{+3}_{-2}	0.88^{+2}_{-2}	0.61/2	0.02^{+5}_{-5}	0.66/5
(1,0,0)	(1,0,0)	0.998^{+4}_{-4}	0.92^{+8}_{-8}	0.91^{+8}_{-8}	0.17/2	0.00^{+0}_{-0}	0/0
(1,0,0)	(-1,0,0)	1.167^{+4}_{-3}	0.83^{+6}_{-5}	0.85^{+5}_{-4}	1.5/2	-0.01^{+1}_{-1}	4.2/5
(1,0,0)	(0,1,0)	1.082^{+3}_{-4}	0.86^{+4}_{-3}	0.87^{+5}_{-3}	0.21/2	0.00^{+1}_{-1}	8/8
$\kappa_Q = 2100 \longrightarrow \kappa_{Q'} = 2500, \quad \kappa_q = 4226$							
p	p'	ω	$h_+^L(\omega)$	$h_+(\omega)^{rc}$	χ^2/dof	$h_-(\omega)$	χ^2/dof
(0,0,0)	(0,0,0)	1.000^{+0}_{-0}	1.02^{+3}_{-3}	1.00^{+0}_{-0}	0.09/2	0.00^{+0}_{-0}	0/0
(0,0,0)	(1,0,0)	1.051^{+2}_{-2}	0.95^{+3}_{-3}	0.94^{+1}_{-1}	2.9/2	-0.06^{+4}_{-4}	18/5
(1,0,0)	(0,0,0)	1.040^{+2}_{-2}	0.90^{+3}_{-2}	0.88^{+2}_{-2}	0.5/2	0.02^{+5}_{-5}	0.56/5
(1,0,0)	(1,0,0)	0.998^{+4}_{-4}	0.92^{+8}_{-8}	0.905^{+8}_{-8}	0.28/2	$-0.92^{+2.0}_{-1.4}$	1/5
(1,0,0)	(-1,0,0)	1.189^{+4}_{-4}	0.82^{+5}_{-4}	0.83^{+5}_{-4}	1.2/2	0.01^{+1}_{-1}	4/5
(1,0,0)	(0,1,0)	1.093^{+4}_{-4}	0.85^{+4}_{-3}	0.85^{+4}_{-3}	0.1/2	0.01^{+1}_{-2}	5.9/8
$\kappa_Q = 2100 \longrightarrow \kappa_{Q'} = 2900, \quad \kappa_q = 4226$							
p	p'	ω	$h_+^L(\omega)$	$h_+(\omega)^{rc}$	χ^2/dof	$h_-(\omega)$	χ^2/dof
(0,0,0)	(0,0,0)	1.000^{+0}_{-0}	1.04^{+3}_{-2}	1.00^{+0}_{-0}	0.087/2	0.00^{+0}_{-0}	0/0
(0,0,0)	(1,0,0)	1.068^{+2}_{-3}	0.94^{+3}_{-3}	0.92^{+2}_{-1}	3/2	-0.01^{+4}_{-4}	16/5
(1,0,0)	(0,0,0)	1.040^{+2}_{-2}	0.92^{+3}_{-2}	0.89^{+2}_{-2}	0.3/2	0.03^{+4}_{-5}	0.44/5
(1,0,0)	(1,0,0)	1.001^{+4}_{-4}	0.91^{+8}_{-8}	0.88^{+8}_{-8}	0.69/2	$0.03^{+9.89}_{-9.66}$	1.7/5
(1,0,0)	(-1,0,0)	1.221^{+4}_{-4}	0.80^{+5}_{-4}	0.81^{+4}_{-4}	0.88/2	0.02^{+1}_{-1}	3.9/5
(1,0,0)	(0,1,0)	1.111^{+4}_{-4}	0.84^{+4}_{-3}	0.83^{+4}_{-3}	0.1/2	0.03^{+2}_{-2}	4.3/8
$\kappa_Q = 2100 \longrightarrow \kappa_{Q'} = 3300, \quad \kappa_q = 4226$							
p	p'	ω	$h_+^L(\omega)$	$h_+(\omega)^{rc}$	χ^2/dof	$h_-(\omega)$	χ^2/dof
(0,0,0)	(0,0,0)	1.000^{+0}_{-0}	1.05^{+2}_{-3}	1.00^{+0}_{-0}	0.11/2	0.00^{+0}_{-0}	0/0
(0,0,0)	(1,0,0)	1.098^{+3}_{-4}	0.92^{+3}_{-3}	0.89^{+2}_{-2}	3.1/2	0.04^{+4}_{-4}	15/5
(1,0,0)	(0,0,0)	1.040^{+2}_{-2}	0.94^{+3}_{-2}	0.90^{+2}_{-2}	0.12/2	0.05^{+5}_{-5}	0.71/5
(1,0,0)	(1,0,0)	1.010^{+5}_{-5}	0.88^{+8}_{-9}	0.84^{+7}_{-8}	1.6/2	$0.40^{+9.55}_{-9.41}$	2.8/5
(1,0,0)	(-1,0,0)	1.274^{+4}_{-5}	0.78^{+5}_{-4}	0.79^{+4}_{-4}	0.48/2	0.04^{+2}_{-2}	4/5
(1,0,0)	(0,1,0)	1.142^{+4}_{-5}	0.82^{+4}_{-4}	0.80^{+3}_{-3}	0.11/2	0.07^{+3}_{-2}	3.3/8

$\kappa_Q = 2900 \longrightarrow \kappa_{Q'} = 2100, \quad \kappa_q = 4226$							
p	p'	ω	$h_+^L(\omega)$	$h_+(\omega)^{rc}$	χ^2/dof	$h_-(\omega)$	χ^2/dof
(0,0,0)	(0,0,0)	1.000^{+0}_{-0}	1.07^{+3}_{-3}	1.00^{+0}_{-0}	0.65/2	0.00^{+0}_{-0}	0/0
(0,0,0)	(1,0,0)	1.040^{+2}_{-2}	1.01^{+3}_{-3}	0.95^{+1}_{-1}	3/2	-0.20^{+4}_{-4}	21/5
(1,0,0)	(0,0,0)	1.068^{+2}_{-3}	0.89^{+3}_{-3}	0.85^{+2}_{-2}	0.25/2	-0.01^{+4}_{-4}	0.45/5
(1,0,0)	(1,0,0)	1.001^{+4}_{-4}	0.96^{+9}_{-8}	0.90^{+7}_{-8}	0.055/2	$0.75^{+9.66}_{-0.9}$	0.72/5
(1,0,0)	(-1,0,0)	1.221^{+4}_{-4}	0.79^{+5}_{-4}	0.78^{+4}_{-4}	4/2	-0.04^{+1}_{-1}	8.1/5
(1,0,0)	(0,1,0)	1.111^{+4}_{-4}	0.86^{+4}_{-4}	0.83^{+3}_{-3}	0.52/2	-0.02^{+2}_{-2}	6.8/8
$\kappa_Q = 2900 \longrightarrow \kappa_{Q'} = 2500, \quad \kappa_q = 4226$							
p	p'	ω	$h_+^L(\omega)$	$h_+(\omega)^{rc}$	χ^2/dof	$h_-(\omega)$	χ^2/dof
(0,0,0)	(0,0,0)	1.000^{+0}_{-0}	1.08^{+3}_{-3}	1.00^{+0}_{-0}	0.61/2	0.00^{+0}_{-0}	0/0
(0,0,0)	(1,0,0)	1.051^{+2}_{-2}	1.00^{+3}_{-3}	0.94^{+1}_{-1}	3.1/2	-0.15^{+4}_{-3}	20/5
(1,0,0)	(0,0,0)	1.068^{+2}_{-3}	0.90^{+3}_{-2}	0.85^{+2}_{-2}	0.3/2	-0.01^{+4}_{-4}	0.57/5
(1,0,0)	(1,0,0)	0.999^{+5}_{-5}	0.97^{+9}_{-8}	0.90^{+7}_{-7}	0.065/2	$0.95^{+1.1}_{-1.5}$	0.98/5
(1,0,0)	(-1,0,0)	1.246^{+4}_{-5}	0.79^{+5}_{-4}	0.76^{+4}_{-4}	3.2/2	-0.03^{+1}_{-1}	7.5/5
(1,0,0)	(0,1,0)	1.122^{+4}_{-4}	0.86^{+4}_{-4}	0.81^{+3}_{-3}	0.21/2	-0.01^{+1}_{-1}	5/8
$\kappa_Q = 2900 \longrightarrow \kappa_{Q'} = 2900, \quad \kappa_q = 4226$							
p	p'	ω	$h_+^L(\omega)$	$h_+(\omega)^{rc}$	χ^2/dof	$h_-(\omega)$	χ^2/dof
(0,0,0)	(0,0,0)	1.000^{+0}_{-0}	1.09^{+2}_{-2}	1.00^{+0}_{-0}	1.1/2	0.00^{+0}_{-0}	0/0
(0,0,0)	(1,0,0)	1.068^{+2}_{-3}	0.99^{+3}_{-3}	0.92^{+1}_{-1}	3.4/2	-0.10^{+3}_{-3}	19/5
(1,0,0)	(0,0,0)	1.068^{+2}_{-3}	0.92^{+3}_{-2}	0.86^{+2}_{-2}	0.24/2	-0.00^{+4}_{-4}	0.68/5
(1,0,0)	(1,0,0)	0.997^{+5}_{-6}	0.96^{+9}_{-8}	0.88^{+8}_{-8}	0.49/2	0.00^{+0}_{-0}	0/0
(1,0,0)	(-1,0,0)	1.283^{+5}_{-5}	0.77^{+4}_{-4}	0.75^{+4}_{-4}	2.4/2	-0.01^{+1}_{-1}	7/5
(1,0,0)	(0,1,0)	1.140^{+5}_{-5}	0.84^{+4}_{-4}	0.80^{+4}_{-3}	0.12/2	0.01^{+1}_{-1}	3.5/8
$\kappa_Q = 2900 \longrightarrow \kappa_{Q'} = 3300, \quad \kappa_q = 4226$							
p	p'	ω	$h_+^L(\omega)$	$h_+(\omega)^{rc}$	χ^2/dof	$h_-(\omega)$	χ^2/dof
(0,0,0)	(0,0,0)	1.000^{+0}_{-0}	1.106^{+3}_{-3}	1.00^{+0}_{-0}	0.34/2	0.00^{+0}_{-0}	0/0
(0,0,0)	(1,0,0)	1.098^{+3}_{-4}	0.97^{+3}_{-3}	0.90^{+1}_{-2}	3.7/2	-0.04^{+3}_{-3}	18/5
(1,0,0)	(0,0,0)	1.068^{+2}_{-3}	0.94^{+3}_{-2}	0.87^{+2}_{-2}	0.13/2	0.02^{+4}_{-4}	1.1/5
(1,0,0)	(1,0,0)	1.000^{+6}_{-7}	0.91^{+9}_{-9}	0.83^{+8}_{-8}	2.2/2	$0.62^{+1.2}_{-0.93}$	3.3/5
(1,0,0)	(-1,0,0)	1.344^{+6}_{-7}	0.75^{+4}_{-4}	0.73^{+4}_{-4}	1.6/2	0.01^{+1}_{-1}	6.5/5
(1,0,0)	(0,1,0)	1.172^{+6}_{-6}	0.82^{+4}_{-4}	0.77^{+3}_{-3}	0.13/2	0.03^{+1}_{-1}	2.6/8

$\kappa_Q = 2100 \longrightarrow \kappa_{Q'} = 2100, \quad \kappa_q = 4262$							
\mathbf{p}	\mathbf{p}'	ω	$h_+^L(\omega)$	$h_+(\omega)^{rc}$	χ^2/dof	$h_-(\omega)$	χ^2/dof
(0,0,0)	(0,0,0)	1.000^{+0}_{-0}	1.04^{+3}_{-4}	1.00^{+0}_{-0}	0.086/2	0.00^{+0}_{-0}	0/0
(0,0,0)	(1,0,0)	1.043^{+2}_{-3}	0.97^{+4}_{-4}	0.95^{+3}_{-2}	2.4/2	-0.09^{+5}_{-6}	13/5
(1,0,0)	(0,0,0)	1.043^{+2}_{-3}	0.87^{+4}_{-4}	0.84^{+3}_{-3}	0.75/2	0.01^{+7}_{-6}	0.89/5
(1,0,0)	(1,0,0)	1.001^{+5}_{-5}	$0.82^{+11}_{-13} \ 0.79^{+12}_{-11}$	0.14/2	0.00^{+0}_{-0}	0/0	
(1,0,0)	(-1,0,0)	1.173^{+5}_{-6}	0.88^{+8}_{-8}	0.89^{+7}_{-7}	0.6/2	-0.00^{+1}_{-1}	3/5
(1,0,0)	(0,1,0)	1.087^{+5}_{-5}	0.86^{+7}_{-5}	0.85^{+6}_{-4}	0.12/2	0.01^{+2}_{-2}	3.6/8
$\kappa_Q = 2100 \longrightarrow \kappa_{Q'} = 2500, \quad \kappa_q = 4262$							
\mathbf{p}	\mathbf{p}'	ω	$h_+^L(\omega)$	$h_+(\omega)^{rc}$	χ^2/dof	$h_-(\omega)$	χ^2/dof
(0,0,0)	(0,0,0)	1.000^{+0}_{-0}	1.04^{+3}_{-4}	1.00^{+0}_{-0}	0.51/2	0.00^{+0}_{-0}	0/0
(0,0,0)	(1,0,0)	1.054^{+3}_{-3}	0.97^{+4}_{-4}	0.94^{+2}_{-2}	2.1/2	-0.05^{+5}_{-6}	11/5
(1,0,0)	(0,0,0)	1.043^{+2}_{-3}	0.88^{+4}_{-4}	0.85^{+3}_{-3}	0.73/2	-0.01^{+6}_{-6}	0.9/5
(1,0,0)	(1,0,0)	1.001^{+5}_{-6}	0.81^{+12}_{-14}	0.78^{+12}_{-12}	0.099/2	$0.44^{+2.6}_{-1.8}$	1.1/5
(1,0,0)	(-1,0,0)	1.196^{+5}_{-6}	0.87^{+8}_{-7}	0.88^{+7}_{-7}	0.48/2	0.00^{+1}_{-1}	2.9/5
(1,0,0)	(0,1,0)	1.099^{+5}_{-6}	0.85^{+6}_{-5}	0.83^{+6}_{-4}	0.22/2	0.01^{+3}_{-2}	2.4/8
$\kappa_Q = 2100 \longrightarrow \kappa_{Q'} = 2900, \quad \kappa_q = 4262$							
\mathbf{p}	\mathbf{p}'	ω	$h_+^L(\omega)$	$h_+(\omega)^{rc}$	χ^2/dof	$h_-(\omega)$	χ^2/dof
(0,0,0)	(0,0,0)	1.000^{+0}_{-0}	1.06^{+3}_{-4}	1.00^{+0}_{-0}	0.44/2	0.00^{+0}_{-0}	0/0
(0,0,0)	(1,0,0)	1.071^{+3}_{-3}	0.96^{+4}_{-4}	0.93^{+2}_{-2}	2/2	-0.00^{+5}_{-6}	9.6/5
(1,0,0)	(0,0,0)	1.043^{+2}_{-3}	0.90^{+4}_{-4}	0.86^{+3}_{-3}	0.51/2	-0.02^{+6}_{-7}	0.73/5
(1,0,0)	(1,0,0)	1.005^{+6}_{-7}	0.80^{+12}_{-14}	0.75^{+12}_{-12}	0.21/2	$0.83^{+1.2}_{-0.89}$	1.4/5
(1,0,0)	(-1,0,0)	1.229^{+6}_{-7}	0.86^{+7}_{-7}	0.86^{+7}_{-7}	0.36/2	0.01^{+2}_{-2}	2.8/5
(1,0,0)	(0,1,0)	1.117^{+5}_{-6}	0.83^{+6}_{-5}	0.80^{+5}_{-4}	0.27/2	0.03^{+3}_{-3}	1.7/8
$\kappa_Q = 2100 \longrightarrow \kappa_{Q'} = 3300, \quad \kappa_q = 4262$							
\mathbf{p}	\mathbf{p}'	ω	$h_+^L(\omega)$	$h_+(\omega)^{rc}$	χ^2/dof	$h_-(\omega)$	χ^2/dof
(0,0,0)	(0,0,0)	1.000^{+0}_{-0}	1.07^{+3}_{-4}	1.00^{+0}_{-0}	0.17/2	0.00^{+0}_{-0}	0/0
(0,0,0)	(1,0,0)	1.103^{+4}_{-5}	0.94^{+4}_{-5}	0.90^{+2}_{-2}	2/2	0.05^{+5}_{-6}	8.5/5
(1,0,0)	(0,0,0)	1.043^{+2}_{-3}	0.93^{+3}_{-4}	0.88^{+2}_{-2}	0.22/2	-0.01^{+8}_{-8}	0.68/5
(1,0,0)	(1,0,0)	1.015^{+7}_{-7}	0.75^{+12}_{-15}	0.70^{+12}_{-13}	0.9/2	$0.99^{+0.72}_{-0.58}$	2/5
(1,0,0)	(-1,0,0)	1.286^{+6}_{-8}	0.84^{+7}_{-7}	0.83^{+6}_{-6}	0.22/2	0.02^{+3}_{-3}	2.7/5
(1,0,0)	(0,1,0)	1.150^{+6}_{-7}	0.81^{+6}_{-5}	0.78^{+5}_{-4}	0.19/2	0.06^{+3}_{-3}	1.5/8

$\kappa_Q = 2900 \longrightarrow \kappa_{Q'} = 2100, \quad \kappa_q = 4262$							
p	p'	ω	$h_+^L(\omega)$	$h_+(\omega)^{rc}$	χ^2/dof	$h_-(\omega)$	χ^2/dof
(0,0,0)	(0,0,0)	1.000^{+0}_{-0}	1.09^{+3}_{-4}	1.00^{+0}_{-0}	1.3/2	0.00^{+0}_{-0}	0/0
(0,0,0)	(1,0,0)	1.043^{+2}_{-3}	1.02^{+4}_{-4}	0.95^{+2}_{-2}	2.8/2	-0.19^{+5}_{-5}	12/5
(1,0,0)	(0,0,0)	1.071^{+3}_{-3}	0.88^{+5}_{-4}	0.83^{+3}_{-3}	0.22/2	0.01^{+6}_{-6}	1.1/5
(1,0,0)	(1,0,0)	1.005^{+6}_{-7}	0.85^{+13}_{-12}	0.79^{+12}_{-11}	0.085/2	$0.23^{+1.0}_{-1.1}$	1/5
(1,0,0)	(-1,0,0)	1.229^{+6}_{-7}	0.84^{+8}_{-7}	0.81^{+7}_{-7}	1.6/2	-0.04^{+2}_{-2}	5.9/5
(1,0,0)	(0,1,0)	1.117^{+5}_{-6}	0.86^{+7}_{-6}	0.82^{+6}_{-5}	0.21/2	-0.00^{+3}_{-3}	4/8
$\kappa_Q = 2900 \longrightarrow \kappa_{Q'} = 2500, \quad \kappa_q = 4262$							
p	p'	ω	$h_+^L(\omega)$	$h_+(\omega)^{rc}$	χ^2/dof	$h_-(\omega)$	χ^2/dof
(0,0,0)	(0,0,0)	1.000^{+0}_{-0}	1.10^{+3}_{-4}	1.00^{+0}_{-0}	0.85/2	0.00^{+0}_{-0}	0/0
(0,0,0)	(1,0,0)	1.054^{+3}_{-3}	1.02^{+4}_{-4}	0.94^{+2}_{-2}	2.8/2	-0.14^{+5}_{-5}	11/5
(1,0,0)	(0,0,0)	1.071^{+3}_{-3}	0.89^{+4}_{-4}	0.83^{+3}_{-3}	0.3/2	-0.01^{+5}_{-5}	1.2/5
(1,0,0)	(1,0,0)	1.002^{+7}_{-7}	0.86^{+13}_{-13}	0.78^{+12}_{-11}	0.17/2	$-0.18^{+1.7}_{-2}$	1.4/5
(1,0,0)	(-1,0,0)	1.256^{+6}_{-7}	0.83^{+7}_{-7}	0.80^{+6}_{-7}	1.3/2	-0.02^{+1}_{-1}	5.5/5
(1,0,0)	(0,1,0)	1.129^{+6}_{-7}	0.85^{+6}_{-6}	0.80^{+5}_{-5}	0.13/2	0.00^{+2}_{-2}	2.8/8
$\kappa_Q = 2900 \longrightarrow \kappa_{Q'} = 2900, \quad \kappa_q = 4262$							
p	p'	ω	$h_+^L(\omega)$	$h_+(\omega)^{rc}$	χ^2/dof	$h_-(\omega)$	χ^2/dof
(0,0,0)	(0,0,0)	1.000^{+0}_{-0}	1.11^{+3}_{-3}	1.00^{+0}_{-0}	0.29/2	0.00^{+0}_{-0}	0/0
(0,0,0)	(1,0,0)	1.071^{+3}_{-3}	1.00^{+4}_{-4}	0.92^{+2}_{-2}	3/2	-0.08^{+5}_{-5}	10/5
(1,0,0)	(0,0,0)	1.071^{+3}_{-3}	0.91^{+4}_{-4}	0.84^{+2}_{-2}	0.28/2	-0.02^{+5}_{-5}	1.3/5
(1,0,0)	(1,0,0)	1.001^{+7}_{-8}	0.85^{+14}_{-13}	0.77^{+13}_{-12}	0.092/2	0.00^{+0}_{-0}	0/0
(1,0,0)	(-1,0,0)	1.295^{+7}_{-8}	0.82^{+7}_{-6}	0.78^{+6}_{-6}	1/2	-0.01^{+1}_{-1}	5.1/5
(1,0,0)	(0,1,0)	1.148^{+6}_{-7}	0.84^{+6}_{-6}	0.78^{+6}_{-5}	0.22/2	0.01^{+1}_{-1}	2/8
$\kappa_Q = 2900 \longrightarrow \kappa_{Q'} = 3300, \quad \kappa_q = 4262$							
p	p'	ω	$h_+^L(\omega)$	$h_+(\omega)^{rc}$	χ^2/dof	$h_-(\omega)$	χ^2/dof
(0,0,0)	(0,0,0)	1.000^{+0}_{-0}	1.12^{+3}_{-4}	1.00^{+0}_{-0}	0.034/2	0.00^{+0}_{-0}	0/0
(0,0,0)	(1,0,0)	1.103^{+4}_{-5}	0.98^{+4}_{-4}	0.89^{+2}_{-2}	3.2/2	-0.01^{+5}_{-4}	9.8/5
(1,0,0)	(0,0,0)	1.071^{+3}_{-3}	0.94^{+4}_{-4}	0.85^{+2}_{-2}	0.16/2	-0.02^{+5}_{-5}	1.5/5
(1,0,0)	(1,0,0)	1.005^{+8}_{-9}	0.79^{+14}_{-15}	0.71^{+13}_{-13}	1/2	$1.86^{+1.7}_{-1.5}$	2.1/5
(1,0,0)	(-1,0,0)	1.359^{+8}_{-10}	0.79^{+6}_{-7}	0.76^{+6}_{-6}	0.72/2	0.01^{+1}_{-1}	4.5/5
(1,0,0)	(0,1,0)	1.182^{+7}_{-9}	0.81^{+6}_{-6}	0.75^{+4}_{-5}	0.25/2	0.03^{+2}_{-2}	1.7/8

C.2 Interpolation of $h_+(\omega)$ to the mass of the strange quark.

These tables list the form factor $h_+(\omega)$ for a spectator quark at the mass of the strange quark. The form factor $h_+(\omega)^{\text{rc}}$ is the radiatively corrected and normalised *physical* form factor. The χ^2/dof correspond to the goodness-of-fit of the interpolation to $h_+(\omega)$. The velocities ω have also been interpolated; the χ^2/dof are all of $\mathcal{O}(1)$.

$\kappa_Q = 2100 \longrightarrow \kappa_{Q'} = 2100, \quad \kappa_q = 0.1419$				
\mathbf{p}	\mathbf{p}'	ω	$h_+(\omega)^{\text{rc}}$	χ^2/dof
(0,0,0)	(1,0,0)	1.039^{+1}_{-1}	0.95^{+1}_{-1}	0/1
(1,0,0)	(0,0,0)	1.039^{+1}_{-1}	0.90^{+2}_{-2}	5.1/1
(1,0,0)	(1,0,0)	1.000^{+3}_{-3}	0.99^{+5}_{-5}	7.1/1
(1,0,0)	(-1,0,0)	1.162^{+3}_{-3}	0.82^{+4}_{-3}	1.1/1
(1,0,0)	(0,1,0)	1.080^{+3}_{-3}	0.88^{+4}_{-3}	1.1/1
$\kappa_Q = 2100 \longrightarrow \kappa_{Q'} = 2500, \quad \kappa_q = 0.1419$				
\mathbf{p}	\mathbf{p}'	ω	$h_+(\omega)^{\text{rc}}$	χ^2/dof
(0,0,0)	(1,0,0)	1.049^{+2}_{-1}	0.94^{+1}_{-1}	0.28/1
(1,0,0)	(0,0,0)	1.039^{+1}_{-1}	0.90^{+2}_{-2}	5.7/1
(1,0,0)	(1,0,0)	1.000^{+3}_{-3}	1.00^{+6}_{-6}	5.5/1
(1,0,0)	(-1,0,0)	1.183^{+2}_{-3}	0.80^{+4}_{-3}	1.1/1
(1,0,0)	(0,1,0)	1.090^{+3}_{-3}	0.85^{+3}_{-3}	1.2/1
$\kappa_Q = 2100 \longrightarrow \kappa_{Q'} = 2900, \quad \kappa_q = 0.1419$				
\mathbf{p}	\mathbf{p}'	ω	$h_+(\omega)^{\text{rc}}$	χ^2/dof
(0,0,0)	(1,0,0)	1.065^{+2}_{-2}	0.92^{+1}_{-1}	0.4/1
(1,0,0)	(0,0,0)	1.039^{+1}_{-1}	0.91^{+2}_{-2}	7.3/1
(1,0,0)	(1,0,0)	1.000^{+4}_{-4}	0.98^{+6}_{-6}	5.6/1
(1,0,0)	(-1,0,0)	1.213^{+3}_{-3}	0.78^{+3}_{-3}	1.2/1
(1,0,0)	(0,1,0)	1.106^{+3}_{-3}	0.84^{+3}_{-3}	1.9/1
$\kappa_Q = 2100 \longrightarrow \kappa_{Q'} = 3300, \quad \kappa_q = 0.1419$				
\mathbf{p}	\mathbf{p}'	ω	$h_+(\omega)^{\text{rc}}$	χ^2/dof
(0,0,0)	(1,0,0)	1.093^{+3}_{-3}	0.89^{+1}_{-1}	0.35/1
(1,0,0)	(0,0,0)	1.039^{+1}_{-1}	0.92^{+1}_{-2}	6.5/1
(1,0,0)	(1,0,0)	1.007^{+4}_{-4}	0.96^{+5}_{-6}	4.1/1
(1,0,0)	(-1,0,0)	1.263^{+4}_{-4}	0.75^{+3}_{-3}	1.2/1
(1,0,0)	(0,1,0)	1.135^{+4}_{-4}	0.82^{+2}_{-2}	2.5/1

$\kappa_Q = 2900 \longrightarrow \kappa_{Q'} = 2100, \quad \kappa_q = 0.1419$				
p	p'	ω	$h_+(\omega)^{\text{rc}}$	χ^2/dof
(0,0,0)	(1,0,0)	1.039^{+1}_{-1}	0.96^{+1}_{-1}	0.056/1
(1,0,0)	(0,0,0)	1.065^{+2}_{-2}	0.86^{+1}_{-1}	0.36/1
(1,0,0)	(1,0,0)	1.000^{+4}_{-4}	1.00^{+5}_{-5}	5.8/1
(1,0,0)	(-1,0,0)	1.213^{+3}_{-3}	0.75^{+3}_{-3}	0.59/1
(1,0,0)	(0,1,0)	1.106^{+3}_{-3}	0.84^{+3}_{-2}	0.16/1
$\kappa_Q = 2900 \longrightarrow \kappa_{Q'} = 2500, \quad \kappa_q = 0.1419$				
p	p'	ω	$h_+(\omega)^{\text{rc}}$	χ^2/dof
(0,0,0)	(1,0,0)	1.049^{+2}_{-1}	0.94^{+1}_{-1}	0.021/1
(1,0,0)	(0,0,0)	1.065^{+2}_{-2}	0.86^{+1}_{-1}	0.82/1
(1,0,0)	(1,0,0)	0.999^{+4}_{-4}	1.00^{+5}_{-5}	7.2/1
(1,0,0)	(-1,0,0)	1.237^{+4}_{-3}	0.73^{+3}_{-2}	0.85/1
(1,0,0)	(0,1,0)	1.117^{+4}_{-4}	0.82^{+3}_{-2}	0.33/1
$\kappa_Q = 2900 \longrightarrow \kappa_{Q'} = 2900, \quad \kappa_q = 0.1419$				
p	p'	ω	$h_+(\omega)^{\text{rc}}$	χ^2/dof
(0,0,0)	(1,0,0)	1.065^{+2}_{-2}	0.93^{+1}_{-1}	0.01/1
(1,0,0)	(0,0,0)	1.065^{+2}_{-2}	0.87^{+1}_{-1}	2.1/1
(1,0,0)	(1,0,0)	1.000^{+4}_{-4}	0.98^{+5}_{-5}	5.3/1
(1,0,0)	(-1,0,0)	1.272^{+4}_{-4}	0.71^{+3}_{-2}	1.2/1
(1,0,0)	(0,1,0)	1.134^{+4}_{-4}	0.81^{+3}_{-2}	0.55/1
$\kappa_Q = 2900 \longrightarrow \kappa_{Q'} = 3300, \quad \kappa_q = 0.1419$				
p	p'	ω	$h_+(\omega)^{\text{rc}}$	χ^2/dof
(0,0,0)	(1,0,0)	1.093^{+3}_{-3}	0.90^{+1}_{-1}	0.33/1
(1,0,0)	(0,0,0)	1.065^{+2}_{-2}	0.88^{+1}_{-1}	5.2/1
(1,0,0)	(1,0,0)	0.999^{+5}_{-5}	0.94^{+5}_{-5}	3.1/1
(1,0,0)	(-1,0,0)	1.330^{+5}_{-5}	0.69^{+3}_{-3}	0.79/1
(1,0,0)	(0,1,0)	1.164^{+5}_{-5}	0.79^{+2}_{-2}	1.7/1

C.3 Extrapolation of $h_+(\omega)$ to the chiral limit.

These tables list the form factor $h_+(\omega)$ for a spectator quark of zero mass. The form factor $h_+(\omega)^{\text{rc}}$ is the radiatively corrected and normalised *physical* form factor. The χ^2/dof correspond to the goodness-of-fit of the extrapolation to $h_+(\omega)$. The velocities ω have also been extrapolated; the χ^2/dof are all of $\mathcal{O}(1)$.

$\kappa_Q = 2100 \longrightarrow \kappa_{Q'} = 2100, \quad \kappa_q = 4315$				
p	p'	ω	$h_+(\omega)^{\text{rc}}$	χ^2/dof
(0,0,0)	(1,0,0)	1.043^{+3}_{-2}	0.94^{+2}_{-2}	0.00/1
(1,0,0)	(0,0,0)	1.043^{+3}_{-2}	0.88^{+3}_{-2}	5.1/1
(1,0,0)	(1,0,0)	1.000^{+6}_{-5}	1.00^{+9}_{-9}	7.1/1
(1,0,0)	(-1,0,0)	1.177^{+6}_{-5}	0.85^{+6}_{-5}	1.1/1
(1,0,0)	(0,1,0)	1.088^{+5}_{-5}	0.87^{+6}_{-4}	1.1/1
$\kappa_Q = 2100 \longrightarrow \kappa_{Q'} = 2500, \quad \kappa_q = 4315$				
p	p'	ω	$h_+(\omega)^{\text{rc}}$	χ^2/dof
(0,0,0)	(1,0,0)	1.054^{+3}_{-3}	0.93^{+2}_{-2}	0.28/1
(1,0,0)	(0,0,0)	1.043^{+3}_{-2}	0.88^{+3}_{-2}	5.7/1
(1,0,0)	(1,0,0)	0.999^{+6}_{-5}	1.00^{+10}_{-9}	5.5/1
(1,0,0)	(-1,0,0)	1.200^{+6}_{-5}	0.83^{+7}_{-5}	1.1/1
(1,0,0)	(0,1,0)	1.100^{+6}_{-5}	0.84^{+6}_{-5}	1.2/1
$\kappa_Q = 2100 \longrightarrow \kappa_{Q'} = 2900, \quad \kappa_q = 4315$				
p	p'	ω	$h_+(\omega)^{\text{rc}}$	χ^2/dof
(0,0,0)	(1,0,0)	1.072^{+3}_{-3}	0.91^{+2}_{-2}	0.4/1
(1,0,0)	(0,0,0)	1.043^{+3}_{-2}	0.90^{+3}_{-2}	7.3/1
(1,0,0)	(1,0,0)	0.999^{+6}_{-5}	0.97^{+9}_{-10}	5.6/1
(1,0,0)	(-1,0,0)	1.235^{+6}_{-5}	0.81^{+6}_{-5}	1.2/1
(1,0,0)	(0,1,0)	1.118^{+6}_{-5}	0.83^{+5}_{-4}	1.9/1
$\kappa_Q = 2100 \longrightarrow \kappa_{Q'} = 3300, \quad \kappa_q = 4315$				
p	p'	ω	$h_+(\omega)^{\text{rc}}$	χ^2/dof
(0,0,0)	(1,0,0)	1.106^{+4}_{-4}	0.89^{+2}_{-2}	0.35/1
(1,0,0)	(0,0,0)	1.043^{+3}_{-2}	0.91^{+2}_{-3}	6.5/1
(1,0,0)	(1,0,0)	1.012^{+7}_{-6}	0.91^{+9}_{-10}	4.1/1
(1,0,0)	(-1,0,0)	1.294^{+6}_{-6}	0.79^{+5}_{-5}	1.2/1
(1,0,0)	(0,1,0)	1.153^{+6}_{-6}	0.81^{+4}_{-3}	2.5/1

$\kappa_Q = 2900 \longrightarrow \kappa_{Q'} = 2100, \quad \kappa_q = 4315$				
p	p'	ω	$h_+(\omega)^{\text{rc}}$	χ^2/dof
(0,0,0)	(1,0,0)	1.043^{+3}_{-2}	0.95^{+2}_{-2}	0.056/1
(1,0,0)	(0,0,0)	1.072^{+3}_{-3}	0.83^{+3}_{-2}	0.36/1
(1,0,0)	(1,0,0)	0.999^{+6}_{-5}	1.02^{+8}_{-9}	5.8/1
(1,0,0)	(-1,0,0)	1.235^{+6}_{-5}	0.78^{+5}_{-4}	0.59/1
(1,0,0)	(0,1,0)	1.118^{+6}_{-5}	0.83^{+5}_{-4}	0.16/1
$\kappa_Q = 2900 \longrightarrow \kappa_{Q'} = 2500, \quad \kappa_q = 4315$				
p	p'	ω	$h_+(\omega)^{\text{rc}}$	χ^2/dof
(0,0,0)	(1,0,0)	1.054^{+3}_{-3}	0.94^{+2}_{-2}	0.021/1
(1,0,0)	(0,0,0)	1.072^{+3}_{-3}	0.83^{+2}_{-2}	0.82/1
(1,0,0)	(1,0,0)	0.997^{+6}_{-6}	1.02^{+8}_{-9}	7.2/1
(1,0,0)	(-1,0,0)	1.262^{+6}_{-5}	0.76^{+5}_{-3}	0.85/1
(1,0,0)	(0,1,0)	1.130^{+6}_{-6}	0.82^{+5}_{-4}	0.33/1
$\kappa_Q = 2900 \longrightarrow \kappa_{Q'} = 2900, \quad \kappa_q = 4315$				
p	p'	ω	$h_+(\omega)^{\text{rc}}$	χ^2/dof
(0,0,0)	(1,0,0)	1.072^{+3}_{-3}	0.92^{+2}_{-2}	0.00/1
(1,0,0)	(0,0,0)	1.072^{+3}_{-3}	0.85^{+2}_{-2}	2.1/1
(1,0,0)	(1,0,0)	0.998^{+7}_{-7}	0.99^{+8}_{-9}	5.3/1
(1,0,0)	(-1,0,0)	1.302^{+7}_{-7}	0.74^{+5}_{-4}	1.2/1
(1,0,0)	(0,1,0)	1.150^{+7}_{-7}	0.80^{+5}_{-4}	0.55/1
$\kappa_Q = 2900 \longrightarrow \kappa_{Q'} = 3300, \quad \kappa_q = 4315$				
p	p'	ω	$h_+(\omega)^{\text{rc}}$	χ^2/dof
(0,0,0)	(1,0,0)	1.106^{+4}_{-4}	0.89^{+2}_{-2}	0.33/1
(1,0,0)	(0,0,0)	1.072^{+3}_{-3}	0.86^{+2}_{-3}	5.2/1
(1,0,0)	(1,0,0)	0.996^{+7}_{-8}	0.88^{+9}_{-10}	3.1/1
(1,0,0)	(-1,0,0)	1.371^{+7}_{-8}	0.73^{+4}_{-4}	0.79/1
(1,0,0)	(0,1,0)	1.186^{+7}_{-9}	0.79^{+4}_{-4}	1.7/1

Appendix D

Pseudoscalar \rightarrow Vector

D.1 The form factor $h_{A_1}(\omega)$ at fixed light quark mass

This appendix lists all values of the form factor $h_{A_1}(\omega)$ of the decay $\bar{B} \rightarrow D^* l \bar{\nu}$. For details of the fitting method see Chapter 5.

In the following tables I use the notation :

- $h_{A_1}^L(\omega) = \frac{h_{A_1}(\omega)}{[1+\beta_{A_1}(\omega)]} [1 + \beta_{A_1}(1)]$; this is the unnormalised but radiatively corrected lattice form factor. The *physical* form factor is obtained by dividing with the $(0,0,0) \rightarrow (0,0,0)$ form factor.

$\kappa_Q = 2100 \longrightarrow \kappa_{Q'} = 2100, \quad \kappa_q = 4144$				
p	p'	ω	$h_{A_1}^L(\omega)$	$\chi^2/d.o.f.$
(0,0,0)	(0,0,0)	1.000^{+0}_{-0}	0.85^{+2}_{-2}	4.2/2
(0,0,0)	(1,0,0)	1.040^{+2}_{-2}	0.83^{+2}_{-2}	5.1/2
(1,0,0)	(0,0,0)	1.037^{+1}_{-1}	0.79^{+2}_{-2}	0.21/2
(1,0,0)	(1,0,0)	1.000^{+3}_{-3}	0.80^{+5}_{-5}	2.9/2
(1,0,0)	(-1,0,0)	1.157^{+3}_{-3}	0.73^{+3}_{-3}	0.83/2
(1,0,0)	(0,1,0)	1.079^{+3}_{-3}	0.77^{+3}_{-2}	7.1/2
$\kappa_Q = 2100 \longrightarrow \kappa_{Q'} = 2500, \quad \kappa_q = 4144$				
p	p'	ω	$h_{A_1}^L(\omega)$	$\chi^2/d.o.f.$
(0,0,0)	(0,0,0)	1.000^{+0}_{-0}	0.85^{+2}_{-2}	5/2
(0,0,0)	(1,0,0)	1.049^{+2}_{-2}	0.81^{+2}_{-2}	5.6/2
(1,0,0)	(0,0,0)	1.037^{+1}_{-1}	0.79^{+2}_{-2}	0.2/2
(1,0,0)	(1,0,0)	1.001^{+3}_{-3}	0.80^{+5}_{-6}	2.6/2
(1,0,0)	(-1,0,0)	1.176^{+3}_{-3}	0.71^{+3}_{-3}	0.47/2
(1,0,0)	(0,1,0)	1.088^{+3}_{-3}	0.76^{+3}_{-3}	6.3/2
$\kappa_Q = 2100 \longrightarrow \kappa_{Q'} = 2900, \quad \kappa_q = 4144$				
p	p'	ω	$h_{A_1}^L(\omega)$	$\chi^2/d.o.f.$
(0,0,0)	(0,0,0)	1.000^{+0}_{-0}	0.84^{+2}_{-2}	5/2
(0,0,0)	(1,0,0)	1.062^{+2}_{-2}	0.79^{+2}_{-2}	6.2/2
(1,0,0)	(0,0,0)	1.037^{+1}_{-1}	0.78^{+2}_{-2}	0.21/2
(1,0,0)	(1,0,0)	1.002^{+4}_{-4}	0.79^{+5}_{-6}	2.2/2
(1,0,0)	(-1,0,0)	1.201^{+4}_{-4}	0.68^{+3}_{-3}	0.31/2
(1,0,0)	(0,1,0)	1.102^{+3}_{-4}	0.74^{+3}_{-3}	5.3/2
$\kappa_Q = 2100 \longrightarrow \kappa_{Q'} = 3300, \quad \kappa_q = 4144$				
p	p'	ω	$h_{A_1}^L(\omega)$	$\chi^2/d.o.f.$
(0,0,0)	(0,0,0)	1.000^{+0}_{-0}	0.83^{+2}_{-2}	4.2/2
(0,0,0)	(1,0,0)	1.083^{+3}_{-3}	0.76^{+2}_{-2}	7/2
(1,0,0)	(0,0,0)	1.037^{+1}_{-1}	0.77^{+2}_{-2}	0.26/2
(1,0,0)	(1,0,0)	1.007^{+4}_{-4}	0.77^{+5}_{-7}	1.8/2
(1,0,0)	(-1,0,0)	1.240^{+4}_{-4}	0.65^{+3}_{-3}	0.35/2
(1,0,0)	(0,1,0)	1.124^{+4}_{-4}	0.71^{+3}_{-2}	4.1/2

$\kappa_Q = 2900 \longrightarrow \kappa_{Q'} = 2100, \quad \kappa_q = 4144$				
\mathbf{p}	\mathbf{p}'	ω	$h_{A_1}^L(\omega)$	$\chi^2/d.o.f.$
(0,0,0)	(0,0,0)	1.000^{+0}_{-0}	0.89^{+2}_{-2}	2/2
(0,0,0)	(1,0,0)	1.040^{+2}_{-2}	0.86^{+2}_{-2}	3.8/2
(1,0,0)	(0,0,0)	1.062^{+2}_{-2}	0.78^{+2}_{-2}	0.59/2
(1,0,0)	(1,0,0)	1.003^{+3}_{-4}	0.84^{+5}_{-5}	2/2
(1,0,0)	(-1,0,0)	1.206^{+3}_{-3}	0.69^{+3}_{-3}	3.1/2
(1,0,0)	(0,1,0)	1.104^{+3}_{-3}	0.75^{+3}_{-2}	6.9/2
$\kappa_Q = 2900 \longrightarrow \kappa_{Q'} = 2500, \quad \kappa_q = 4144$				
\mathbf{p}	\mathbf{p}'	ω	$h_{A_1}^L(\omega)$	$\chi^2/d.o.f.$
(0,0,0)	(0,0,0)	1.000^{+0}_{-0}	0.89^{+2}_{-2}	2.3/2
(0,0,0)	(1,0,0)	1.049^{+2}_{-2}	0.85^{+2}_{-2}	4.1/2
(1,0,0)	(0,0,0)	1.062^{+2}_{-2}	0.78^{+2}_{-2}	0.5/2
(1,0,0)	(1,0,0)	1.001^{+4}_{-4}	0.83^{+5}_{-5}	1.9/2
(1,0,0)	(-1,0,0)	1.227^{+3}_{-3}	0.68^{+3}_{-3}	2.4/2
(1,0,0)	(0,1,0)	1.114^{+3}_{-4}	0.74^{+3}_{-2}	6.3/2
$\kappa_Q = 2900 \longrightarrow \kappa_{Q'} = 2500, \quad \kappa_q = 4144$				
\mathbf{p}	\mathbf{p}'	ω	$h_{A_1}^L(\omega)$	$\chi^2/d.o.f.$
(0,0,0)	(0,0,0)	1.000^{+0}_{-0}	0.89^{+2}_{-2}	2.3/2
(0,0,0)	(1,0,0)	1.049^{+2}_{-2}	0.85^{+2}_{-2}	4.1/2
(1,0,0)	(0,0,0)	1.062^{+2}_{-2}	0.78^{+2}_{-2}	0.5/2
(1,0,0)	(1,0,0)	1.001^{+4}_{-4}	0.83^{+5}_{-5}	1.9/2
(1,0,0)	(-1,0,0)	1.227^{+3}_{-3}	0.68^{+3}_{-3}	2.4/2
(1,0,0)	(0,1,0)	1.114^{+3}_{-4}	0.74^{+3}_{-2}	6.3/2
$\kappa_Q = 2900 \longrightarrow \kappa_{Q'} = 2900, \quad \kappa_q = 4144$				
\mathbf{p}	\mathbf{p}'	ω	$h_{A_1}^L(\omega)$	$\chi^2/d.o.f.$
(0,0,0)	(0,0,0)	1.000^{+0}_{-0}	0.88^{+2}_{-2}	2.6/2
(0,0,0)	(1,0,0)	1.062^{+2}_{-2}	0.83^{+2}_{-2}	4.4/2
(1,0,0)	(0,0,0)	1.062^{+2}_{-2}	0.78^{+2}_{-2}	0.46/2
(1,0,0)	(1,0,0)	1.000^{+4}_{-4}	0.82^{+5}_{-5}	1.6/2
(1,0,0)	(-1,0,0)	1.257^{+4}_{-4}	0.67^{+3}_{-3}	2/2
(1,0,0)	(0,1,0)	1.128^{+4}_{-4}	0.73^{+3}_{-2}	5.2/2
$\kappa_Q = 2900 \longrightarrow \kappa_{Q'} = 3300, \quad \kappa_q = 4144$				
\mathbf{p}	\mathbf{p}'	ω	$h_{A_1}^L(\omega)$	$\chi^2/d.o.f.$
(0,0,0)	(0,0,0)	1.000^{+0}_{-0}	0.86^{+2}_{-2}	2.9/2
(0,0,0)	(1,0,0)	1.083^{+3}_{-3}	0.80^{+2}_{-2}	4.8/2
(1,0,0)	(0,0,0)	1.062^{+2}_{-2}	0.76^{+2}_{-2}	0.47/2
(1,0,0)	(1,0,0)	1.000^{+5}_{-5}	0.80^{+5}_{-6}	1.3/2
(1,0,0)	(-1,0,0)	1.300^{+5}_{-4}	0.63^{+3}_{-3}	2.1/2
(1,0,0)	(0,1,0)	1.150^{+4}_{-4}	0.70^{+2}_{-2}	3.6/2

$\kappa_Q = 2500 \longrightarrow \kappa_{Q'} = 2500, \quad \kappa_q = 4144$				
\mathbf{p}	\mathbf{p}'	ω	$h_{A_1}^L(\omega)$	$\chi^2/d.o.f.$
(0,0,0)	(0,0,0)	1.000^{+0}_{-0}	0.87^{+2}_{-2}	3.6/2
(0,0,0)	(1,0,0)	1.049^{+2}_{-2}	0.83^{+2}_{-2}	4.8/2
(1,0,0)	(0,0,0)	1.047^{+3}_{-3}	0.79^{+2}_{-2}	0.35/2
(1,0,0)	(1,0,0)	1.000^{+3}_{-4}	0.81^{+5}_{-5}	2.3/2
(1,0,0)	(-1,0,0)	1.197^{+3}_{-3}	0.71^{+3}_{-3}	1.2/2
(1,0,0)	(0,1,0)	1.098^{+3}_{-3}	0.76^{+2}_{-2}	6.7/2
$\kappa_Q = 2500 \longrightarrow \kappa_{Q'} = 3300, \quad \kappa_q = 4144$				
\mathbf{p}	\mathbf{p}'	ω	$h_{A_1}^L(\omega)$	$\chi^2/d.o.f.$
(0,0,0)	(0,0,0)	1.000^{+0}_{-0}	0.85^{+2}_{-2}	3.8/2
(0,0,0)	(1,0,0)	1.083^{+3}_{-3}	0.78^{+2}_{-2}	5.9/2
(1,0,0)	(0,0,0)	1.047^{+3}_{-3}	0.77^{+2}_{-2}	0.37/2
(1,0,0)	(1,0,0)	1.003^{+4}_{-4}	0.78^{+5}_{-7}	1.6/2
(1,0,0)	(-1,0,0)	1.265^{+4}_{-4}	0.64^{+3}_{-3}	0.99/2
(1,0,0)	(0,1,0)	1.134^{+4}_{-4}	0.70^{+3}_{-2}	4.1/2
$\kappa_Q = 3300 \longrightarrow \kappa_{Q'} = 2500, \quad \kappa_q = 4144$				
\mathbf{p}	\mathbf{p}'	ω	$h_{A_1}^L(\omega)$	$\chi^2/d.o.f.$
(0,0,0)	(0,0,0)	1.000^{+0}_{-0}	0.90^{+2}_{-2}	1.5/2
(0,0,0)	(1,0,0)	1.049^{+2}_{-2}	0.87^{+2}_{-2}	3.5/2
(1,0,0)	(0,0,0)	1.088^{+2}_{-2}	0.76^{+2}_{-2}	0.52/2
(1,0,0)	(1,0,0)	1.007^{+4}_{-4}	0.85^{+5}_{-6}	1.3/2
(1,0,0)	(-1,0,0)	1.276^{+4}_{-4}	0.65^{+3}_{-3}	3.9/2
(1,0,0)	(0,1,0)	1.141^{+4}_{-4}	0.73^{+3}_{-2}	4.7/2
$\kappa_Q = 3300 \longrightarrow \kappa_{Q'} = 3300, \quad \kappa_q = 4144$				
\mathbf{p}	\mathbf{p}'	ω	$h_{A_1}^L(\omega)$	$\chi^2/d.o.f.$
(0,0,0)	(0,0,0)	1.000^{+0}_{-0}	0.88^{+2}_{-2}	1.9/2
(0,0,0)	(1,0,0)	1.083^{+3}_{-3}	0.82^{+2}_{-2}	4/2
(1,0,0)	(0,0,0)	1.088^{+2}_{-2}	0.76^{+2}_{-2}	0.47/2
(1,0,0)	(1,0,0)	0.999^{+5}_{-5}	0.83^{+5}_{-6}	0.98/2
(1,0,0)	(-1,0,0)	1.357^{+5}_{-5}	0.63^{+3}_{-3}	3.6/2
(1,0,0)	(0,1,0)	1.178^{+5}_{-5}	0.70^{+2}_{-2}	2.6/2

$\kappa_Q = 2100 \longrightarrow \kappa_{Q'} = 2100, \quad \kappa_q = 4226$				
\mathbf{p}	\mathbf{p}'	ω	$h_{A_1}^L(\omega)$	$\chi^2/d.o.f.$
(0,0,0)	(0,0,0)	1.000_{-0}^{+0}	0.87_{-3}^{+2}	4.5/2
(0,0,0)	(1,0,0)	1.044_{-3}^{+2}	0.84_{-3}^{+3}	5.2/2
(1,0,0)	(0,0,0)	1.040_{-2}^{+2}	0.78_{-3}^{+3}	0.68/2
(1,0,0)	(1,0,0)	1.004_{-4}^{+4}	0.75_{-9}^{+8}	2.2/2
(1,0,0)	(-1,0,0)	1.169_{-4}^{+4}	0.76_{-5}^{+6}	0.24/2
(1,0,0)	(0,1,0)	1.087_{-4}^{+4}	0.79_{-4}^{+4}	4.2/2
$\kappa_Q = 2100 \longrightarrow \kappa_{Q'} = 2500, \quad \kappa_q = 4226$				
\mathbf{p}	\mathbf{p}'	ω	$h_{A_1}^L(\omega)$	$\chi^2/d.o.f.$
(0,0,0)	(0,0,0)	1.000_{-0}^{+0}	0.87_{-3}^{+2}	4.2/2
(0,0,0)	(1,0,0)	1.055_{-3}^{+3}	0.82_{-3}^{+3}	5.3/2
(1,0,0)	(0,0,0)	1.040_{-2}^{+2}	0.78_{-3}^{+3}	0.56/2
(1,0,0)	(1,0,0)	1.005_{-4}^{+4}	0.74_{-9}^{+8}	1.6/2
(1,0,0)	(-1,0,0)	1.190_{-5}^{+5}	0.74_{-5}^{+5}	0.089/2
(1,0,0)	(0,1,0)	1.097_{-5}^{+5}	0.78_{-4}^{+4}	3.6/2
$\kappa_Q = 2100 \longrightarrow \kappa_{Q'} = 2900, \quad \kappa_q = 4226$				
\mathbf{p}	\mathbf{p}'	ω	$h_{A_1}^L(\omega)$	$\chi^2/d.o.f.$
(0,0,0)	(0,0,0)	1.000_{-0}^{+0}	0.86_{-2}^{+2}	3.2/2
(0,0,0)	(1,0,0)	1.069_{-4}^{+4}	0.81_{-3}^{+3}	5.4/2
(1,0,0)	(0,0,0)	1.040_{-2}^{+2}	0.78_{-3}^{+3}	0.51/2
(1,0,0)	(1,0,0)	1.007_{-5}^{+5}	0.73_{-9}^{+9}	0.94/2
(1,0,0)	(-1,0,0)	1.218_{-6}^{+5}	0.72_{-5}^{+5}	29/2
(1,0,0)	(0,1,0)	1.113_{-5}^{+5}	0.76_{-3}^{+4}	3/2
$\kappa_Q = 2100 \longrightarrow \kappa_{Q'} = 3300, \quad \kappa_q = 4226$				
\mathbf{p}	\mathbf{p}'	ω	$h_{A_1}^L(\omega)$	$\chi^2/d.o.f.$
(0,0,0)	(0,0,0)	1.000_{-0}^{+0}	0.85_{-2}^{+2}	2.1/2
(0,0,0)	(1,0,0)	1.093_{-5}^{+5}	0.78_{-3}^{+3}	5/2
(1,0,0)	(0,0,0)	1.040_{-2}^{+2}	0.77_{-3}^{+3}	0.5/2
(1,0,0)	(1,0,0)	1.013_{-6}^{+6}	0.71_{-11}^{+9}	0.33/2
(1,0,0)	(-1,0,0)	1.261_{-7}^{+6}	0.69_{-5}^{+5}	5/2
(1,0,0)	(0,1,0)	1.137_{-7}^{+7}	0.72_{-4}^{+4}	2.2/2

$\kappa_Q = 2900 \longrightarrow \kappa_{Q'} = 2100, \quad \kappa_q = 4226$				
\mathbf{p}	\mathbf{p}'	ω	$h_{A_1}^L(\omega)$	$\chi^2/d.o.f.$
(0,0,0)	(0,0,0)	1.000^{+0}_{-0}	0.90^{+3}_{-2}	3.4/2
(0,0,0)	(1,0,0)	1.044^{+2}_{-3}	0.88^{+3}_{-3}	4.4/2
(1,0,0)	(0,0,0)	1.068^{+2}_{-3}	0.78^{+3}_{-3}	1.4/2
(1,0,0)	(1,0,0)	1.008^{+5}_{-4}	0.78^{+8}_{-9}	1.6/2
(1,0,0)	(-1,0,0)	1.223^{+5}_{-5}	0.72^{+5}_{-5}	1.2/2
(1,0,0)	(0,1,0)	1.115^{+5}_{-4}	0.77^{+4}_{-3}	4.5/2
$\kappa_Q = 2900 \longrightarrow \kappa_{Q'} = 2500, \quad \kappa_q = 4226$				
\mathbf{p}	\mathbf{p}'	ω	$h_{A_1}^L(\omega)$	$\chi^2/d.o.f.$
(0,0,0)	(0,0,0)	1.000^{+0}_{-0}	0.90^{+2}_{-2}	3.1/2
(0,0,0)	(1,0,0)	1.055^{+3}_{-3}	0.86^{+3}_{-3}	4.4/2
(1,0,0)	(0,0,0)	1.068^{+2}_{-3}	0.78^{+3}_{-3}	1.2/2
(1,0,0)	(1,0,0)	1.006^{+5}_{-5}	0.77^{+9}_{-9}	1.2/2
(1,0,0)	(-1,0,0)	1.246^{+5}_{-5}	0.71^{+5}_{-5}	0.83/2
(1,0,0)	(0,1,0)	1.126^{+5}_{-5}	0.76^{+4}_{-4}	3.9/2
$\kappa_Q = 2900 \longrightarrow \kappa_{Q'} = 2900, \quad \kappa_q = 4226$				
\mathbf{p}	\mathbf{p}'	ω	$h_{A_1}^L(\omega)$	$\chi^2/d.o.f.$
(0,0,0)	(0,0,0)	1.000^{+0}_{-0}	0.89^{+2}_{-2}	2.7/2
(0,0,0)	(1,0,0)	1.069^{+4}_{-4}	0.85^{+2}_{-3}	4.3/2
(1,0,0)	(0,0,0)	1.068^{+2}_{-3}	0.78^{+3}_{-2}	1/2
(1,0,0)	(1,0,0)	1.005^{+5}_{-5}	0.76^{+9}_{-10}	0.69/2
(1,0,0)	(-1,0,0)	1.279^{+6}_{-6}	0.71^{+5}_{-5}	0.62/2
(1,0,0)	(0,1,0)	1.142^{+6}_{-6}	0.76^{+4}_{-4}	3/2
$\kappa_Q = 2900 \longrightarrow \kappa_{Q'} = 3300, \quad \kappa_q = 4226$				
\mathbf{p}	\mathbf{p}'	ω	$h_{A_1}^L(\omega)$	$\chi^2/d.o.f.$
(0,0,0)	(0,0,0)	1.000^{+0}_{-0}	0.88^{+2}_{-2}	1.9/2
(0,0,0)	(1,0,0)	1.093^{+5}_{-5}	0.81^{+2}_{-3}	3.9/2
(1,0,0)	(0,0,0)	1.068^{+2}_{-3}	0.76^{+3}_{-3}	0.99/2
(1,0,0)	(1,0,0)	1.006^{+6}_{-7}	0.74^{+10}_{-11}	0.21/2
(1,0,0)	(-1,0,0)	1.328^{+8}_{-8}	0.66^{+4}_{-5}	0.71/2
(1,0,0)	(0,1,0)	1.167^{+7}_{-7}	0.71^{+4}_{-4}	2.1/2

$\kappa_Q = 2100 \longrightarrow \kappa_{Q'} = 2100, \quad \kappa_q = 4262$				
\mathbf{p}	\mathbf{p}'	ω	$h_{A_1}^L(\omega)$	$\chi^2/d.o.f.$
(0,0,0)	(0,0,0)	1.000^{+0}_{-0}	0.89^{+3}_{-4}	3.6/2
(0,0,0)	(1,0,0)	1.047^{+4}_{-4}	0.86^{+4}_{-5}	4.5/2
(1,0,0)	(0,0,0)	1.043^{+2}_{-3}	0.80^{+5}_{-4}	0.67/2
(1,0,0)	(1,0,0)	1.008^{+6}_{-6}	0.68^{+13}_{-14}	1.6/2
(1,0,0)	(-1,0,0)	1.176^{+6}_{-6}	0.81^{+9}_{-8}	0.11/2
(1,0,0)	(0,1,0)	1.092^{+6}_{-6}	0.8^{+971}_{-959}	2.1/2
$\kappa_Q = 2100 \longrightarrow \kappa_{Q'} = 2500, \quad \kappa_q = 4262$				
\mathbf{p}	\mathbf{p}'	ω	$h_{A_1}^L(\omega)$	$\chi^2/d.o.f.$
(0,0,0)	(0,0,0)	1.000^{+0}_{-0}	0.89^{+3}_{-4}	2.4/2
(0,0,0)	(1,0,0)	1.058^{+4}_{-4}	0.85^{+4}_{-5}	4.2/2
(1,0,0)	(0,0,0)	1.043^{+2}_{-3}	0.80^{+5}_{-4}	0.54/2
(1,0,0)	(1,0,0)	1.009^{+6}_{-8}	0.67^{+14}_{-15}	0.94/2
(1,0,0)	(-1,0,0)	1.197^{+7}_{-7}	0.79^{+8}_{-8}	0.13/2
(1,0,0)	(0,1,0)	1.103^{+7}_{-7}	0.79^{+7}_{-6}	1.7/2
$\kappa_Q = 2100 \longrightarrow \kappa_{Q'} = 2900, \quad \kappa_q = 4262$				
\mathbf{p}	\mathbf{p}'	ω	$h_{A_1}^L(\omega)$	$\chi^2/d.o.f.$
(0,0,0)	(0,0,0)	1.000^{+0}_{-0}	0.88^{+3}_{-3}	1.3/2
(0,0,0)	(1,0,0)	1.074^{+5}_{-5}	0.83^{+4}_{-5}	3.5/2
(1,0,0)	(0,0,0)	1.043^{+2}_{-3}	0.79^{+4}_{-4}	0.5/2
(1,0,0)	(1,0,0)	1.011^{+7}_{-8}	0.65^{+15}_{-16}	0.34/2
(1,0,0)	(-1,0,0)	1.227^{+7}_{-8}	0.77^{+7}_{-8}	0.18/2
(1,0,0)	(0,1,0)	1.119^{+7}_{-8}	0.77^{+8}_{-6}	1.3/2
$\kappa_Q = 2100 \longrightarrow \kappa_{Q'} = 3300, \quad \kappa_q = 4262$				
\mathbf{p}	\mathbf{p}'	ω	$h_{A_1}^L(\omega)$	$\chi^2/d.o.f.$
(0,0,0)	(0,0,0)	1.000^{+0}_{-0}	0.87^{+3}_{-3}	0.6/2
(0,0,0)	(1,0,0)	1.098^{+7}_{-7}	0.81^{+4}_{-5}	2.6/2
(1,0,0)	(0,0,0)	1.043^{+2}_{-3}	0.79^{+4}_{-4}	0.54/2
(1,0,0)	(1,0,0)	1.018^{+8}_{-9}	0.62^{+15}_{-17}	0.15/2
(1,0,0)	(-1,0,0)	1.272^{+9}_{-9}	0.75^{+7}_{-8}	0.24/2
(1,0,0)	(0,1,0)	1.145^{+9}_{-9}	0.73^{+8}_{-7}	0.99/2

$\kappa_Q = 2900 \longrightarrow \kappa_{Q'} = 2100, \quad \kappa_q = 4262$				
\mathbf{p}	\mathbf{p}'	ω	$h_{A_1}^L(\omega)$	$\chi^2/d.o.f.$
(0,0,0)	(0,0,0)	1.000^{+0}_{-0}	0.92^{+3}_{-3}	3.4/2
(0,0,0)	(1,0,0)	1.047^{+4}_{-4}	0.90^{+4}_{-4}	4.2/2
(1,0,0)	(0,0,0)	1.071^{+3}_{-3}	0.79^{+5}_{-4}	1.5/2
(1,0,0)	(1,0,0)	1.012^{+6}_{-7}	0.69^{+15}_{-13}	1.3/2
(1,0,0)	(-1,0,0)	1.232^{+6}_{-7}	0.76^{+8}_{-8}	0.22/2
(1,0,0)	(0,1,0)	1.122^{+7}_{-7}	0.79^{+7}_{-6}	2.5/2
$\kappa_Q = 2900 \longrightarrow \kappa_{Q'} = 2500, \quad \kappa_q = 4262$				
\mathbf{p}	\mathbf{p}'	ω	$h_{A_1}^L(\omega)$	$\chi^2/d.o.f.$
(0,0,0)	(0,0,0)	1.000^{+0}_{-0}	0.92^{+3}_{-3}	2.6/2
(0,0,0)	(1,0,0)	1.058^{+4}_{-4}	0.88^{+4}_{-4}	3.8/2
(1,0,0)	(0,0,0)	1.071^{+3}_{-3}	0.79^{+4}_{-4}	1.4/2
(1,0,0)	(1,0,0)	1.010^{+7}_{-8}	0.68^{+15}_{-14}	0.76/2
(1,0,0)	(-1,0,0)	1.257^{+7}_{-9}	0.75^{+8}_{-8}	0.068/2
(1,0,0)	(0,1,0)	1.134^{+7}_{-8}	0.78^{+7}_{-6}	2/2
$\kappa_Q = 2900 \longrightarrow \kappa_{Q'} = 2900, \quad \kappa_q = 4262$				
\mathbf{p}	\mathbf{p}'	ω	$h_{A_1}^L(\omega)$	$\chi^2/d.o.f.$
(0,0,0)	(0,0,0)	1.000^{+0}_{-0}	0.91^{+2}_{-3}	1.6/2
(0,0,0)	(1,0,0)	1.074^{+5}_{-5}	0.87^{+4}_{-4}	3.1/2
(1,0,0)	(0,0,0)	1.071^{+3}_{-3}	0.79^{+4}_{-4}	1.3/2
(1,0,0)	(1,0,0)	1.010^{+8}_{-8}	0.67^{+16}_{-14}	0.25/2
(1,0,0)	(-1,0,0)	1.291^{+8}_{-9}	0.76^{+8}_{-8}	58/2
(1,0,0)	(0,1,0)	1.150^{+8}_{-9}	0.76^{+7}_{-6}	1.5/2
$\kappa_Q = 2900 \longrightarrow \kappa_{Q'} = 2900, \quad \kappa_q = 4262$				
\mathbf{p}	\mathbf{p}'	ω	$h_{A_1}^L(\omega)$	$\chi^2/d.o.f.$
(0,0,0)	(0,0,0)	1.000^{+0}_{-0}	0.91^{+2}_{-3}	1.6/2
(0,0,0)	(1,0,0)	1.074^{+5}_{-5}	0.87^{+4}_{-4}	3.1/2
(1,0,0)	(0,0,0)	1.071^{+3}_{-3}	0.79^{+4}_{-4}	1.3/2
(1,0,0)	(1,0,0)	1.010^{+8}_{-8}	0.67^{+16}_{-14}	0.25/2
(1,0,0)	(-1,0,0)	1.291^{+8}_{-9}	0.76^{+8}_{-8}	0.0/2
(1,0,0)	(0,1,0)	1.150^{+8}_{-9}	0.76^{+7}_{-6}	1.5/2

D.2 Interpolation of $h_{A_1}(\omega)$ to the mass of the strange quark.

These tables list the form factor $h_{A_1}(\omega)$ for a spectator quark at the mass of the strange quark. The form factor $h_{A_1}^{\text{rc}}(\omega)$ is the radiatively corrected and normalised *physical* form factor. The χ^2/dof correspond to the goodness-of-fit of the interpolation to $h_{A_1}(\omega)$. The velocities ω have also been interpolated to κ_s ; the χ^2/dof are all of $\mathcal{O}(1)$.

$\kappa_Q = 2100 \longrightarrow \kappa_{Q'} = 2100, \quad \kappa_q = 0.1419$				
p	p'	ω	$h_{A_1}^{\text{rc}}(\omega)$	χ^2/dof
(0,0,0)	(1,0,0)	1.042^{+2}_{-2}	1.00^{+2}_{-2}	0/1
(1,0,0)	(0,0,0)	1.039^{+1}_{-1}	0.94^{+3}_{-2}	5.1/1
(1,0,0)	(1,0,0)	1.000^{+4}_{-4}	0.97^{+7}_{-7}	7.1/1
(1,0,0)	(-1,0,0)	1.164^{+6}_{-3}	0.87^{+6}_{-4}	1.1/1
(1,0,0)	(0,1,0)	1.083^{+3}_{-3}	0.94^{+4}_{-4}	1.1/1
$\kappa_Q = 2100 \longrightarrow \kappa_{Q'} = 2500, \quad \kappa_q = 0.1419$				
p	p'	ω	$h_{A_1}^{\text{rc}}(\omega)$	χ^2/dof
(0,0,0)	(1,0,0)	1.052^{+2}_{-2}	0.99^{+2}_{-2}	0.28/1
(1,0,0)	(0,0,0)	1.039^{+1}_{-1}	0.94^{+3}_{-2}	5.7/1
(1,0,0)	(1,0,0)	1.000^{+4}_{-4}	0.97^{+7}_{-7}	5.5/1
(1,0,0)	(-1,0,0)	1.183^{+4}_{-4}	0.85^{+5}_{-4}	1.1/1
(1,0,0)	(0,1,0)	1.093^{+4}_{-4}	0.93^{+4}_{-4}	1.2/1
$\kappa_Q = 2100 \longrightarrow \kappa_{Q'} = 2900, \quad \kappa_q = 0.1419$				
p	p'	ω	$h_{A_1}^{\text{rc}}(\omega)$	χ^2/dof
(0,0,0)	(1,0,0)	1.066^{+3}_{-3}	0.98^{+2}_{-2}	0/1
(1,0,0)	(0,0,0)	1.039^{+1}_{-1}	0.95^{+3}_{-2}	5.1/1
(1,0,0)	(1,0,0)	1.000^{+4}_{-4}	0.98^{+7}_{-8}	7.1/1
(1,0,0)	(-1,0,0)	1.210^{+4}_{-4}	0.83^{+5}_{-4}	1.1/1
(1,0,0)	(0,1,0)	1.108^{+4}_{-4}	0.92^{+4}_{-3}	1.1/1
$\kappa_Q = 2100 \longrightarrow \kappa_{Q'} = 3300, \quad \kappa_q = 0.1419$				
p	p'	ω	$h_{A_1}^{\text{rc}}(\omega)$	χ^2/dof
(0,0,0)	(1,0,0)	1.088^{+4}_{-4}	0.96^{+2}_{-2}	0.35/1
(1,0,0)	(0,0,0)	1.039^{+1}_{-1}	0.95^{+3}_{-2}	6.5/1
(1,0,0)	(1,0,0)	1.010^{+5}_{-5}	0.97^{+8}_{-9}	4.1/1
(1,0,0)	(-1,0,0)	1.251^{+5}_{-5}	0.82^{+5}_{-4}	1.2/1
(1,0,0)	(0,1,0)	1.131^{+5}_{-5}	0.90^{+4}_{-3}	2.5/1

$\kappa_Q = 2900 \longrightarrow \kappa_{Q'} = 2100, \quad \kappa_q = 0.1419$				
\mathbf{p}	\mathbf{p}'	ω	$h_{A_1}^{\text{rc}}(\omega)$	χ^2/dof
(0,0,0)	(1,0,0)	1.042_{-2}^{+2}	1.00_{-2}^{+1}	0.056/1
(1,0,0)	(0,0,0)	1.065_{-2}^{+2}	0.90_{-2}^{+3}	0.36/1
(1,0,0)	(1,0,0)	1.000_{-4}^{+4}	0.99_{-7}^{+6}	5.8/1
(1,0,0)	(-1,0,0)	1.214_{-4}^{+4}	0.79_{-4}^{+5}	0.59/1
(1,0,0)	(0,1,0)	1.110_{-4}^{+4}	0.88_{-3}^{+4}	0.16/1
$\kappa_Q = 2900 \longrightarrow \kappa_{Q'} = 2500, \quad \kappa_q = 0.1419$				
\mathbf{p}	\mathbf{p}'	ω	$h_{A_1}^{\text{rc}}(\omega)$	χ^2/dof
(0,0,0)	(1,0,0)	1.052_{-2}^{+2}	1.00_{-1}^{+1}	0.021/1
(1,0,0)	(0,0,0)	1.065_{-2}^{+2}	0.90_{-2}^{+3}	0.82/1
(1,0,0)	(1,0,0)	1.003_{-4}^{+4}	0.99_{-7}^{+6}	7.2/1
(1,0,0)	(-1,0,0)	1.237_{-4}^{+4}	0.79_{-4}^{+5}	0.85/1
(1,0,0)	(0,1,0)	1.120_{-4}^{+4}	0.88_{-3}^{+4}	0.33/1
$\kappa_Q = 2900 \longrightarrow \kappa_{Q'} = 2900, \quad \kappa_q = 0.1419$				
\mathbf{p}	\mathbf{p}'	ω	$h_{A_1}^{\text{rc}}(\omega)$	χ^2/dof
(0,0,0)	(1,0,0)	1.066_{-3}^{+3}	1.00_{-1}^{+2}	0.0/1
(1,0,0)	(0,0,0)	1.065_{-2}^{+2}	0.91_{-2}^{+3}	2.1/1
(1,0,0)	(1,0,0)	1.000_{-5}^{+5}	0.99_{-8}^{+7}	5.3/1
(1,0,0)	(-1,0,0)	1.268_{-5}^{+4}	0.79_{-4}^{+4}	1.2/1
(1,0,0)	(0,1,0)	1.135_{-5}^{+5}	0.88_{-3}^{+4}	0.55/1
$\kappa_Q = 2900 \longrightarrow \kappa_{Q'} = 3300, \quad \kappa_q = 0.1419$				
\mathbf{p}	\mathbf{p}'	ω	$h_{A_1}^{\text{rc}}(\omega)$	χ^2/dof
(0,0,0)	(1,0,0)	1.088_{-4}^{+4}	0.97_{-1}^{+2}	0.33/1
(1,0,0)	(0,0,0)	1.065_{-2}^{+2}	0.91_{-2}^{+3}	5.2/1
(1,0,0)	(1,0,0)	1.000_{-6}^{+5}	0.99_{-9}^{+8}	3.1/1
(1,0,0)	(-1,0,0)	1.320_{-6}^{+6}	0.75_{-4}^{+4}	0.79/1
(1,0,0)	(0,1,0)	1.158_{-6}^{+6}	0.85_{-3}^{+4}	1.7/1

D.3 Extrapolation of $h_{A_1}(\omega)$ to the chiral limit.

These tables list the form factor $h_{A_1}(\omega)$ for a spectator quark of mass zero. The form factor $h_{A_1}^{\text{rc}}(\omega)$ is the radiatively corrected and normalised *physical* form factor. The χ^2/dof correspond to the goodness-of-fit of the extrapolation to $h_{A_1}(\omega)$. The velocities ω have also been extrapolated to κ_s ; the χ^2/dof are all of $\mathcal{O}(1)$.

$\kappa_Q = 2100 \longrightarrow \kappa_{Q'} = 2100, \quad \kappa_q = 4315$				
p	p'	ω	$h_{A_1}^{\text{rc}}(\omega)$	χ^2/dof
(0,0,0)	(1,0,0)	1.049^{+4}_{-4}	0.944^{+2}_{-2}	0.00/1
(1,0,0)	(0,0,0)	1.043^{+3}_{-2}	0.86^{+4}_{-3}	5.1/1
(1,0,0)	(1,0,0)	1.008^{+6}_{-6}	0.87^{+10}_{-12}	7.1/1
(1,0,0)	(-1,0,0)	1.181^{+7}_{-7}	0.83^{+8}_{-7}	1.1/1
(1,0,0)	(0,1,0)	1.095^{+6}_{-6}	0.91^{+6}_{-5}	1.1/1
$\kappa_Q = 2100 \longrightarrow \kappa_{Q'} = 2500, \quad \kappa_q = 4315$				
p	p'	ω	$h_{A_1}^{\text{rc}}(\omega)$	χ^2/dof
(0,0,0)	(1,0,0)	1.060^{+5}_{-4}	0.93^{+3}_{-3}	0.28/1
(1,0,0)	(0,0,0)	1.043^{+3}_{-2}	0.86^{+3}_{-3}	5.7/1
(1,0,0)	(1,0,0)	1.008^{+7}_{-7}	0.87^{+12}_{-12}	5.5/1
(1,0,0)	(-1,0,0)	1.204^{+7}_{-7}	0.81^{+8}_{-7}	1.1/1
(1,0,0)	(0,1,0)	1.106^{+7}_{-7}	0.90^{+6}_{-4}	1.2/1
$\kappa_Q = 2100 \longrightarrow \kappa_{Q'} = 2900, \quad \kappa_q = 4315$				
p	p'	ω	$h_{A_1}^{\text{rc}}(\omega)$	χ^2/dof
(0,0,0)	(1,0,0)	1.077^{+6}_{-5}	0.92^{+3}_{-3}	0.4/1
(1,0,0)	(0,0,0)	1.043^{+3}_{-2}	0.87^{+4}_{-3}	7.3/1
(1,0,0)	(1,0,0)	1.011^{+8}_{-8}	0.89^{+12}_{-13}	5.6/1
(1,0,0)	(-1,0,0)	1.235^{+8}_{-8}	0.80^{+8}_{-6}	1.2/1
(1,0,0)	(0,1,0)	1.124^{+9}_{-7}	0.90^{+6}_{-5}	1.9/1
$\kappa_Q = 2100 \longrightarrow \kappa_{Q'} = 3300, \quad \kappa_q = 4315$				
p	p'	ω	$h_{A_1}^{\text{rc}}(\omega)$	χ^2/dof
(0,0,0)	(1,0,0)	1.103^{+8}_{-7}	0.91^{+3}_{-3}	0.35/1
(1,0,0)	(0,0,0)	1.043^{+3}_{-3}	0.87^{+4}_{-3}	6.5/1
(1,0,0)	(1,0,0)	1.018^{+9}_{-9}	0.90^{+12}_{-14}	4.1/1
(1,0,0)	(-1,0,0)	1.283^{+9}_{-9}	0.80^{+8}_{-7}	1.2/1
(1,0,0)	(0,1,0)	1.151^{+9}_{-9}	0.88^{+7}_{-5}	2.5/1

$\kappa_Q = 2900 \longrightarrow \kappa_{Q'} = 2100, \quad \kappa_q = 4315$				
\mathbf{p}	\mathbf{p}'	ω	$h_{A_1}^{\text{rc}}(\omega)$	χ^2/dof
(0,0,0)	(1,0,0)	1.049^{+4}_{-4}	0.96^{+3}_{-3}	0.056/1
(1,0,0)	(0,0,0)	1.072^{+3}_{-3}	0.83^{+4}_{-3}	0.36/1
(1,0,0)	(1,0,0)	1.011^{+6}_{-6}	0.92^{+9}_{-10}	5.8/1
(1,0,0)	(-1,0,0)	1.240^{+7}_{-6}	0.74^{+7}_{-7}	0.59/1
(1,0,0)	(0,1,0)	1.125^{+7}_{-6}	0.85^{+6}_{-5}	0.16/1
$\kappa_Q = 2900 \longrightarrow \kappa_{Q'} = 2500, \quad \kappa_q = 4315$				
\mathbf{p}	\mathbf{p}'	ω	$h_{A_1}^{\text{rc}}(\omega)$	χ^2/dof
(0,0,0)	(1,0,0)	1.060^{+5}_{-4}	0.95^{+3}_{-3}	0.021/1
(1,0,0)	(0,0,0)	1.072^{+3}_{-3}	0.83^{+4}_{-3}	0.82/1
(1,0,0)	(1,0,0)	1.009^{+7}_{-7}	0.92^{+10}_{-11}	7.2/1
(1,0,0)	(-1,0,0)	1.265^{+8}_{-7}	0.74^{+8}_{-7}	0.85/1
(1,0,0)	(0,1,0)	1.138^{+8}_{-7}	0.85^{+6}_{-5}	0.33/1
$\kappa_Q = 2900 \longrightarrow \kappa_{Q'} = 2900, \quad \kappa_q = 4315$				
\mathbf{p}	\mathbf{p}'	ω	$h_{A_1}^{\text{rc}}(\omega)$	χ^2/dof
(0,0,0)	(1,0,0)	1.077^{+6}_{-5}	0.95^{+3}_{-3}	0.00/1
(1,0,0)	(0,0,0)	1.072^{+3}_{-3}	0.83^{+4}_{-3}	2.1/1
(1,0,0)	(1,0,0)	1.008^{+9}_{-8}	0.92^{+10}_{-11}	5.3/1
(1,0,0)	(-1,0,0)	1.302^{+9}_{-9}	0.75^{+8}_{-6}	1.2/1
(1,0,0)	(0,1,0)	1.155^{+9}_{-8}	0.82^{+5}_{-4}	0.55/1
$\kappa_Q = 2900 \longrightarrow \kappa_{Q'} = 3300, \quad \kappa_q = 4315$				
\mathbf{p}	\mathbf{p}'	ω	$h_{A_1}^{\text{rc}}(\omega)$	χ^2/dof
(0,0,0)	(1,0,0)	1.103^{+8}_{-7}	0.93^{+2}_{-3}	0.33/1
(1,0,0)	(0,0,0)	1.072^{+3}_{-3}	0.83^{+4}_{-3}	5.2/1
(1,0,0)	(1,0,0)	1.011^{+10}_{-10}	0.92^{+11}_{-13}	3.1/1
(1,0,0)	(-1,0,0)	1.376^{+11}_{-10}	0.72^{+7}_{-6}	0.79/1
(1,0,0)	(0,1,0)	1.183^{+10}_{-10}	0.82^{+6}_{-5}	1.7/1